AN ANALYSIS OF THE ROTOR BLADE STRESSES OF THE THREE STAGE COMPRESSOR OF THE AMES RESEARCH CENTER 11- BY 11-FOOT TRANSONIC WIND TUNNEL

by

Jules B. Dods, Jr.

Distribution of this report is provided in the interest of information exchange. Responsibility for the contents resides in the author or organization that prepared it.

TABLE OF CONTENTS

i

AN ANALYSIS OF THE ROTOR BLADE STRESSES OF THE
THREE-STAGE COMPRESSOR OF THE AMES RESEARCH CENTER
11- by 11-FOOT TRANSONIC WIND TUNNEL

By Jules B. Dods, Jr.
Raman Aeronautics, Research and Engineering, Inc.

SUMMARY

An experimental investigation to determine the static and dynamic rotor blade stresses of the 3-stage compressor of the Ames Research Center 11- by 11-Foot Transonic Wind Tunnel has been made. The data are presented in terms of total blade stress, defined as the summation of the static and dynamic stresses, for the complete operational range of compressor speeds and tunnel total pressures. A power spectral analysis of selected portions of the data was made to measure the modal frequencies of the blades and the manner in which the frequencies varied with tunnel conditions. The phase angles and coherences between various gage combinations are also presented. The maximum total blade stress of 62.36×10^6 N/m^2 (9045 psi) was measured on the third stage blade at a distance of 0.5461 m $(21.5$ inches$)$ outboard of the blade butt for a tunnel total pressure of 220.12×10^3 N/m^2 (65 in. Hg.). The static stress accounts for 88.6-percent of the total, and the dynamic stress accounts for the remaining 11.4-percent of the total stress. A band-pass frequency analysis of the data indicated that the dynamic stresses are primarily due to vibrations in the 1st bending mode. A series of recommendations are presented to improve the results for any future experimental investigations of the rotor blade stresses.

INTRODUCTION

The static and dynamic aerodynamic loads and the centrifugal loads imposed upon the components of wind tunnel compressors result in rotor blade stresses that vary considerably over the operational envelope of the wind tunnel. Knowledge of the blade stresses is important in evaluating the operational limits of the wind tunnel in terms of compressor speed and wind tunnel total pressure combinations. In addition, the blade stresses must be known

in order to estimate the rotor blade fatigue life, and hence, the maximum number of hours a given set of blades can be run. The consequence of a single blade failure are catastrophic in terms of severe damage to the remaining rotor and stator blades and to the wind tunnel, and in terms of the extensive time required to replace the damaged parts. Thus, tests were initiated and conducted by NASA personnel to determine the rotor blade stresses in the 2nd and 3rd stages of the three-stage compressor of the Ames Research Center 11-by 11-Foot Transonic Wind Tunnel. The tests consisted of measurements of 15 strain gage outputs on two rotor blades for compressor speeds from 430 to 685 RPM and for tunnel total pressures from 16.93×10^3 N/m^2 (5 in. Hg.) to 220.01×10^3 N/m^2 (65 in. Hg.). The data were analyzed to determine the total blade stresses, broadband (root-mean-square) dynamic stresses, and the static stresses. In addition, the spectral characteristics of the dynamic stresses were analyzed to determine the modal frequencies of the blade vibrations, the variation of these frequencies with compressor speed and tunnel total pressure, the power spectral densities, and the phase angle and coherences of various strain gage combinations.

The data analysis and preparation of the report were carried out at Raman Aeronautics, Research and Engineering, Inc., Palo Alto, CA on contract No. NAS2-9112 from Ames Research Center.

NOMENCLATURE

A	constant = 3.65 in equation, $f = AN$ (see figure 13)
C	centrifugal force on blade, N (lb)
D	drag on blade, N (lb)
f	frequency, Hz
G_S	power spectral density of blade stress, $(N/m^2)^2/Hz$ $[(lb/in^2)^2/Hz]$
$G_S(f)$	nondimensional power spectral density function of $S(t)$, $G_S U/q^2 L$
K	strain gage sensitivity, volts/N/m^2 (volts/lb/in^2)
L	lift on blade, N(lb) [also nondimensionalizing factor for $G_S(f)$, m(ft)]
ℓ	length of compressor blade, m (in)
M_∞	free stream Mach number in wind-tunnel test section
M_g	modulus of gage signals, $\sqrt{x^2 + y^2}$
N	3-stage compressor speed, revolutions per minute
P_t, PT	tunnel total pressure, N/m^2 (in. Hg)
q	wind tunnel dynamic pressure, nondimensionalizing factor for $G_S(f)$, $N/m^2(lb/ft^2)$
Q	torque on blade, N-m (lb-ft)
R	resultant force on blade, N (lb)
S-TOTAL	total stress on blade, absolute value of S-MEAN and S-RMS, $N/m^2(lb/in^2)$
S-MEAN	static stress on blade, N/m^2 (lb/in^2)
S-RMS	dynamic stress on blade, N/m^2 (lb/in^2)
S(t)	time varying function of blade stress
T	thrust on blade, N (lb)
U	nondimensionalizing factor for $G_S(f)$, m/sec (ft/sec)
U_c	velocity approaching compressor blades, m/sec (ft/sec)
U_ω	rotational compressor velocity, m/sec (ft/sec)
U_R	resultant velocity on blade, m/sec (ft/sec)
X, Y	generalized notation for gage signals, volts
α	blade angle of attack, deg (see Fig. 2)
β	blade angle ($\alpha+\phi$), deg
γ	coherence between gage signals, $[M_g^2/(G_S X)(G_S Y)]$
ε	angle between L and R vectors, deg
θ	phase angle between X, Y, deg (arctan quadrature-power/co-power)
ϕ	angle between resultant and rotational velocities, deg.

The "model" of the present investigation consists of two strain gage instrumented rotor blades installed in the three-stage compressor of the Ames 11- by 11-Foot Transonic Wind Tunnel. A sectional side view of the compressor showing the number and the arrangement of the entrance and exit vanes, and of the stators and rotors is presented in figure 1. A force diagram for a typical rotor blade is given in figure 2 for reference.

The general arrangement of the 11- by 11-Foot tunnel is given in figure 1.1.1 of reference 1 along with other detailed information. The tunnel is of the closed-return variable density type having an adjustable nozzle with two flexible walls and a slotted test section to permit transonic testing. The Mach number range of the tunnel is from 0.7 to 1.4 and can be operated at unit Reynolds numbers from 5.6×10^6 to $30.8 \times 10^6/m$ (1.7×10^6 to $9.4 \times 10^6/ft$).

INSTRUMENTATION AND DATA ANALYSIS

Data Acquisition System

The locations of the strain gages on the 2nd and 3rd stage rotors of the compressor are shown in figure 3(a) and the locations with respect to the theoretical node points for the first four bending modes are given in figure 3(b). The output from each gage was amplified by an automatic gain-ranging amplifier and recorded with a frequency range from DC to 2.5 kHz (7-1/2 ips.) on a FM tape recorder (Ampex FR-1800, 32-channel). In the automatic mode each amplifier adjusts its own gain step and is locked at that gain during the data acquisition of that particular test point. A dc voltage analogous to the gain is provided by each amplifier and is recorded on the tape recorder. A calibration sine wave signal was also recorded on each tape recorder channel at the beginning of each discrete data point. A timing mechanism furnished timed relay closures to accomplish a variety of tasks in the data acquisition procedure. For example, a relay closure signaled the time code generator to start the tape recorder. Other relays would control the auto-gain amplifiers to seek the proper signal gain level ("reset" mode), to prevent further ranging of the gain once the proper level was reached ("lock" mode), and to record the dc voltage levels corresponding to the various gain steps ("interrogate" mode). In addition to

recording the dynamic strain gage outputs, the static, or mean, strain gage outputs were recorded on separate tape recorder channels in a dc mode.

Data Retrieval System

The data obtained on the magnetic tape during the wind tunnel test was played back using the data "retrieval" system shown in figure 4. The data recorded on the magnetic tapes were divided into four sets, two for the dynamic, or ac mode, and two for the static (mean), or dc mode. Information from previous tests had indicated the desirability of filtering the dynamic signals beyond a frequency of 1 kHz. Accordingly, the low-pass filters shown on Figure 4 were used to eliminate all frequencies above 1 kHz from the dynamic measurement, and above 0.1 Hz (essentially zero) for the static measurements. The resulting dynamic signals were then read by the root-mean-square (RMS) modules and a digital voltmeter (DVM), while an interface scanner introduced the results to the Hewlett-Packard 9830 computer. The static signals were handled directly by the DVM/Scanner unit. The computer then processed the signals and stored the final results on a cassette for printing and plotting. To assist in an analysis of the relative "stress energies" of the various bending modes, the low pass filters were replaced by the Krohn-Hite band-pass filters, and portions of the data were rerun using band-pass frequencies set to have a center frequency near the modal frequencies for the first four bending modes. The data were run separately for each mode.

In addition to the data analysis for determining the overall blade stresses, selected portions of the data were analyzed to determine the power spectral densities of the blade stresses using the system described by Lim and Cameron in reference 2.

RESULTS AND DISCUSSION

Broadband or Overall Stresses

The blade stress data obtained from the wind tunnel test consisted of outputs from 15 strain gages with variations in the tunnel total pressure from 16.93×10^3 N/m^2 (5 in Hg) to 220.12×10^3 N/m^2 (65 in Hg) and for compressor speeds from 430 to 685 RPM. Although the data from all gages were analyzed,

results are presented only for gages 4, 5, 6, 8, 11, and 12 through 16. The data from gages 2, 3, 7, 9, and 10 are believed to be incorrect and, therefore, are not presented. Two of these gages (7 and 9) were located on the camber side of the blade, and thus no comparisons could be made of the stress differences between the camber and the flat side of the blade. However, the remaining gages were distributed quite well longitudinally along the blade and, therefore, it is believed that a reasonably accurate assessment of the overall stresses could be made. The gage indicating the highest stresses (No. 6) was located between valid gages (5 and 11), and the gage indicating the next highest stress was the one nearest the blade root (No. 12), which would be expected to respond more to the first bending mode. (It will be shown later than the highest stresses were found in the first bending mode).

The basic data are presented in the form of total stress, mean (static) stress, and root-mean-square (dynamic) stress for each operating condition. The effect of tunnel total pressure on the stresses is shown in figure 5(a) through (dd) throughout the compressor speed range. The effect of compressor speed on the stresses is shown in figure 6(a) through (u) throughout the tunnel total pressure range. The longitudinal distribution of the blade stresses is shown in figure 7(a) through (r) for various compressor speeds and tunnel total pressures.

In general, the total blade stresses increase in a fairly regular manner with increasing compressor speed, and with increasing total pressure up to 152.39×10^3 N/m^2 (45 in Hg). The data indicate that the compressor blades are probably operating in a stalled condition at 220.12×10^3 N/m^2 (65 in Hg) and in general the stresses tend to decrease at stall. Since it was recognized early in the analysis that gage 6 had the largest stresses at 65 in Hg, the data were reread numerous times during the course of the analysis to ensure reliability. The results were consistent for all readings. Also, as will be shown later, the ratios of mean to total stresses and RMS to total stresses for gage 6 are consistent with the other highly loaded gages. Therefore, it is believed that the data from gage 6 are valid. Unfortunately, there are omissions in the available data at 65 in Hg (N's from 570 to 630, and from 670 to 685), and in the total pressure range between 152.39×10^3 N/m^2 (45 in Hg) and 220.12×10^3 N/m^2 (65 in Hg).

The maximum total stresses for each strain gage with their corresponding tunnel operating condition are shown in the following table. The stresses are

listed in descending order of magnitude. Also shown are the static (MEAN) and dynamic (RMS) stresses and their percentages with respect to the total stresses.

Gage No.	P_t, in Hg	N	S-TOTAL, psi	S-MEAN, psi	Percent S-MEAN / S-TOTAL	S-RMS, psi	Percent, S-RMS / S-TOTAL
6	65	640	9045	8011	88.6	1034	11.4
12	45	685	6092	3216	52.8	2876	47.2
11	45	685	5381	2309	42.9	3072	57.1
5	65	640	4450	4000	89.9	450	10.1
4	45	685	4200	1670	39.8	2530	60.2
8	45	685	4108	1442	35.1	2666	64.9
13	45	680	3816	3053	80.0	763	20.0
15	45	685	3753	3008	80.1	745	19.9
14	45	685	3253	2377	73.1	876	26.9

The maximum total stress (gage 6) occurs on the 3rd stage blade at a distance of 0.5461 m (21.5 in) outboard of the blade root (fig. 3(a)) for a total pressure of 220.12 x 10^3 N/m^2 (65 in Hg). As shown in figure 5(g), it is very likely that the blade is operating in a stalled condition. The next largest total stress occurs for gage 12, which is located nearest to the blade root 0.2413 m (9.5 in) for a total pressure of 152.39 x 10^3 N/m^2 (45 in Hg). As shown in figure 5(p) the blade appears to be unstalled at this pressure. The third largest total stress occurs for gage 11, the next nearest gage to the blade root 0.4445 m (17.5 in), and also for a total pressure of 45 in Hg. This gage also indicates that the blade is unstalled at this pressure. As shown in the above table, there appears to be a large difference in the static and dynamic stress distribution between a stalled and an unstalled blade. To illustrate this phenomena more fully, the following table is presented showing the four most highly loaded gages for a stalled and unstalled blade condition. In each case, blade stalling results in a large reduction in the percentage of dynamic stress to total stress. This result is somewhat unexpected since it might be presumed that the stalled blade would have a more unsteady flow field, and thus larger rather than smaller dynamic stresses.

Gage	Blade Condition	P_t, in Hg	N	S-TOTAL, psi	S-MEAN, psi	Percent S-MEAN / S-TOTAL	S-RMS, psi	Percent, S-RMS / S-TOTAL
6	unstalled	45	670	7598	4995	65.7	2603	34.3
6	stalled	65	640	9045	8011	88.6	1034	11.4
12	unstalled	45	685	6092	3216	52.8	2876	47.2
12	stalled	65	640	4190	3418	81.6	772	18.4
11	unstalled	45	685	5381	2309	42.9	3072	57.1
11	stalled	65	670	3001	2599	86.6	402	13.4
5	unstalled	45	685	4233	1575	37.2	2658	62.8
5	stalled	65	640	4450	4013	90.2	437	9.8

The "peaks" in the dynamic stresses that occur in the data, generally at 640N for the blades operating in a stalled condition (see fig. 5(l), (r),(u), (aa) for example) are repeatable and occur for various gages and in both compressor stages. For these reasons it is believed that the peaks in the data are valid even though the cause is unknown.

Comparisons between the maximum stress levels in the blades of the 2nd and 3rd stages of the compressor are shown in the following table (from figure 5) for the blades in an unstalled condition. The data are for pairs of gages in the two stages that are located at the same blade stations. The total stresses in the 2nd stage blade are only 50 to 62-percent of those of the 3rd stage. As shown in the table, the lower total stresses in the second stage blade are due mostly to lower dynamic stresses.

Gage	Stage	P_t, in Hg	N	S-TOTAL, psi	Percent, $\frac{\text{S-TOTAL 2}}{\text{S-TOTAL 3}}$	S-Mean psi	Percent, $\frac{\text{S-MEAN 2}}{\text{S-MEAN 3}}$	S-RMS psi	Percent, $\frac{\text{S-RMS 2}}{\text{S-RMS 3}}$
6	3	45	670	7598		4995		2603	
13	2		680	3816	50.2	3053	61.1	763	29.3
11	3		685	5381		2309		3072	
14	2		685	3253	60.5	2377	100.3	876	28.5
12	3		685	6092		3216		2876	
15	2		685	3753	61.6	3008	93.5	745	25.9

Comparisons were made of the data obtained from runs made by continuously recording stress levels as the compressor speed was increased at a variable rate (referred to as "sweep" data) with the constant speed data (referred to as "discrete" point data). The results indicate that the sweep data were considerably lower than the discrete point data by a factor of 2 to 2.5 in most cases. The reason for these discrepancies is unknown. The sweep technique has been used previously in the measurement of other parameters (for example, fluctuating pressures) with more reasonable results.

The dynamic blade stresses as a function of tunnel compressor speed are given in figures 8(a) through (j) for a P_t of 152.39 N/m^2 (45 in Hg) and for various band-pass frequencies in comparison with the normal data containing all of the stress energy up to 1 kHz (low-pass). The band-pass frequencies were chosen to include the resonant frequencies of the first four bending modes (see figure 3(b)). These data indicate that for all gages the stress "energy" in the 1st bending mode (band pass from 30-90 Hz) is practically identical to that obtained for the low-pass analysis. The stress "energy" for the other three

modes is seen to be minimal. Thus, the dynamic blade stresses are primarily due to vibration in the 1st bending mode. The band pass analysis for gage 6 did not show the above results. It indicates nearly zero stress in the 1st mode and minimal stress in the other three modes. This indicates that the observed result is due to a reading failure in the HP 9830 analysis equipment. The result was not noticed in time to repeat the analysis on the HP 9830. However, a power spectral density analysis of the data for gage 6 reconfirmed the belief that the majority of the dynamic stress "energy" is also contained in the first bending mode.

In order to indicate the importance of filtering out the data above 1 kHz, the total blade stresses are presented in figure 9 with and without the "Dynamics" low-pass filter. The data are for a few representative gages and operating conditions. The rather large differences in the stress levels illustrate the importance of filtering the data. It is believed that the signals beyond about the 4th bending mode ($\sim$ 700 Hz) are primarily "noise" and therefore are not indicative of true blade stresses. The character of the noise effects beyond 1 kHz will be discussed in the next section of the report.

Power Spectral Analysis of Stresses

The primary purpose of conducting a power spectral analysis of the blade stress data was to measure the modal frequencies and to indicate the manner in which the frequencies varied with compressor speed and with tunnel total pressure. A secondary purpose was to compare various gage combinations and to measure their relative phase angles and coherences. At the beginning of the analysis portion of the investigation it was believed that comparisons of the phase angles and coherences would provide insight into the modal behavior of the blade stresses. However, except for the 1st bending mode, little information of substance was obtained. The reasons for this were twofold – one, the blade stresses were shown to be primarily due to first mode bending which tends to mask any attempt to measure the higher mode phase angles and coherences; and two, the failure of five of the strain gages, one of which was a torsional gage, hampered the selection of gage combinations which would, through phase relationship, indicate torsional and higher vibrational modes. These deficiencies, however, are not too serious considering the primacy of the 1st bending mode stresses, and the low stresses near the leading edge as indicated by the one operational torsional gage 8.

The power spectral analysis consisted of measuring 918 individual power spectral densities and cross-power spectral densities from which were obtained modal frequencies, and phase angles and coherences between selected gages for various test conditions. The results of the analysis are presented in figure 10(a) through (m) showing the variation of the modal frequencies, coherences, and phase angles with compressor speed for various tunnel pressures. For convenience, the same data are shown as a function of tunnel total pressure in figure 11(a) through (i). In general, the modal frequencies agreed with the values obtained from "bench" tests at zero RPM by NASA personnel. The variations with either compressor speed or tunnel total pressure were minimal. The 1st bending mode frequency varied from 42 Hz at N=470 to 62 at N=685.

Values of the coherence were generally near 1.0 for the 1st mode, and decreased rapidly for the higher modes, and, depending on the gage combinations, the phase angles tended to be 0° (in-phase) or 180° out-of-phase. The coherence tended to be higher at larger values of total pressure (compare figure 10(a) and 10(d)). The signals from gages 4 and 5 (figure 10(a) through (e)) were expected to be in-phase ($\Theta \cong 0°$). However, for the most part they were out-of-phase ($\Theta \cong 180°$). An inspection of the signs of the signal (from the HP 9830 system analysis) indicated a sign reversal between these gages in the mean values. Thus, it is probable that the phase angles shown should be changed by 180°. For gages 6 and 12 (figure 10(f) through 10(j)), the phase angle relationship should be correct as shown since the mean values have the proper signs. The signals appear to be in-phase for the 1st and 3rd modes and 180° out-of-phase for the 2nd and 4th modes. Gages 6 and 11 (figure 10(k)) are in-phase for the 1st, 2nd, and 3rd modes and 180° out-of-phase for the 4th mode. The second stage gages, 13, 14 and 15 are shown in figure 10(1) and (m). Gage combinations 13, 14 and 14, 15 are in-phase except for the 2nd mode for the 14, 15 combinations. A summary of these phase angle relationships is given in Table I.

The power spectral density analysis of the data also provided an independent check upon the broadband dynamic stresses measured by the HP 9830 system by integrating the PSDs, and also by measuring the RMS signal strengths as the data were being transferred from the test magnetic tape to the "control loop" of the hybrid system. In general, these values compared very well with those measured by the HP 9830 system.

A series of representative power spectra for the most highly stressed gages (6, 11, and 12) is shown in figures 12(a) through (h). The spectra are for a total pressure of 152.39×10^3 N/m^2 (45 in Hg) and for various compressor speeds, and were analyzed for frequencies up to 20 kHz in order to measure the noise peaks previously mentioned for the regions above 1 kHz. (The majority of the power spectra were, of course, limited to 1 kHz to correspond to the 1 kHz limits used with the HP 9830 system.) The plotted data appear to end at from 3 to 5 kHz instead of 20 kHz. The reason for this is that the spectral values are less than the lowest decade shown, and since the plots are limited to 5 decades, the values do not appear. They are, however, included in the overall integrations.

As previously discussed in the section of the report concerning the band-pass analysis (figure 8), these power spectra show that the peaks for gage 6 compare closely in frequency and amplitude with those for gages 11 and 12, confirming the statement made in a previous section of the report that the majority of the stress "energy" for gage 6 was in the 1st bending mode.

The frequencies of the noise spectral peaks above 1 kHz are presented in figure 13 as a function of compressor speed. These frequencies can be approximated by the equation $f = 3.65$ N. It has been conjectured by NASA personnel that the strain gages act as miniature RF antennas and pick up the peaks from being rotated in an enclosed electromagnetic environment. In any event, these peaks must be considered as being noise because their amplitudes are about two orders of magnitude greater than the 4th bending mode peaks at $f \cong 700$ Hz (see figure 12) and, therefore, it would be unrealistic to believe that the peaks could be caused by higher modal vibrations of the blades. Thus, for the present analysis, the noise spectra is defined as that portion of the power spectra having frequencies >1 kHz. The effect of filtering out the noise spectra upon the dynamic stresses is illustrated for gages 6, 11, and 12 in figure 14. It is recommended that the above definition of the noise be retained for any further tests to determine blade stresses.

CONCLUSIONS AND RECOMMENDATIONS

An analysis of tests conducted to determine the rotor blade stresses of the 3-stage compressor of the Ames Research Center 11- by 11-Foot Transonic Wind Tunnel has resulted in presentations of the blade total stresses, the static stresses, and the dynamic stresses over the operating range of compressor

speeds and tunnel total pressures. A power spectral analysis of selected portions of the data was made to measure the modal frequencies of the rotor blades and the manner in which the frequencies varied with tunnel conditions. The phase angles and coherences between various gage combinations are also presented. The analysis has resulted in the following conclusions and recommendations.

1. The maximum total blade stress of 62.36×10^6 N/m^2 (9045 psi) occurs on the third stage blade at a distance of 0.5461 m (21.5 inches) outboard of the blade root for a $P_t = 220.12 \times 10^3$ N/m^2 (65 in Hg). The static stress accounts for 88.6 percent of the total, and the dynamic stress accounts for the remaining 11.4 percent of the total.

2. The data indicate that the compressor blades are operating in a stalled condition at $P_t = 220.12 \times 10^3$ N/m^2 (65 in Hg) and mostly in an unstalled condition at $P_t = 152.39 \times 10^3$ N/m^2 (45 in Hg).

3. Unexpectedly, blade stalling results in lower dynamic stresses. For example, for the most highly stressed gage No. 6, the ratio of dynamic stresses to total stresses is 34.3 percent for the unstalled blade, and only 11.4 percent for the stalled blade.

4. The total stresses in the 2nd stage rotor blade are only 50 to 60 percent of the stresses in the 3rd stage rotor blade.

5. A band-pass frequency analysis of the data indicated that the dynamic stresses are primarily due to vibrations in the 1st bending mode.

6. The variations of the modal frequencies with either compressor speed or tunnel total pressure were minimal. The measured 1st bending mode frequencies varied from 42 Hz at N=470 to 62 Hz at N=685.

7. Values of the coherence for various gage combinations were generally near 1.0 for the 1st bending mode, and decreased rapidly for the higher modes. The phase angles tended to be 0° (in-phase) or 180° (out-of-phase) in the first mode. The primacy of the 1st bending mode stresses tended to mask the measurements of the higher mode phase angles and coherences.

The following recommendations are given for any further experimental blade stress investigations:

(a) Locate strain gages nearer to the root of the blade, and additional gages near gage 6 to more clearly determine the maximum stresses.

(b) Provide more strain gages on the camber side of the blade, since there is some evidence from previous tests that the stresses may exceed somewhat the values on the flat side of the blade.

(c) In general, provide more redundancy of strain gages, or investigate procedures to prevent gage failures. For the present investigation, failure of one of the torsional gages precluded the measurement of possibly higher stresses near the blade trailing edge. For wide blades, vibration in the torsional mode may induce relatively high longitudinal stresses. However, the one operational torsional gage 8 did not indicate very high stresses near the leading edge.

(d) Because of the considerably lower stresses measured on the 2nd stage blade, eliminate the gages in the 2nd stage, unless significant changes are made to the compressor configuration.

(e) Conduct the tests for several values of tunnel total pressures between 45 in Hg and 65 in Hg to determine more definitely the pressures and compressor speeds for blade stall.

(f) Eliminate tests at the lower compressor speeds and at the lower tunnel total pressures.

(g) Establish definite strain gage signs by pushing on the blade. This procedure will result in more confidence in phase-angle relationships.

(h) Investigate the possibility of strut, stator, and/or rotor redesign in order to avoid responses of the rotor blades to the forced oscillation frequencies of the present compressor configuration.

REFERENCES

1. Anon: Research Facilities Summary. Wind Tunnels – Subsonic, Transonic, and Supersonic. Vol. II – NASA-Ames Research Center, Moffett Field, CA, December 1965.

2. Lim, R. S.; and Cameron, W. D.: Power and Cross-Power Spectrum Analysis by Hybrid Computers. NASA TM X-1324, 1966.

TABLE I.- SUMMARY OF PHASE ANGLES

Gages 4, 5

P_t, in Hg	θ			
	1st Mode*	2nd Mode	3rd Mode	4th Mode
10	180°	180°	0°	180°
20	180°	180°	0°	180°
30	180°	180°	Erratic	180°
45	180°	180°	Erratic	180°
65	180°	180°	Erratic	180°

Gages 6, 12

10	0°	180°(mostly)	0°	0°,180°Erratic
20	0°	180°	0°	180°
30	0°	180°	0°	180°
45	0°	180°	0°	180°
65	0°	180°	0°	180°

Gages 6, 11

45	0°	0°	0°	180°

Gages 13, 14 (2nd Stage)

45	0°	0°	0°	0°,180°@ N 620, 630

Gages 14, 15 (2nd Stage)

45	0°	180°	0°	0°

*Probably 0°; See Discussion in Text

Figure 1.- Sectional side view of the Ames 11- by 11-Foot TWT 3-stage compressor.

DIRECTION OF
ROTOR ROTATION

CENTRIFUGAL FORCE, C
IS PERPENDICULAR TO
T AND Q PLANE

PLANE OF
ROTATION

BLADE REFERENCE
LINE
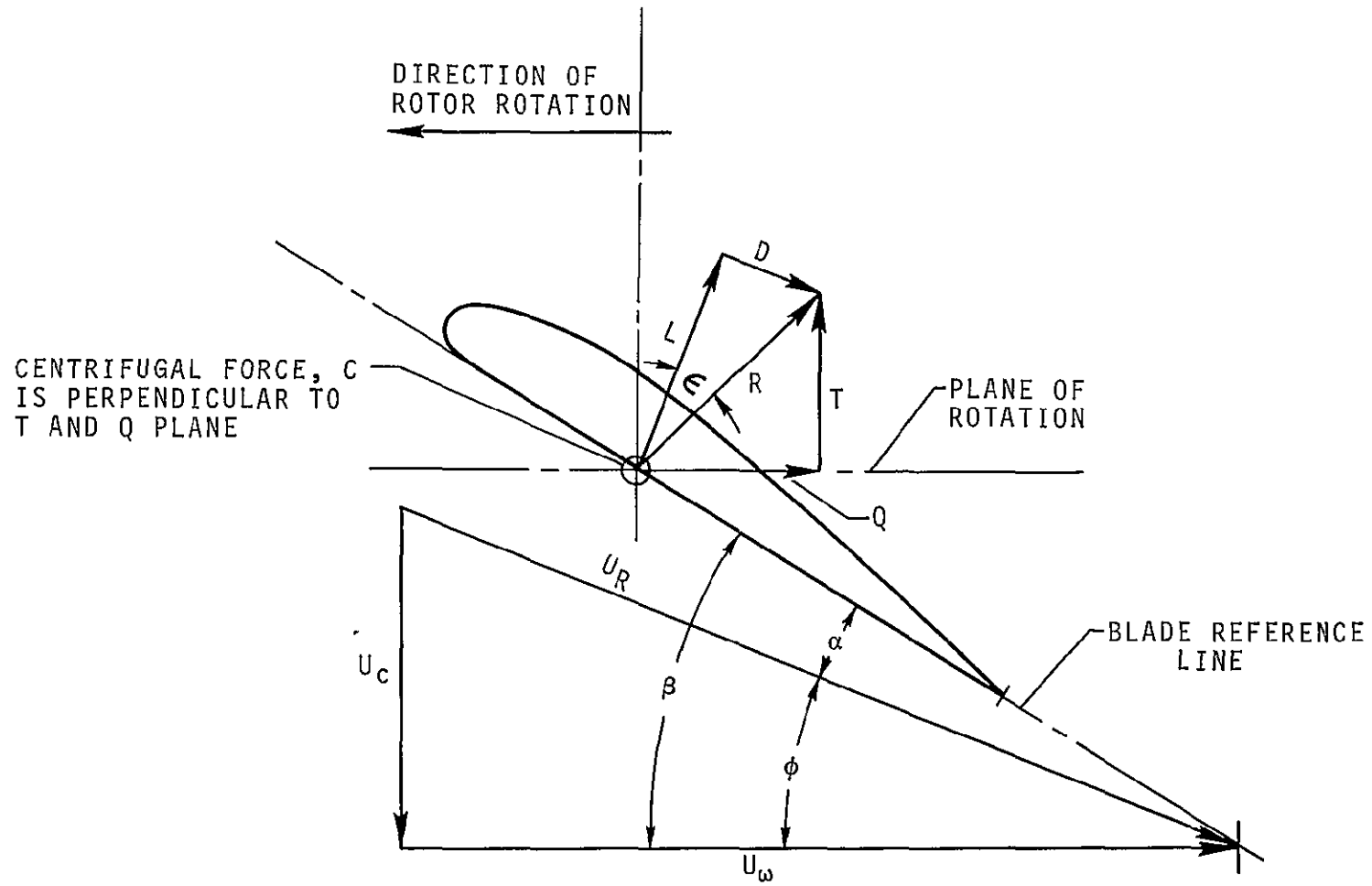
Figure 2.- Force diagram for typical rotor blade.

NOTE: ALL DIMENSIONS ARE
IN METERS (INCHES)
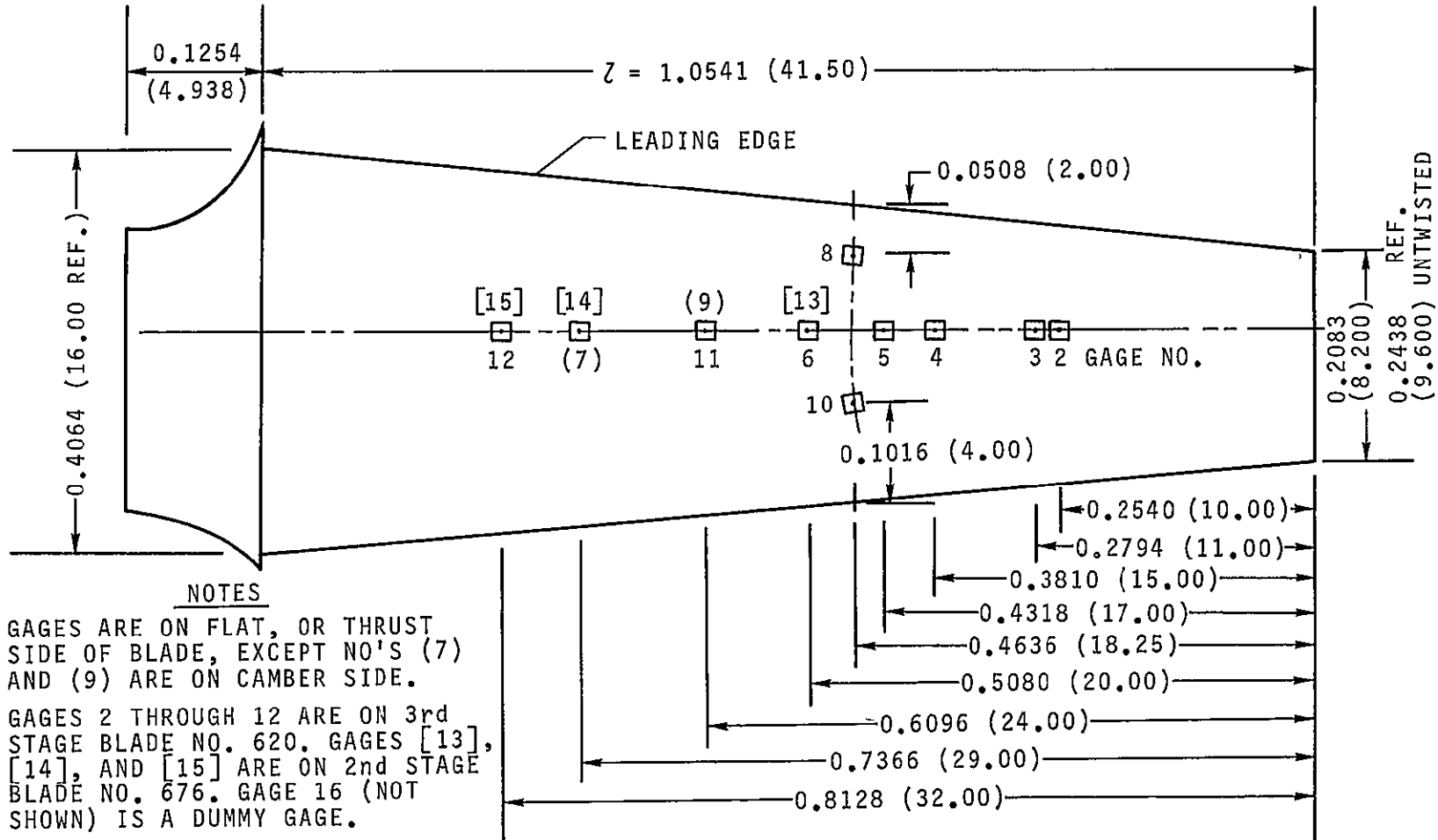
(a) Blade and gage dimensions.

Figure 3.- Location of the strain gages on the rotor blades of the Ames 11- by 11-Foot
TWT 3-stage compressor.
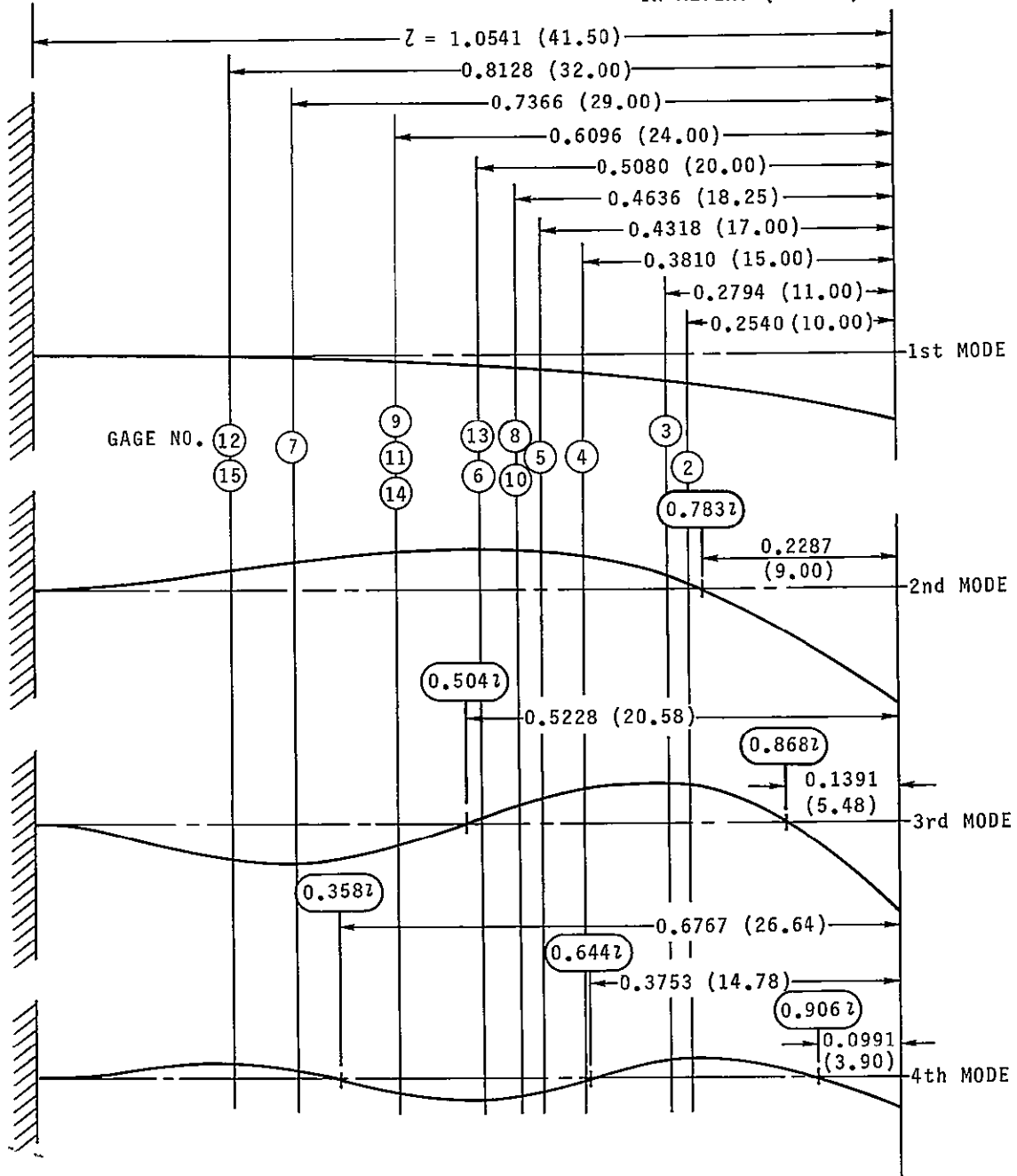
(b) Gage locations with respect to the theoretical mode points.

Figure 3.- Concluded.
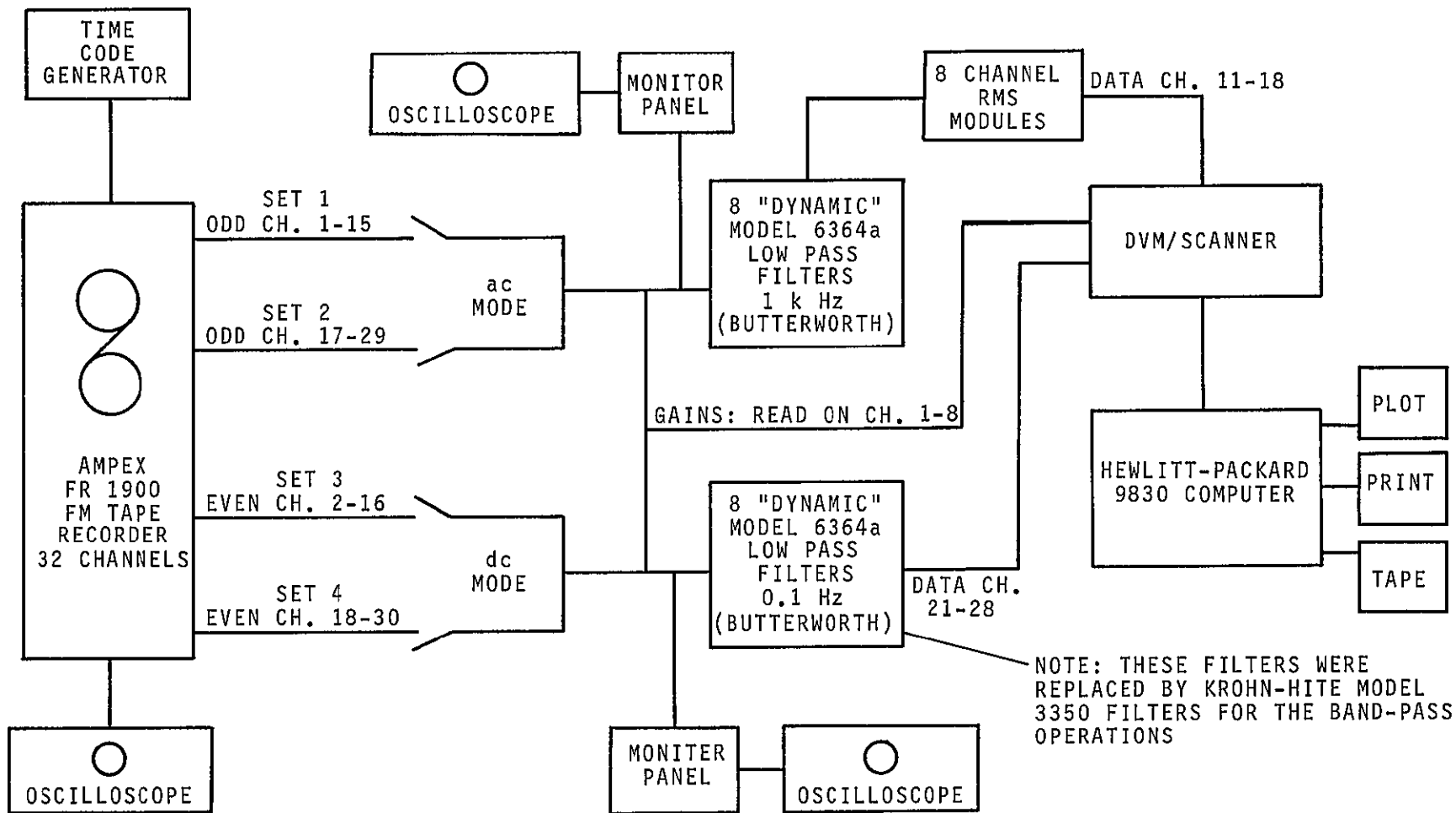
Figure 4.- Block diagram of data retrieval system.
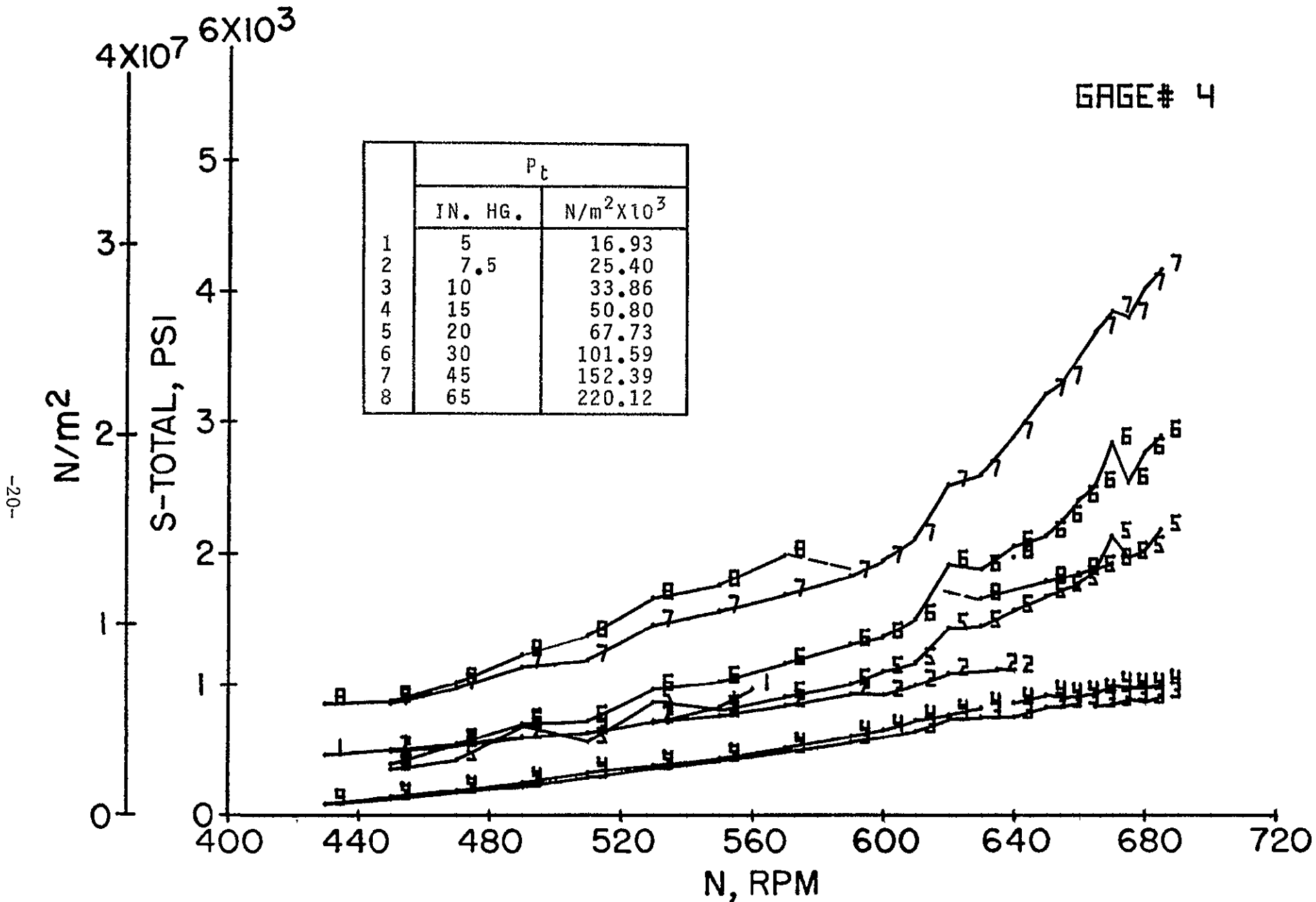
(a) Total stress; gage 4; 3rd stage.

Figure 5.- Effect of compressor speed on the blade stresses as a function of tunnel total pressure.

GAGE# 4

	P_t	
	IN. HG.	$N/m^2 X10^3$
1	5	16.93
2	7.5	25.40
3	10	33.86
4	15	50.80
5	20	67.73
6	30	101.59
7	45	152.39
8	65	220.12
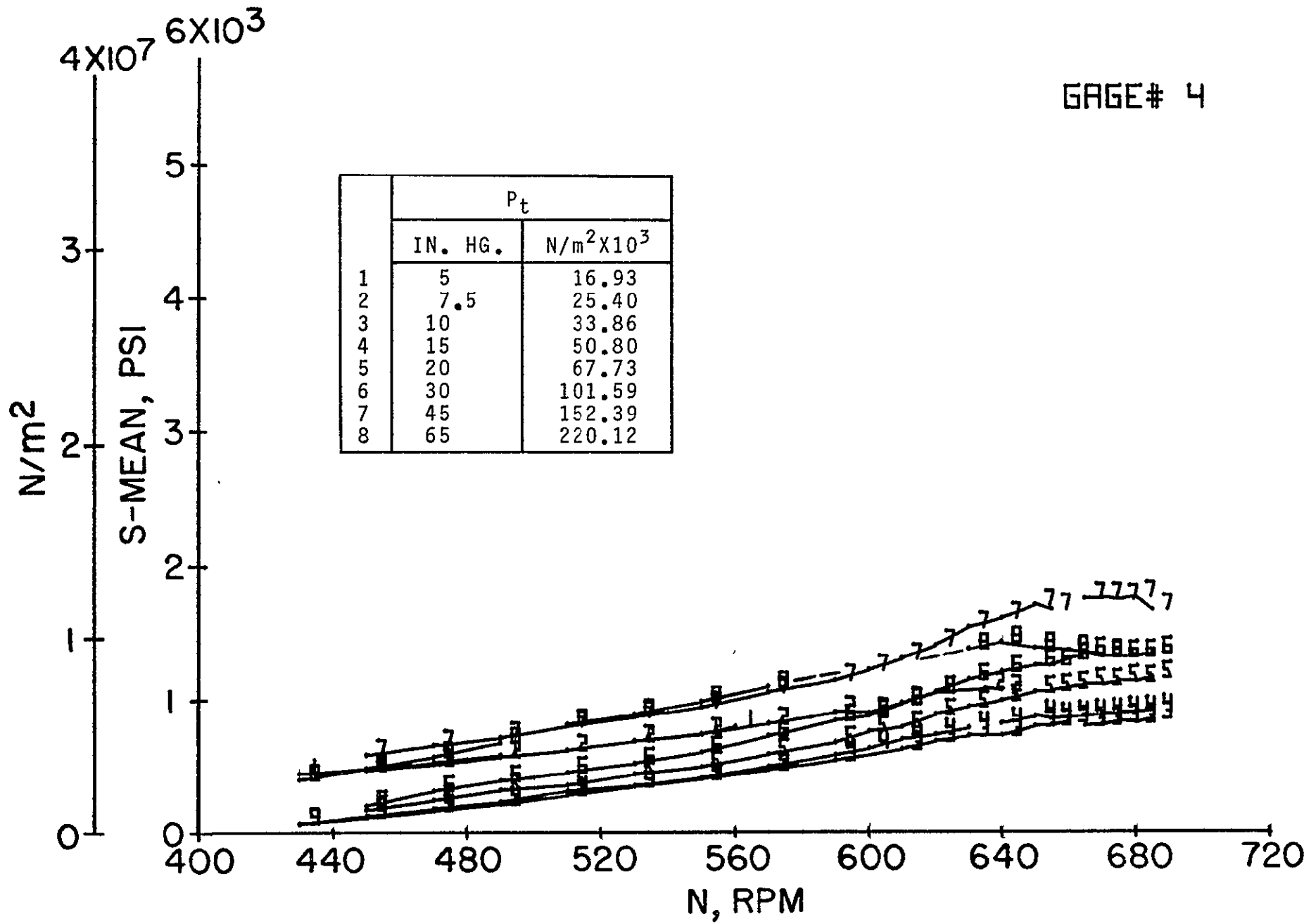
(b) Static stress; gage 4; 3rd stage.

Figure 5.- Continued.
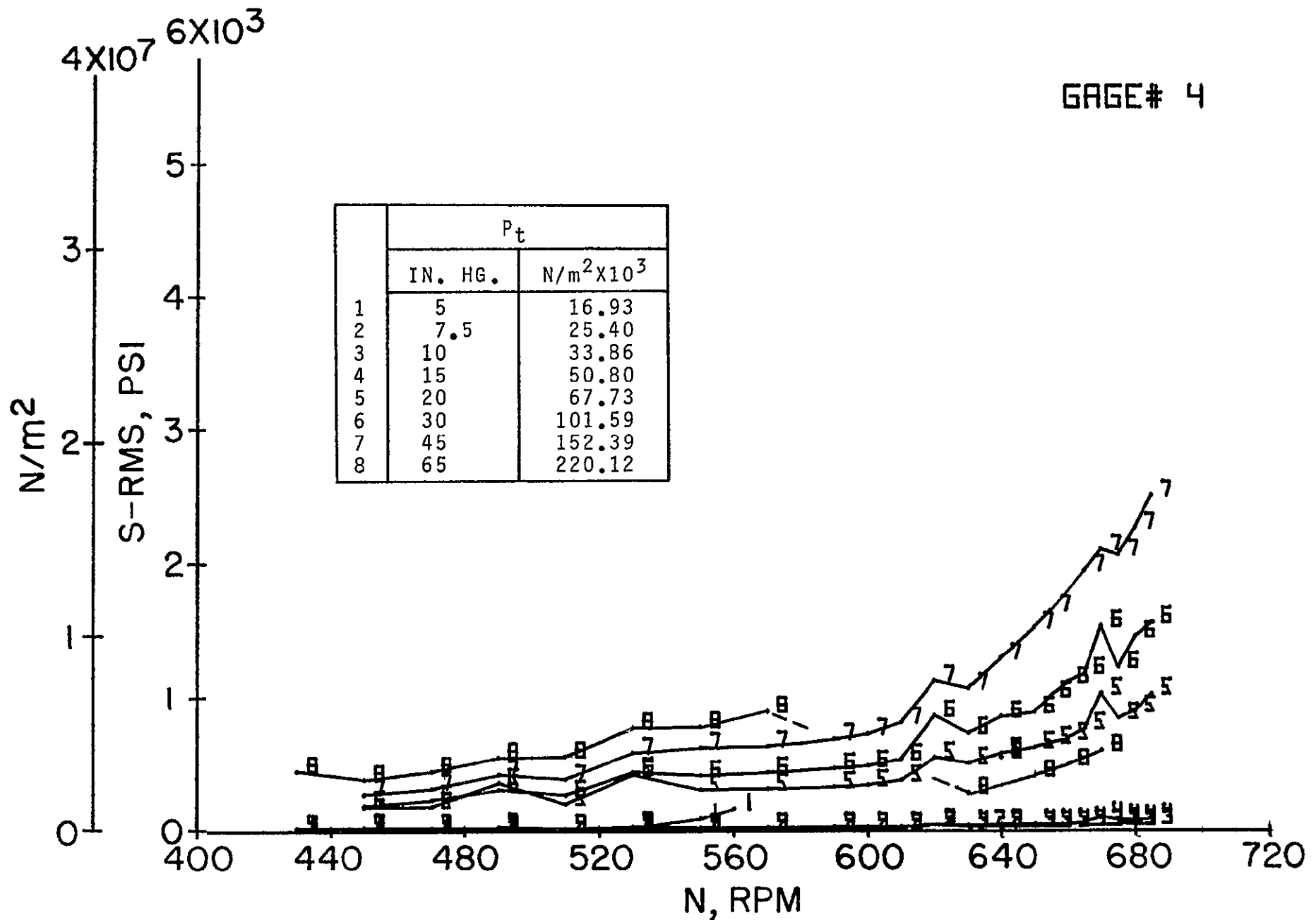
(c) Dynamic stress; gage 4; 3rd stage.
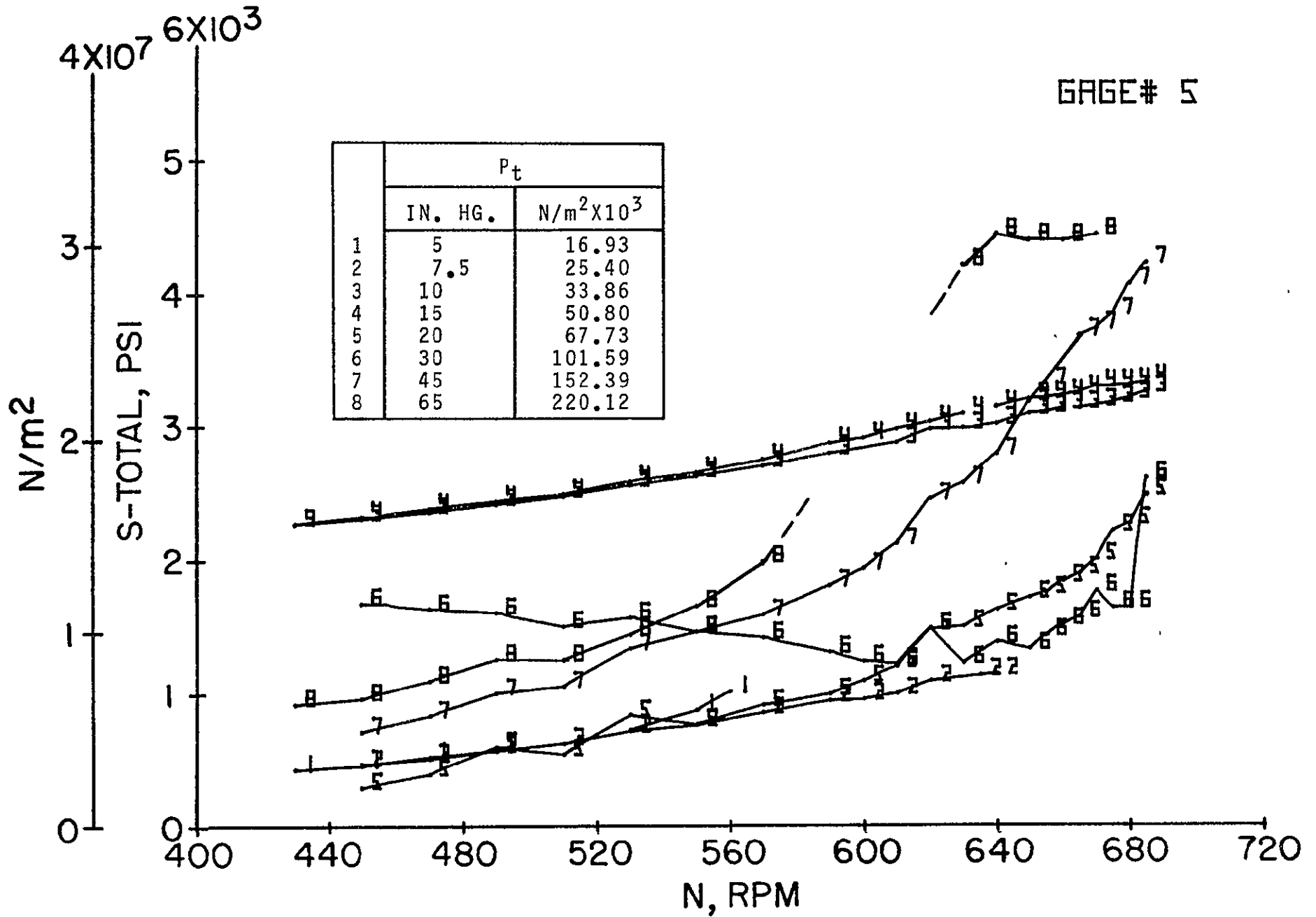
Figure 5.- Continued.

(d) Total stress; gage 5; 3rd stage.
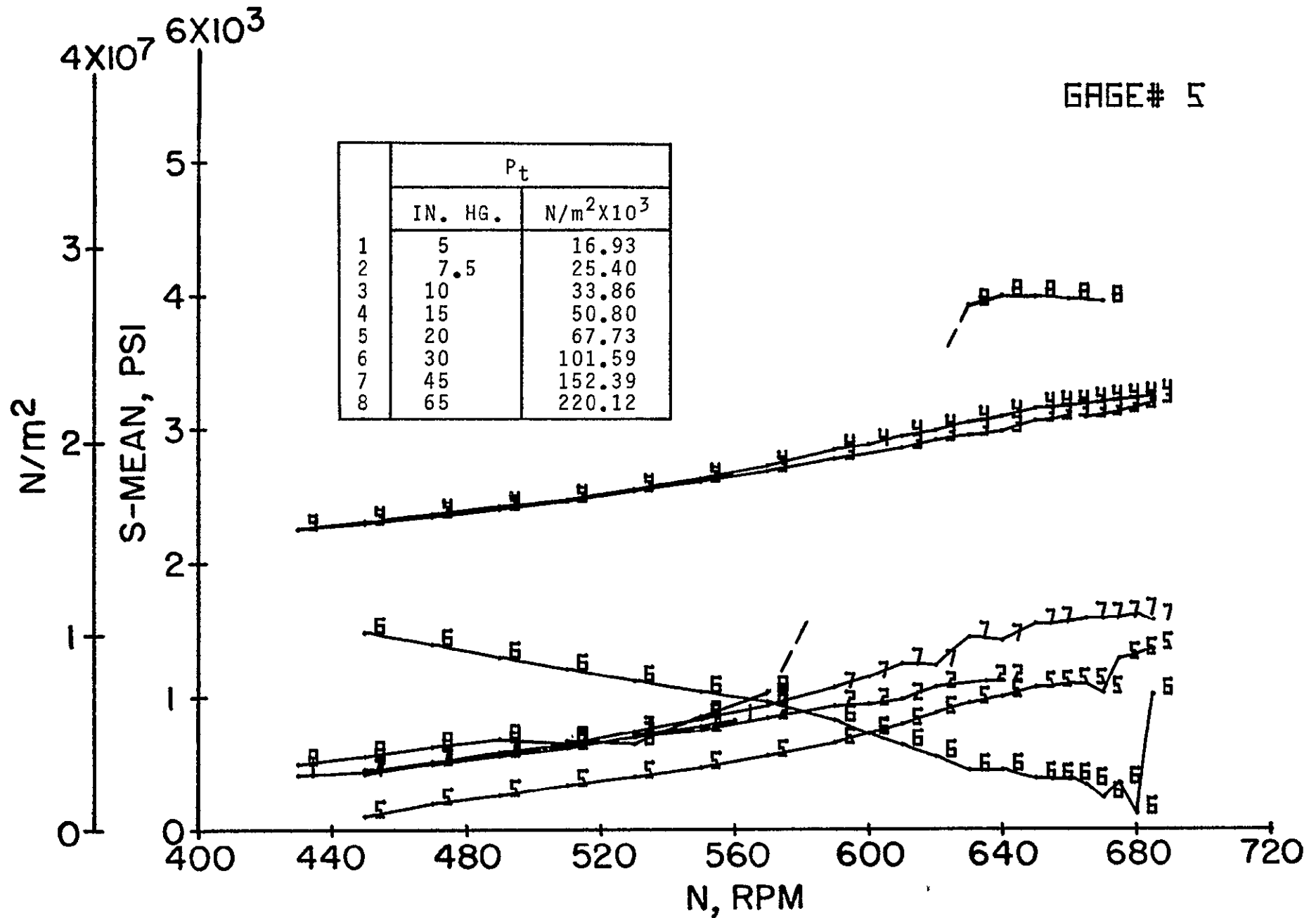
Figure 5.- Continued.

(e) Static stress; gage 5; 3rd stage.
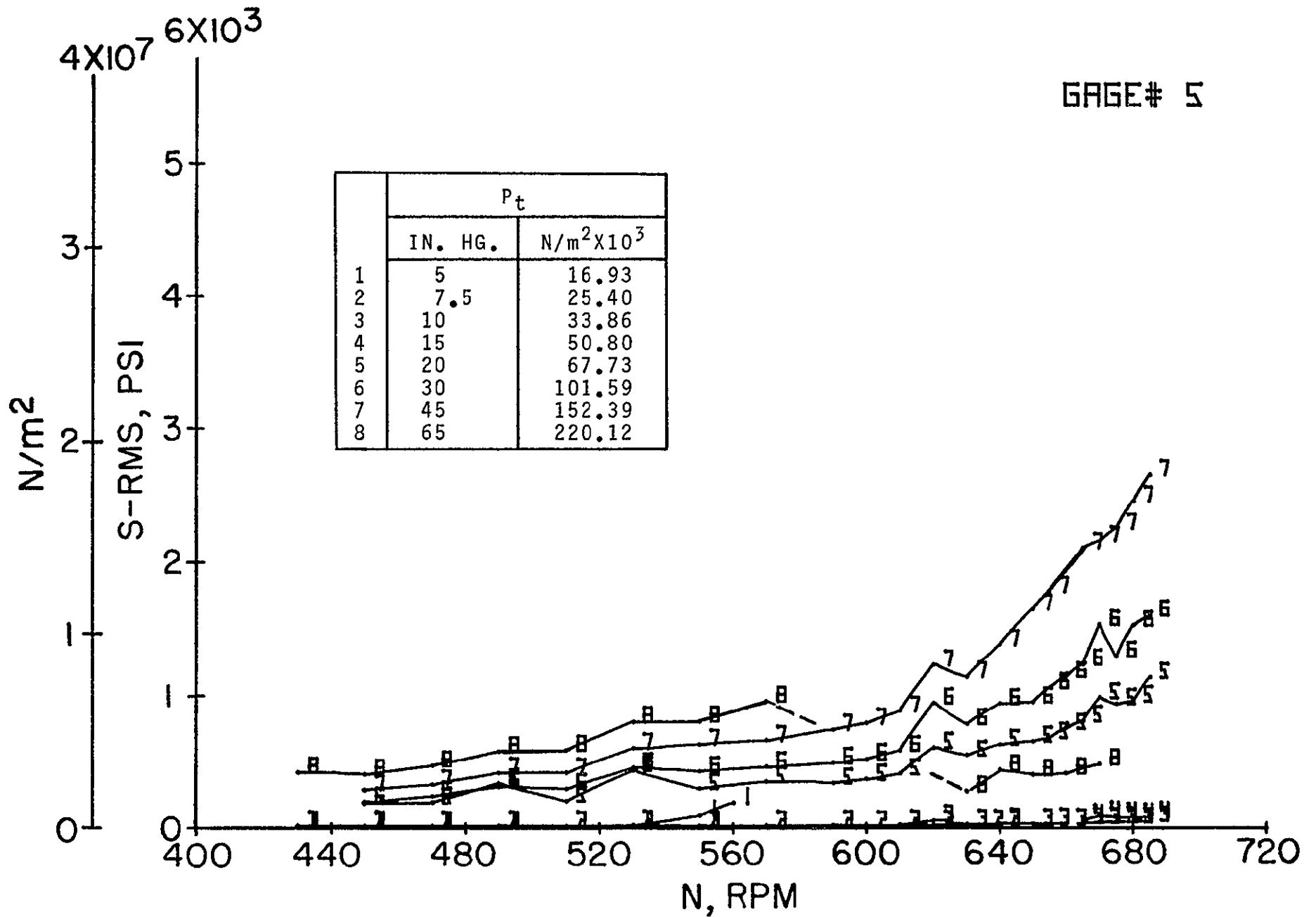
Figure 5.- Continued.

(f) Dynamic stress; gage 5; 3rd stage.
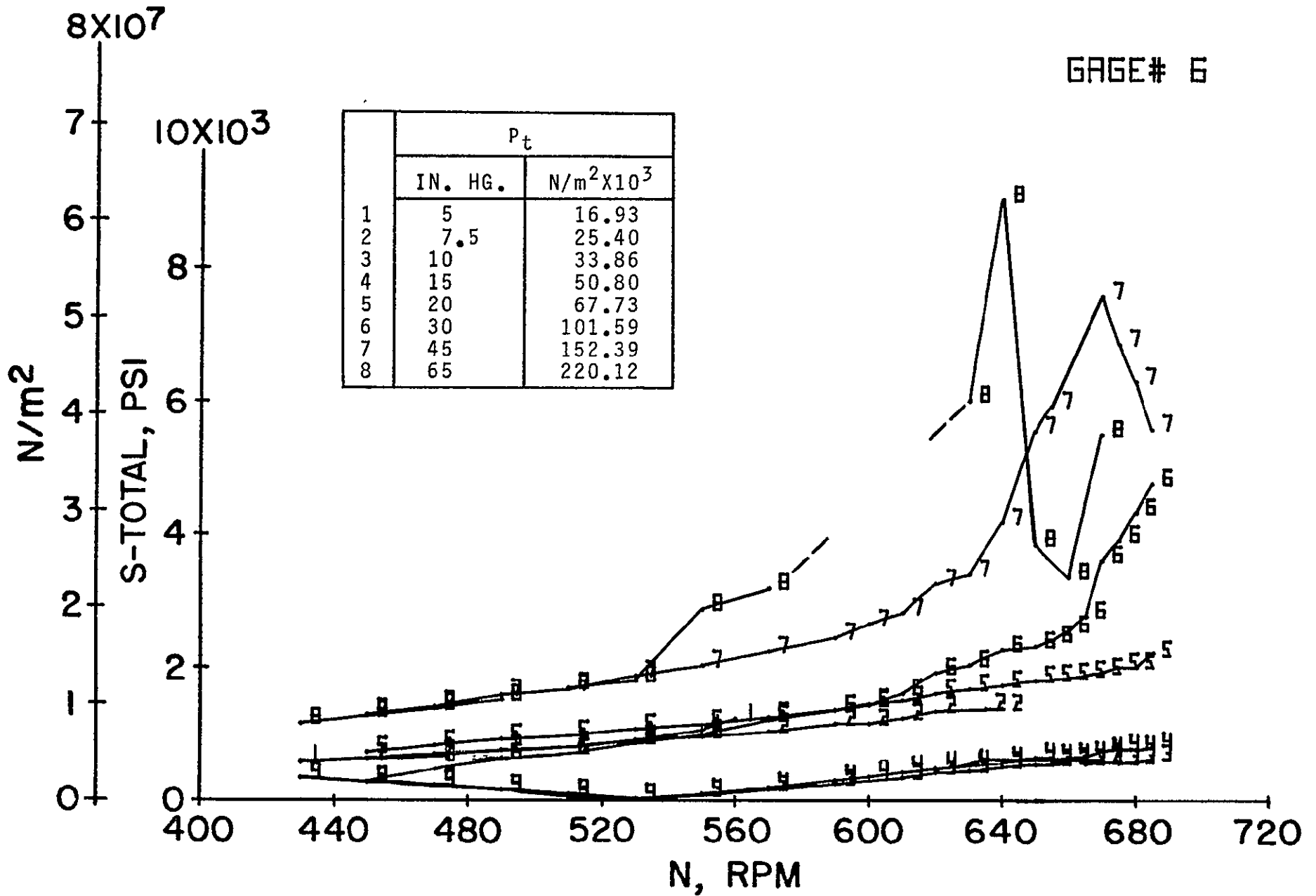
Figure 5.- Continued.

(g) Total stress; gage 6; 3rd stage.
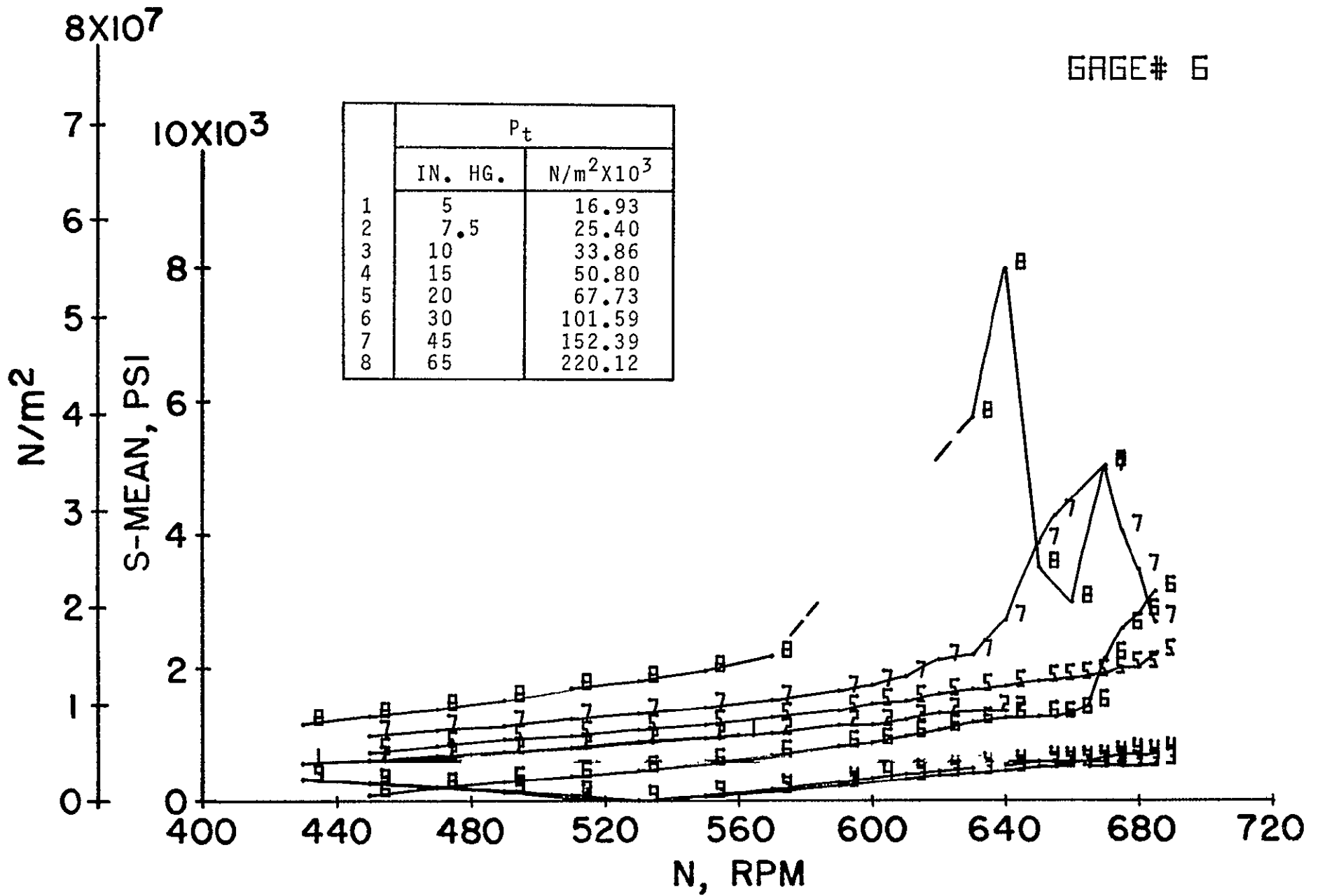
Figure 5.- Continued.

(h) Static stress; gage 6; 3rd stage.
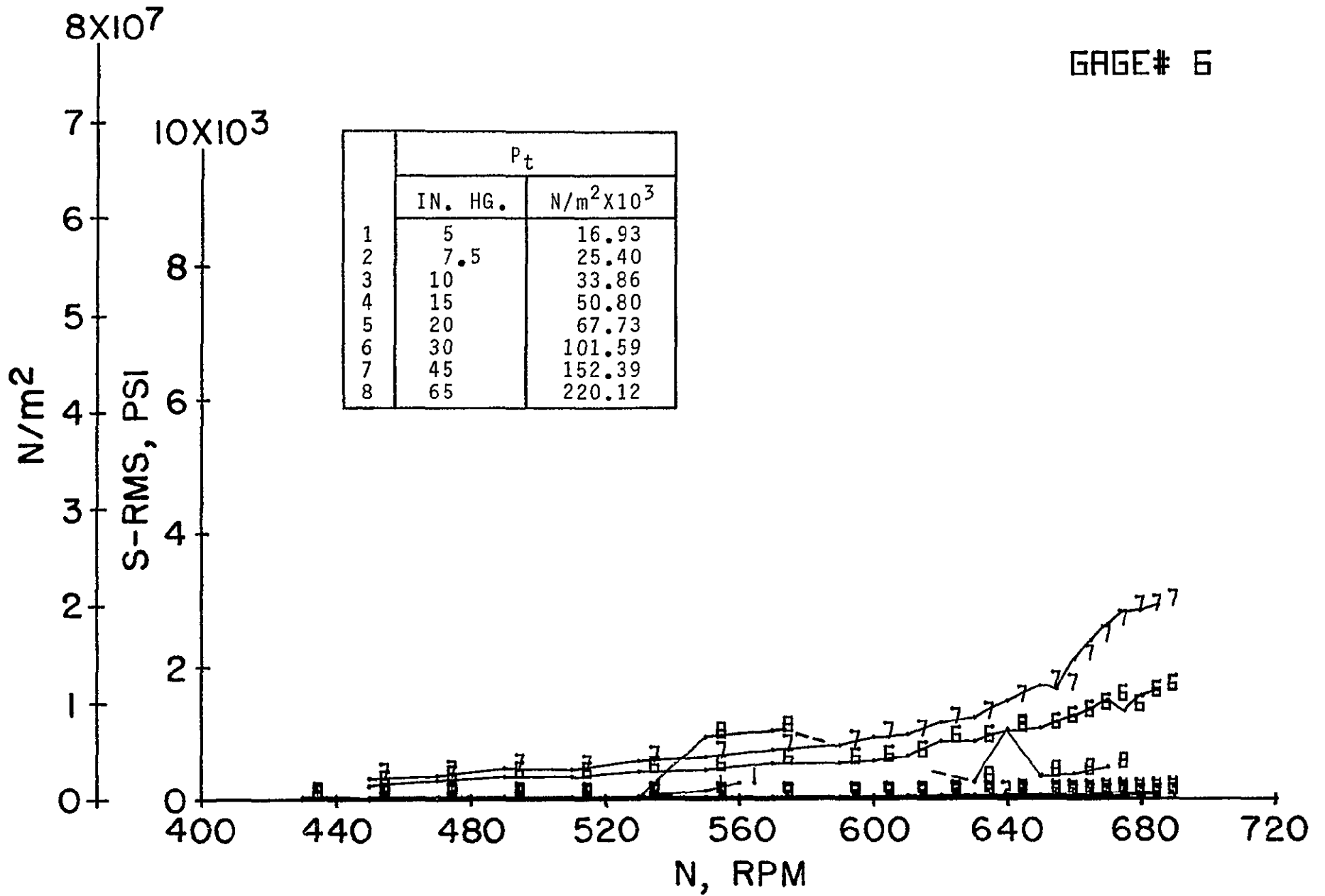
Figure 5.- Continued.

(i) Dynamic stress; gage 6; 3rd stage.
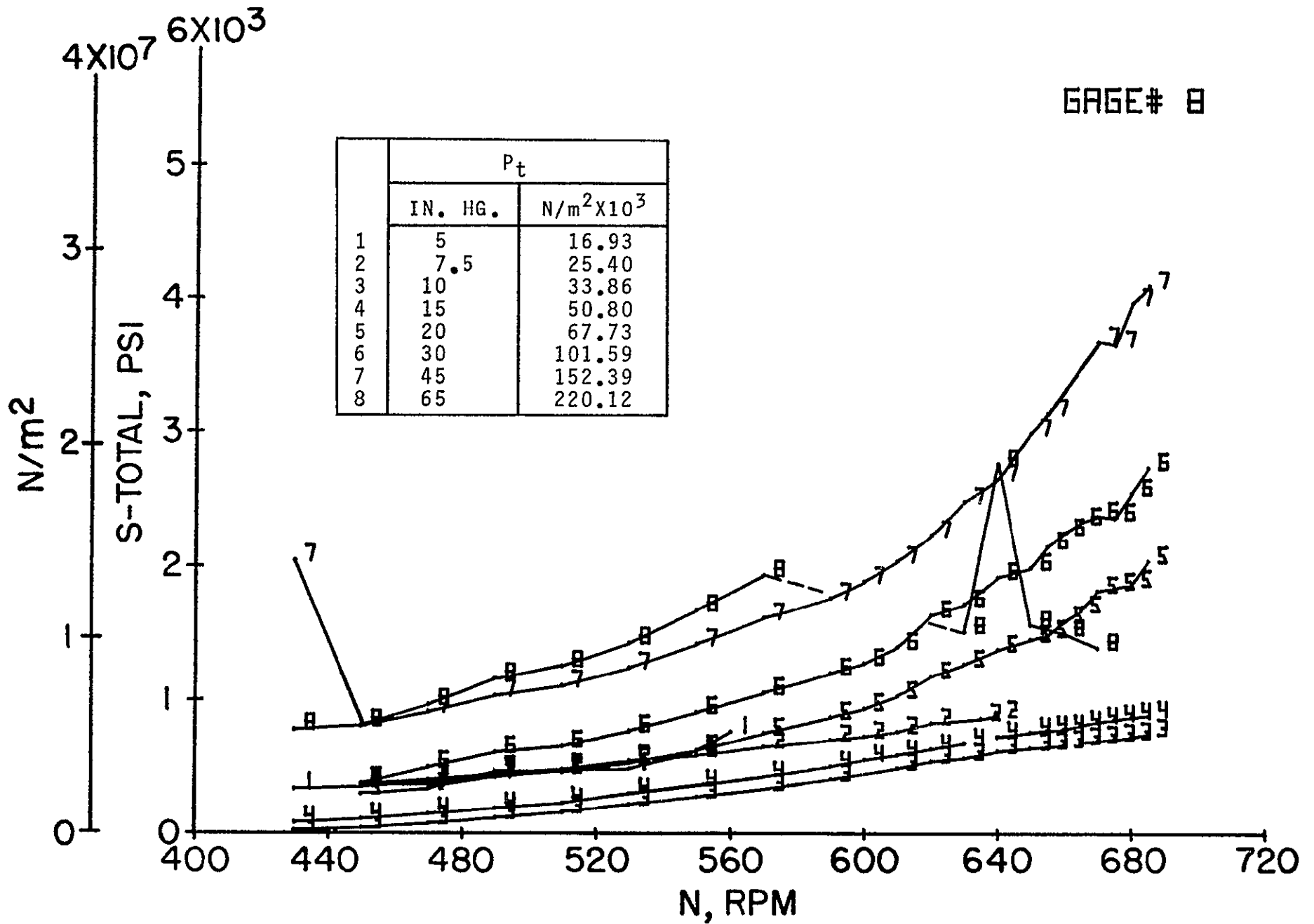
Figure 5.- Continued.

(j) Total stress; gage 8; 3rd stage.
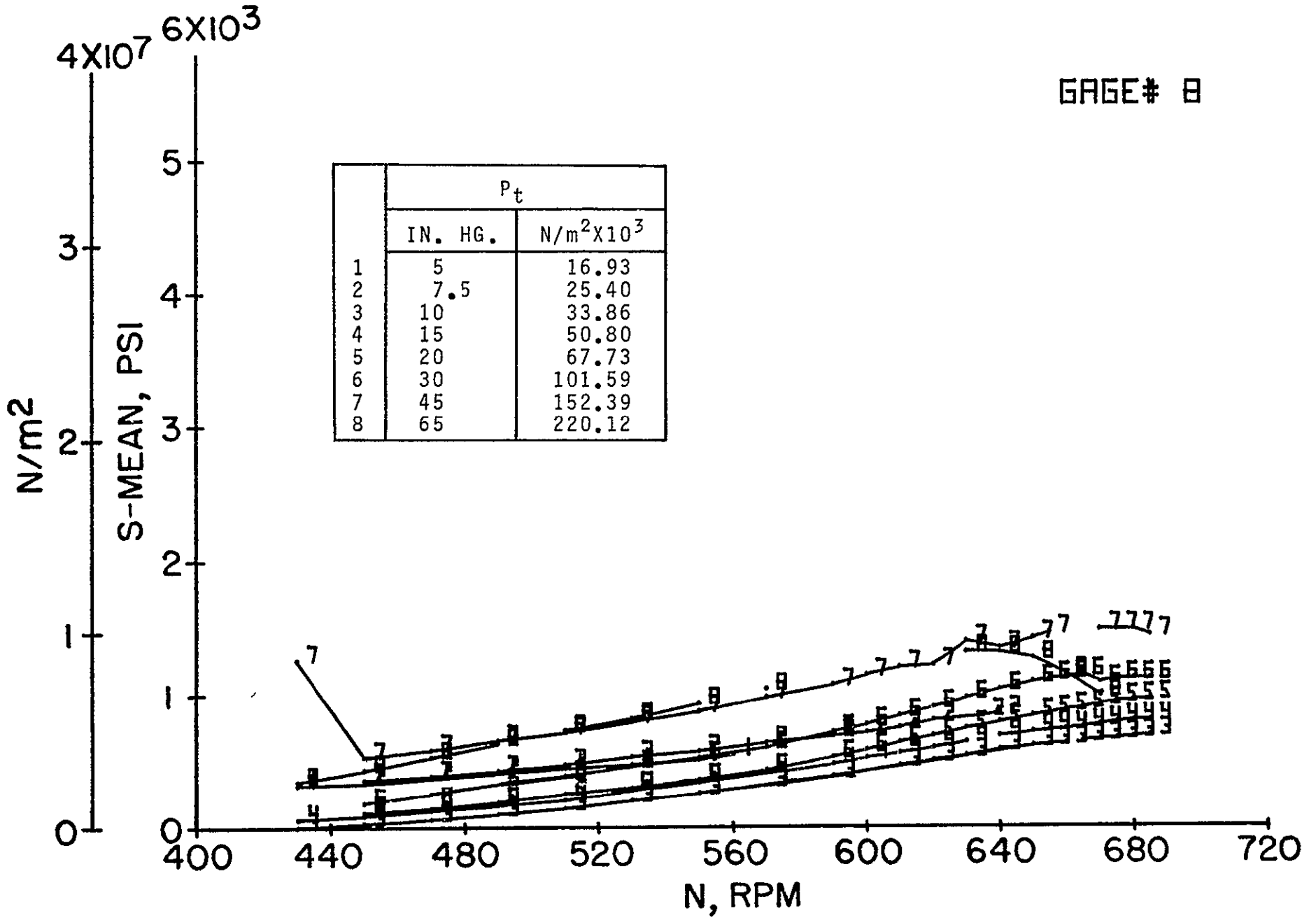
Figure 5.- Continued.

(k) Static stress; gage 8; 3rd stage.
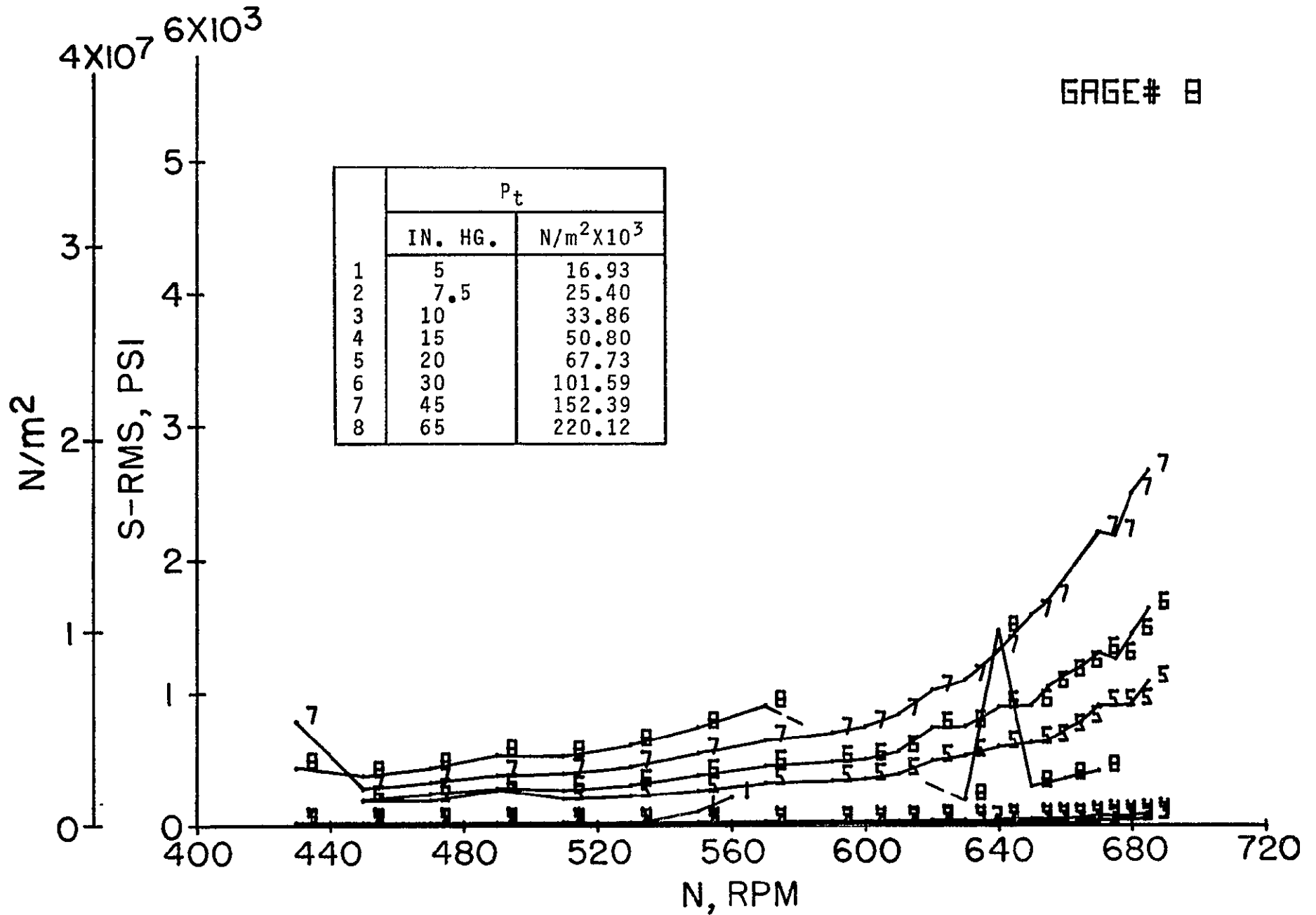
Figure 5.- Continued.

(1) Dynamic stress; gage 8; 3rd stage.

Figure 5.- Continued.

(m) Total stress; gage 11; 3rd stage.

Figure 5.- Continued.

(n) Static stress; gage 11; 3rd stage.

Figure 5.- Continued.

(o) Dynamic stress; gage 11; 3rd stage.

Figure 5.- Continued.

	P_t	
	IN. HG.	$N/m^2 X10^3$
1	5	16.93
2	7.5	25.40
3	10	33.86
4	15	50.80
5	20	67.73
6	30	101.59
7	45	152.39
8	65	220.12

(p) Total stress; gage 12; 3rd stage.

Figure 5.- Continued.

GAGE# 12

	P_t	
	IN. HG.	$N/m^2 X 10^3$
1	5	16.93
2	7.5	25.40
3	10	33.86
4	15	50.80
5	20	67.73
6	30	101.59
7	45	152.39
8	65	220.12

(q) Static stress; gage 12; 3rd stage.

Figure 5.- Continued.

(r) Dynamic stress; gage 12; 3rd stage.

Figure 5.- Continued.

(s) Total stress; gage 13; 2nd stage.

Figure 5.- Continued.

(t) Static stress; gage 13; 2nd stage.

Figure 5.- Continued.

(u) Dynamic stress; gage 13; 2nd stage.

Figure 5.- Continued.

(v) Total stress; gage 14; 2nd stage.

Figure 5.- Continued.

(w) Static stress; gage 14; 2nd stage.

Figure 5.- Continued.

GAGE# 14

	P_t	
	IN. HG.	$N/m^2 X10^3$
1	5	16.93
2	7.5	25.40
3	10	33.86
4	15	50.80
5	20	67.73
6	30	101.59
7	45	152.39
8	65	220.12
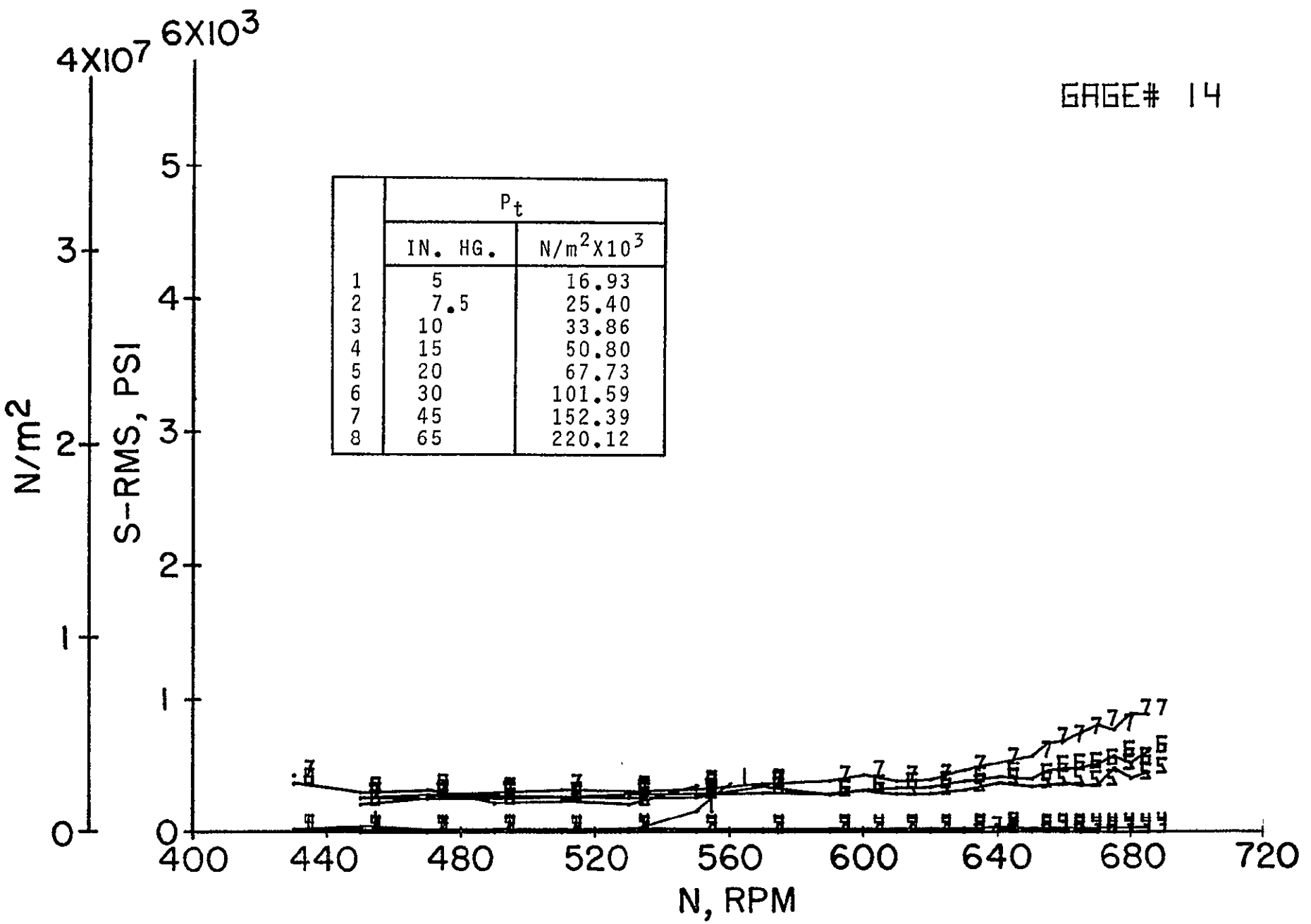
(x) Dynamic stress; gage 14; 2nd stage.

Figure 5.- Continued.

(y) Total stress; gage 15; 2nd stage.

Figure 5.- Continued.

(z) Static stress; gage 15; 2nd stage.

Figure 5.- Continued.

(aa) Dynamic stress; gage 15; 2nd stage.

Figure 5.- Continued.

GAGE# 16

	P_t	
	IN. HG.	$N/m^2 X 10^3$
1	5	16.93
2	7.5	25.40
3	10	33.86
4	15	50.80
5	20	67.73
6	30	101.59
7	45	152.39
8	65	220.12

(bb) Total stress; gage 16; dummy.

Figure 5.- Continued.

(cc) Static stress; gage 16; dummy.

Figure 5.- Continued.

GAGE# 16

	P_t	
	IN. HG.	$N/m^2 \times 10^3$
1	5	16.93
2	7.5	25.40
3	10	33.86
4	15	50.80
5	20	67.73
6	30	101.59
7	45	152.39
8	65	220.12
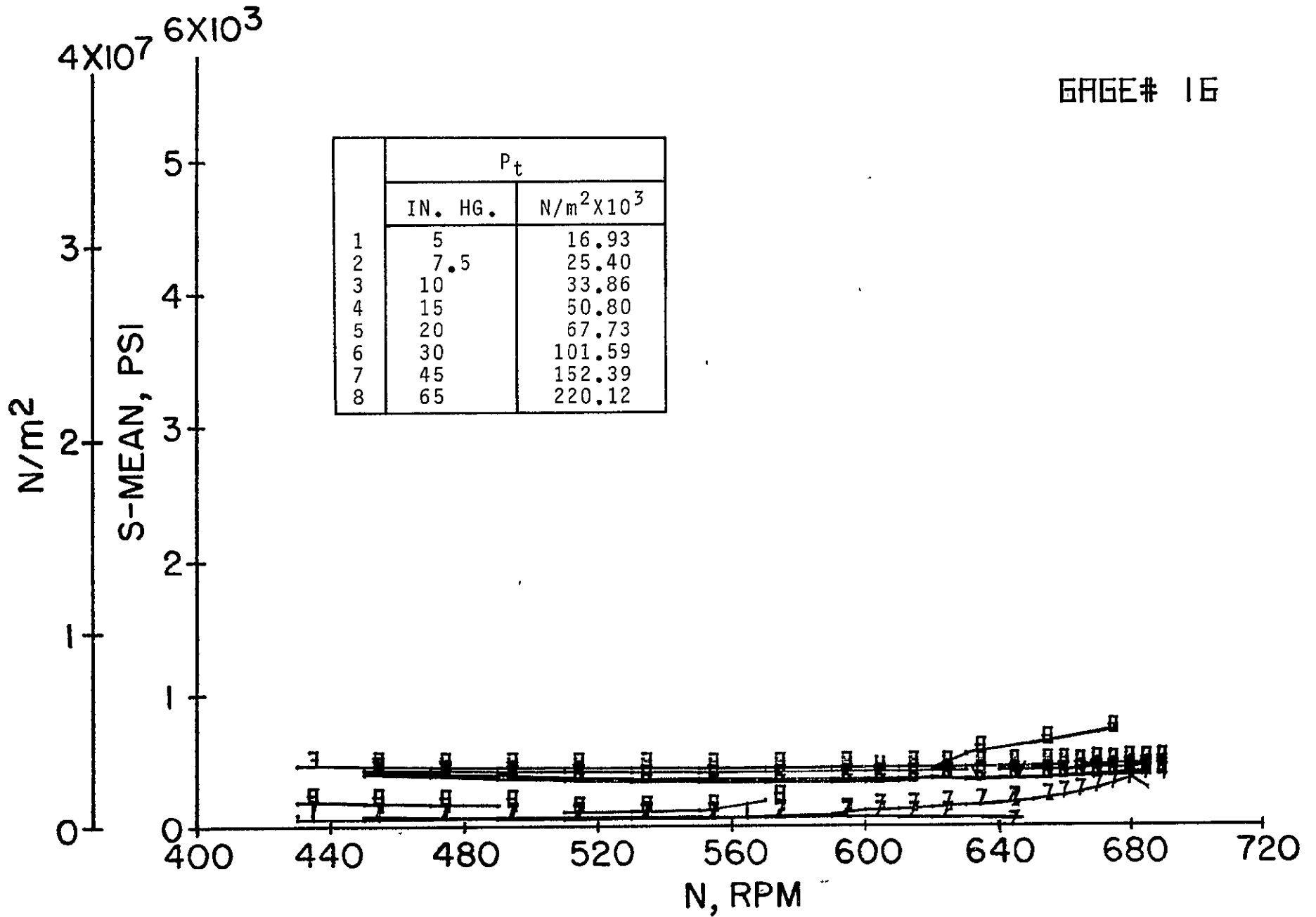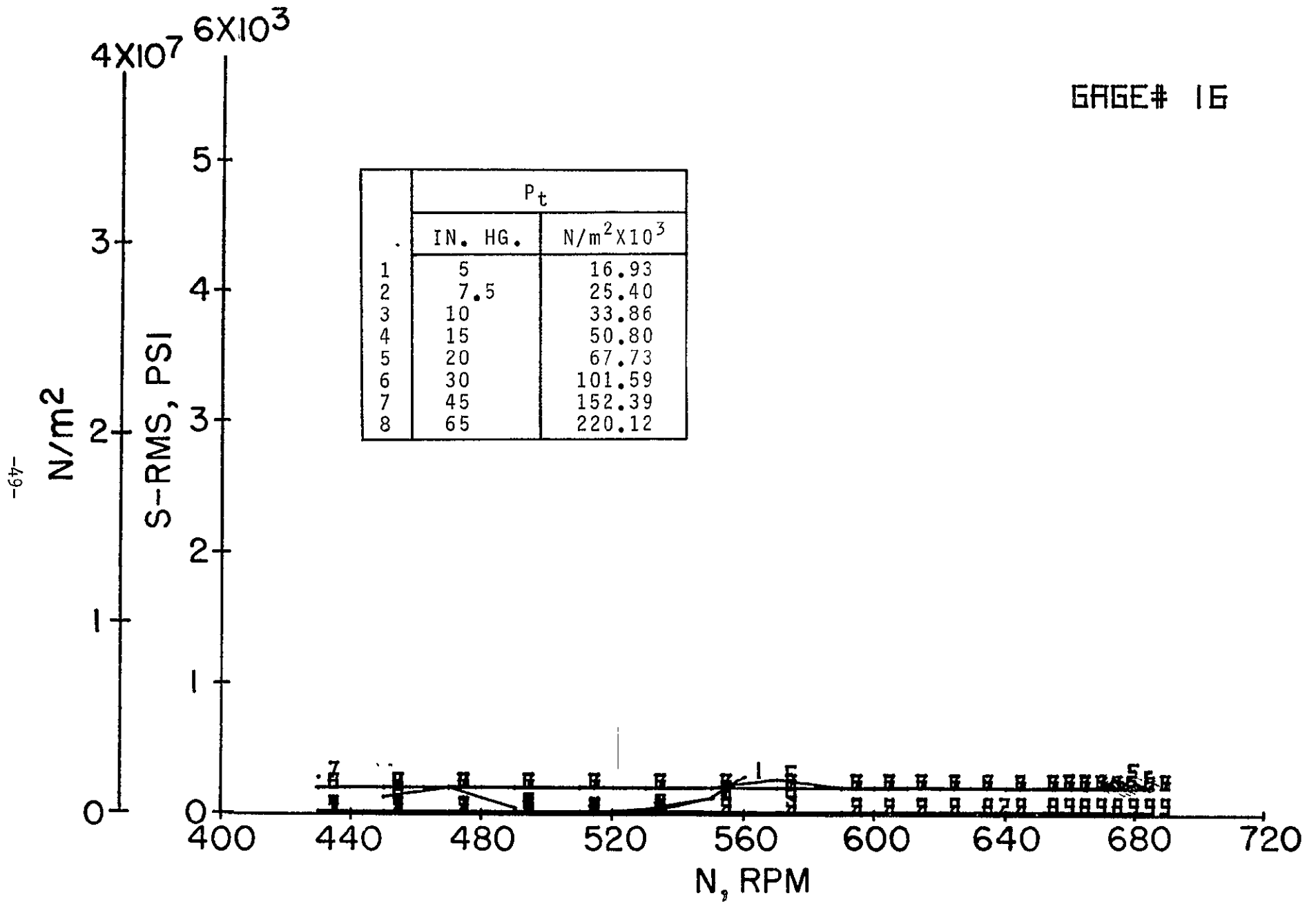
(dd) Dynamic stress; gage 16; dummy.

Figure 5.- Concluded.
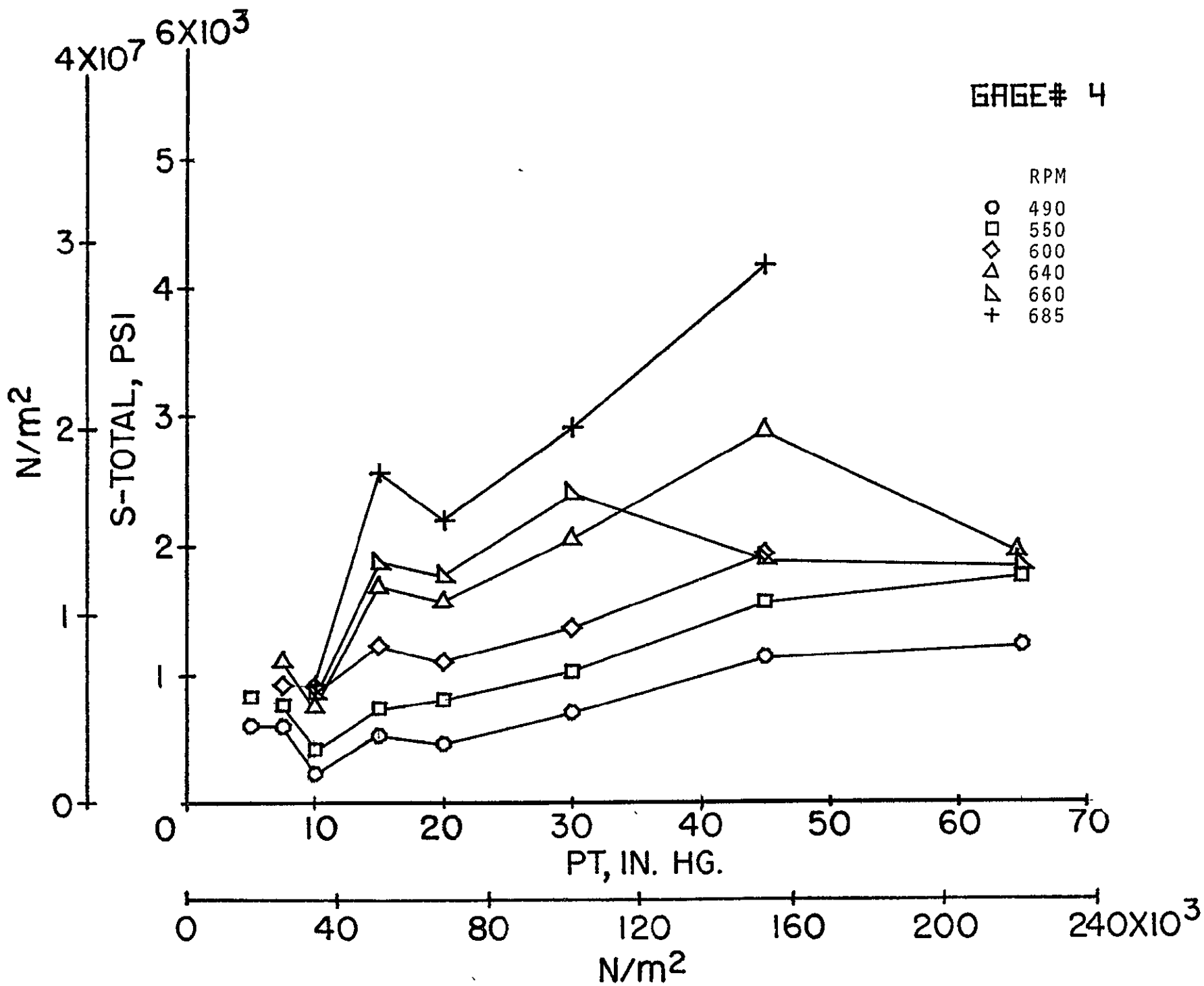
(a) Total stress; gage 4; 3rd stage.

Figure 6.- Effect of compressor speed on the blade stresses as a function of tunnel total pressure.
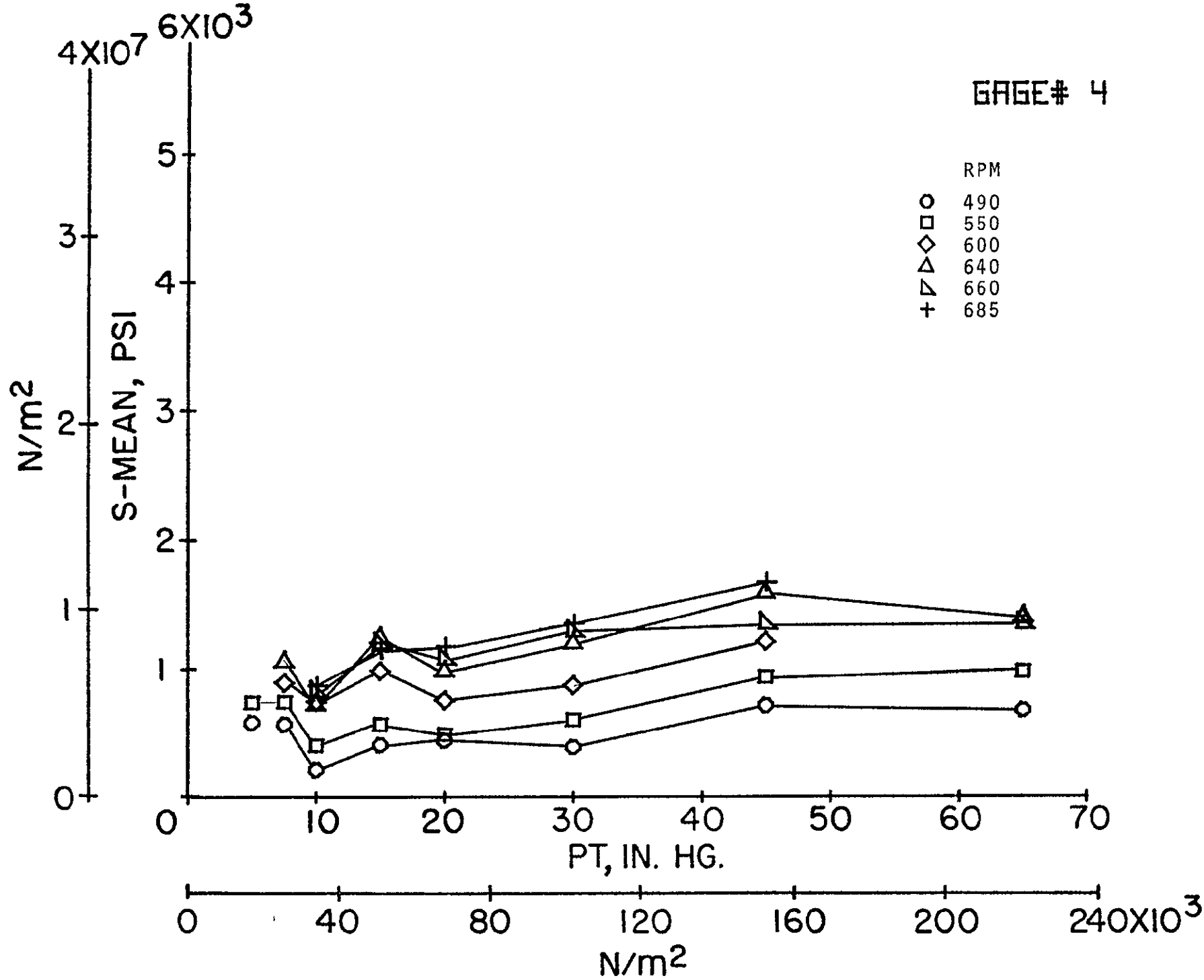
(b) Static stress; gage 4; 3rd stage.
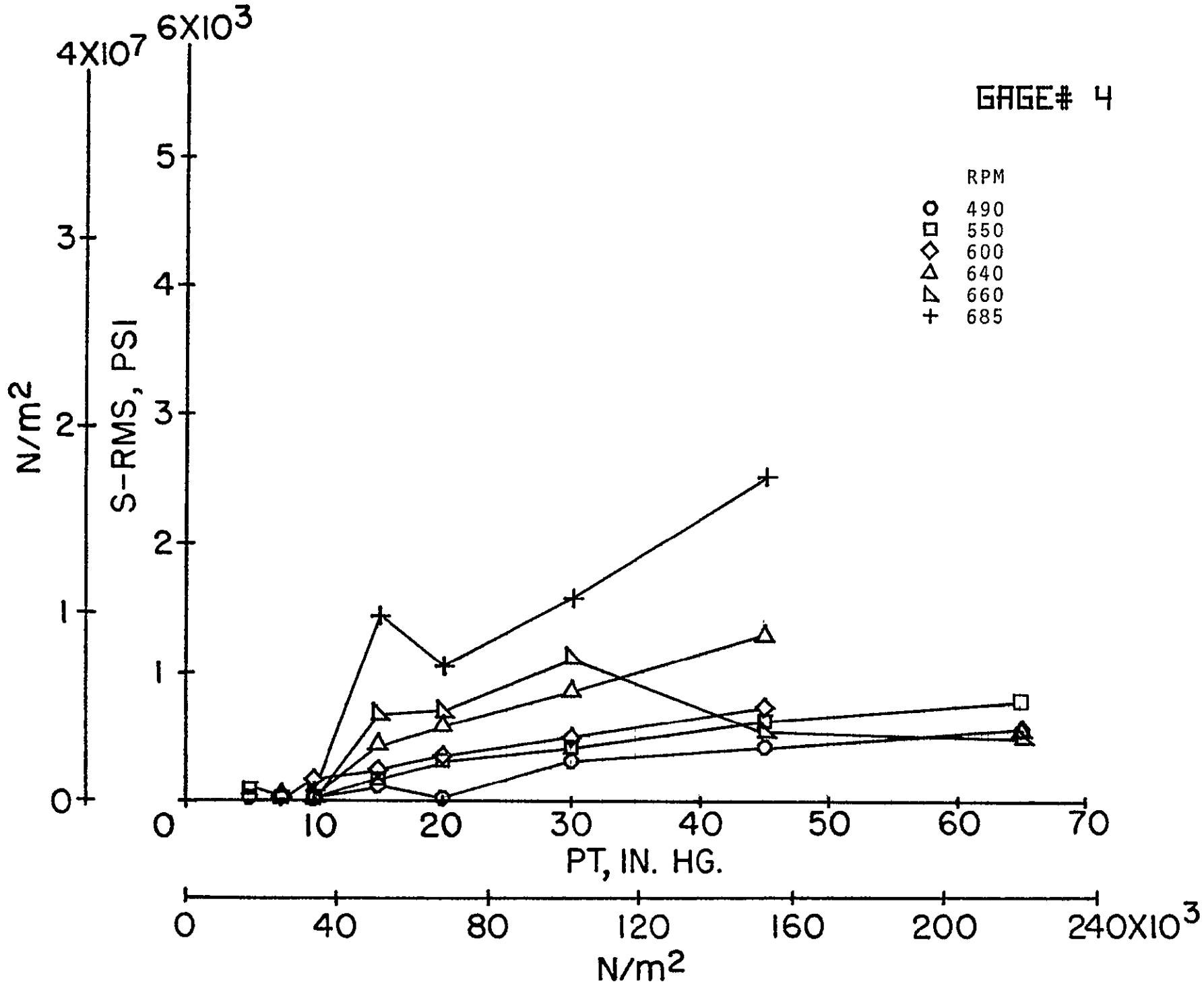
Figure 6.- Continued.

(c) Dynamic stress; gage 4; 3rd stage.
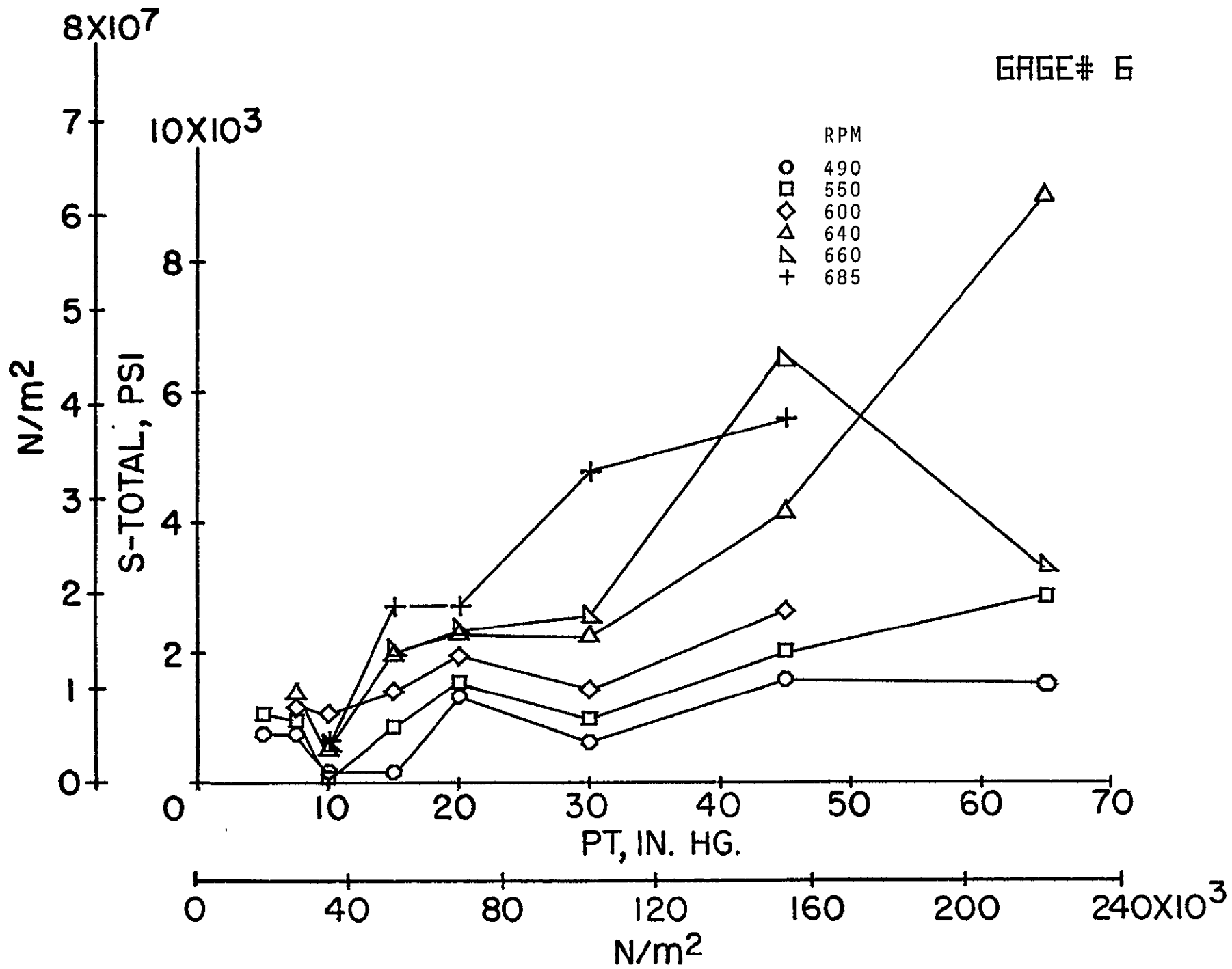
Figure 6.- Continued.

(d) Total stress; gage 6; 3rd stage.
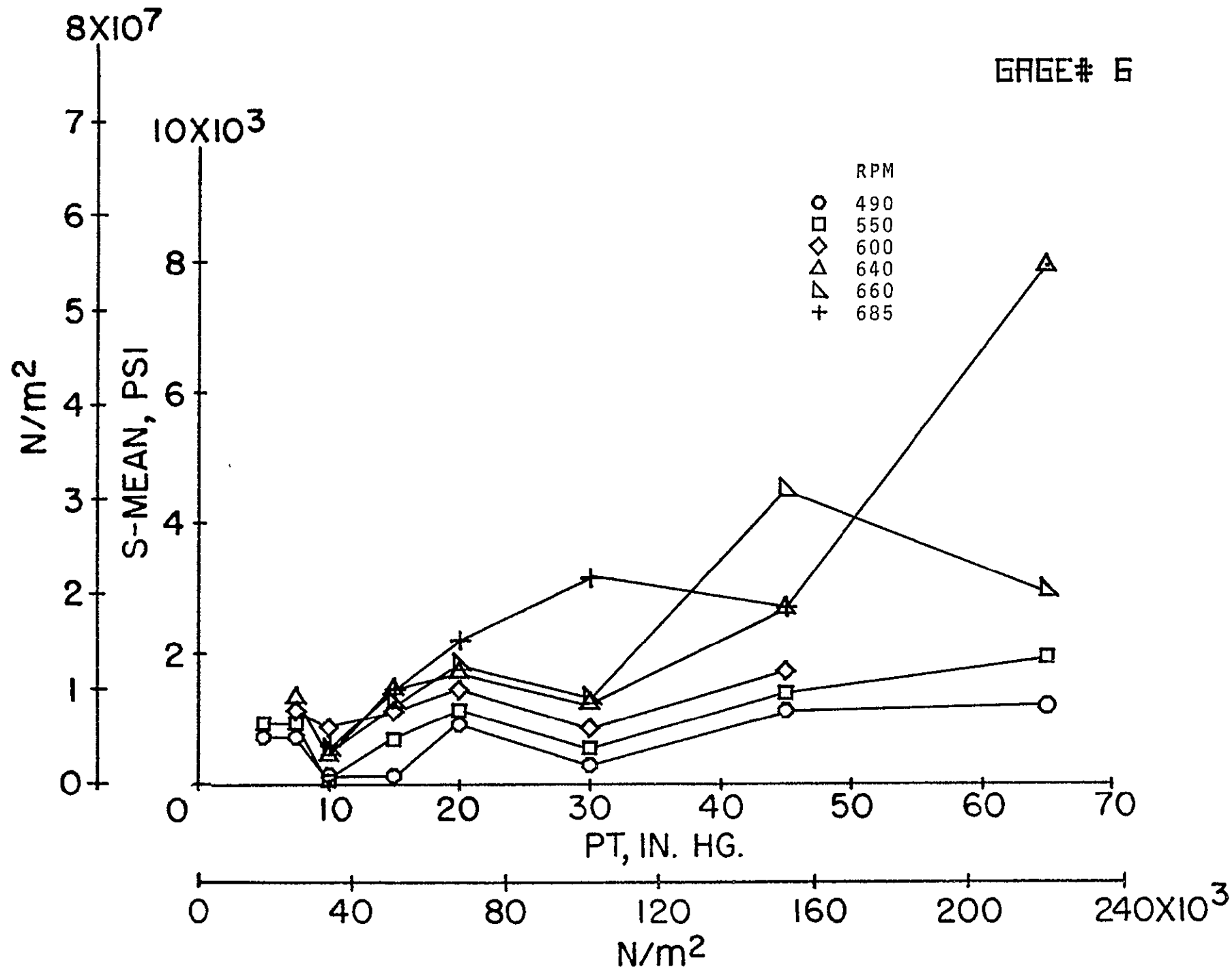
Figure 6.- Continued.

(e) Static stress; gage 6; 3rd stage.
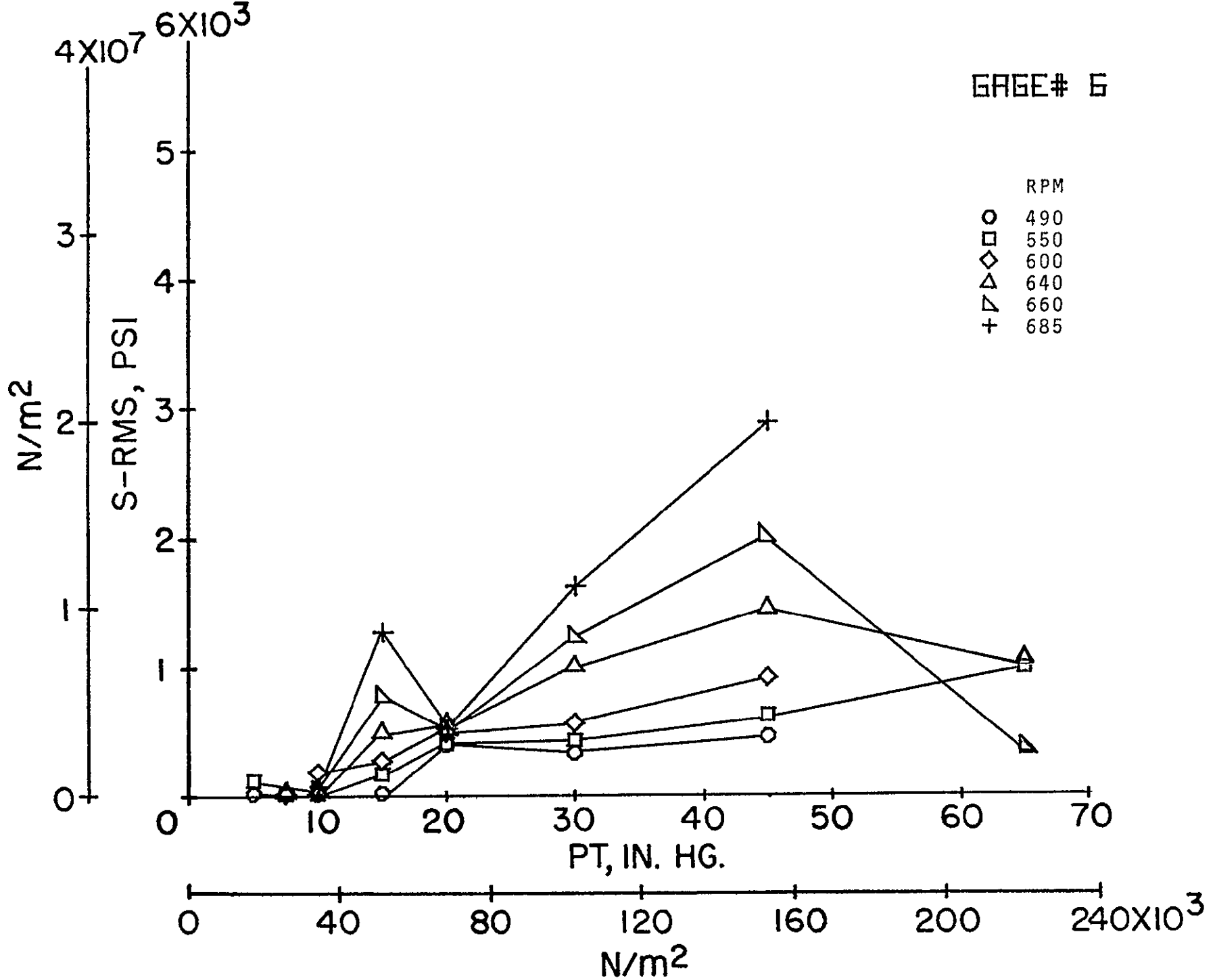
Figure 6.- Continued.

(f) Dynamic stress; gage 6; 3rd stage.
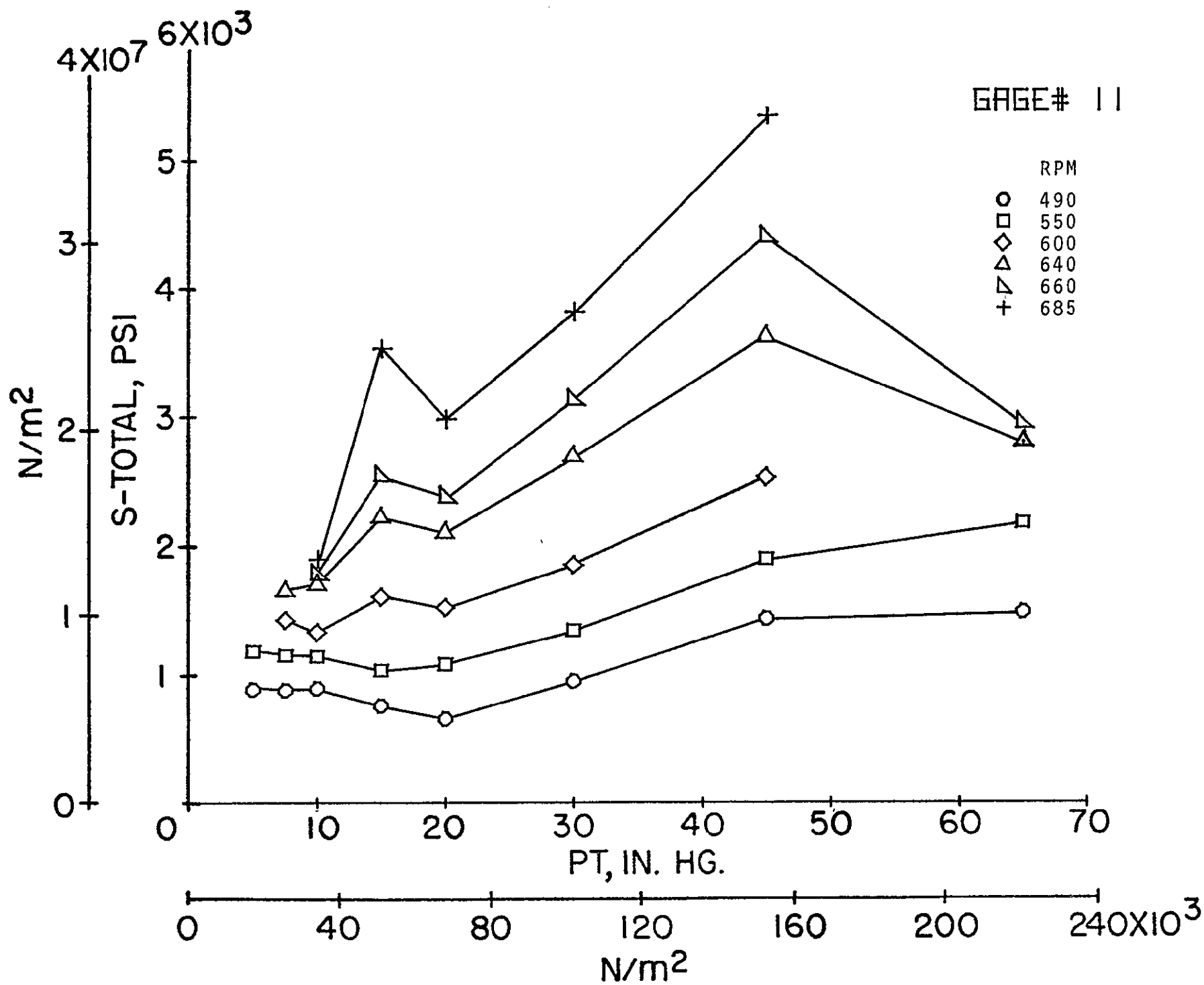
Figure 6.- Continued.

(g) Total stress; gage 11; 3rd stage.
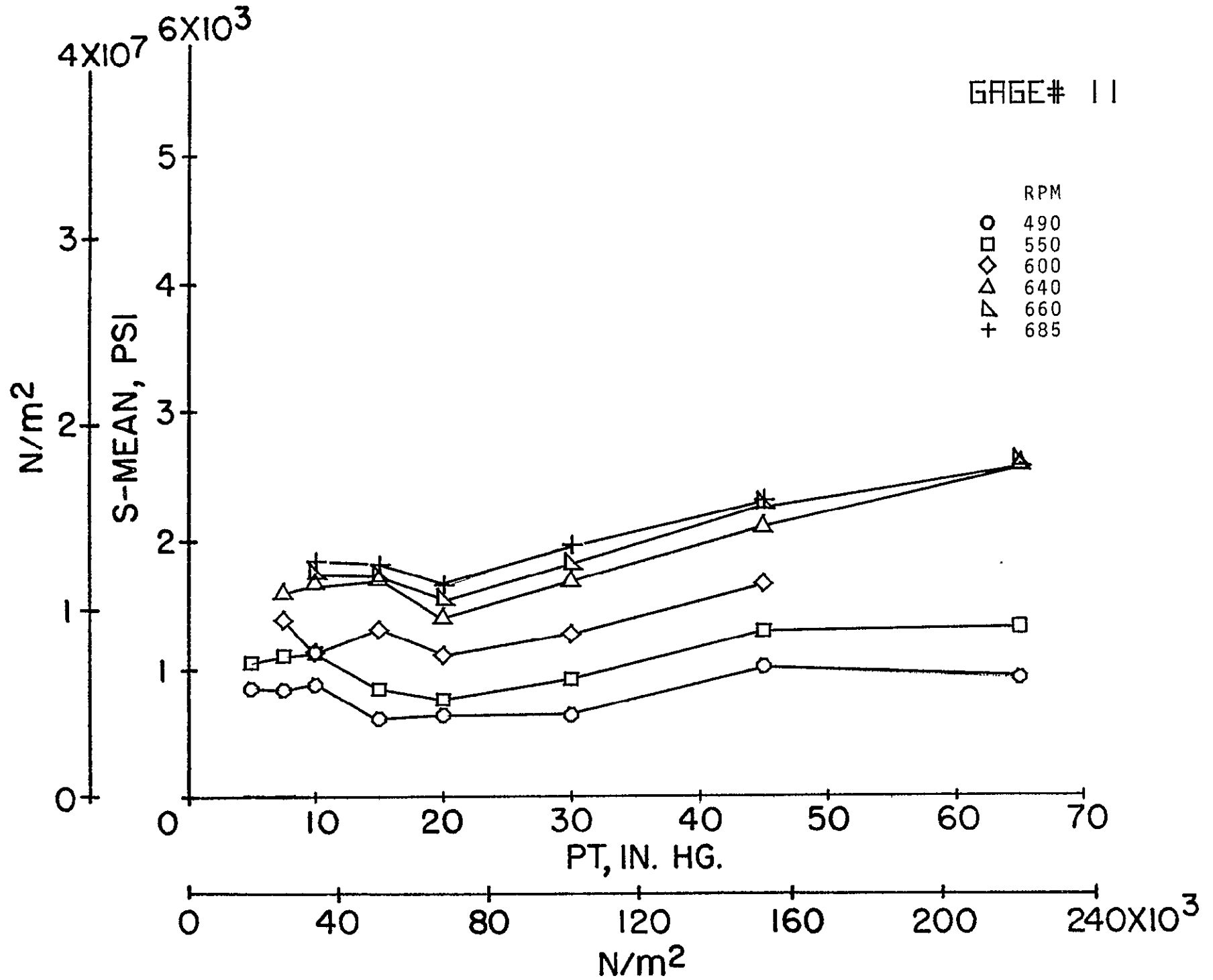
Figure 6.- Continued.

(h) Static stress; gage 11; 3rd stage.
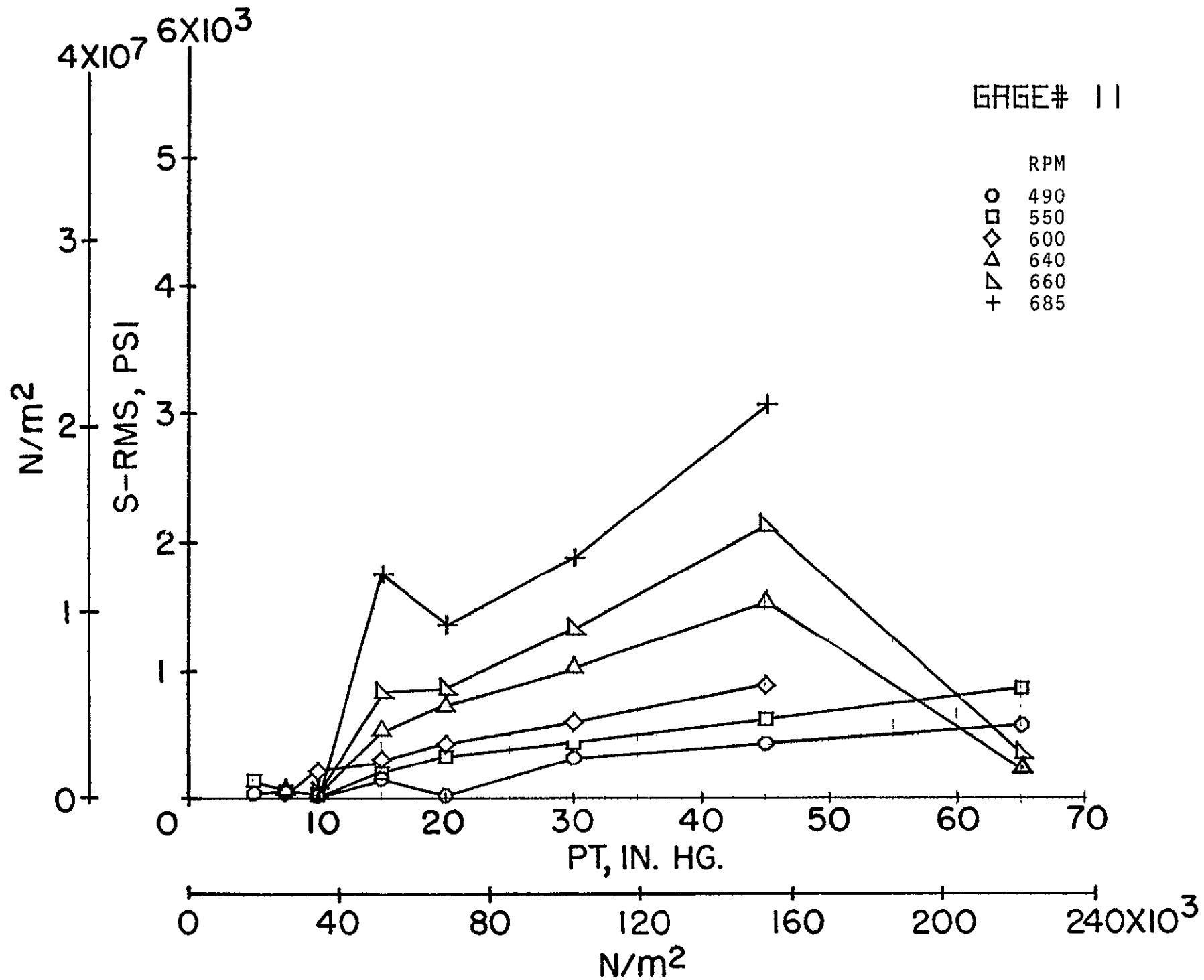
Figure 6.- Continued.

(i) Dynamic stress; gage 11; 3rd stage.
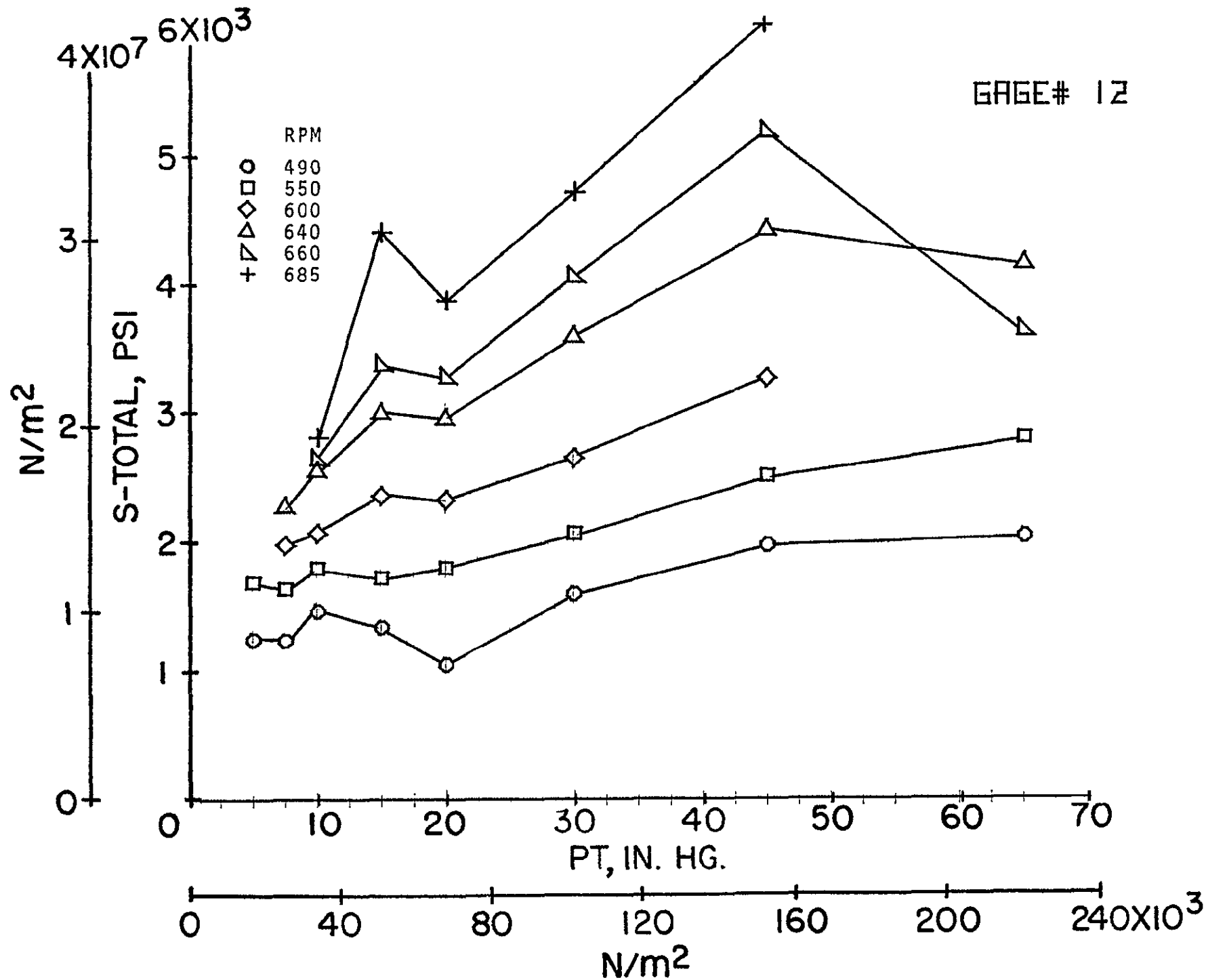
Figure 6.- Continued.

(j) Total stress; gage 12; 3rd stage.

Figure 6.- Continued.
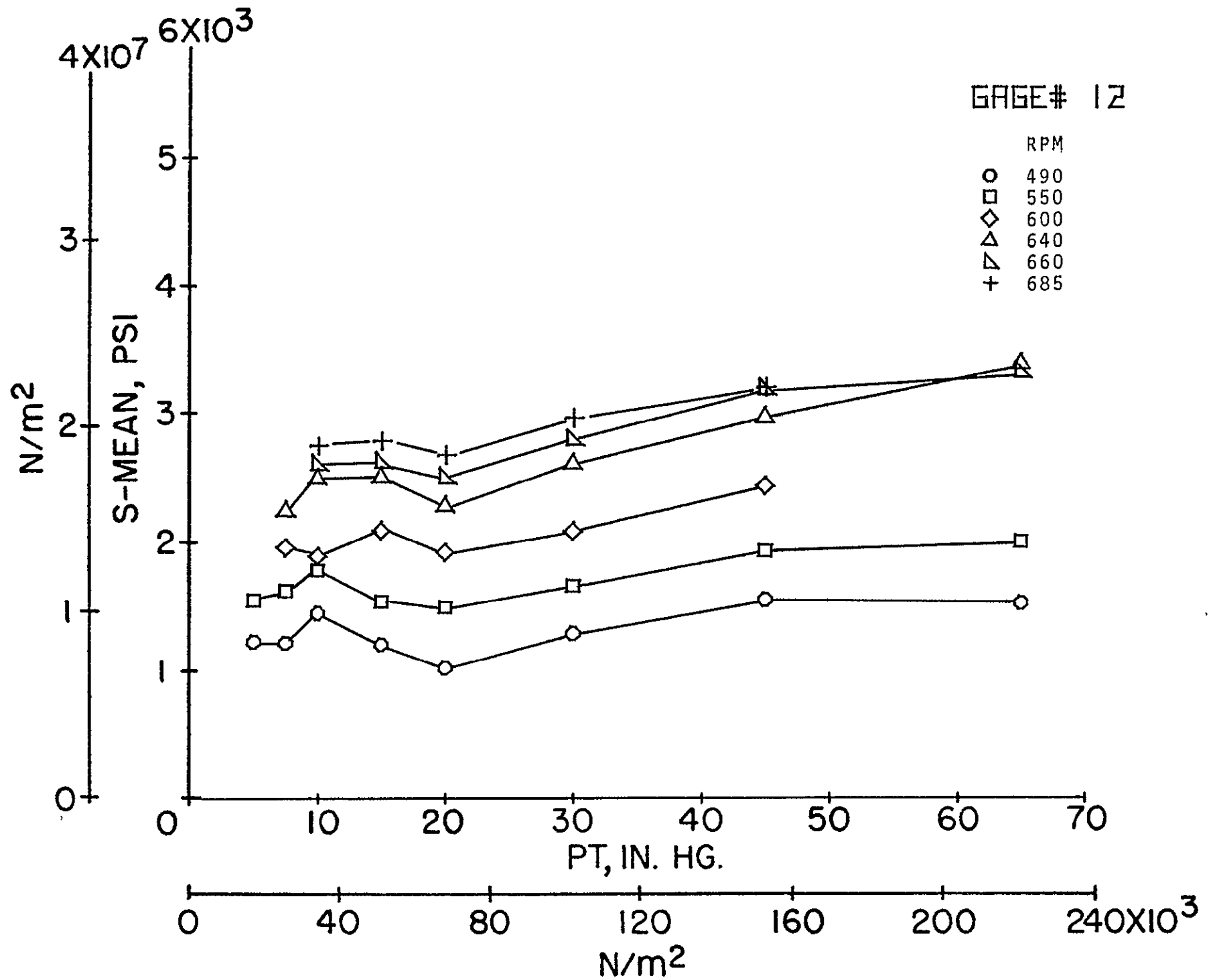
(k) Static stress; gage 12; 3rd stage.
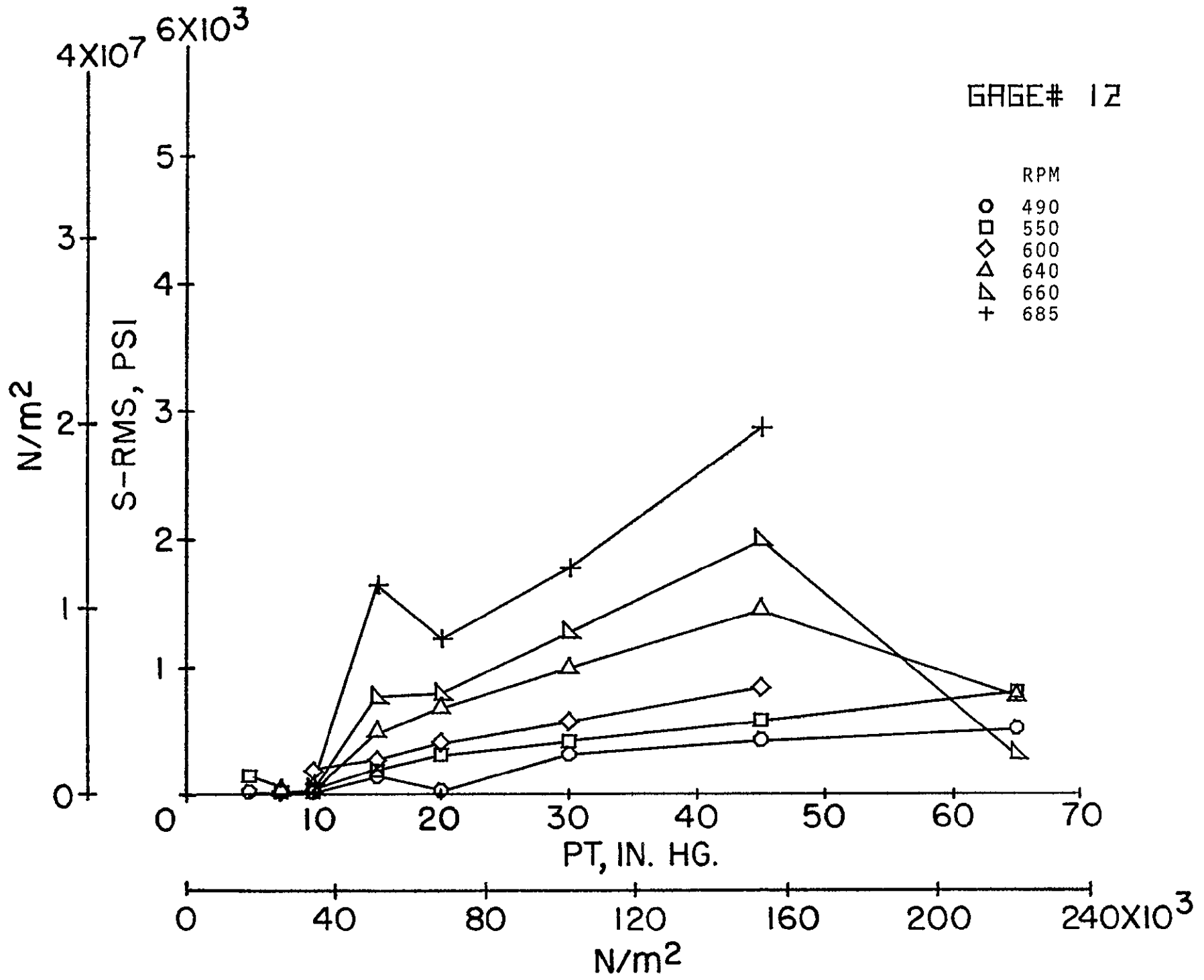
Figure 6.- Continued.

(1) Dynamic stress; gage 12; 3rd stage.
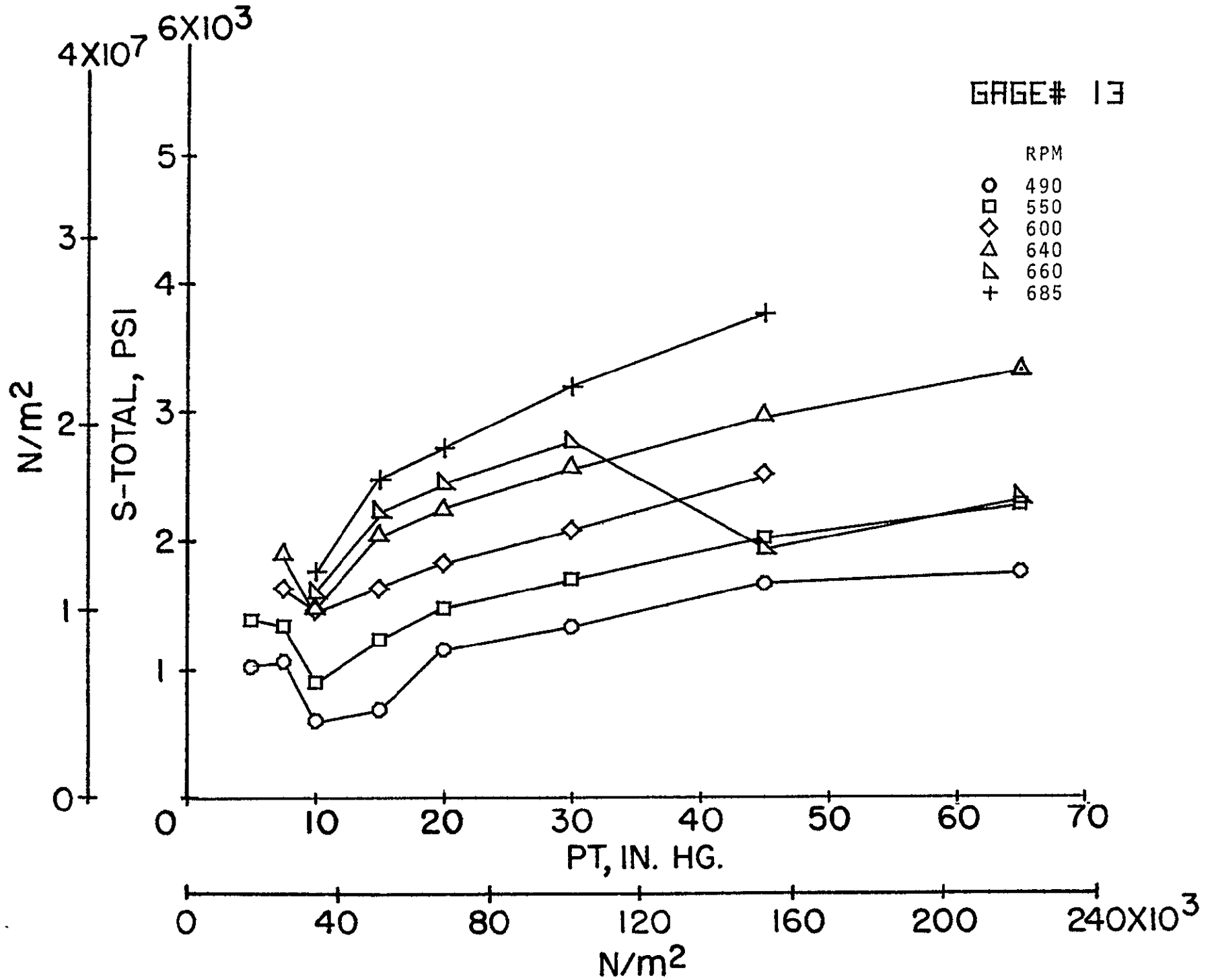
Figure 6.- Continued.

(m) Total stress; gage 13; 2nd stage.
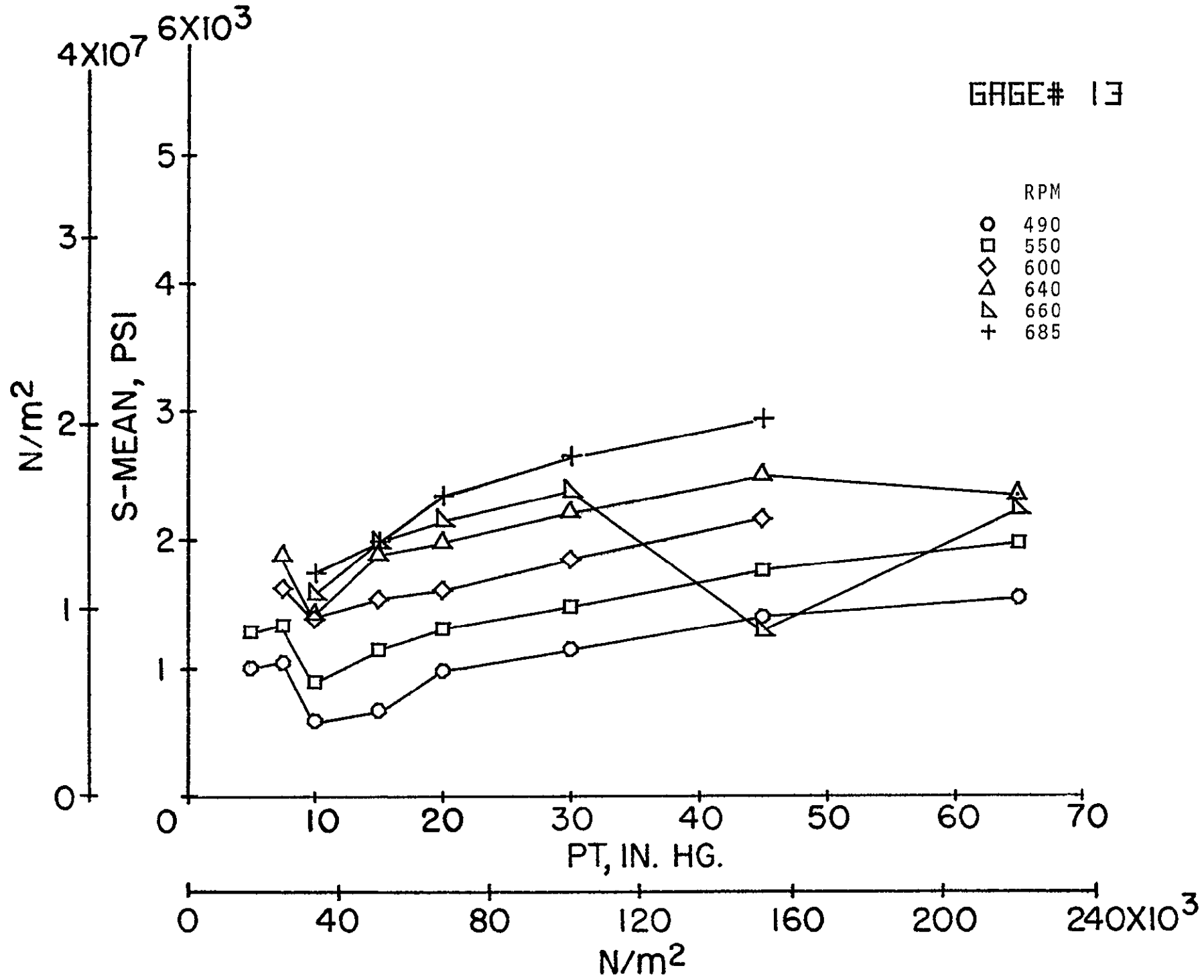
Figure 6.- Continued.

(n) Static stress; gage 13; 2nd stage.
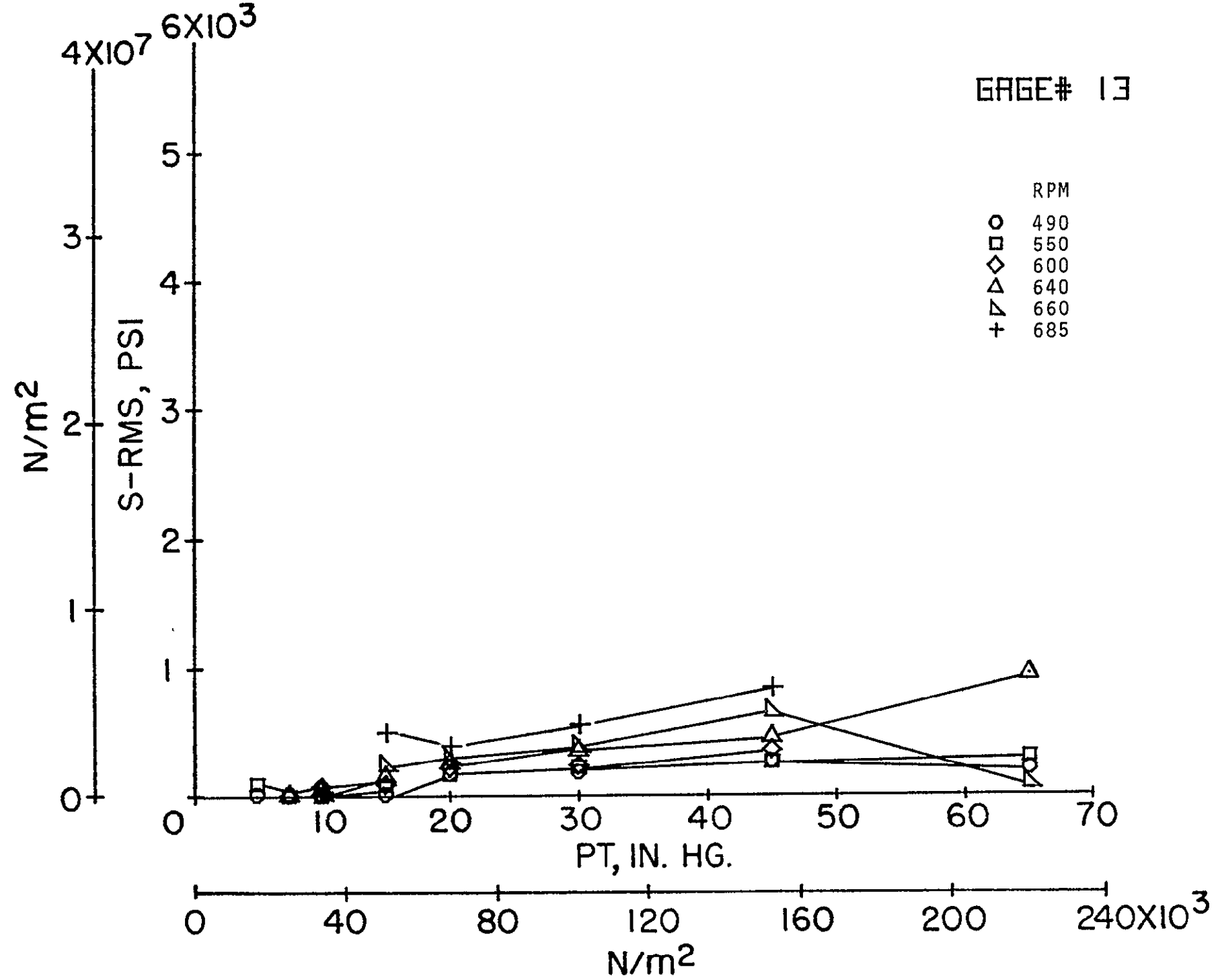
Figure 6.- Continued.

(o) Dynamic stress; gage 13; 2nd stage.
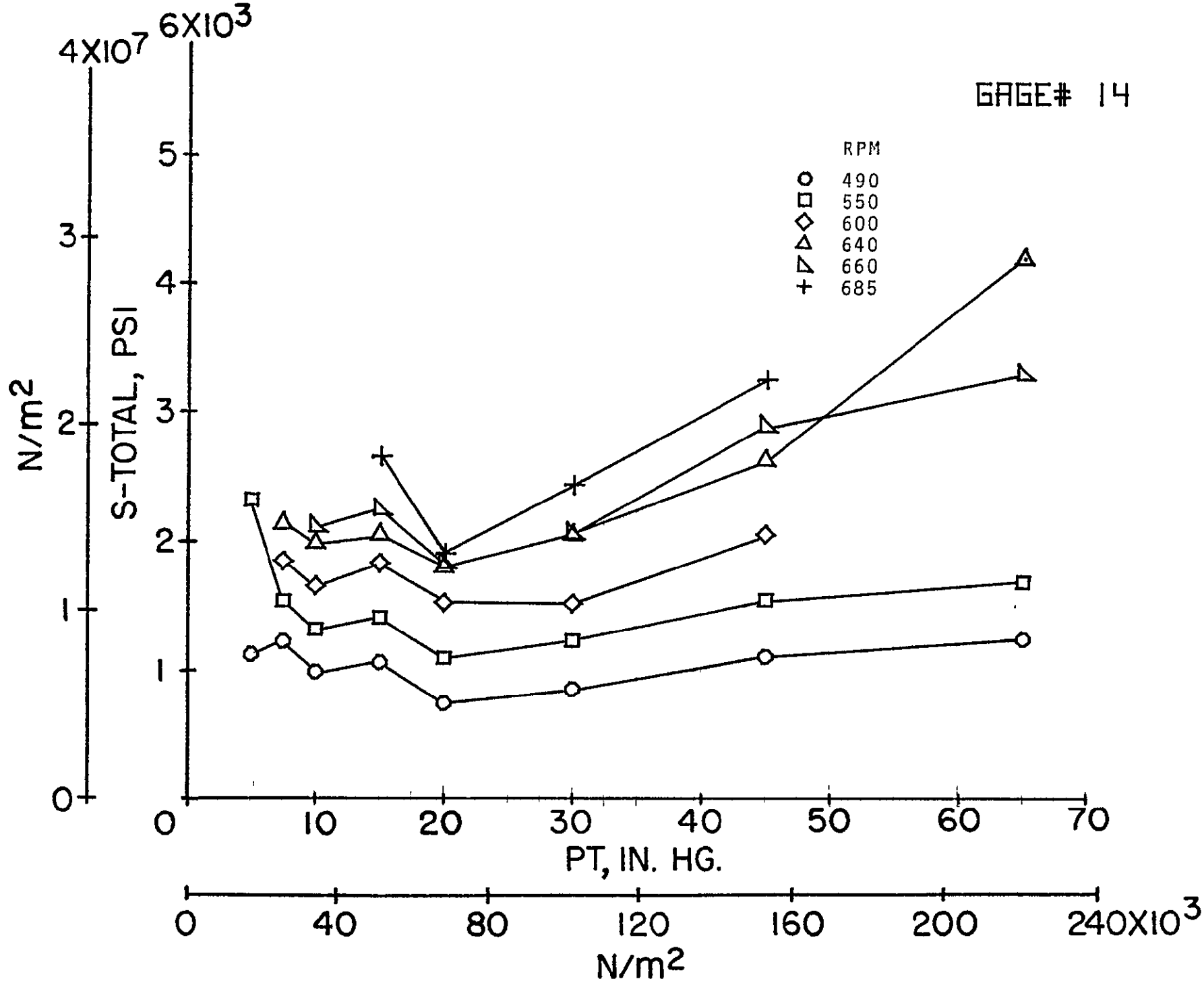
Figure 6.- Continued.

(p) Total stress; gage 14; 2nd stage.
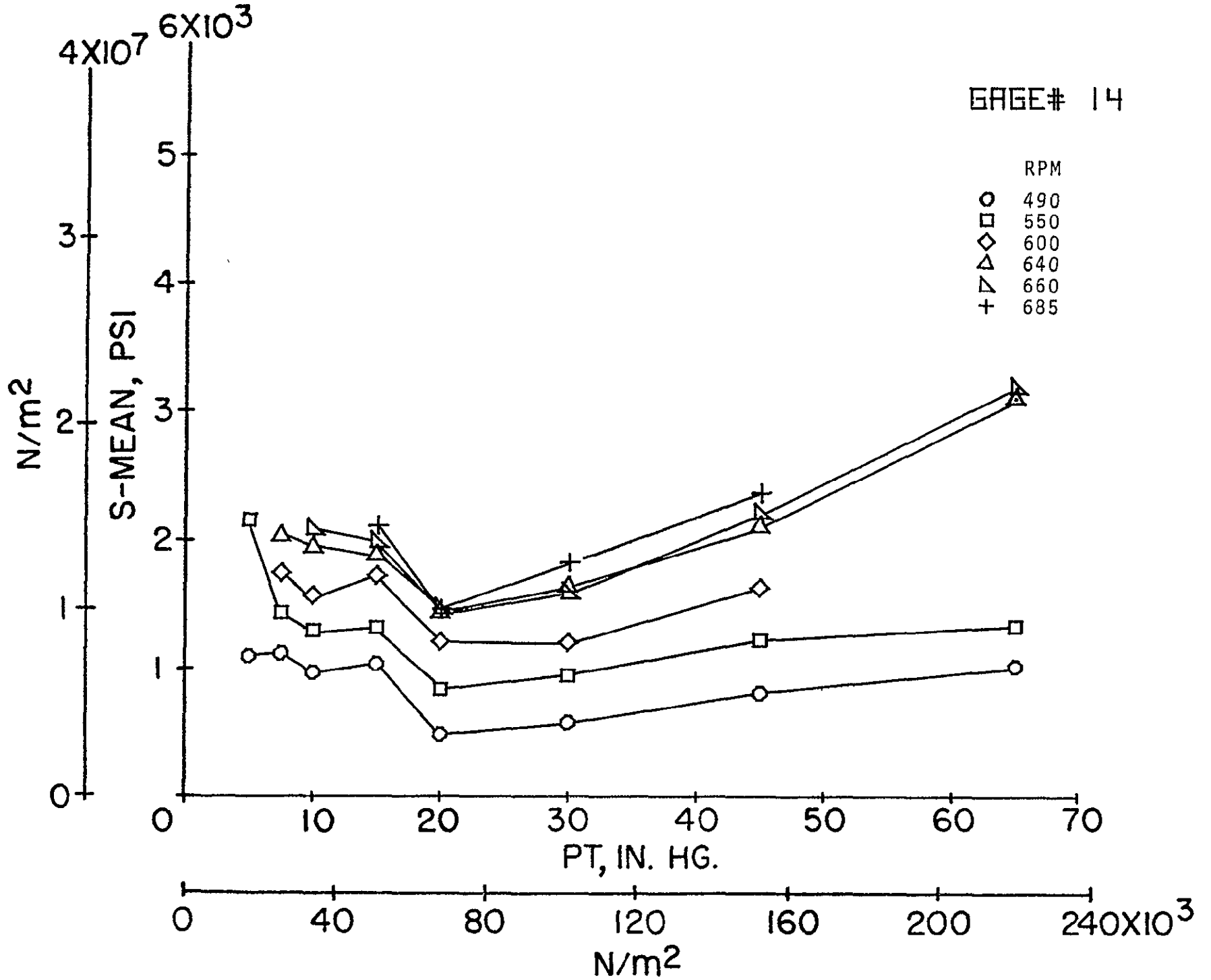
Figure 6.- Continued.

(q) Static stress; gage 14; 2nd stage.
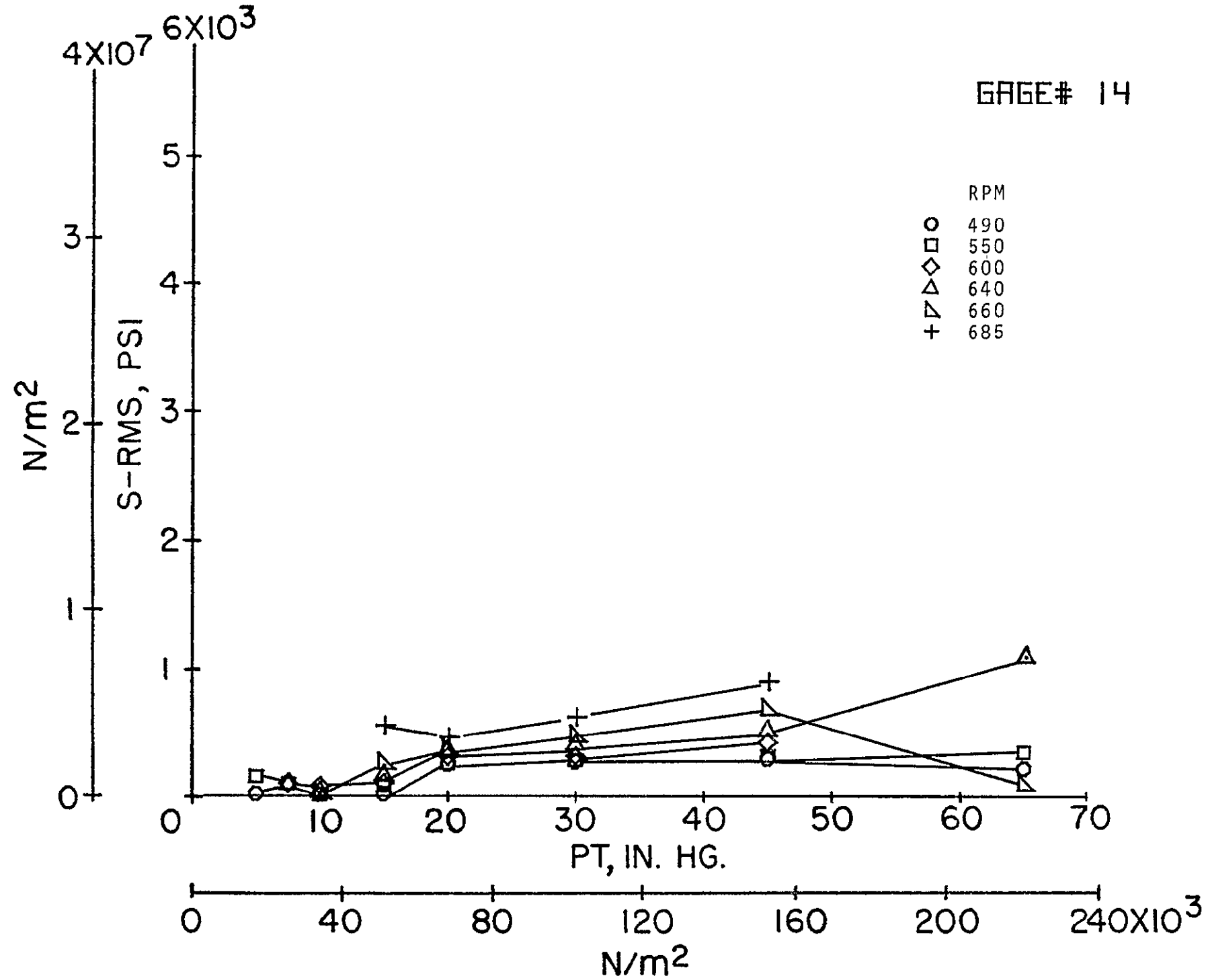
Figure 6.- Continued.

(r) Dynamic stress; gage 14; 2nd stage.
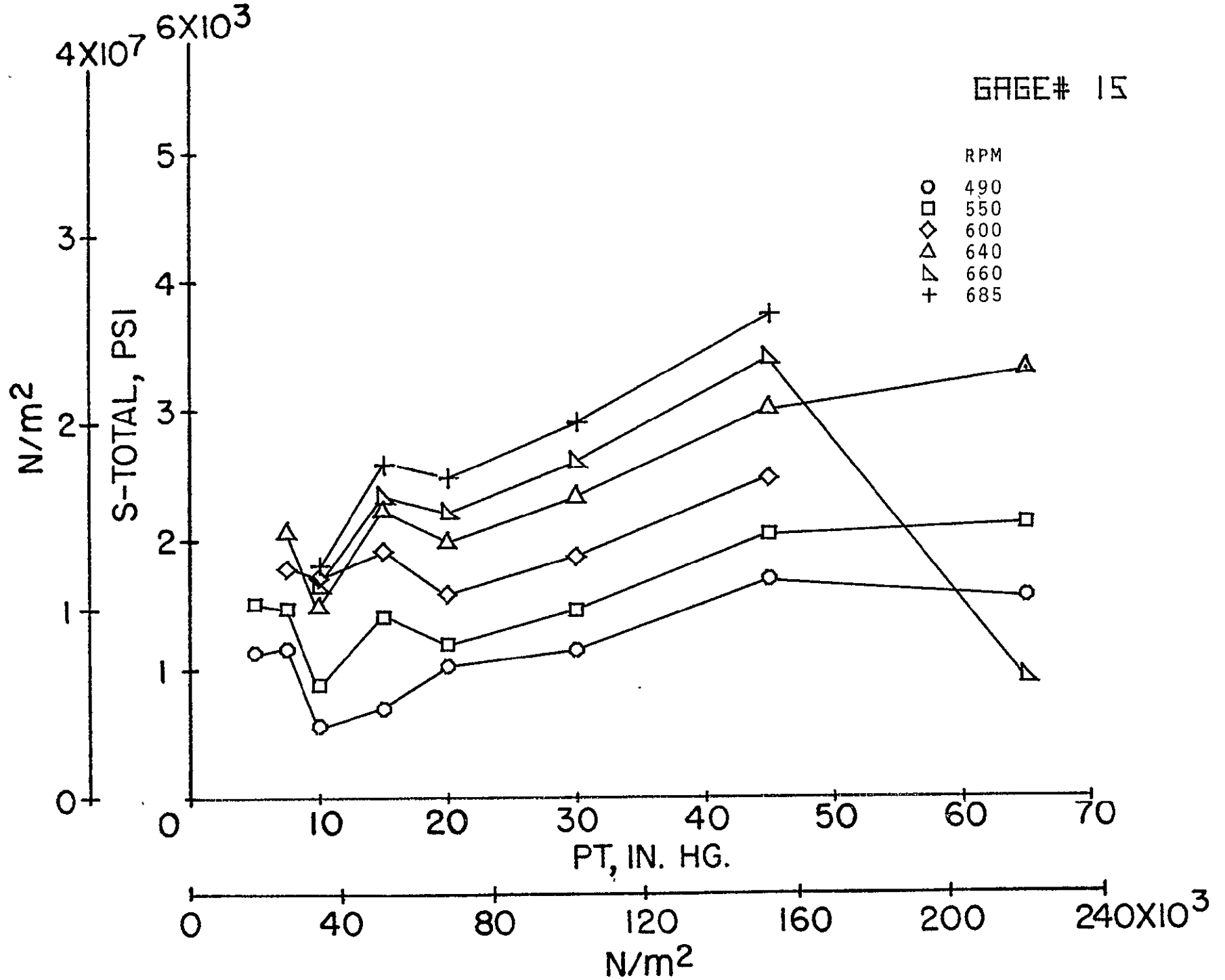
Figure 6.- Continued.

(s) Total stress; gage 15; 2nd stage.
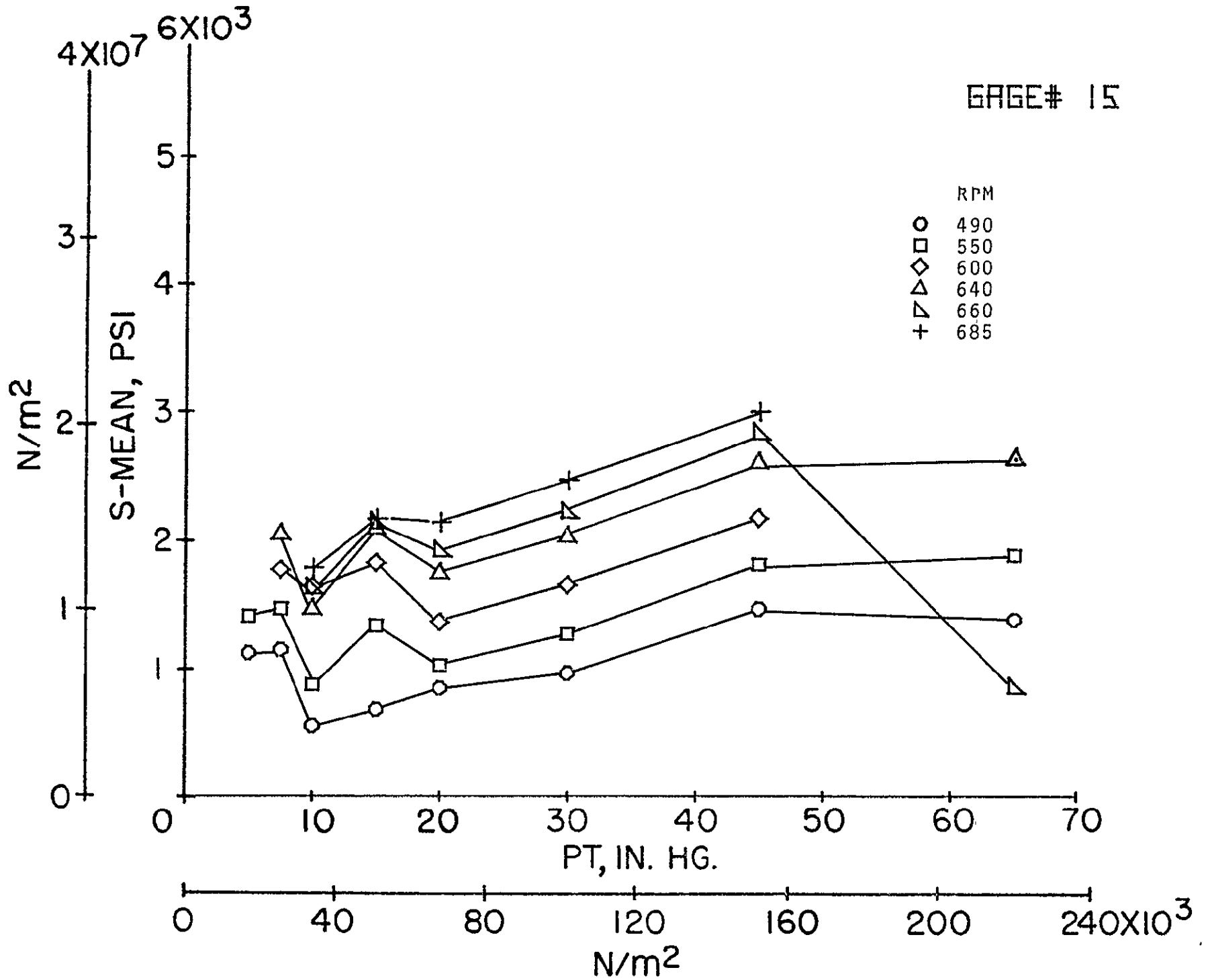
Figure 6.- Continued.

(t) Static stress; gage 15; 2nd stage.

Figure 6.- Continued.
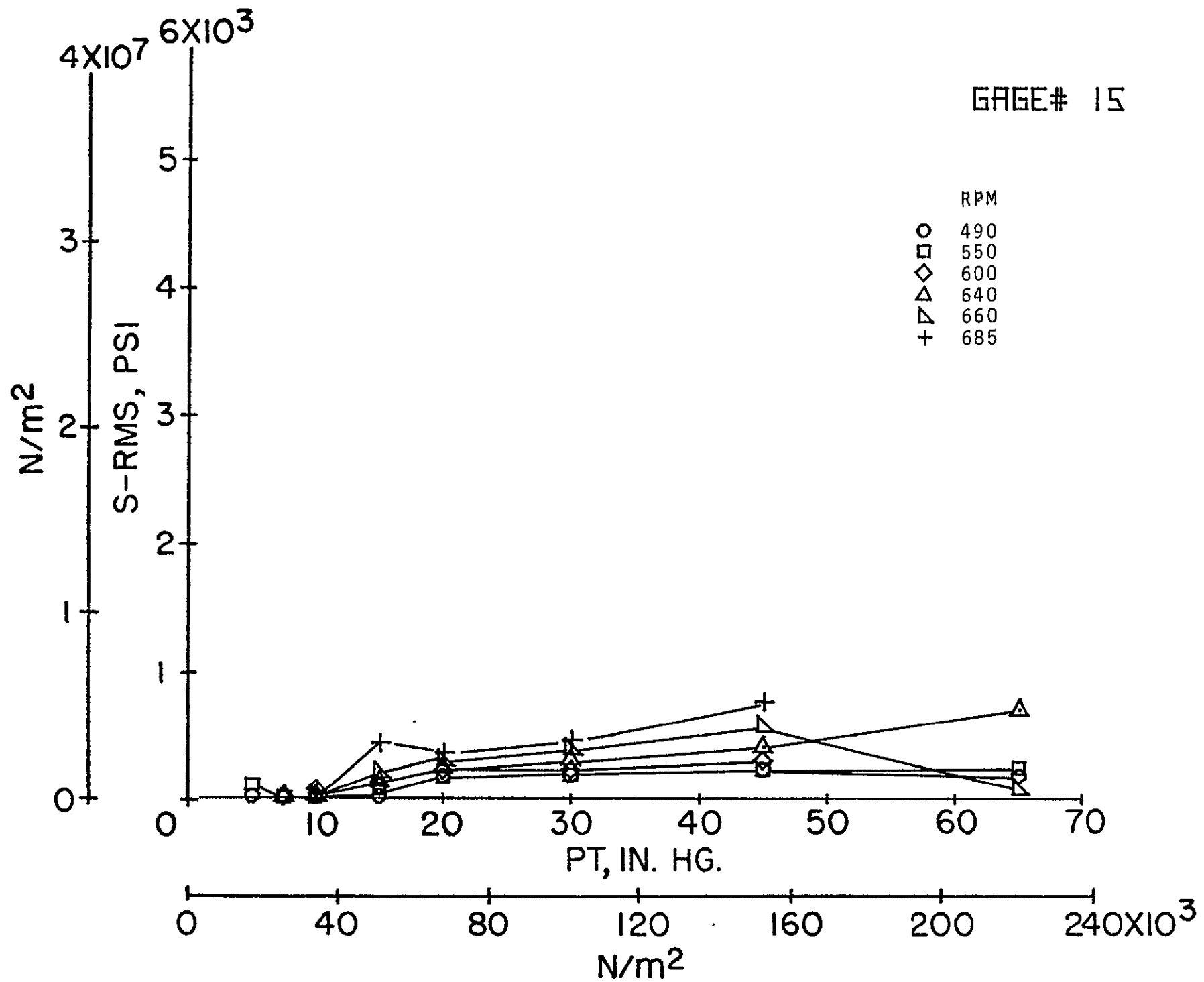
(u) Dynamic stress; gage 15; 2nd stage.

Figure 6.- Concluded.
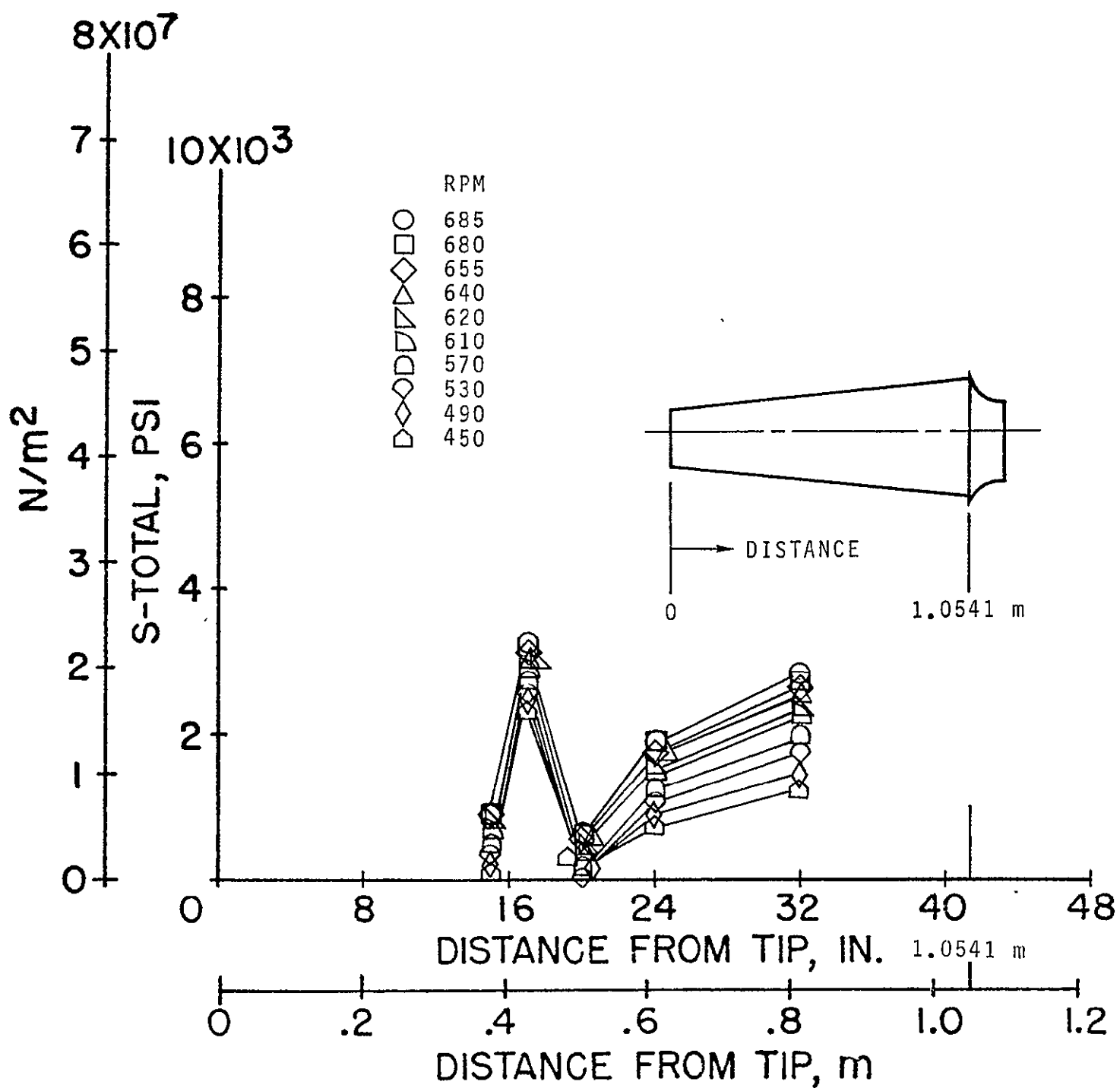
(a) Total stress; $p_t = 33.86 \times 10^3$ N/m^2 (10 in. Hg); 3rd stage.

Figure 7.- Effect of compressor speed on the longitudinal distribution of blade stresses for various tunnel total pressures.
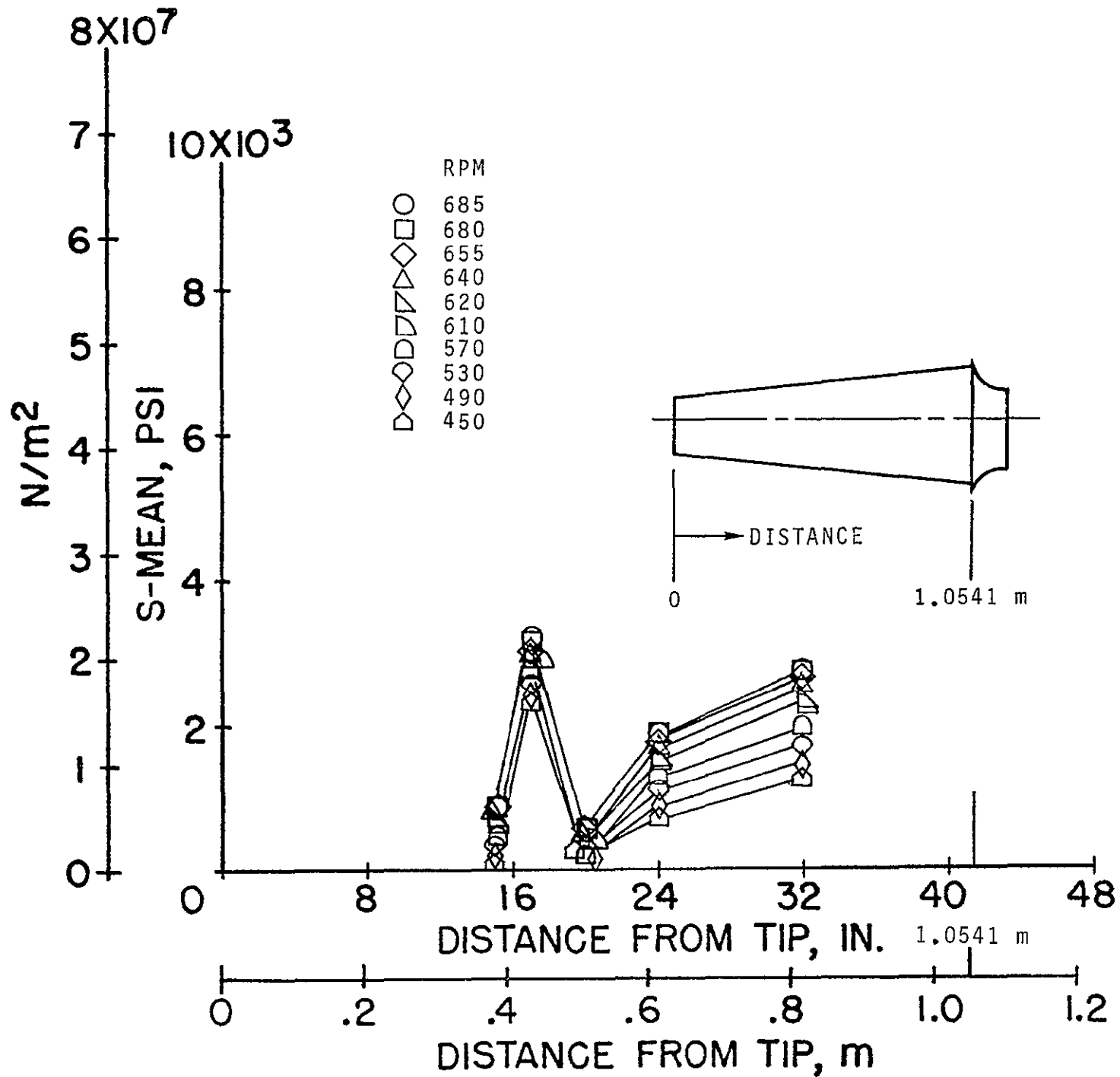
(b) Static stress; $p_t = 33.86 \times 10^3$ N/m^2 (10 in. Hg); 3rd stage.
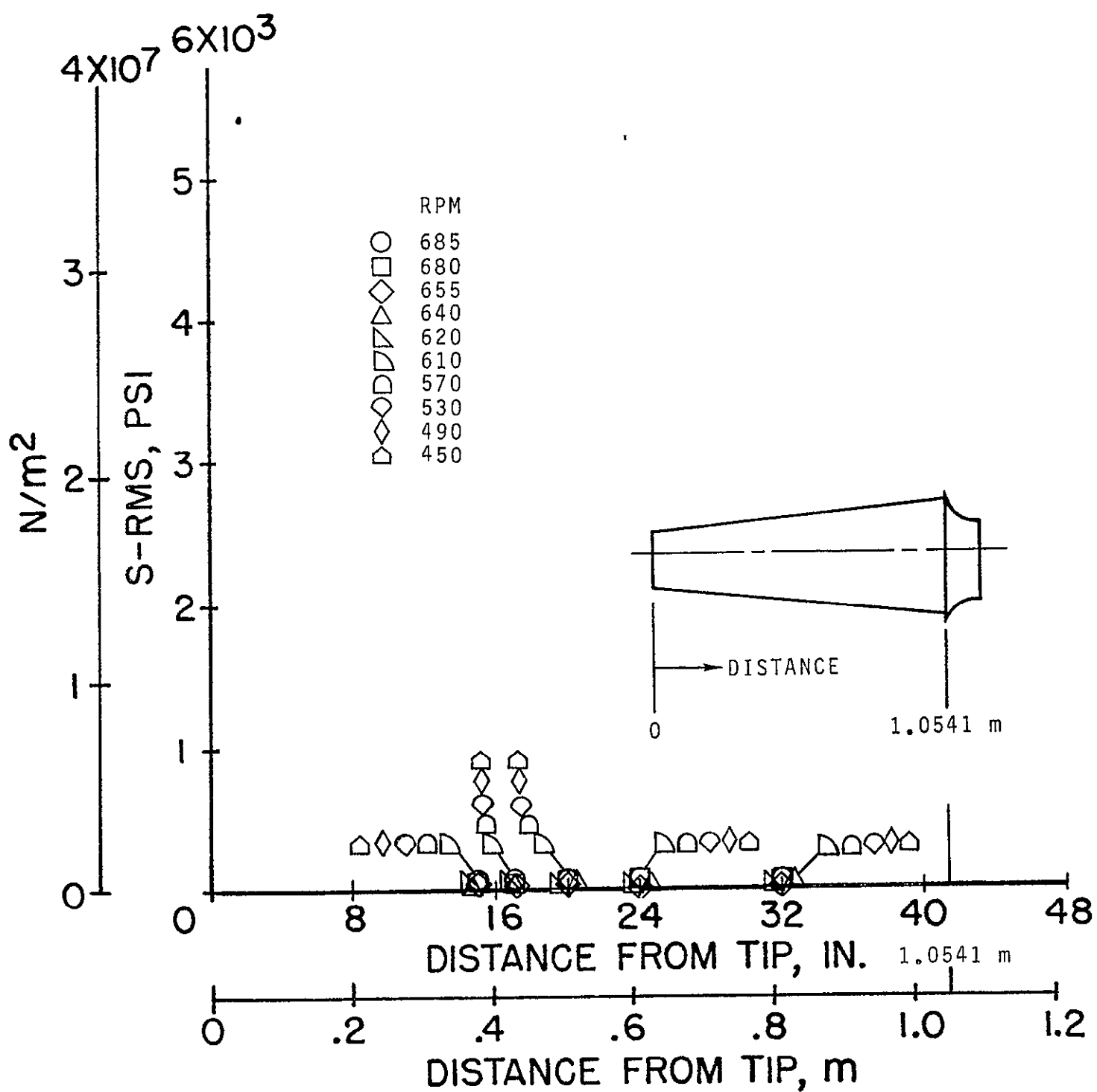
FIGURE 7.- CONTINUED.

(c) Dynamic stress; $p_t = 33.86 \times 10^3$ N/m^2 (10 in. Hg); 3rd stage.
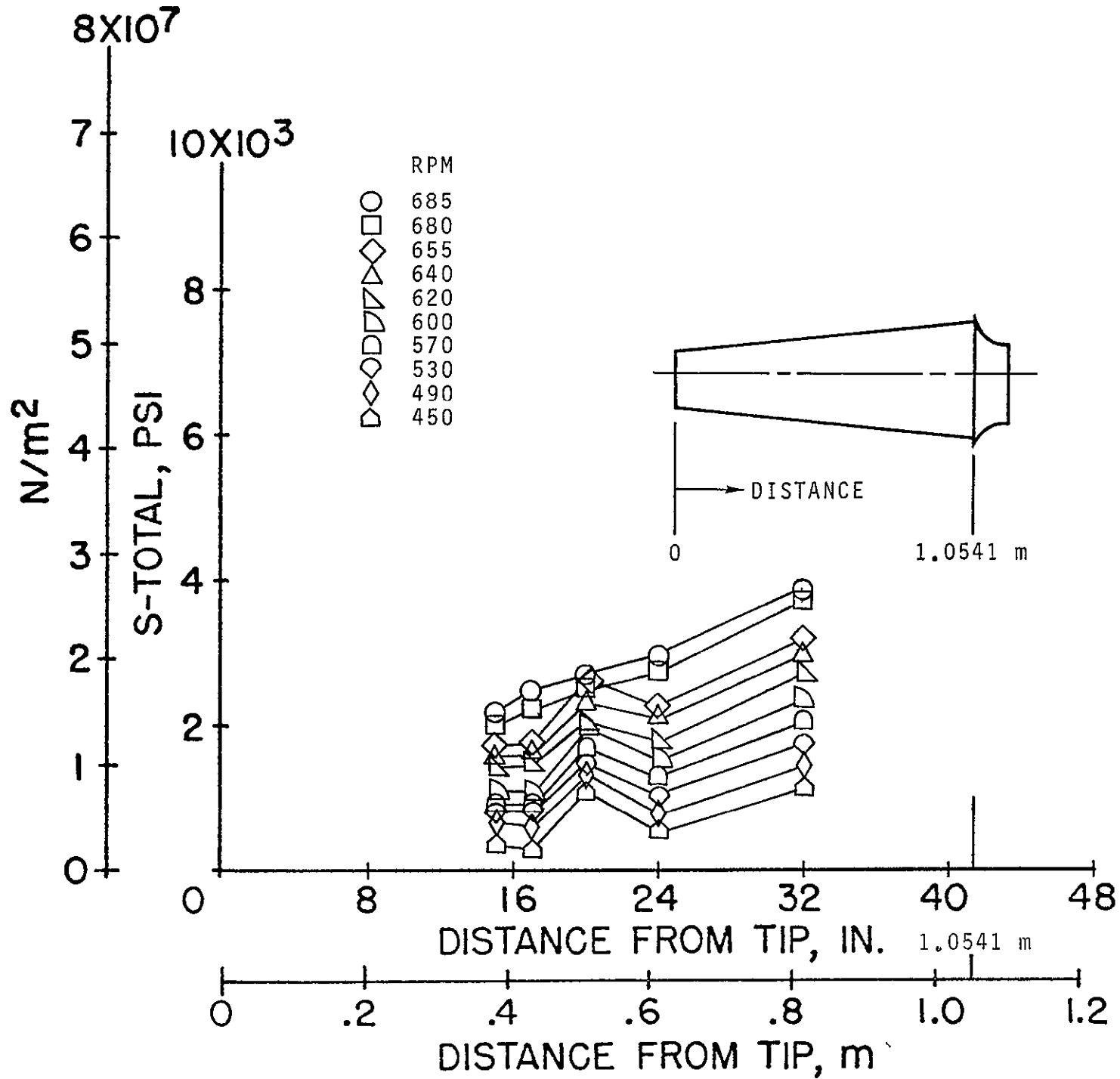
Figure 7.- Continued.

(d) Total stress; p_t = 67.73X10^3 N/m^2 (20 in. Hg); 3rd stage.

Figure 7.- Continued.

(e) Static stress; p_t = 67.73X10^3 N/m^2 (20 in. Hg); 3rd stage.

Figure 7.- Continued.

(f) Dynamic stress; $p_t = 67.73 \times 10^3$ N/m^2 (20 in. Hg); 3rd stage.
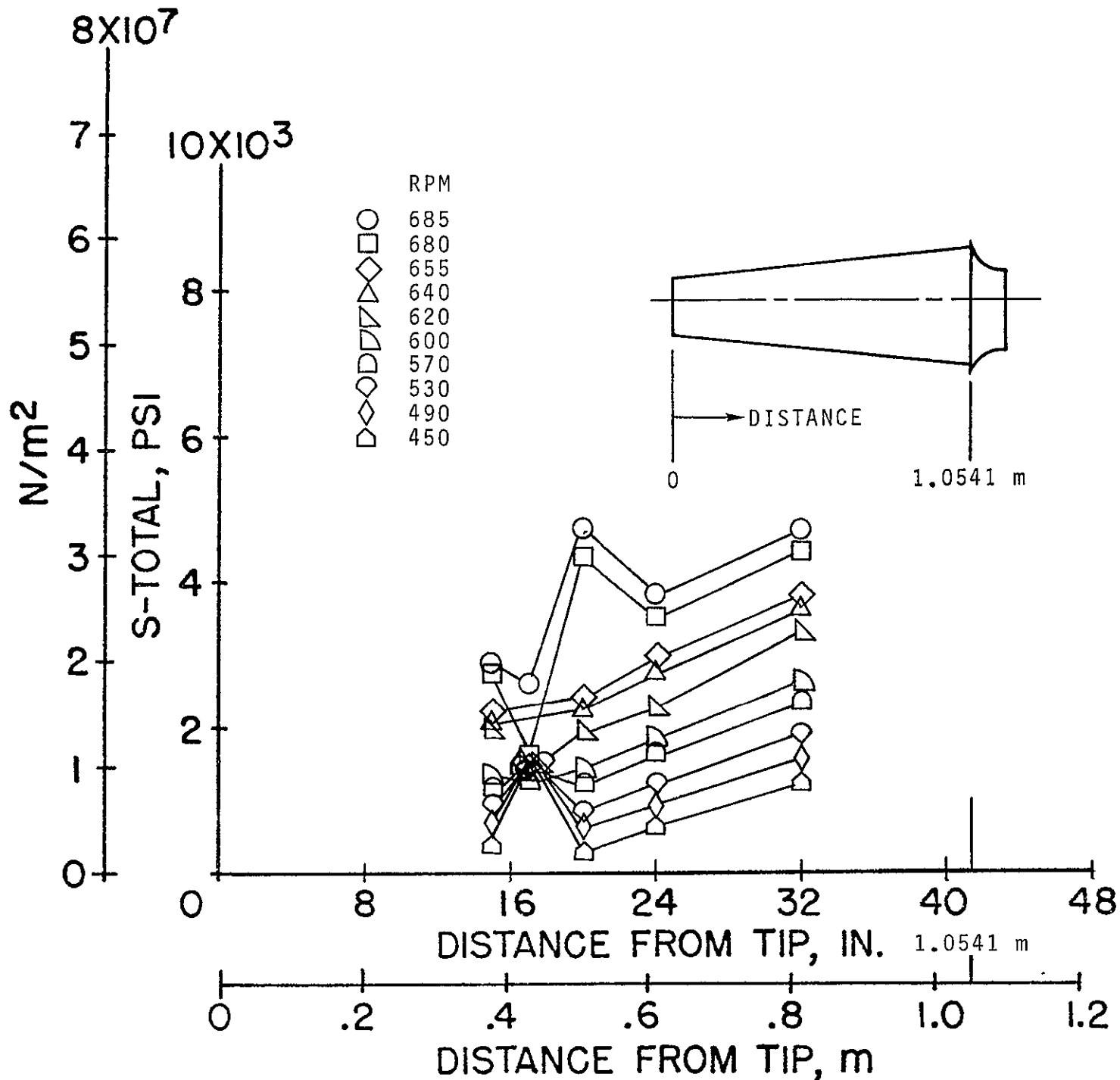
Figure 7.- Continued.

(g) Total stress; p_t = 101.59X10^3 N/m^2 (30 in. Hg); 3rd stage.

Figure 7.- Continued.

(h) Static stress; p_t = 101.59X10^3 N/m^2 (30 in. Hg); 3rd stage.

Figure 7.- Continued.

(i) Dynamic stress; $p_t = 101.59 \times 10^3$ N/m^2 (30 in. Hg); 3rd stage.
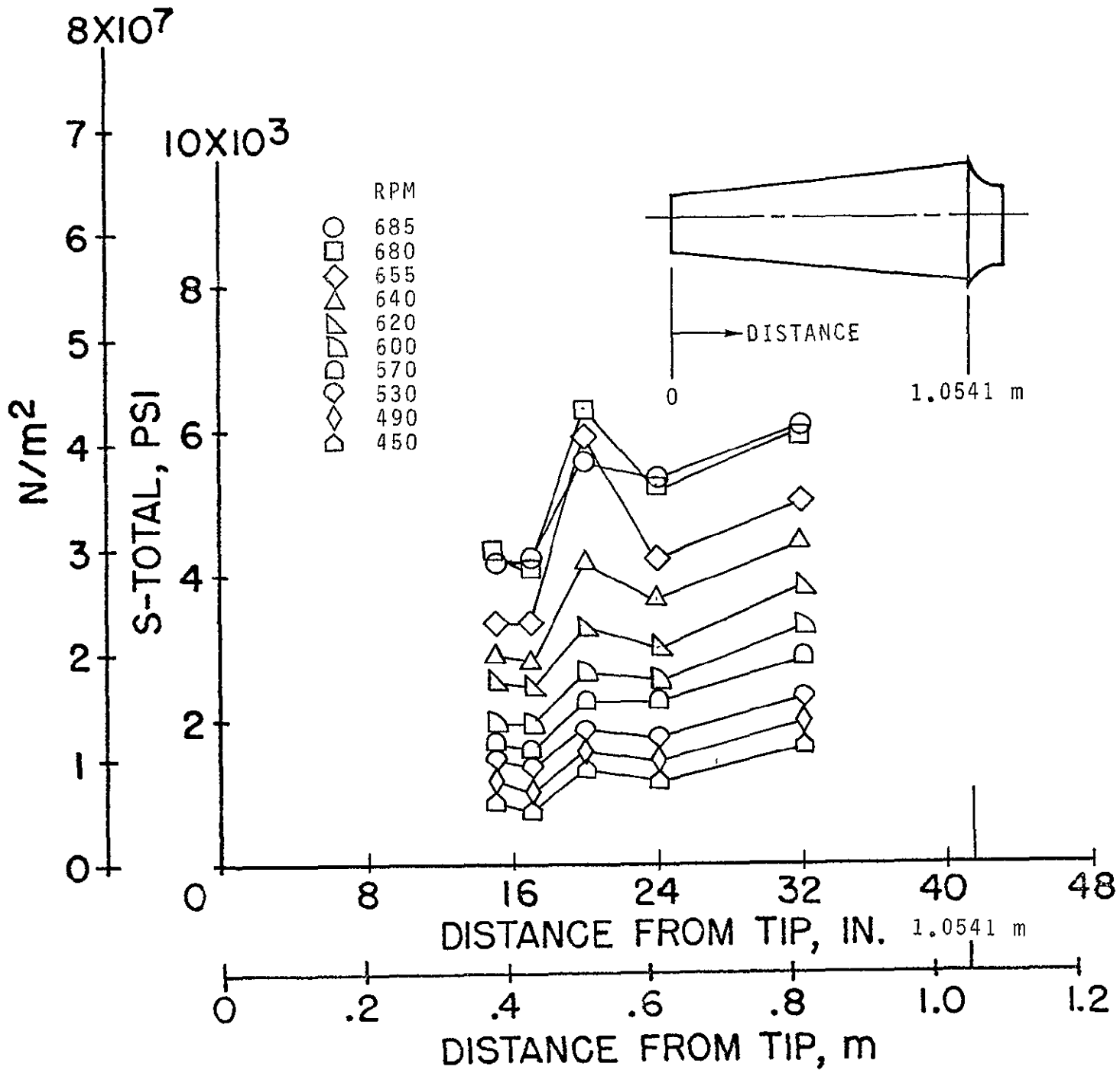
Figure 7.- Continued.

(j) Total stress; $p_t = 152.39 \times 10^3$ N/m^2 (45 in. Hg); 3rd stage.
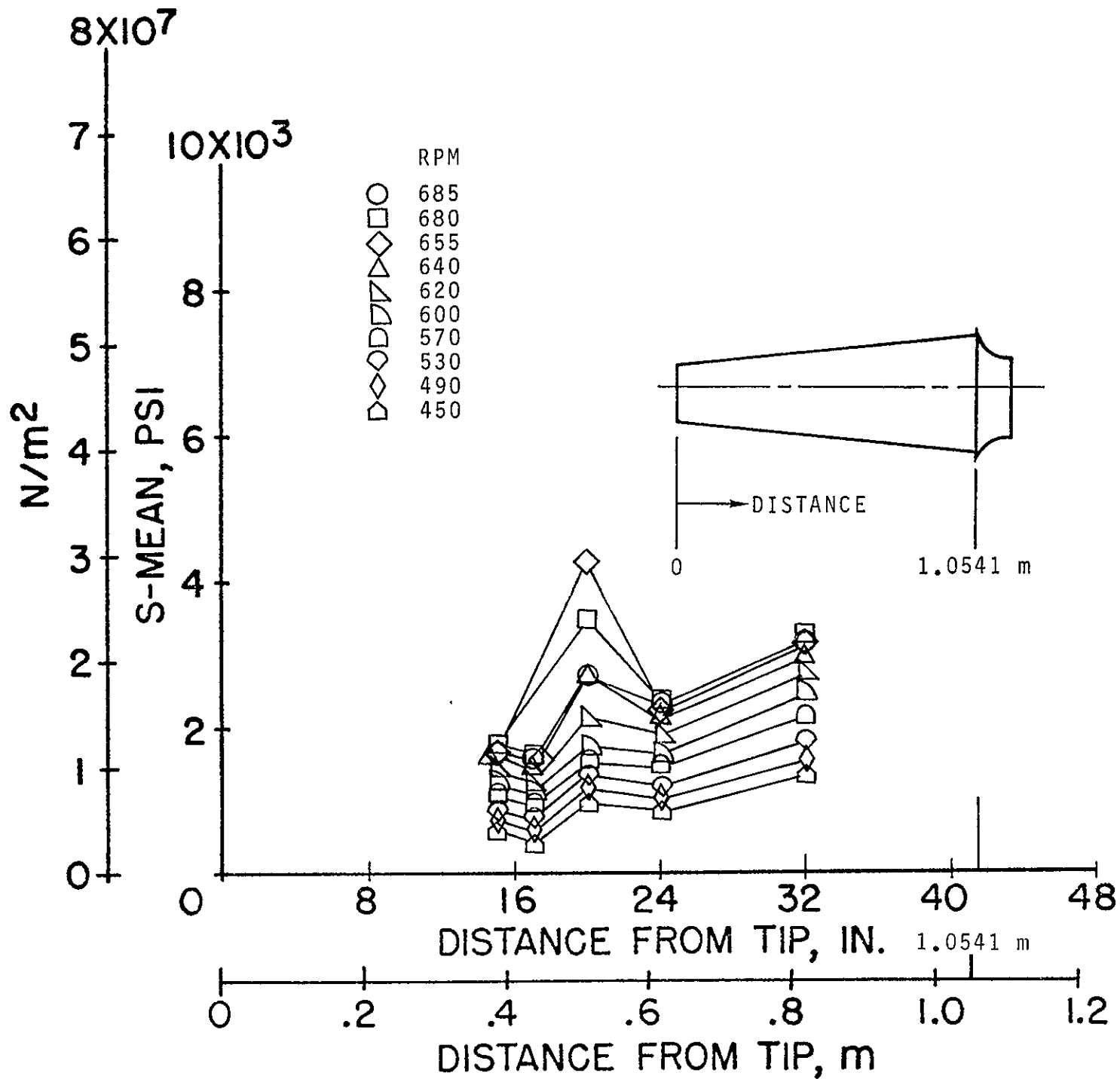
Figure 7.- Continued.

(k) Static stress; p_t = 152.39X10^3 N/m^2 (45 in. Hg); 3rd stage.
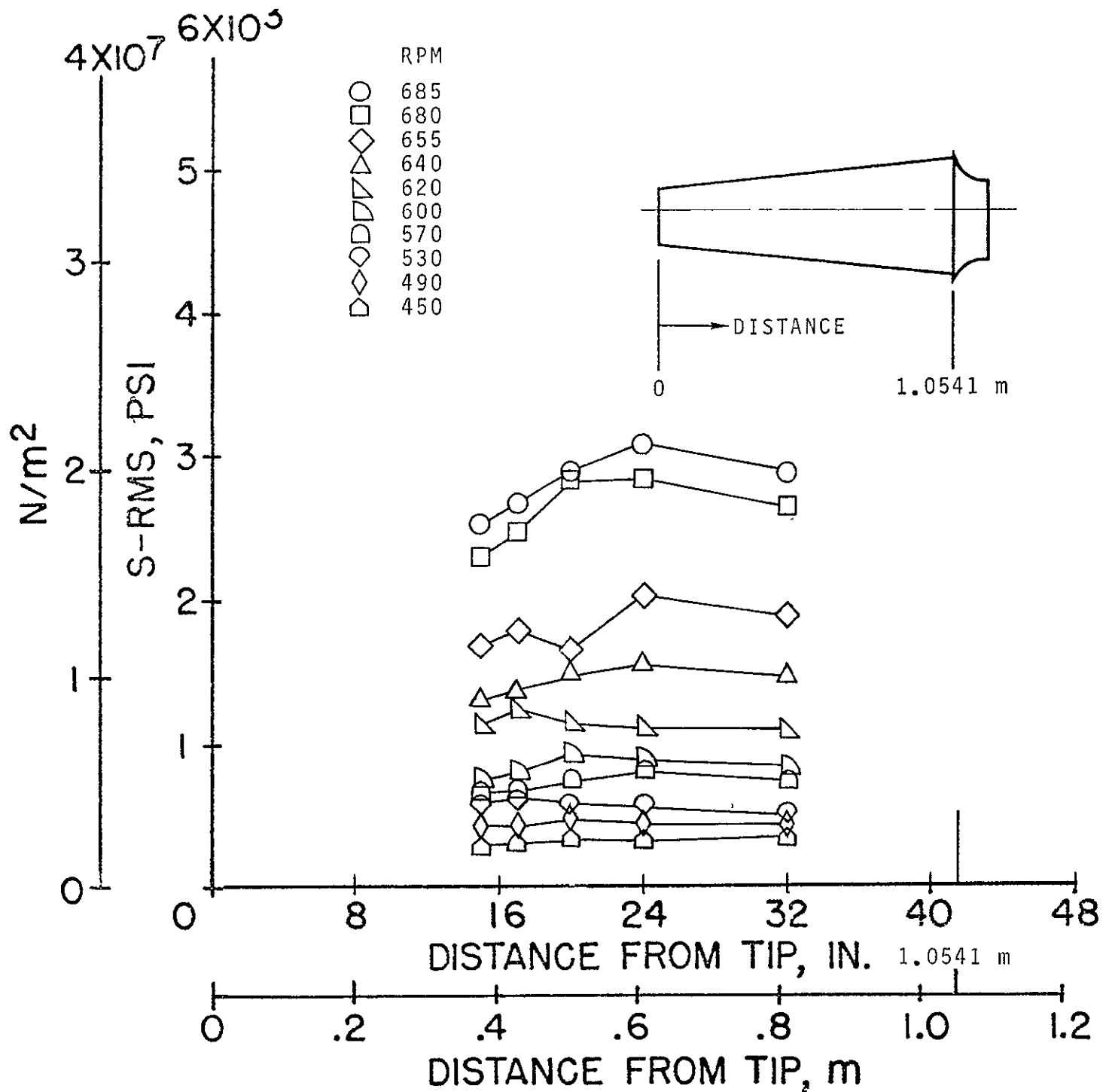
Figure 7.- Continued.

(1) Dynamic stress; p_t = 152.39X10^3 N/m^2 (45 in. Hg); 3rd stage.
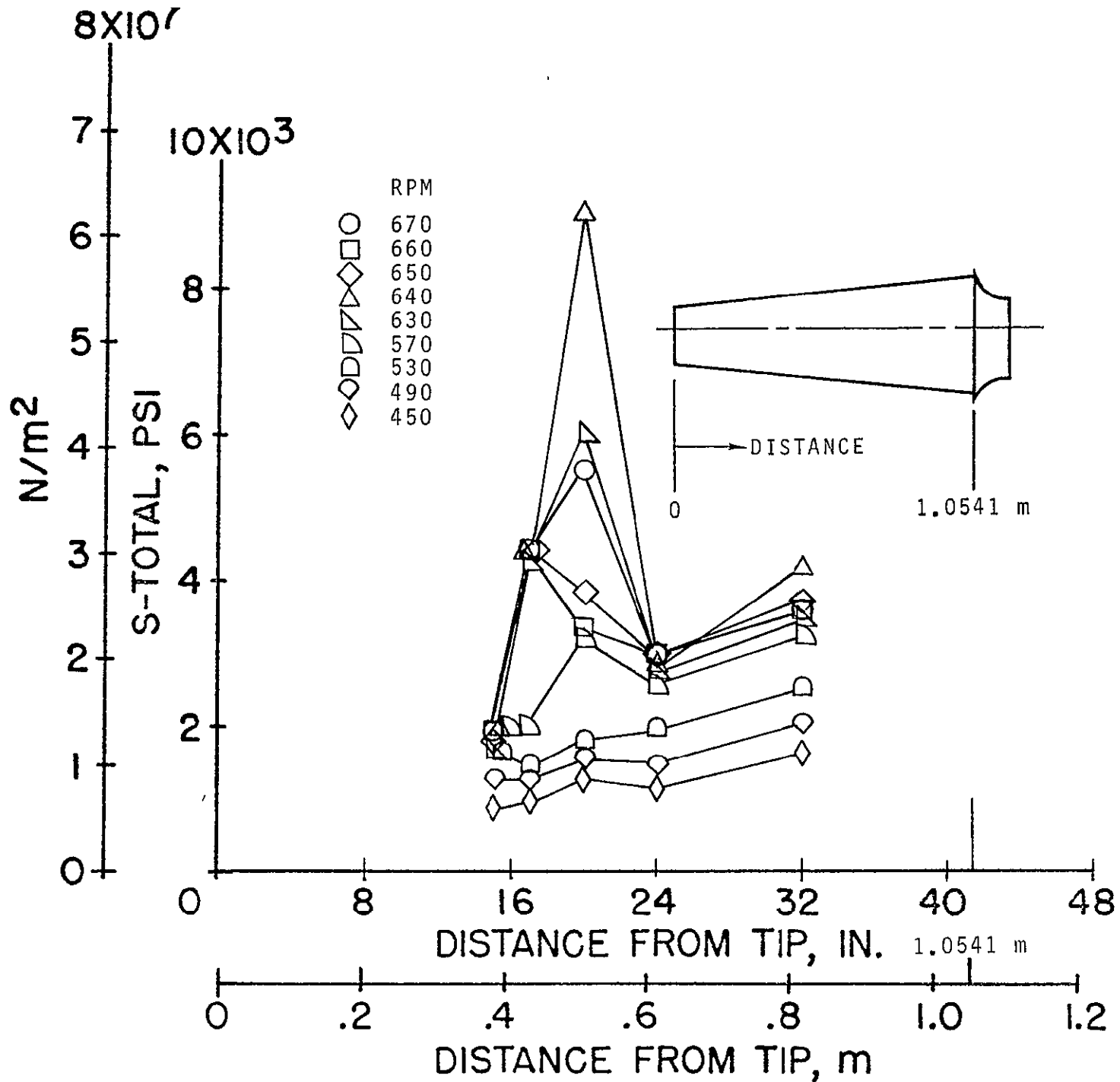
Figure 7.- Continued.

(m) Total stress; p_t = 220.12X10³ N/m² (65 in. Hg); 3rd stage.
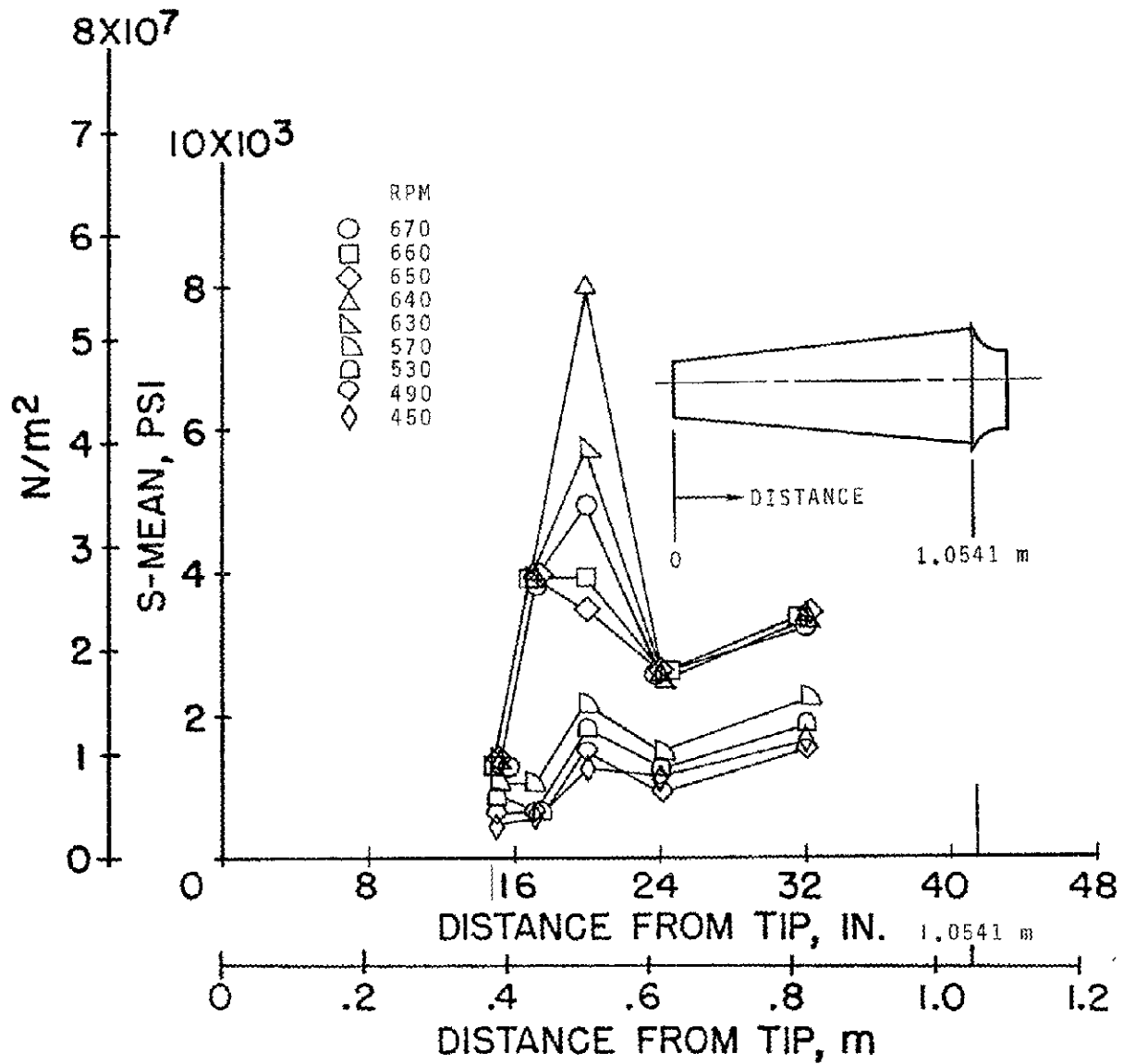
Figure 7.- Continued.

(n) Static stress; p_t = 220.12X10^3 N/m^2 (65 in. Hg); 3rd stage.
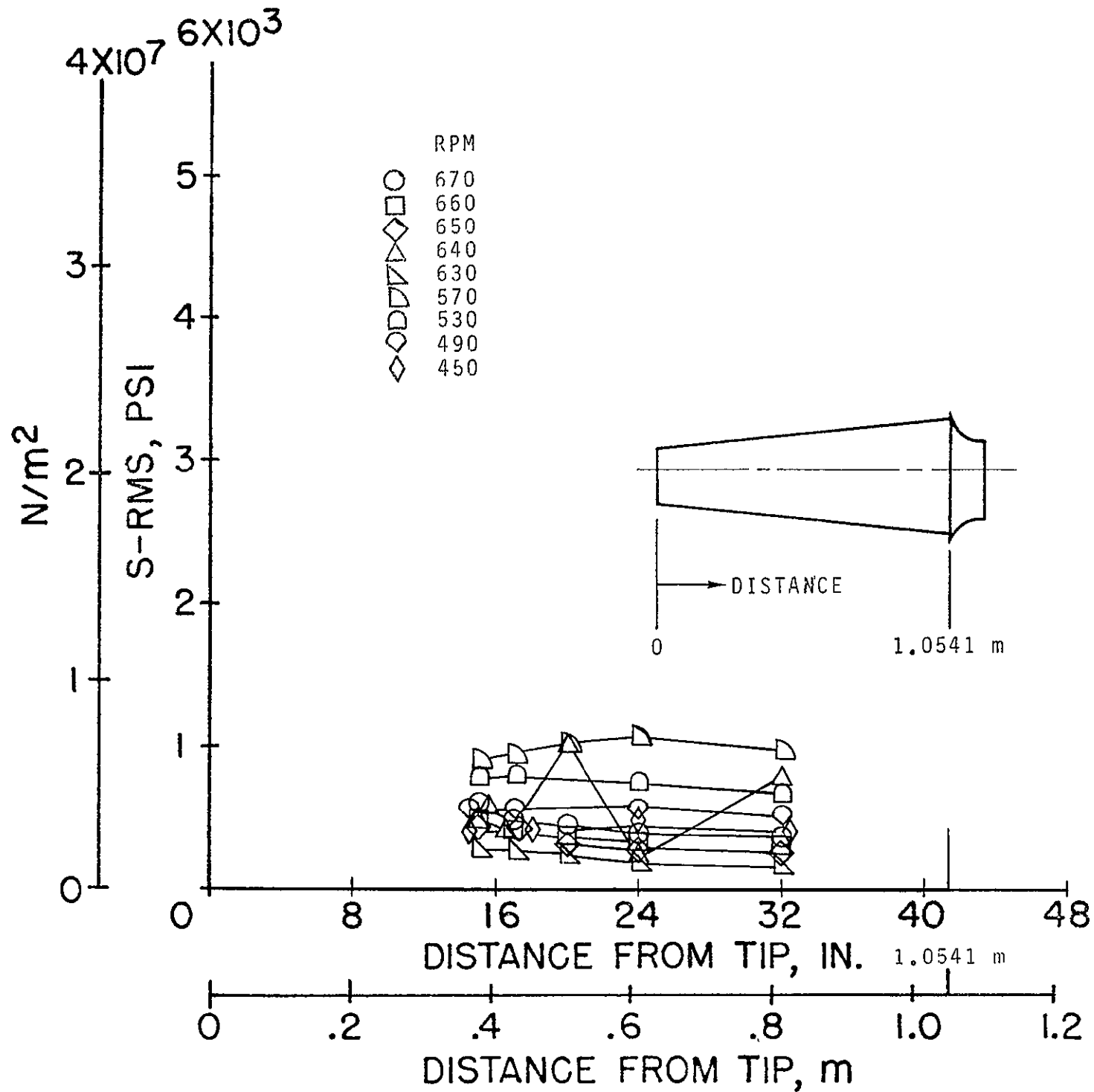
Figure 7.- Continued.

(o) Dynamic stress; p_t = 220.12X10^3 N/m^2 (65 in. Hg); 3rd stage.
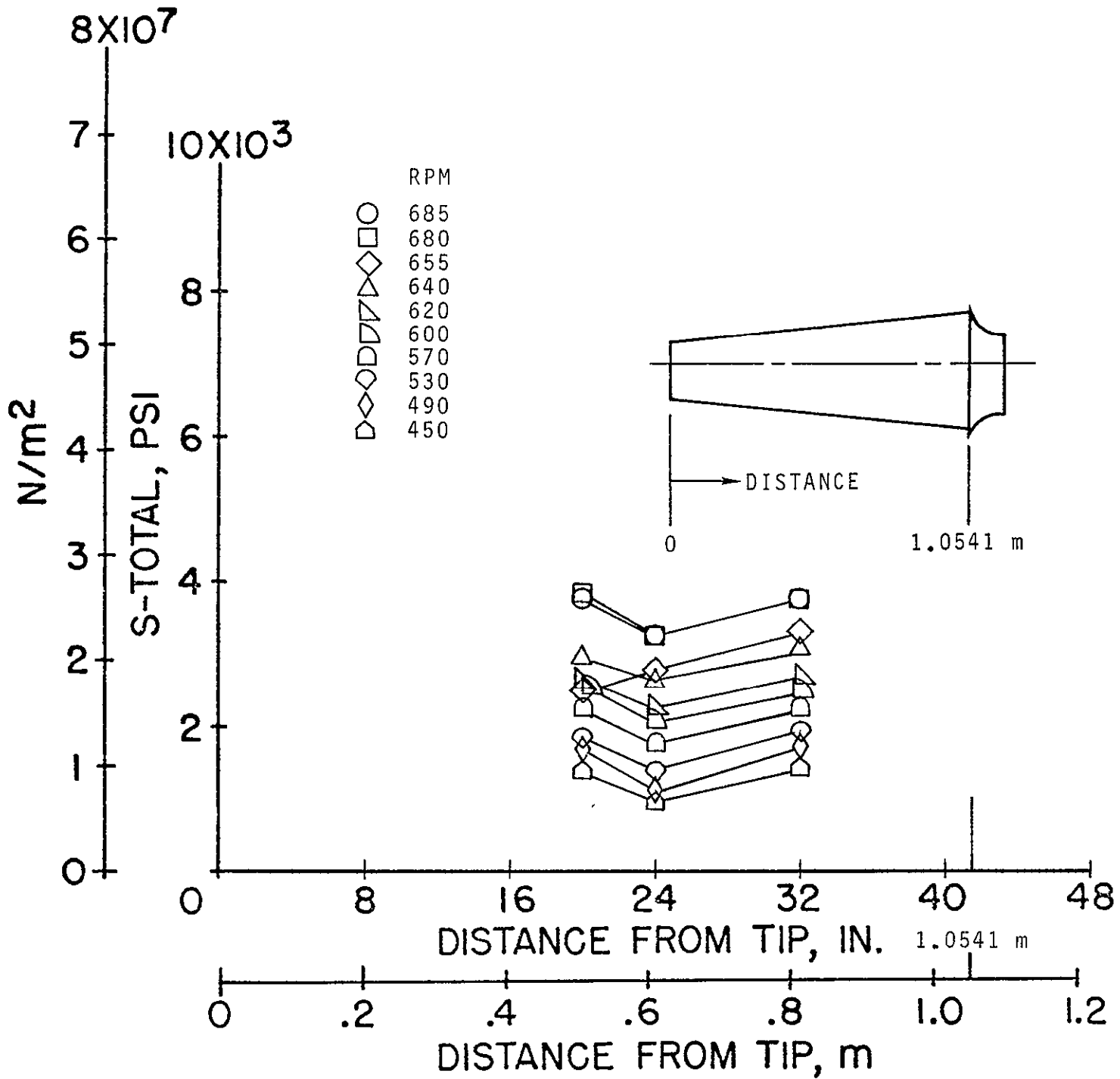
Figure 7.- Continued.

(p) Total stress; $p_t = 152.39 \times 10^3$ N/m^2 (45 in. Hg); 2nd stage.
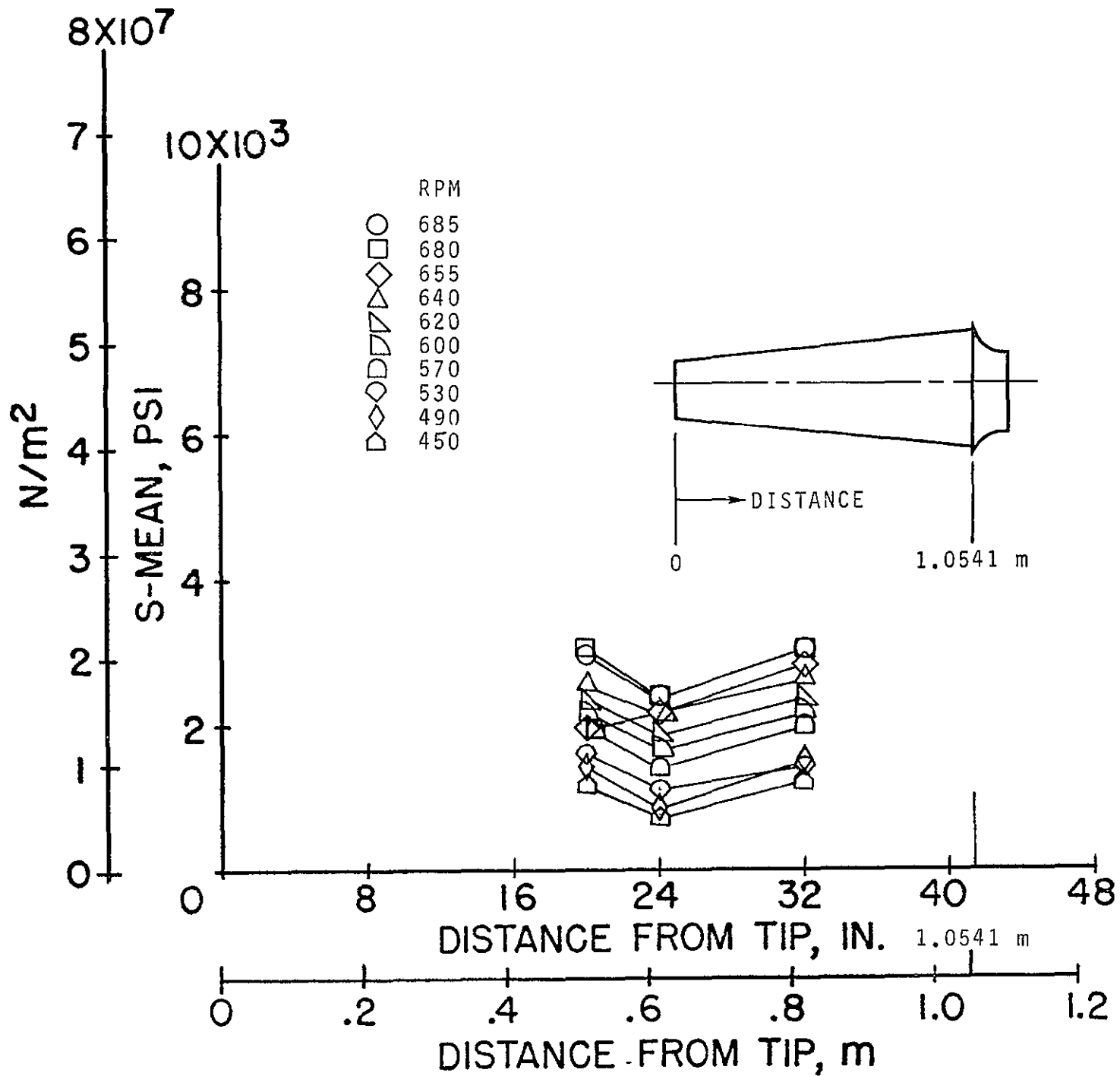
Figure 7.- Continued.

(q) Static stress; p_t = 152.39X10^3 N/m^2 (45 in. Hg); 2nd stage.

Figure 7.- Continued.
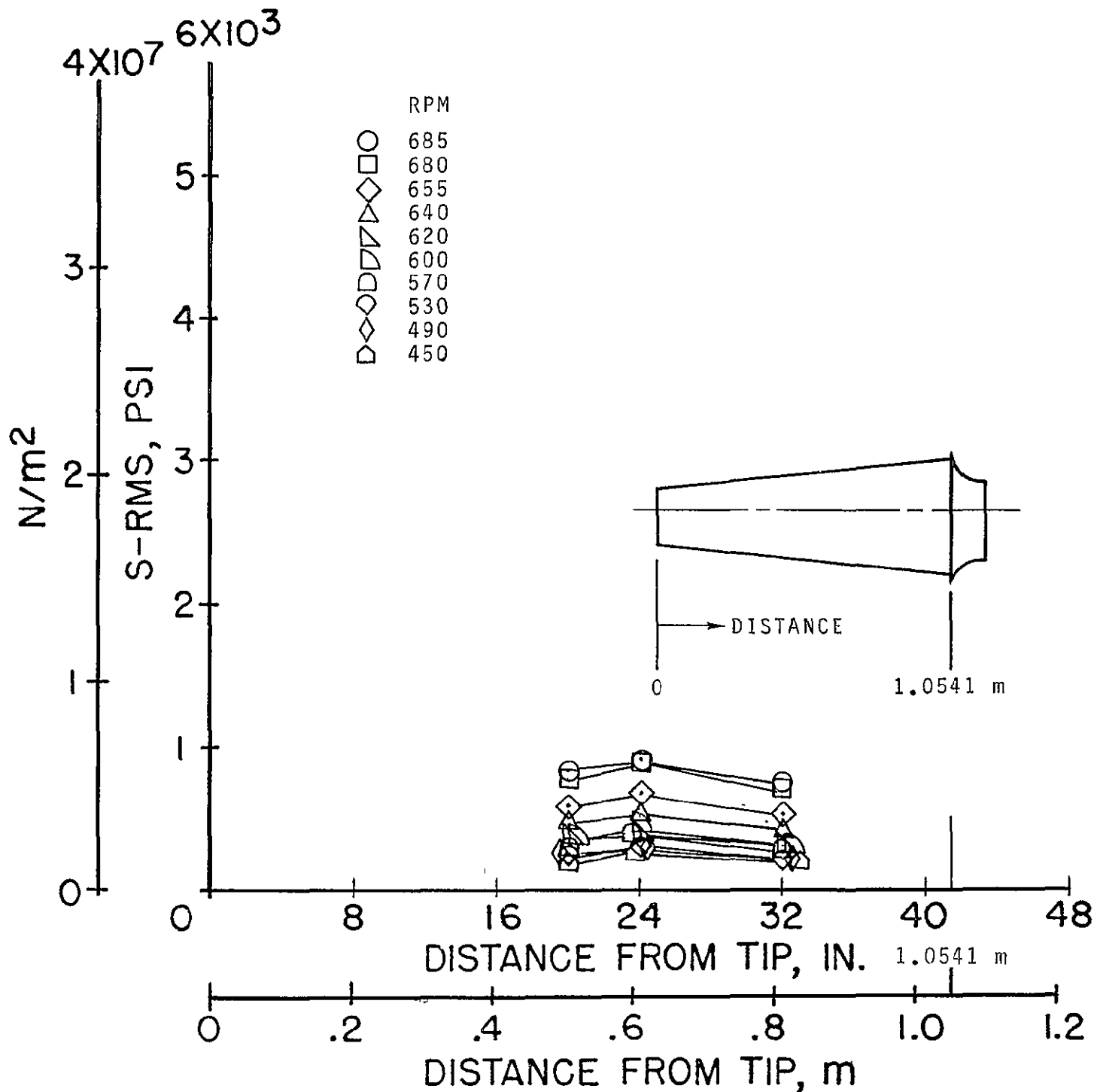
(r) Dynamic stress; $p_t = 152.39 \times 10^3$ N/m^2 (45 in. Hg); 2nd stage.

Figure 7.- Concluded.
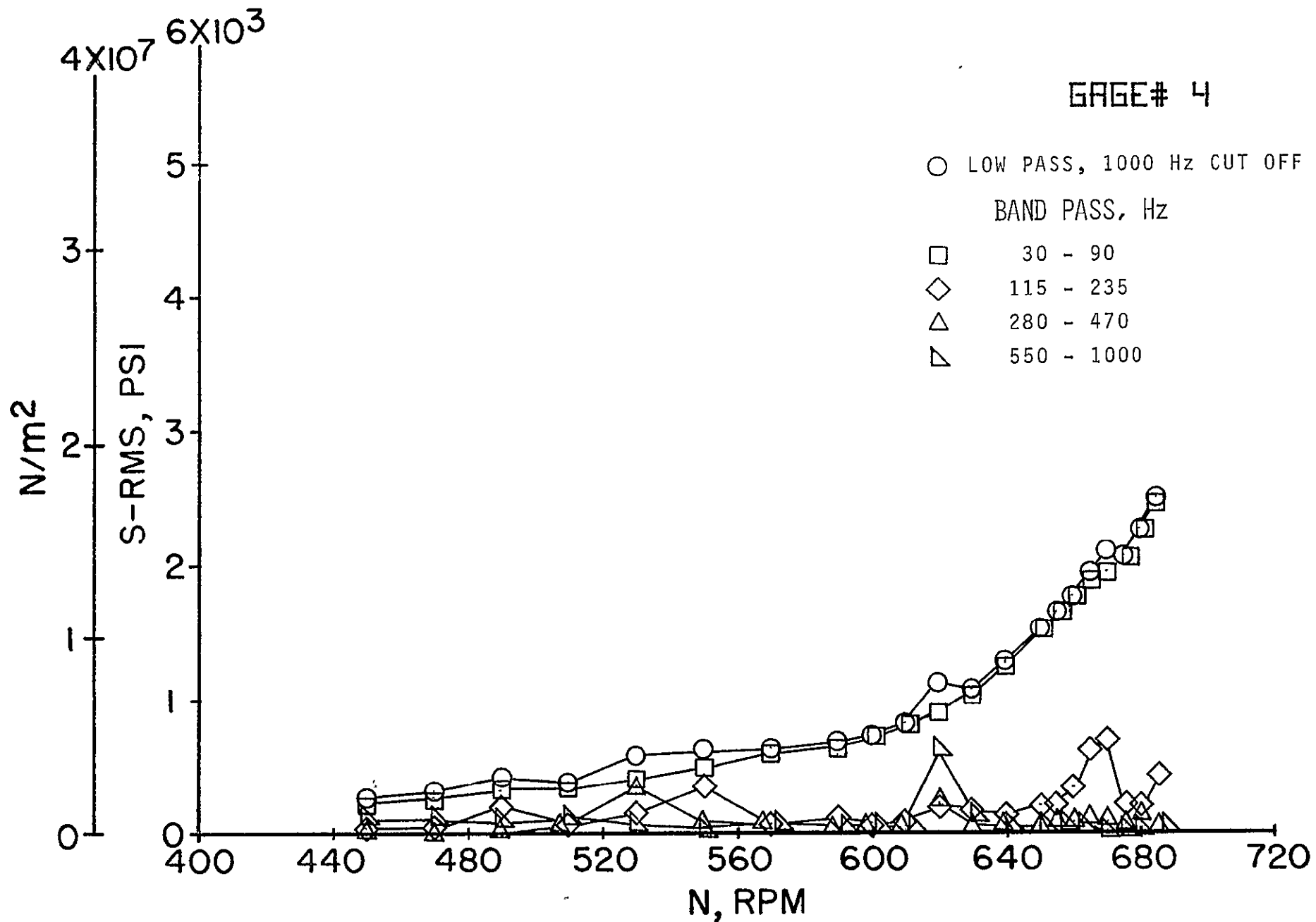
(a) Gage 4; 3rd stage.

Figure 8.- Distribution of the dynamic blade stresses in various band pass frequency ranges as a function of compressor speed at a tunnel total pressure of 152.39X10³ N/m² (45 in. Hg).
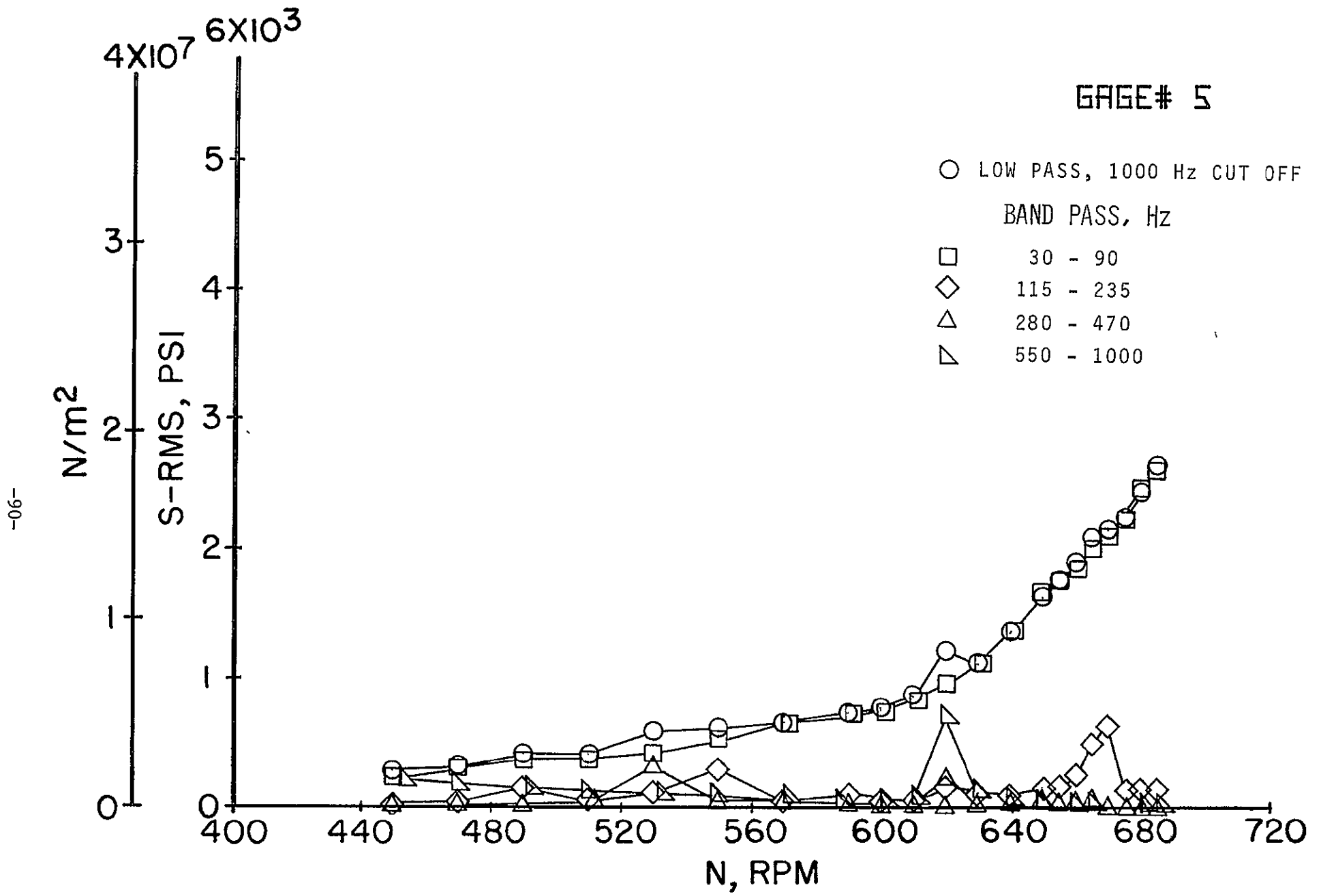
(b) Gage 5; 3rd stage.

Figure 8.- Continued.
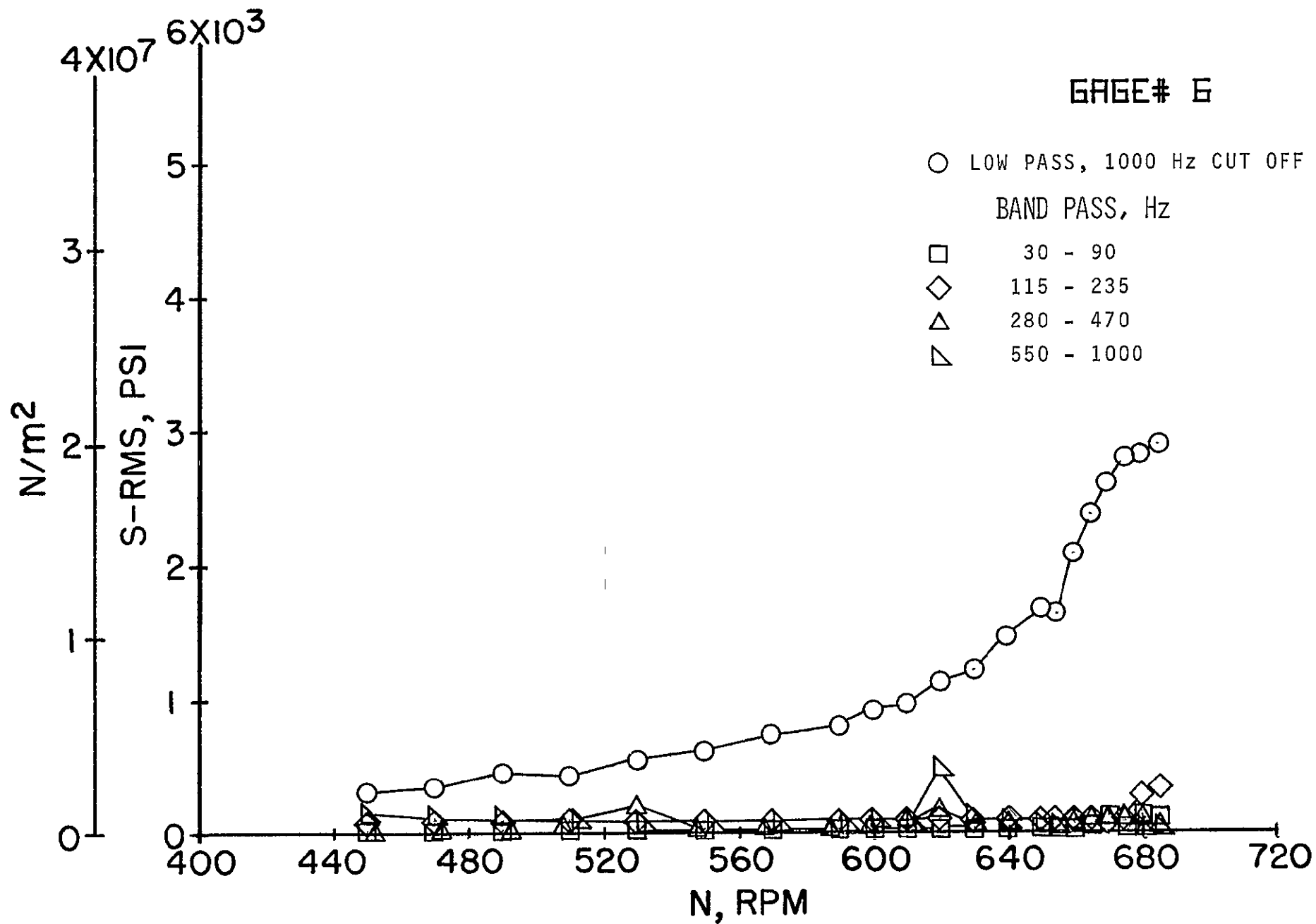
(c) Gage 6; 3rd stage.

Figure 8.- Continued.
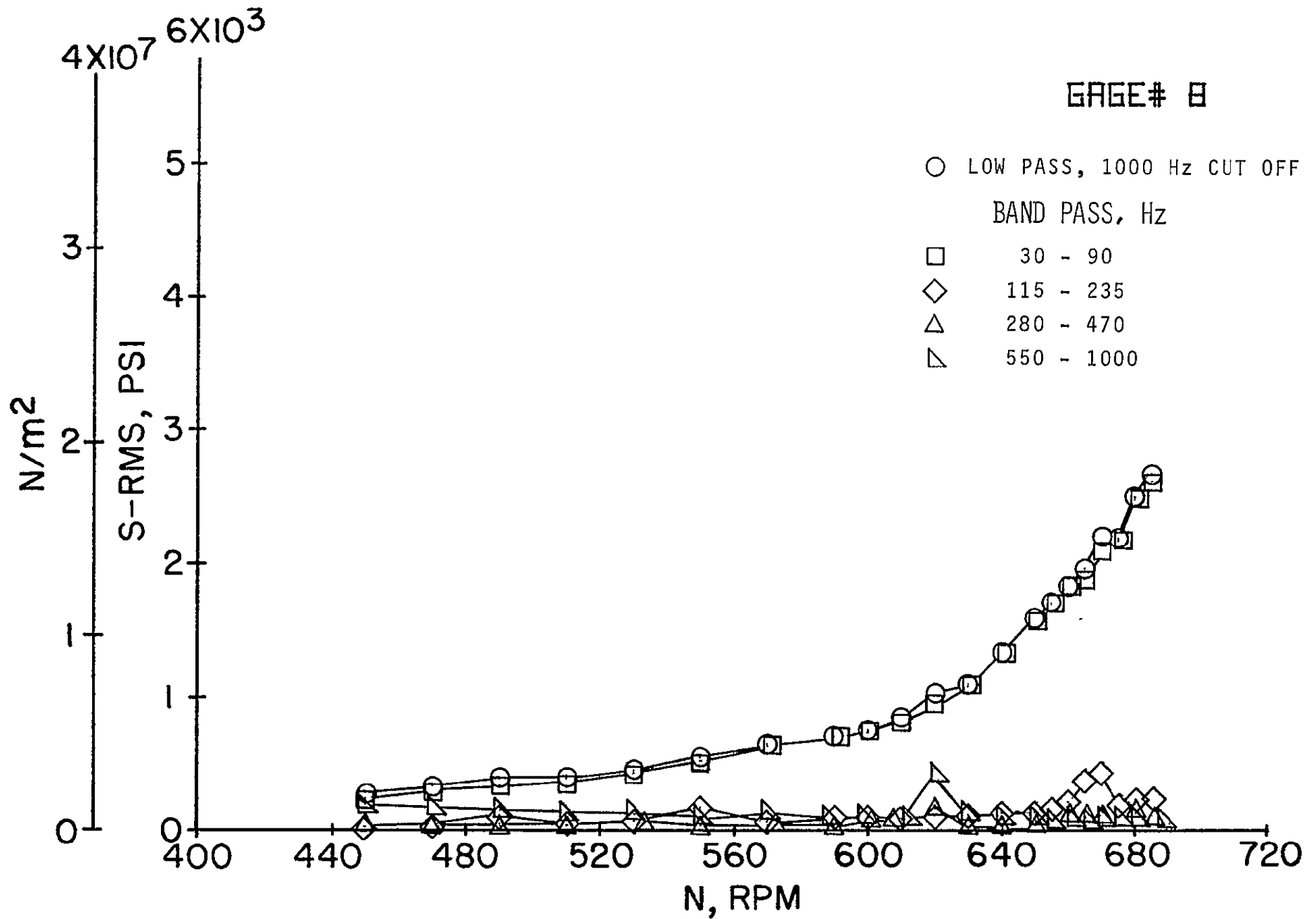
(d) Gage 8; 3rd stage.

Figure 8.- Continued.
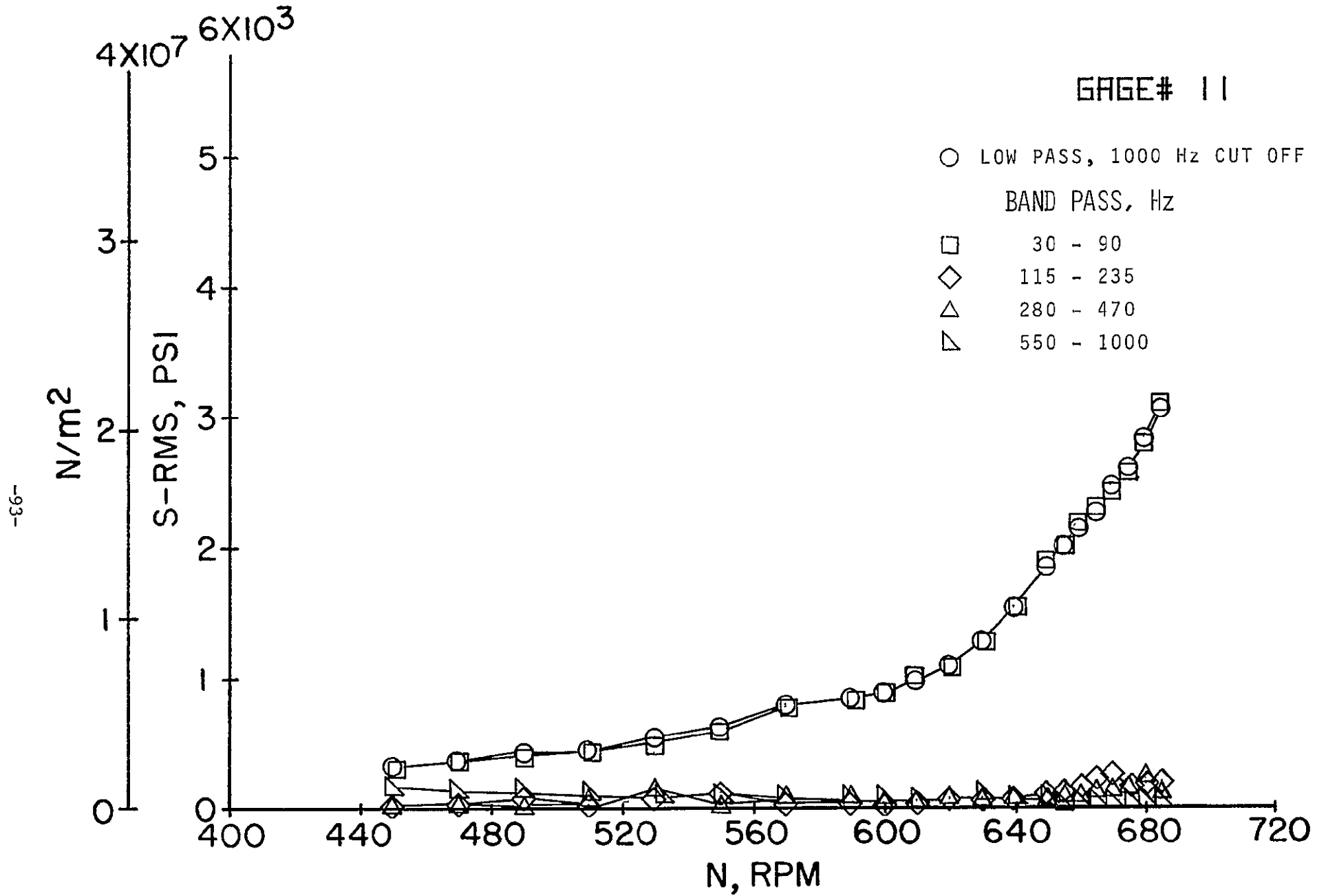
(e) Gage 11; 3rd stage.

Figure 8.- Continued.
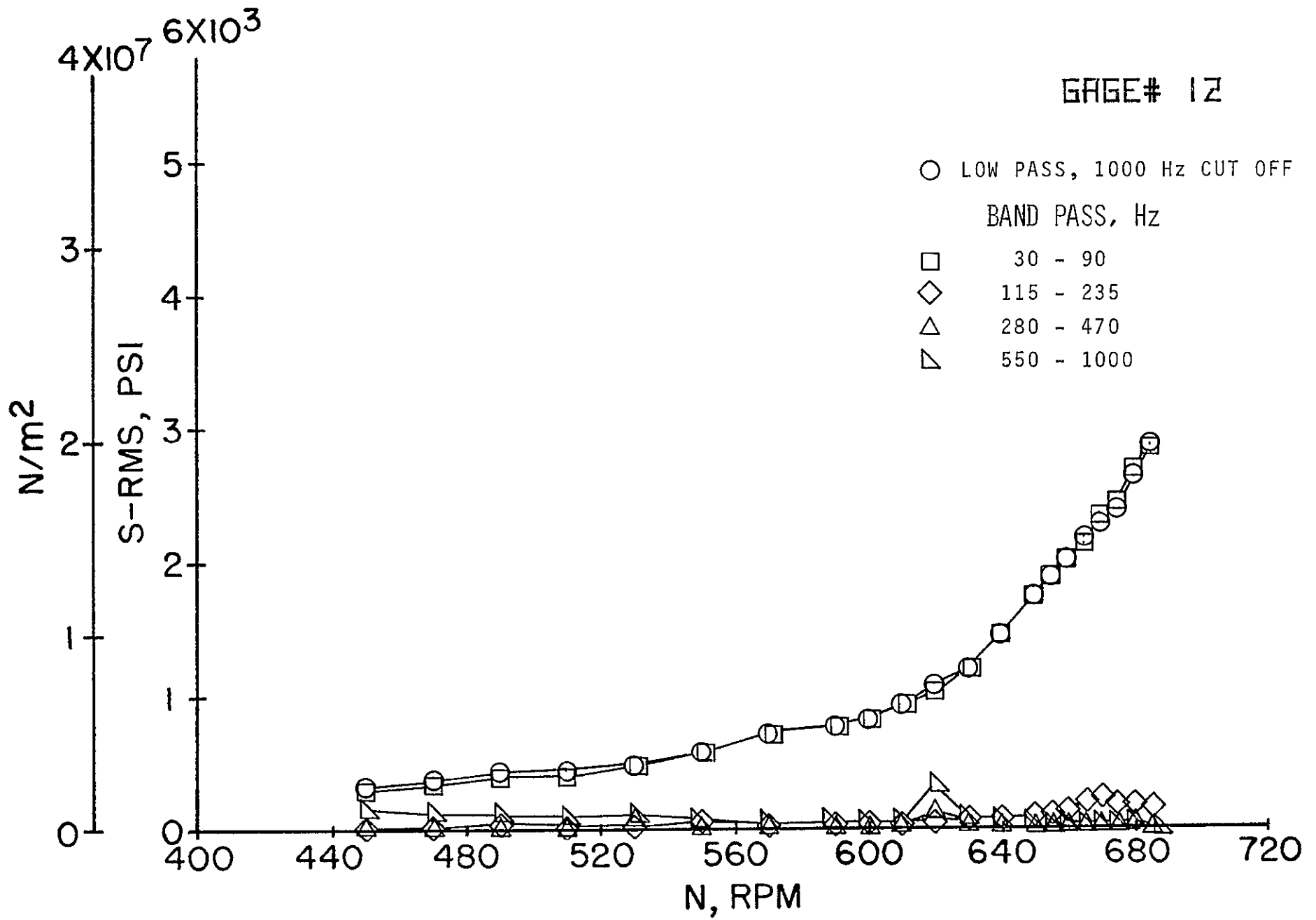
(f) Gage 12; 3rd stage.

Figure 8.- Continued.
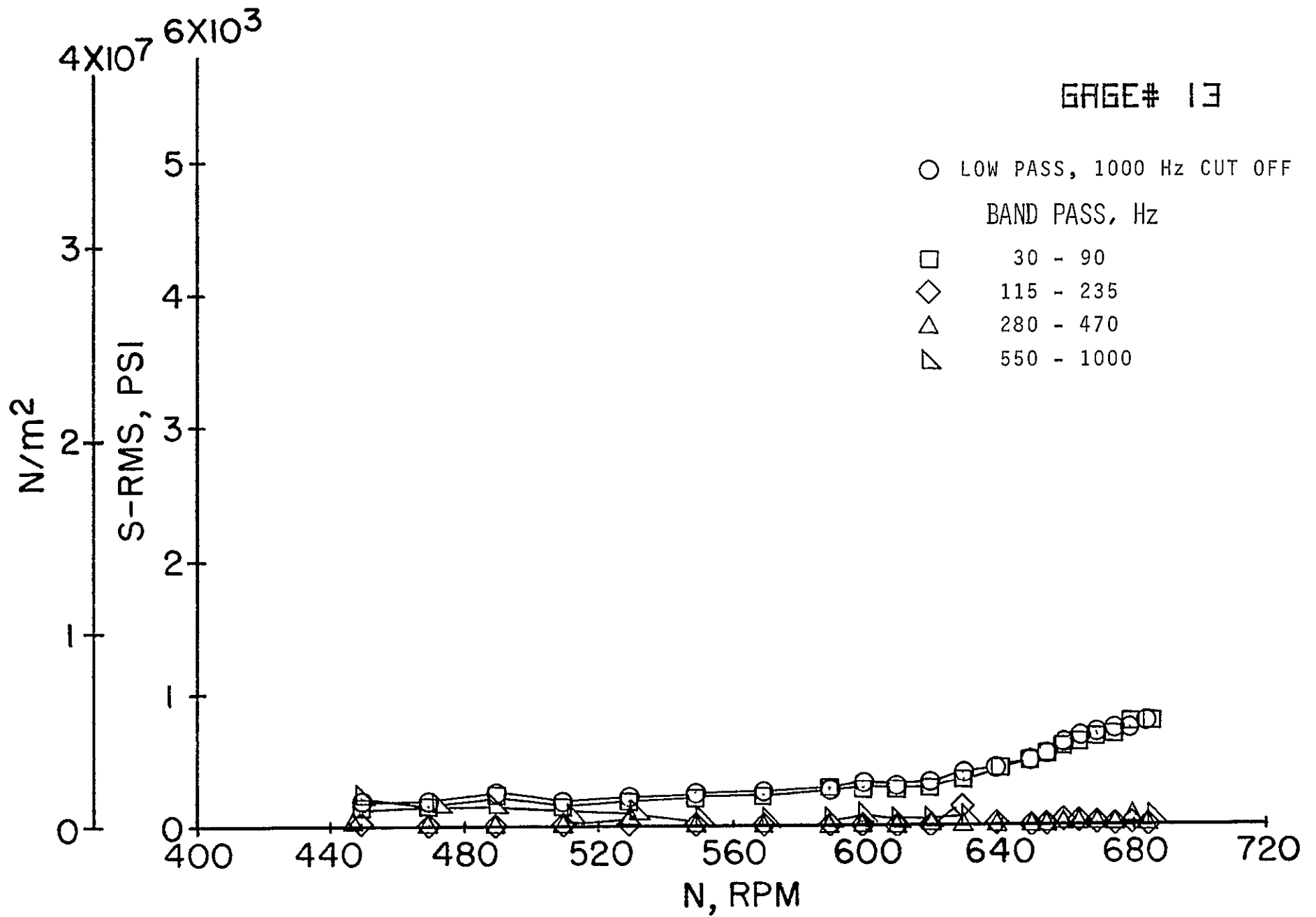
(g) Gage 13; 2nd stage.

Figure 8.- Continued.
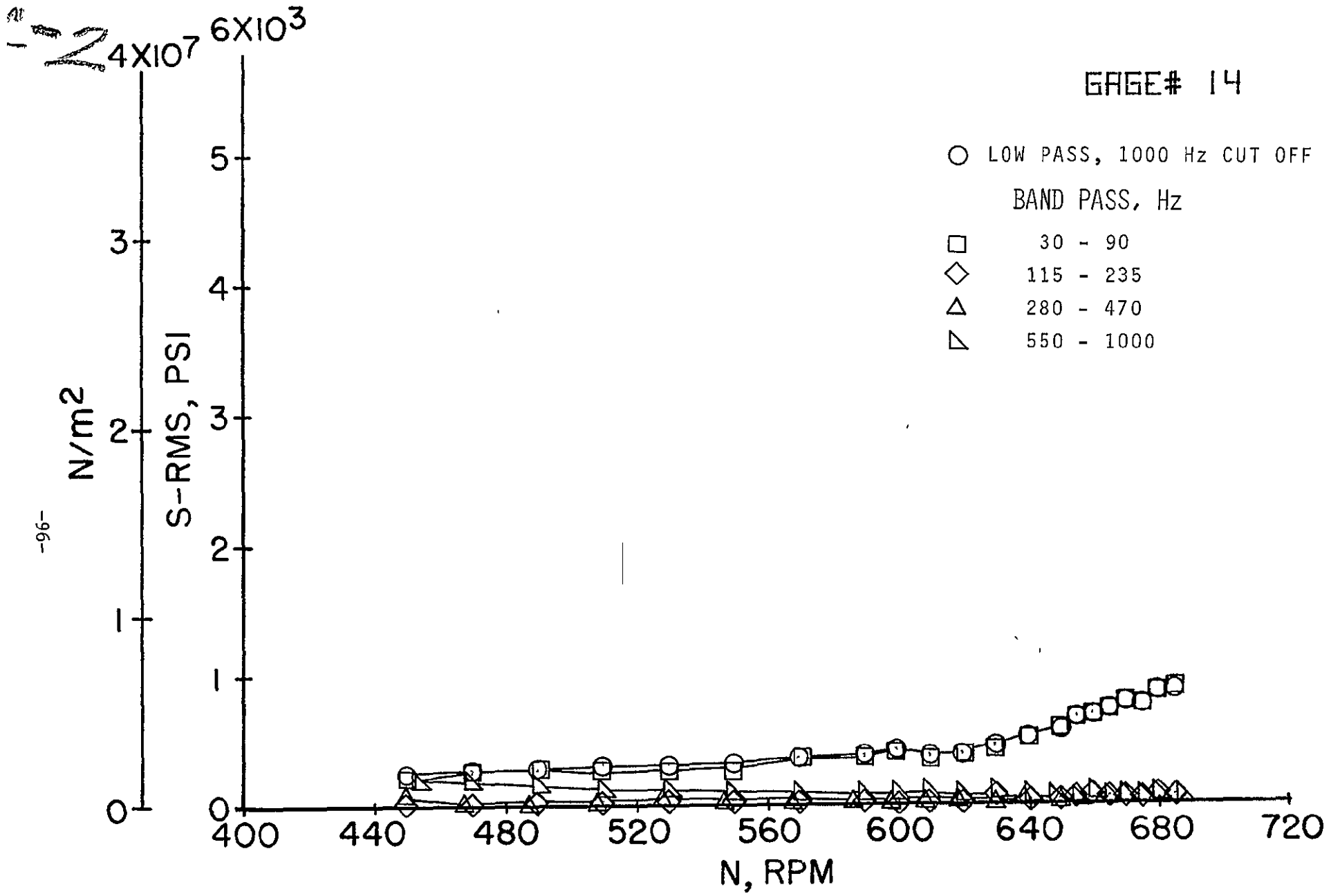
(h) Gage 14; 2nd stage.

Figure 8.- Continued.
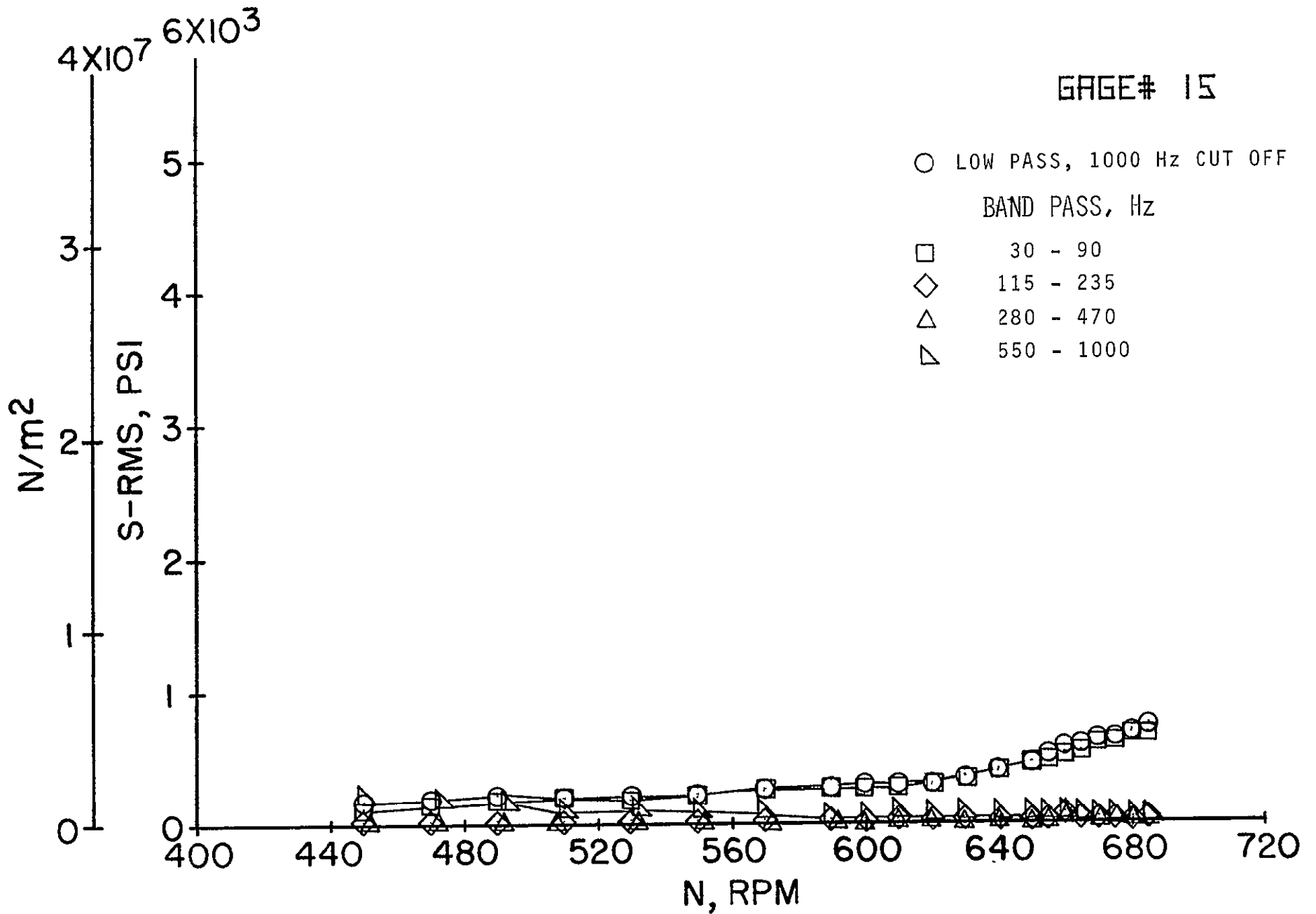
(i) Gage 15; 2nd stage.

Figure 8.- Continued.
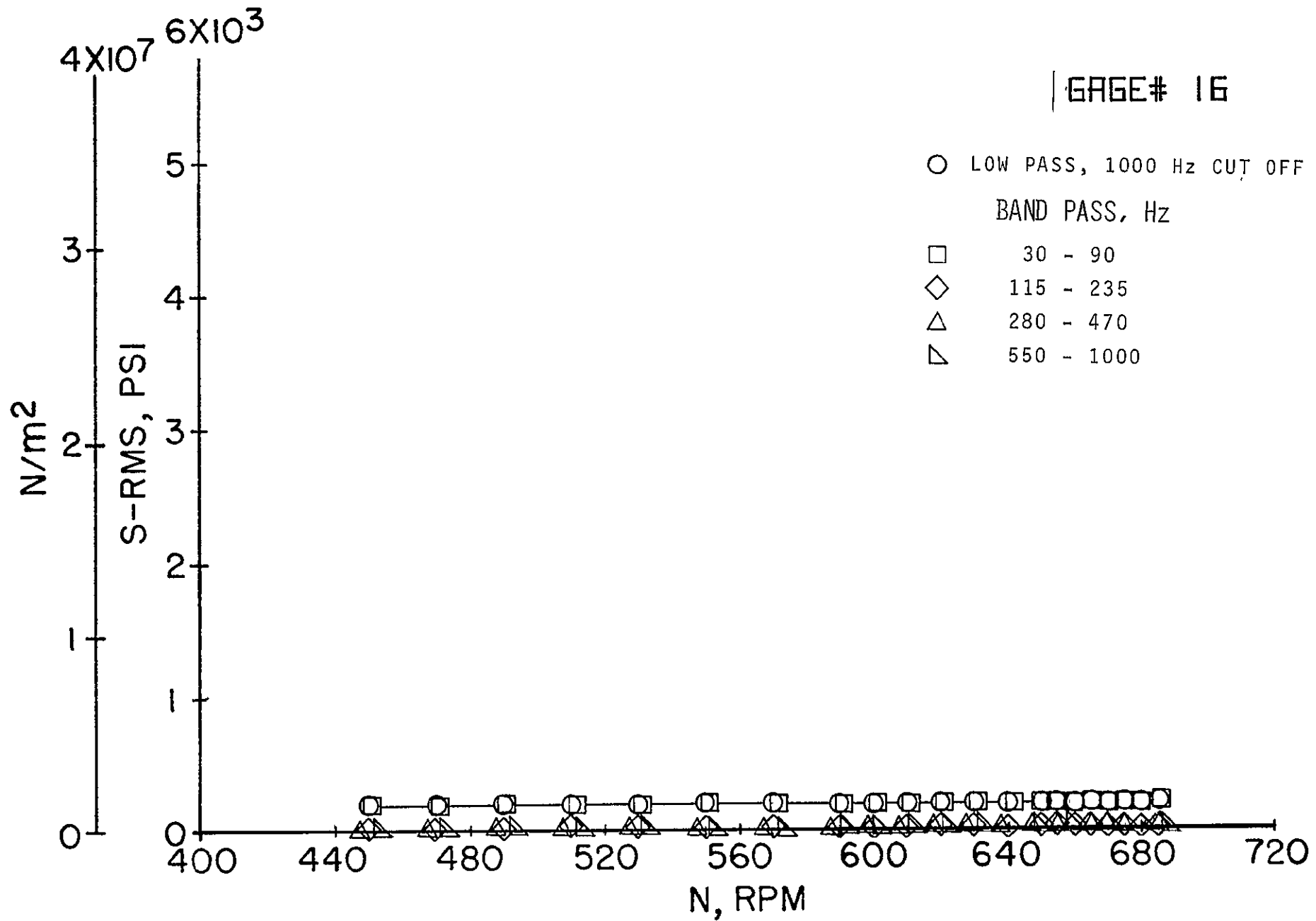
(j) Gage 16; dummy gage.

Figure 8.- Concluded.
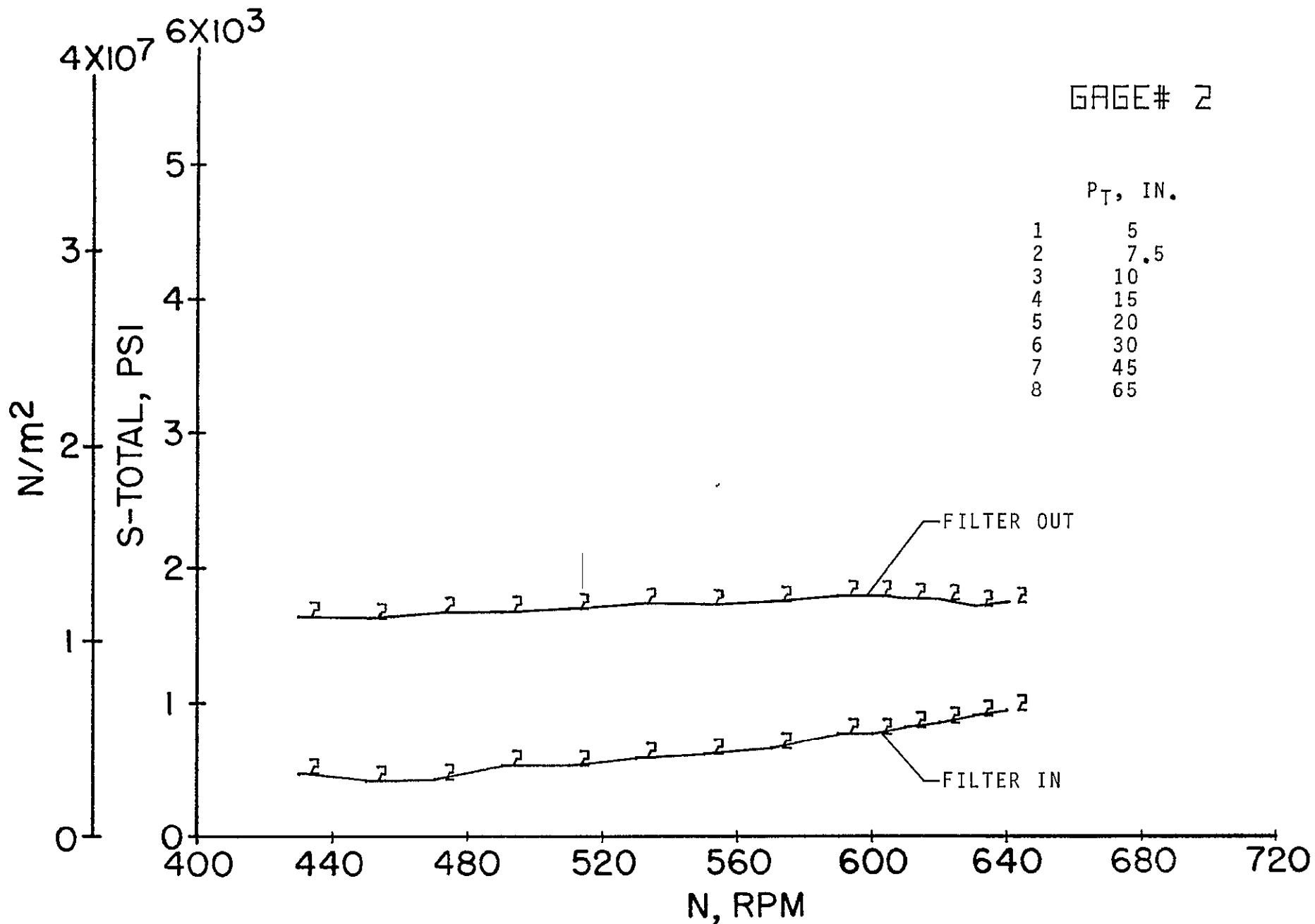
(a) Gage 2; $p_t = 25.40 \times 10^3$ N/m^2 (7.5 in. Hg).

Figure 9.- Effect of a low pass filter with a cut-off frequency of 1 kHz on the total blade stresses for various gages and tunnel total pressures.
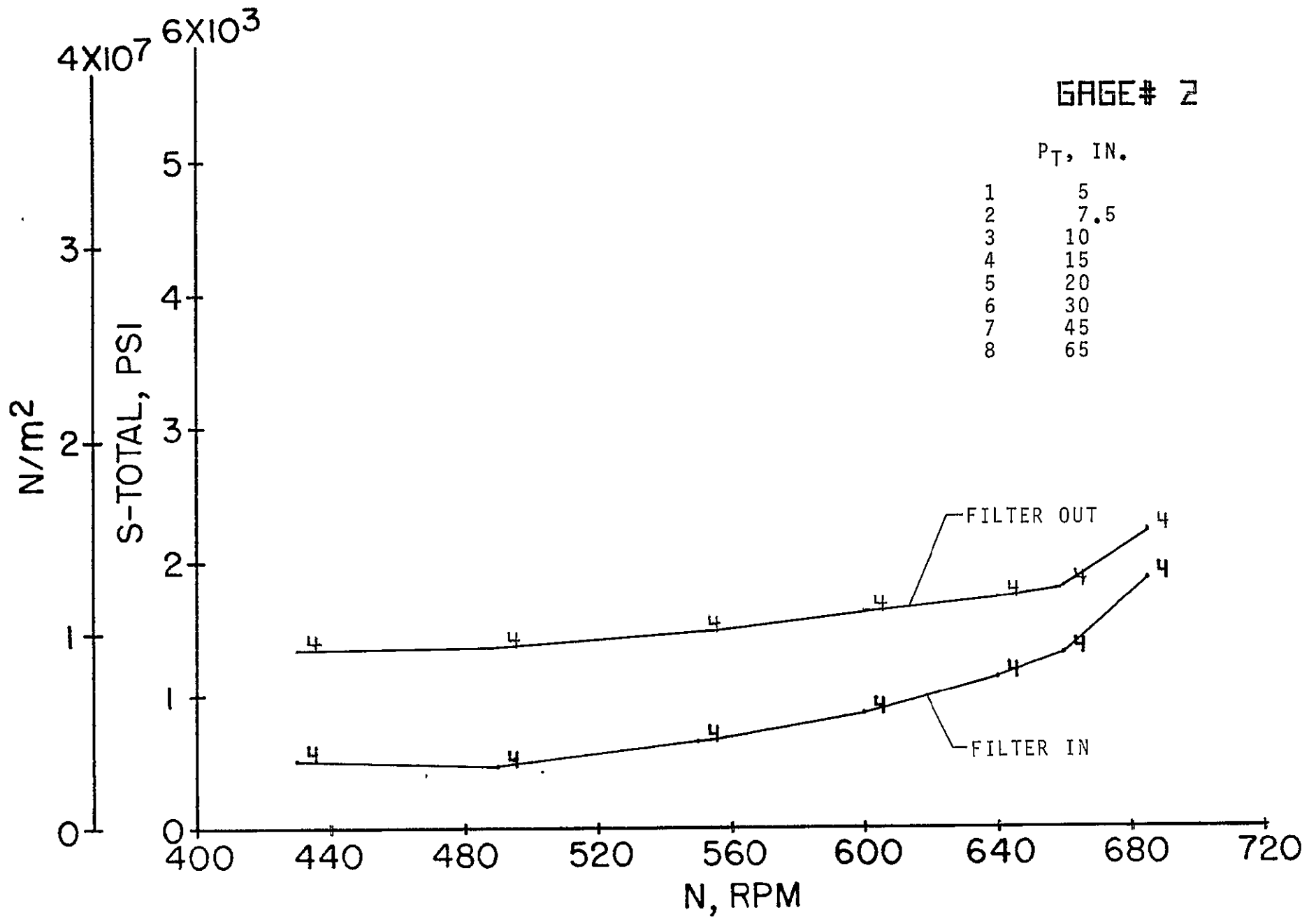
(b) Gage 2; $p_t = 50.80 \times 10^3$ N/m² (15 in. Hg).
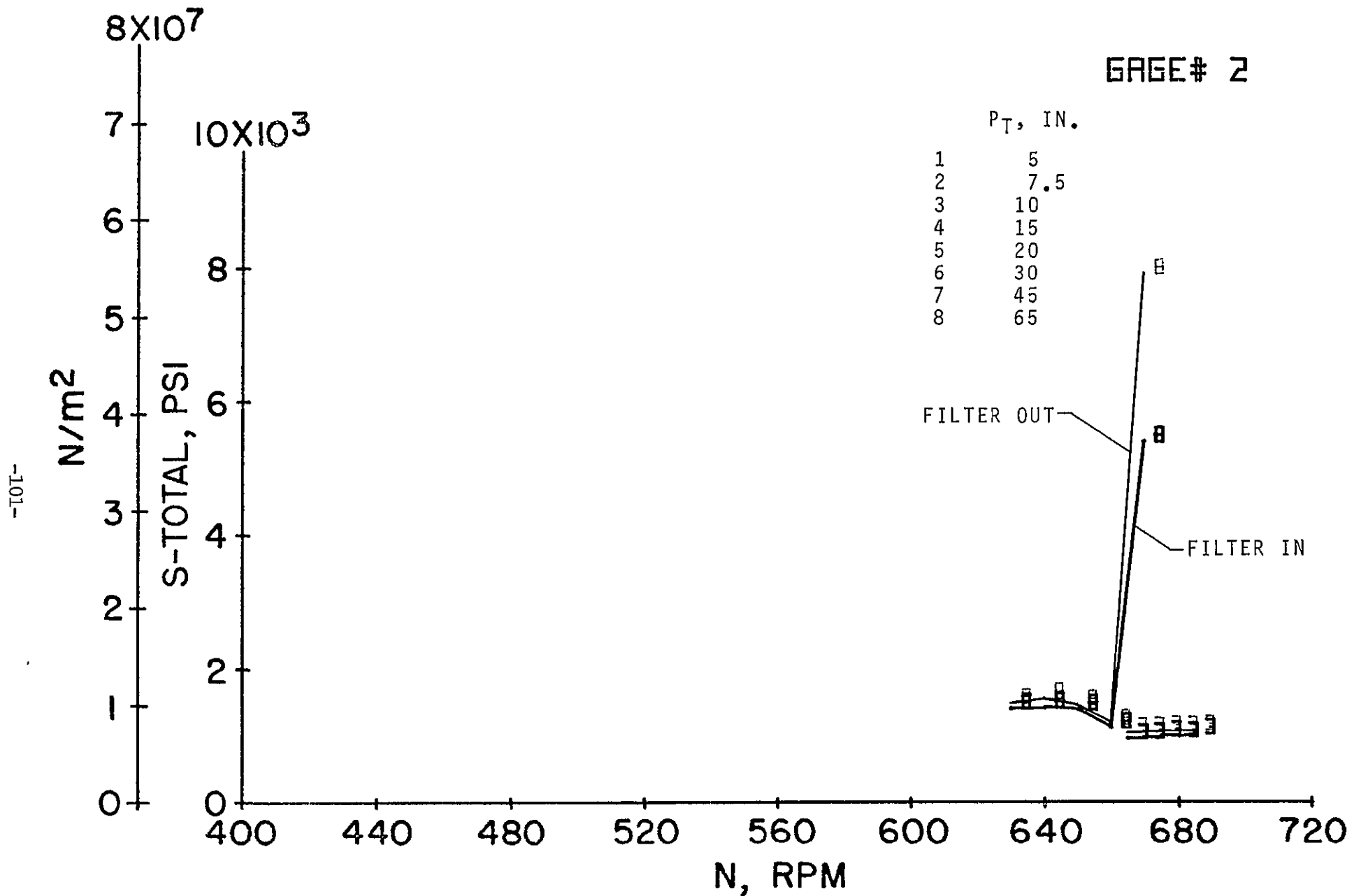
Figure 9.- Continued.

(c) Gage 2; $p_t = 33,86$ and 220.12×10^3 N/m^2 (10 and 65 in. Hg).

Figure 9.- Continued.

(d) Gage 4; p_t = 25.40X10^3 N/m^2 (7.5 in. Hg).
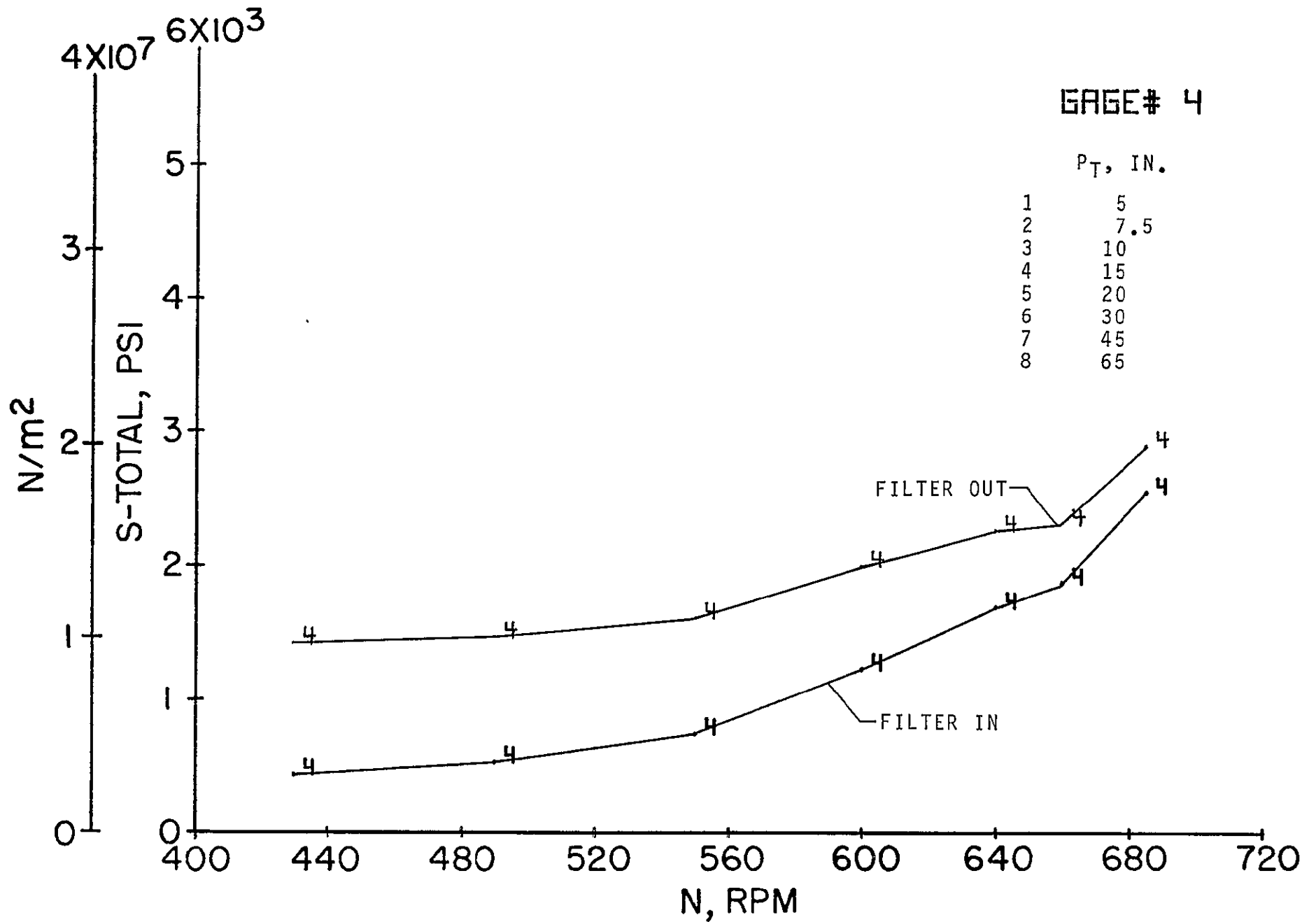
Figure 9.- Continued.

(e) Gage 4; $p_t = 50.80 \times 10^3$ N/m^2 (15 in. Hg).
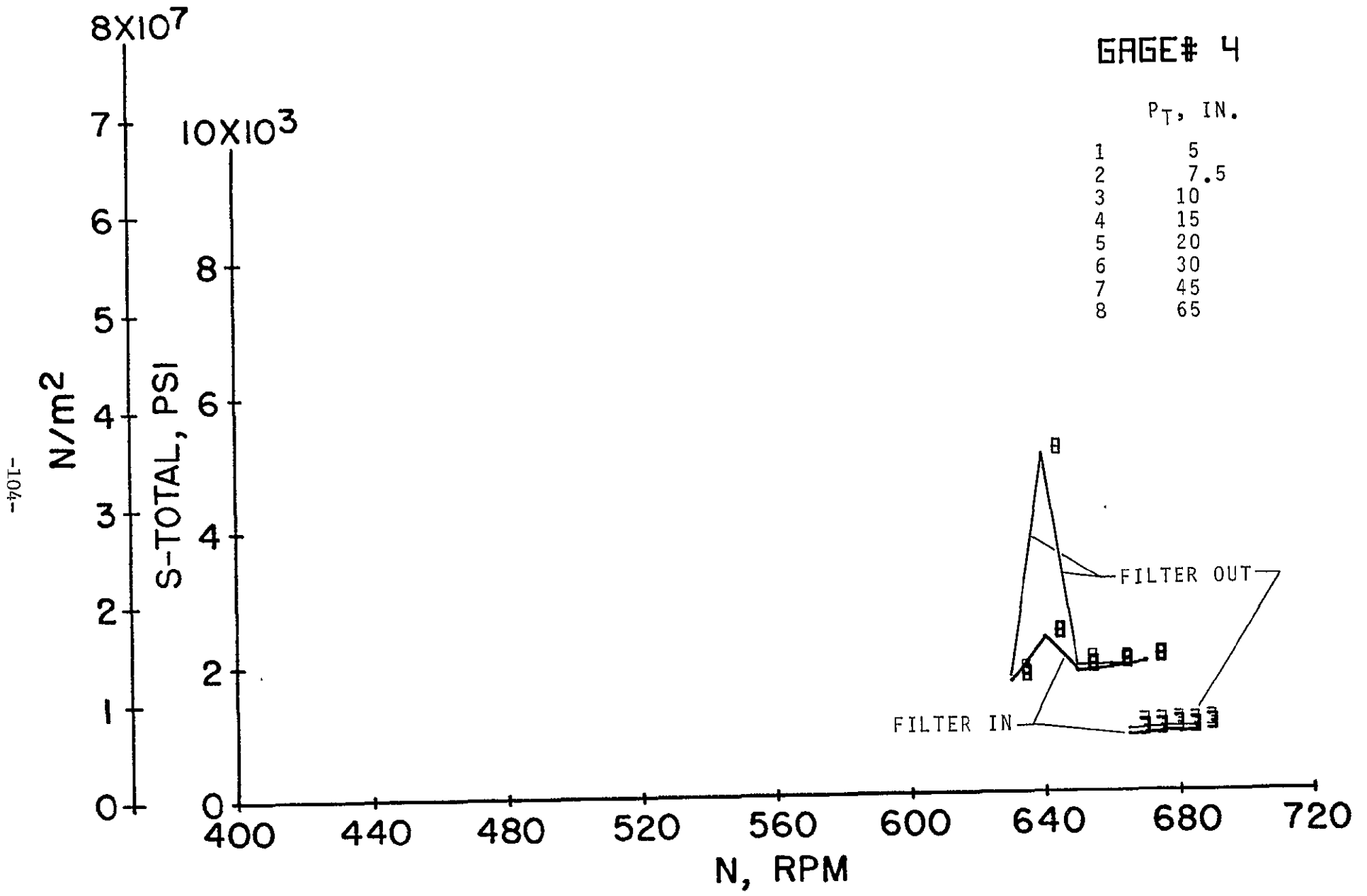
Figure 9.- Continued.

(f) Gage 4; p_t = 33.86 and 220.12X10^3 N/m^2 (10 and 65 in. Hg).

Figure 9.- Continued.

(g) Gage 11; p_t = 25.40X10^3 N/m^2 (7.5 in. Hg).
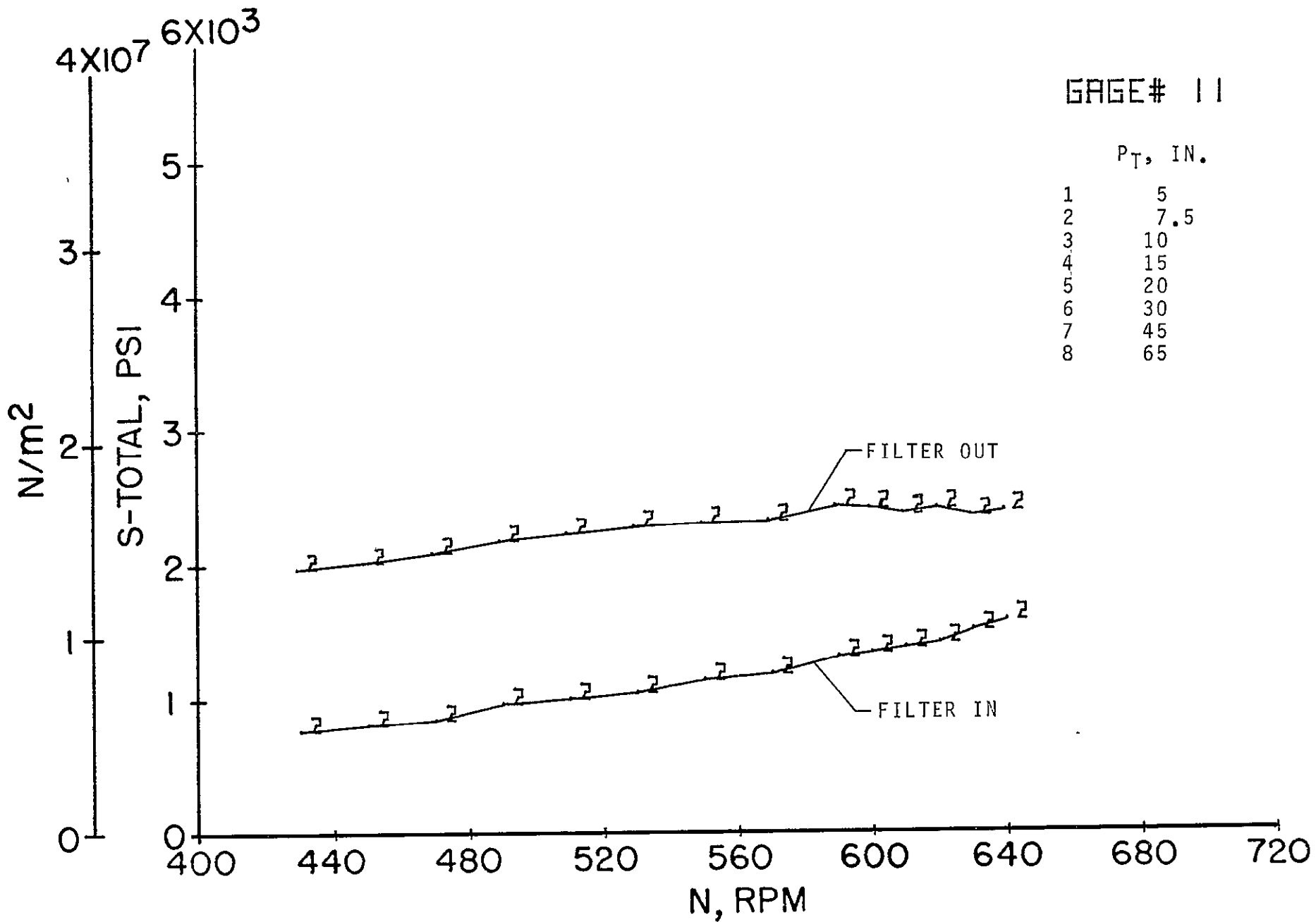
Figure 9 - Continued.

(h) Gage 11; p_t = 50.80X10^3 N/m^2 (15 in. Hg).
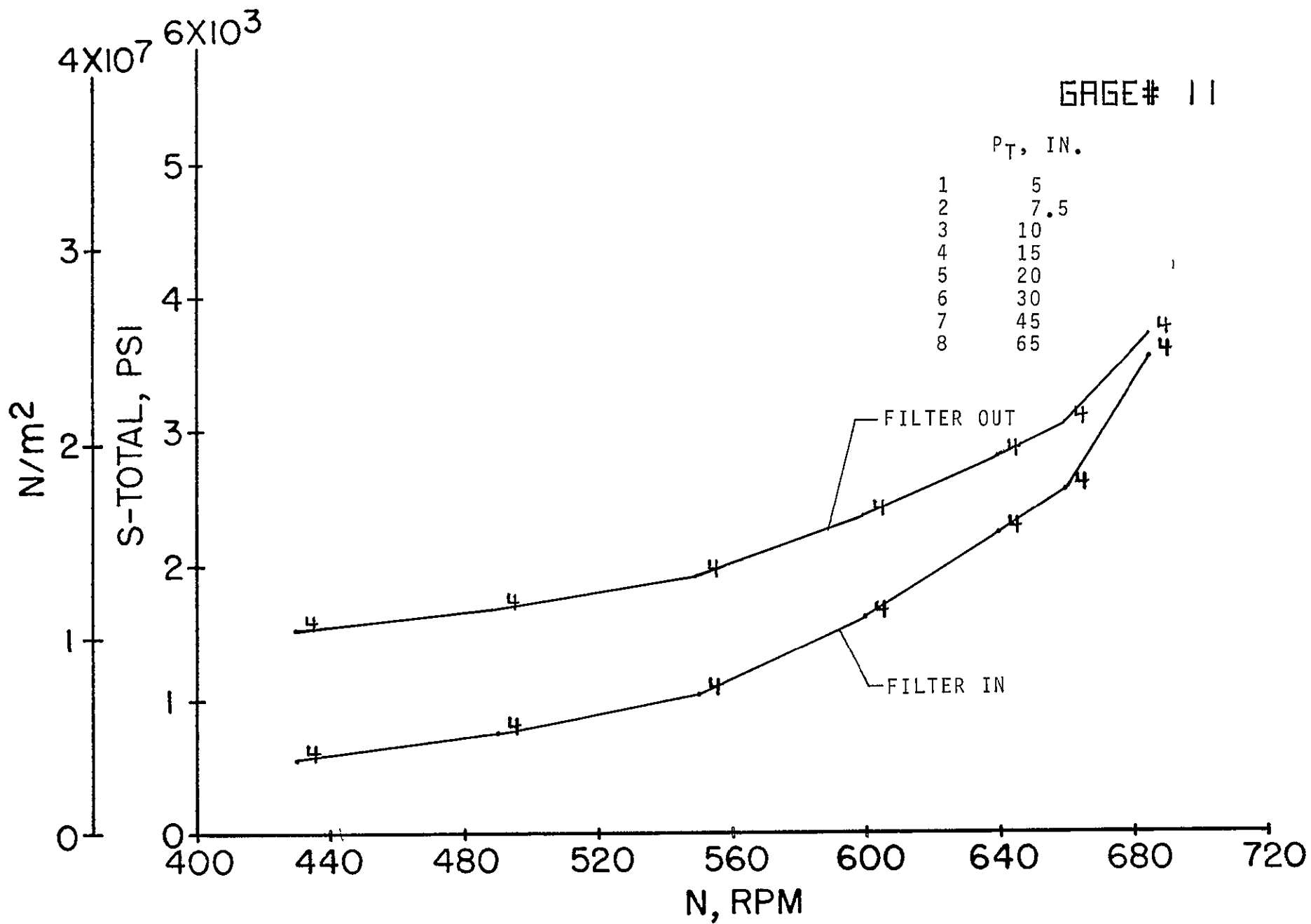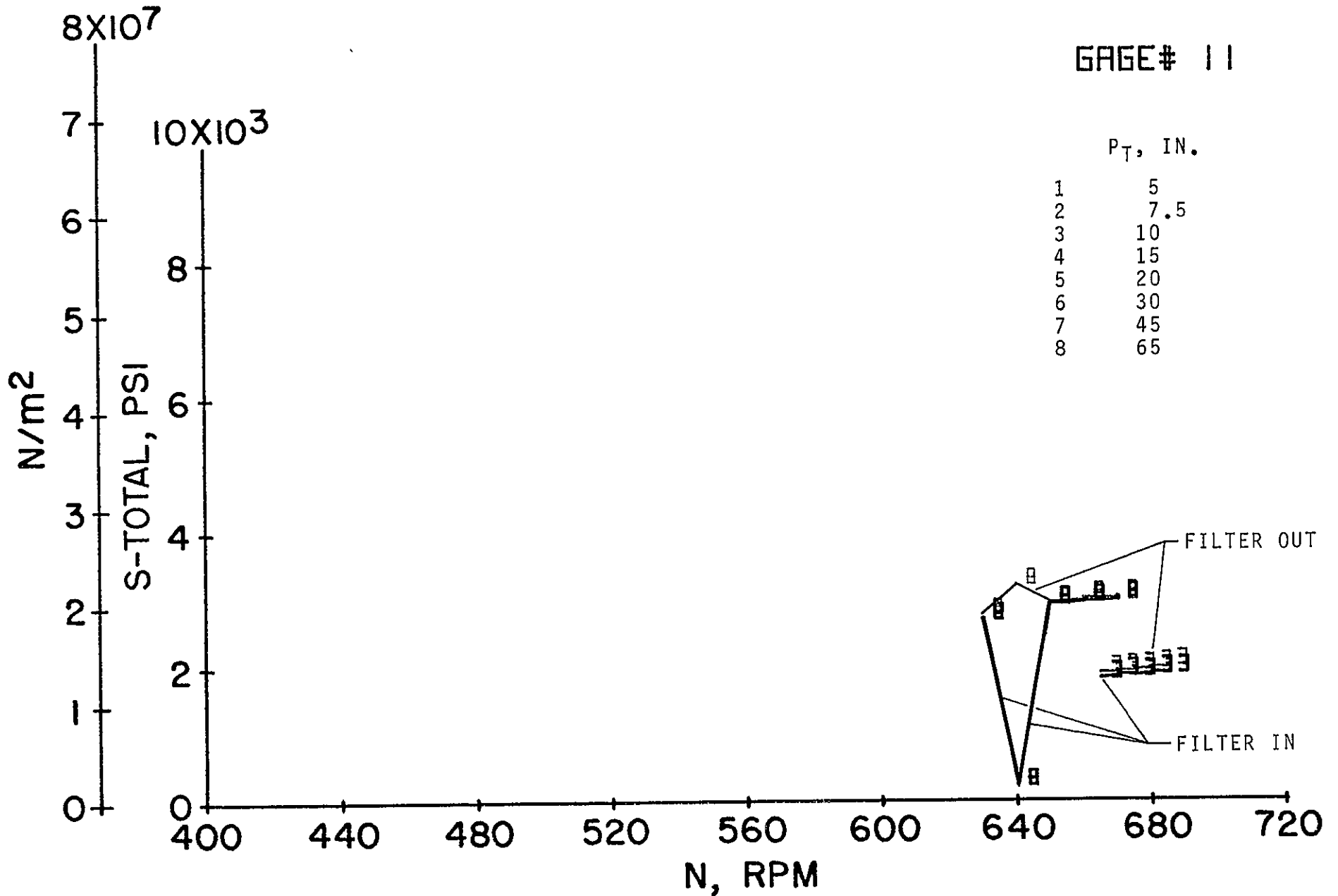
Figure 9.- Continued.

(i) Gage 11; p_t = 33.86 and 220.12X10^3 N/m^2 (10 and 65 in. Hg).

Figure 9.- Continued.

(j) Gage 12; p_t = 25.40X10^3 N/m^2 (7.5 in. Hg).

Figure 9.- Continued.

(k) Gage 12; $p_t = 50.80 \times 10^3$ N/m^2 (15 in. Hg).

Figure 9.- Continued.
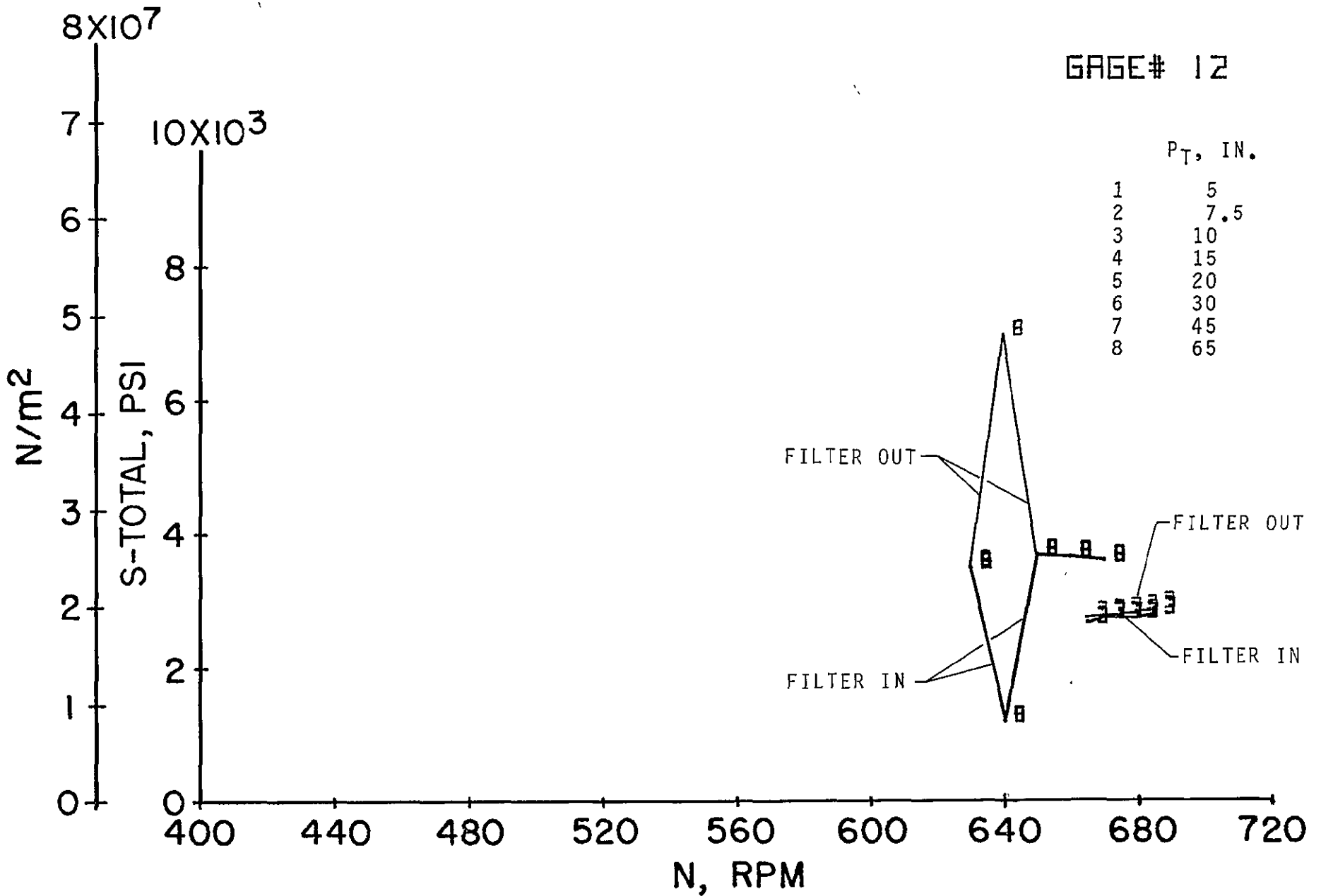
(1) Gage 12; p_t = 33.86 and 220.12X10^3 N/m^2 (10 and 65 in. Hg).

Figure 9.- Concluded.
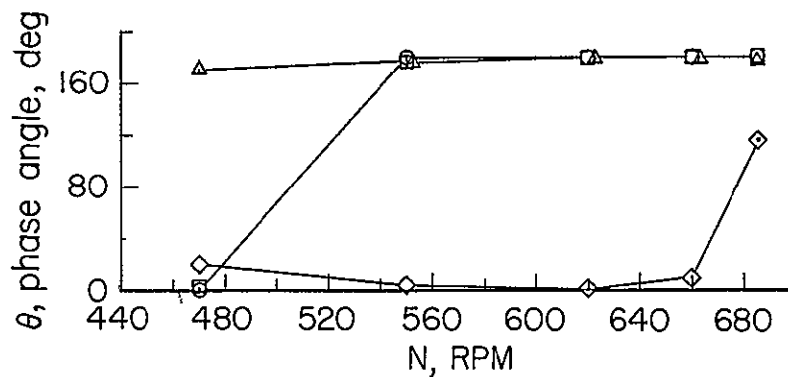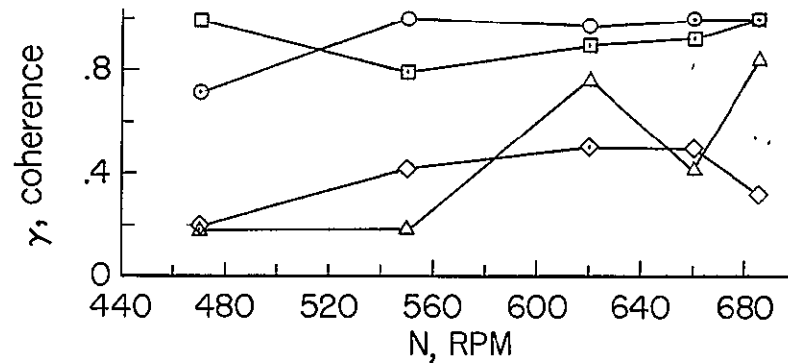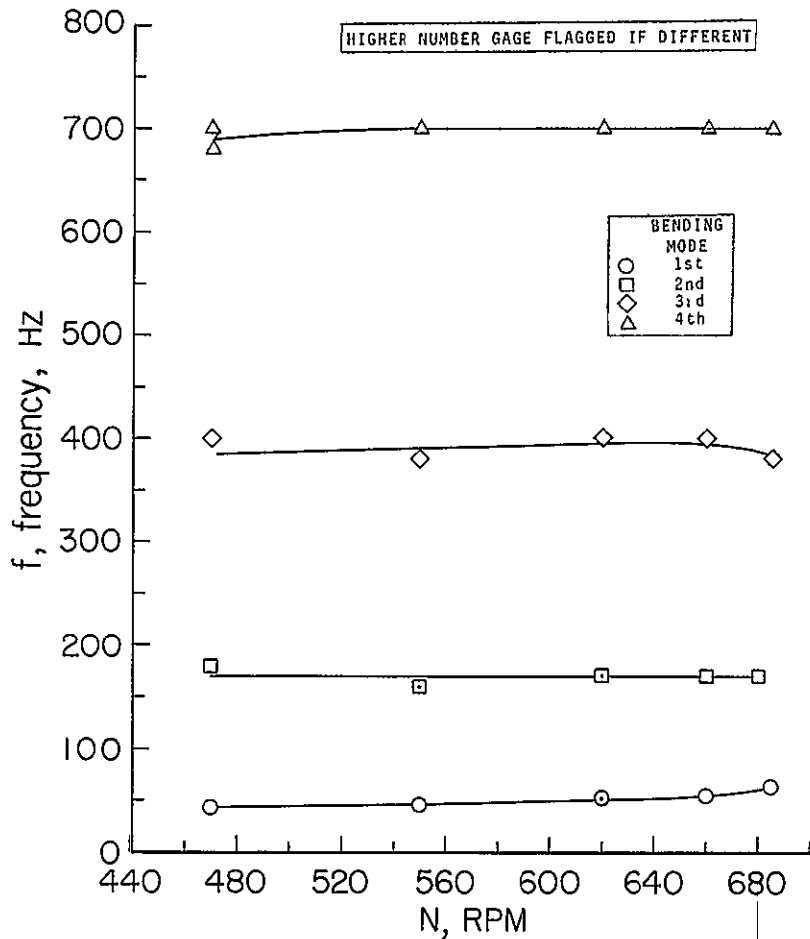
(a) Gages 4,5; p_t = 33.86X10^3 N/m^2 (10 in. Hg).

Figure 10.- Variation of the frequency, phase angle, and coherence with compressor speed for the first four bending modes of the blade for various gage combinations and tunnel total pressures.
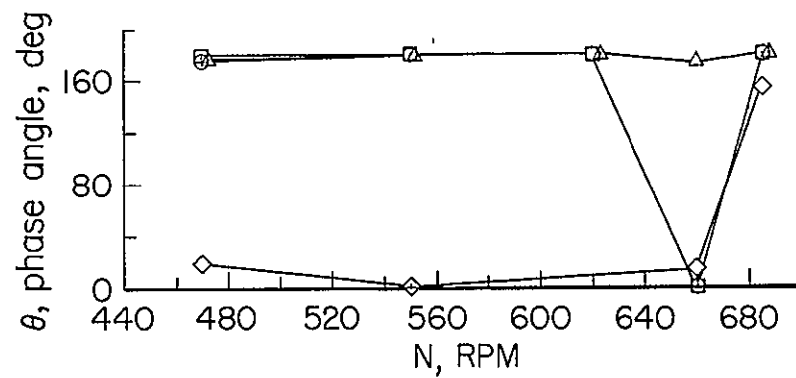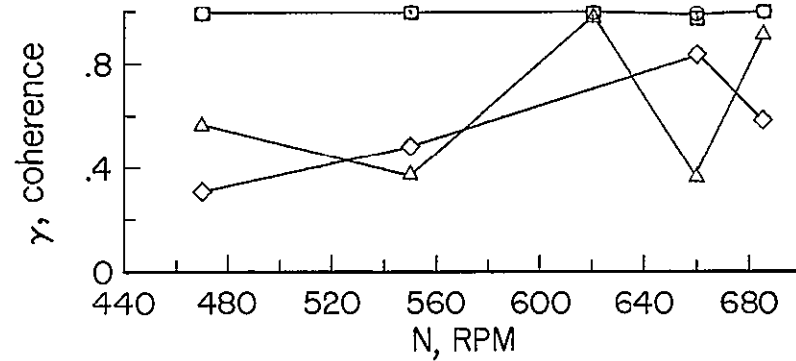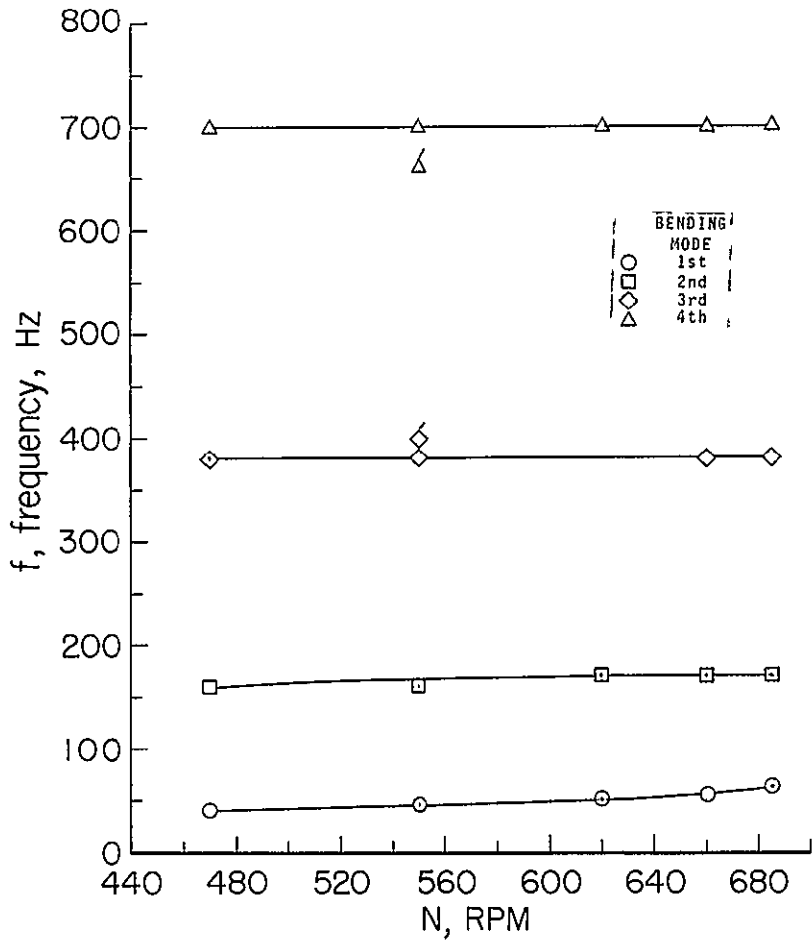
(b) Gages 4,5; p_t = 67.73X10^3 N/m^2 (20 in. Hg).

Figure 10.- Continued.
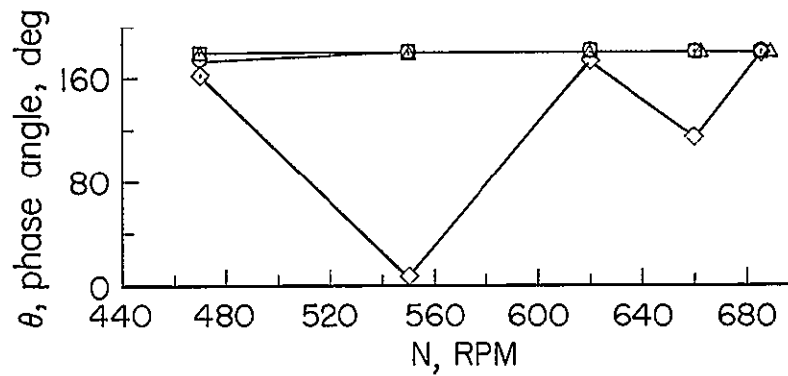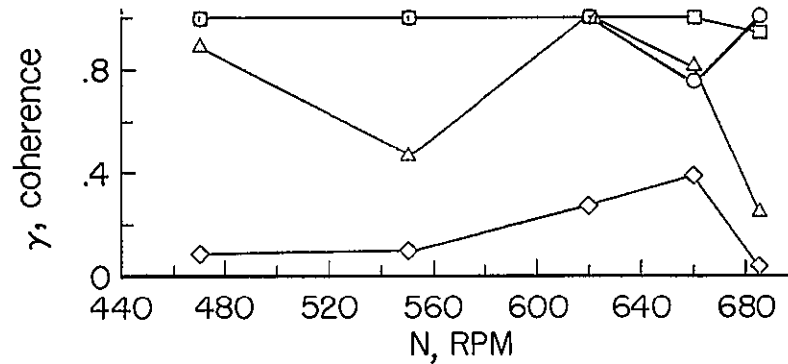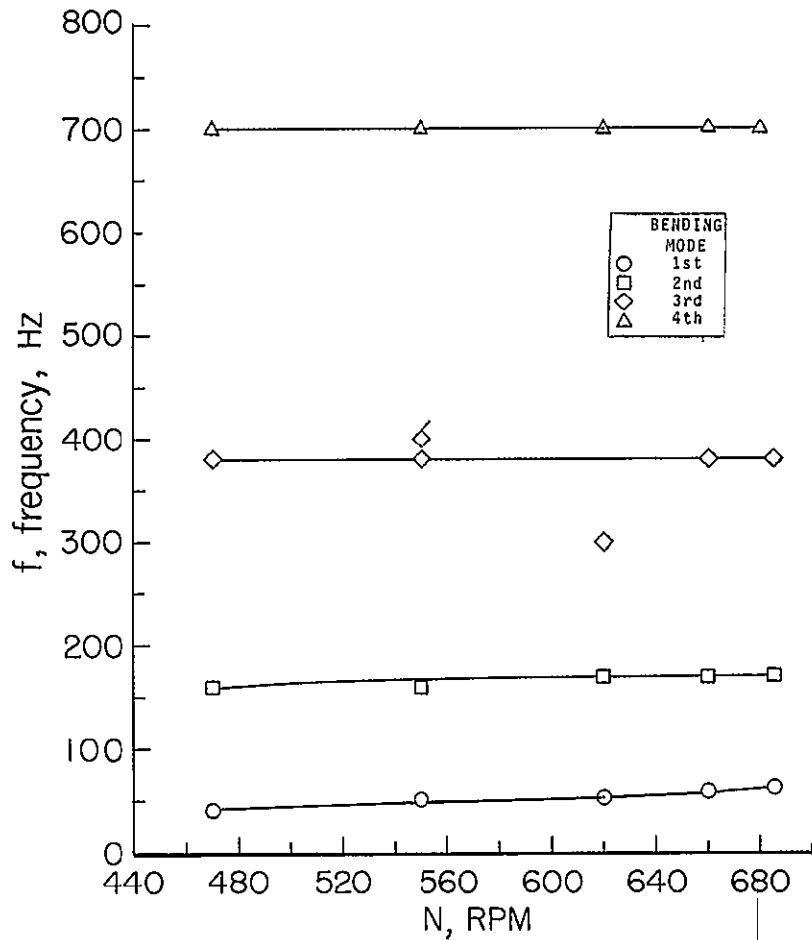
(c) Gages 4,5; p_t = 101.59X10^3 N/m^2 (30 in. Hg).

Figure 10.- Continued.
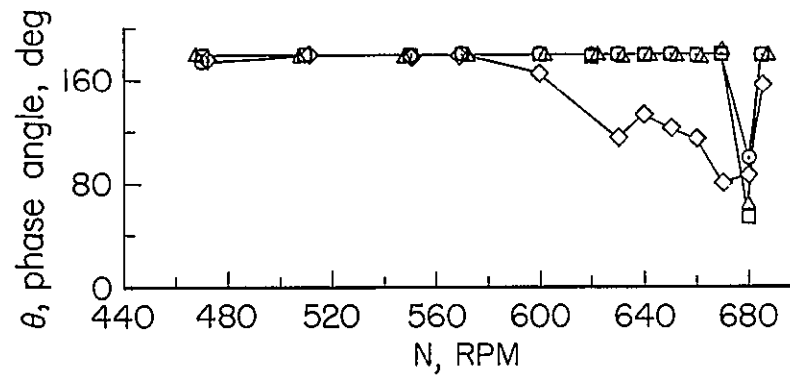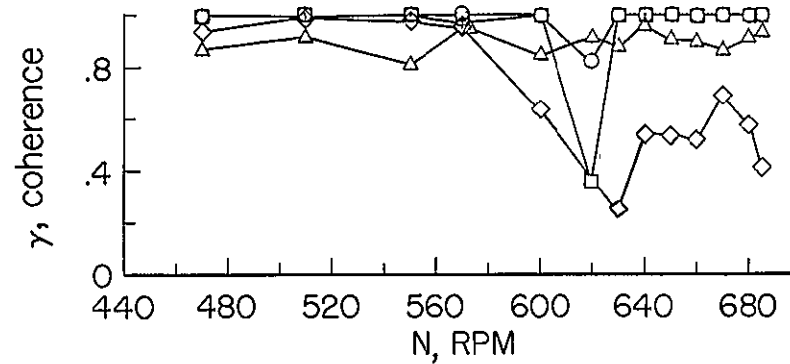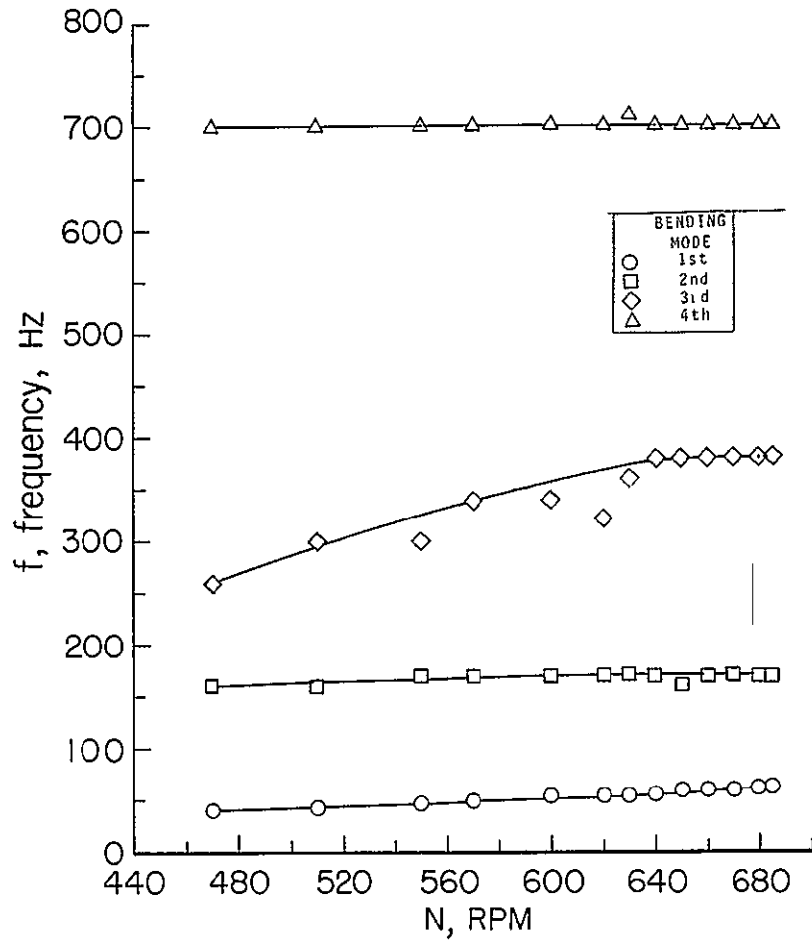
(d) Gages 4,5; p_t = 152.39X10^3 N/m^2 (45 in. Hg).

Figure 10.- Continued.
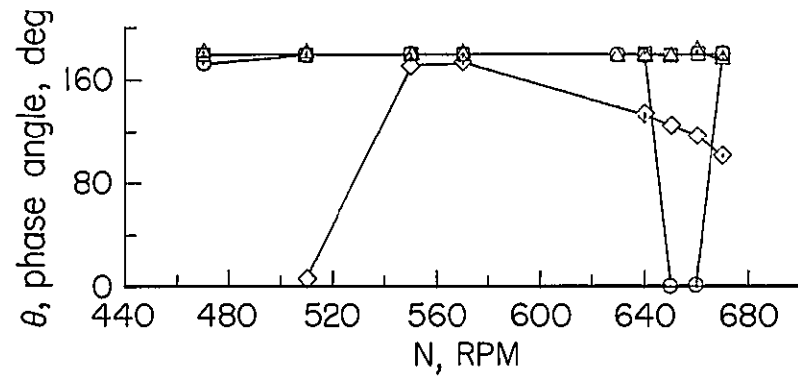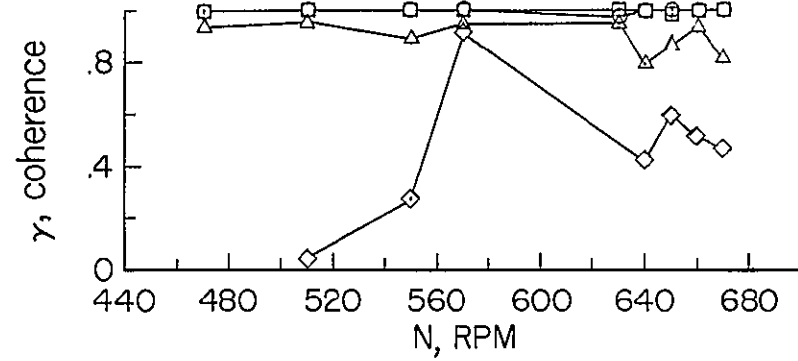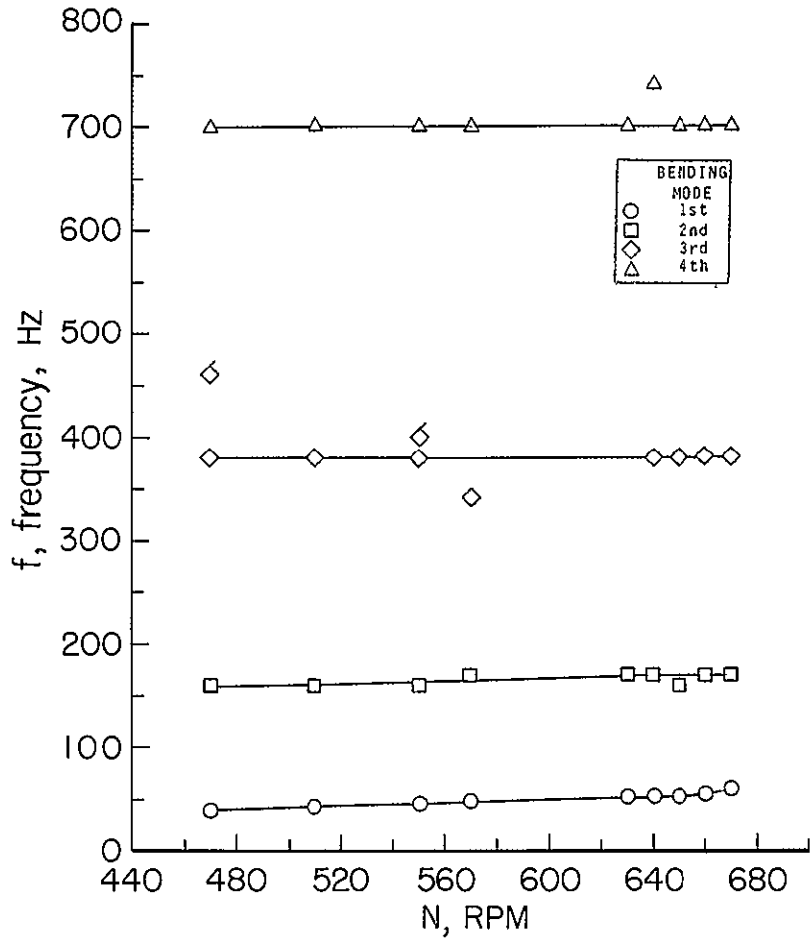
(e) Gages 4,5; p_t = 220.12X10^3 N/m^2 (65 in. Hg).

Figure 10.- Continued.
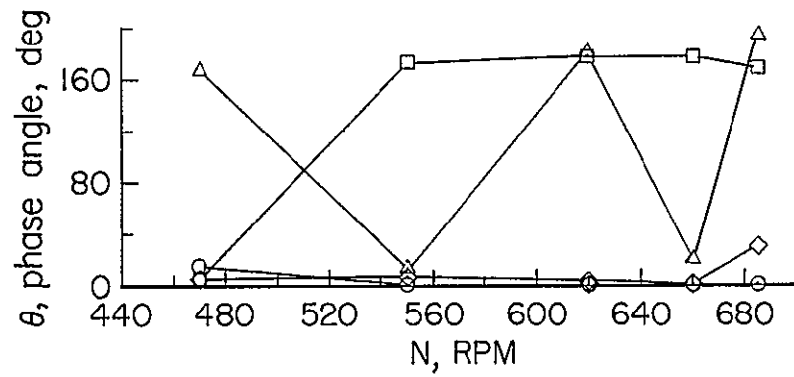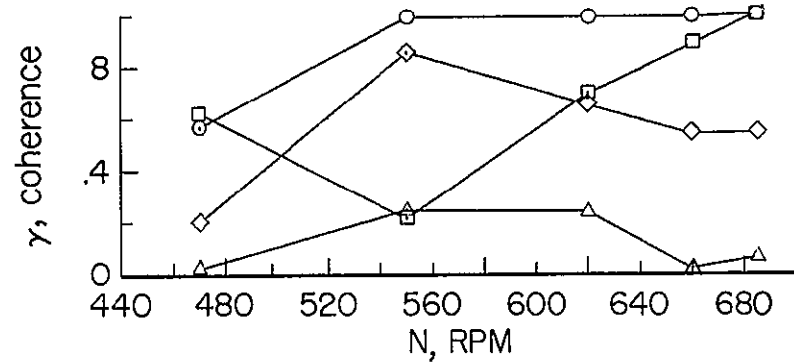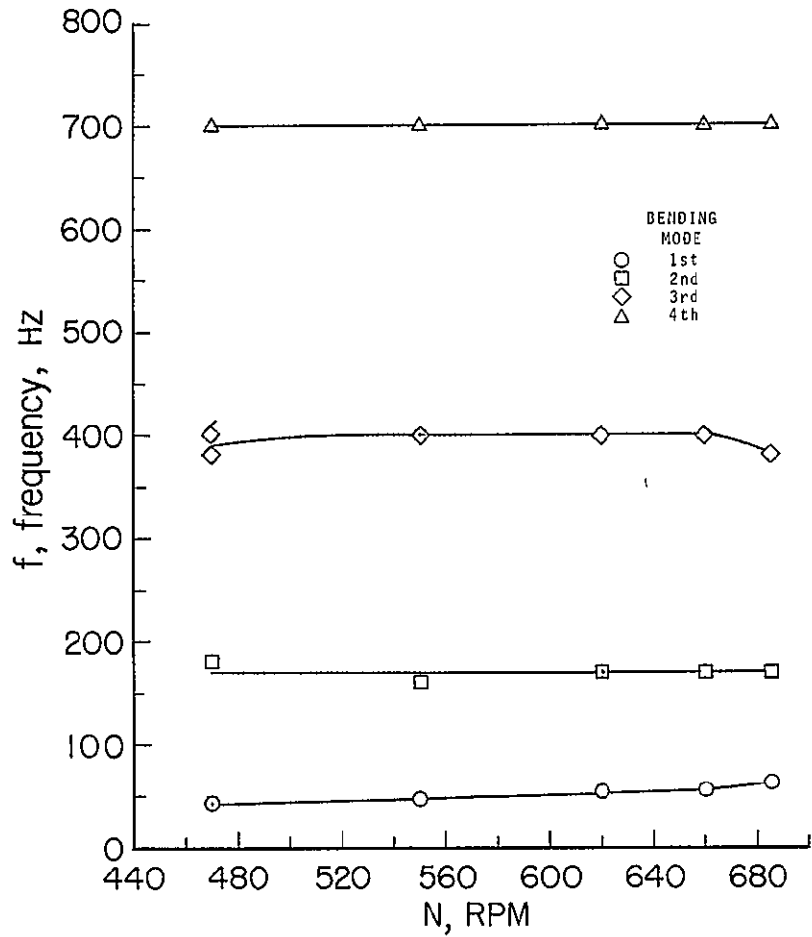
(f) Gages 6,12; $p_t = 33.86 \times 10^3$ N/m^2 (10 in. Hg).

Figure 10.- Continued.
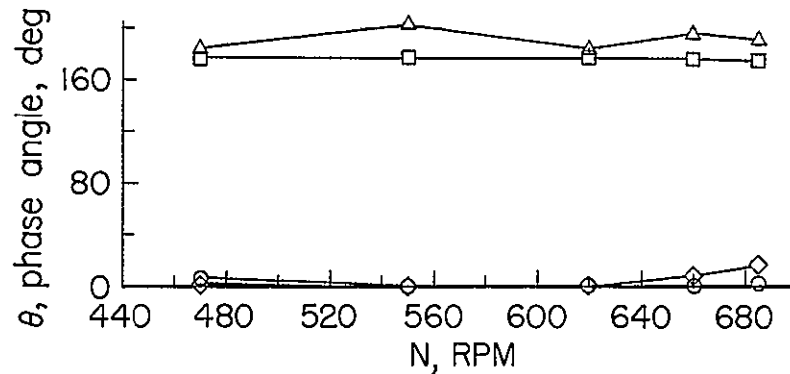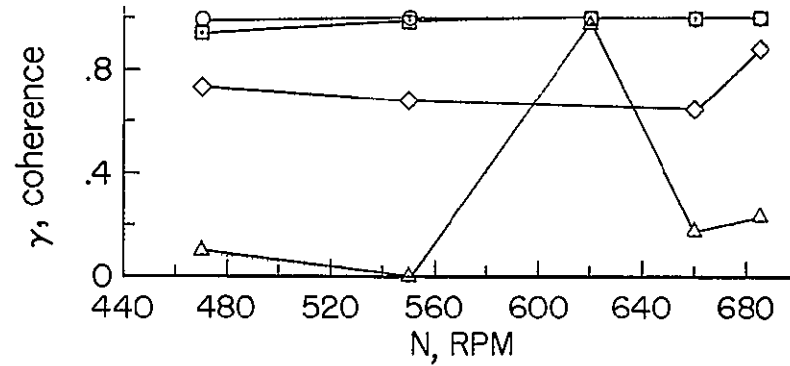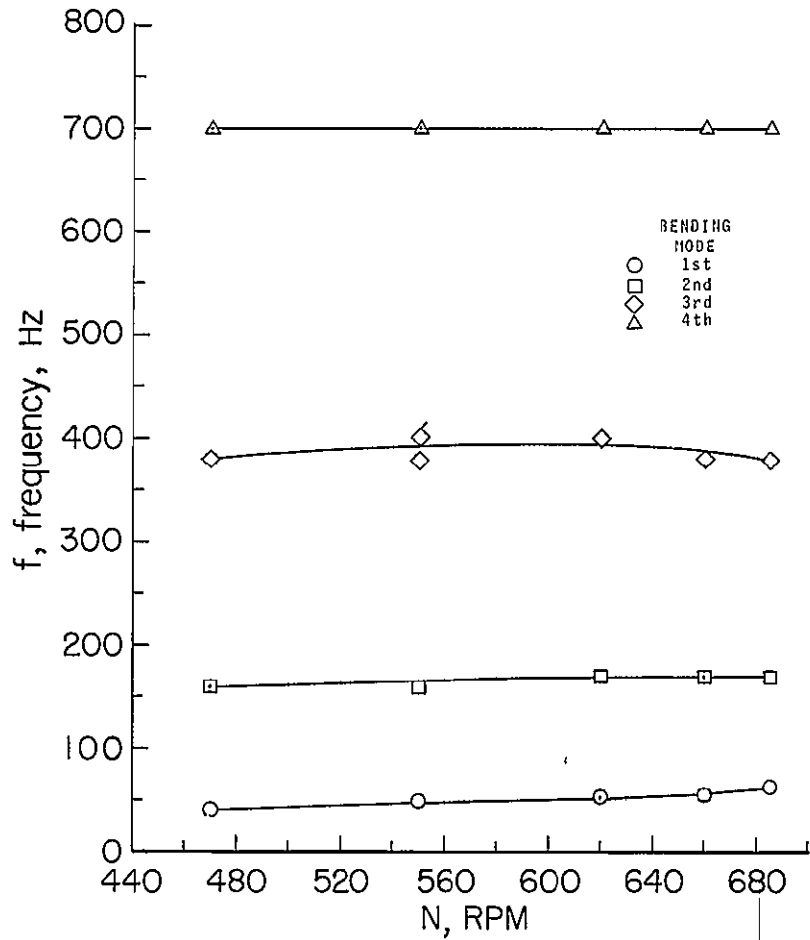
(g) Gages 6,12; p_t = 67.73X10^3 N/m^2 (20 in. Hg).

Figure 10.- Continued.
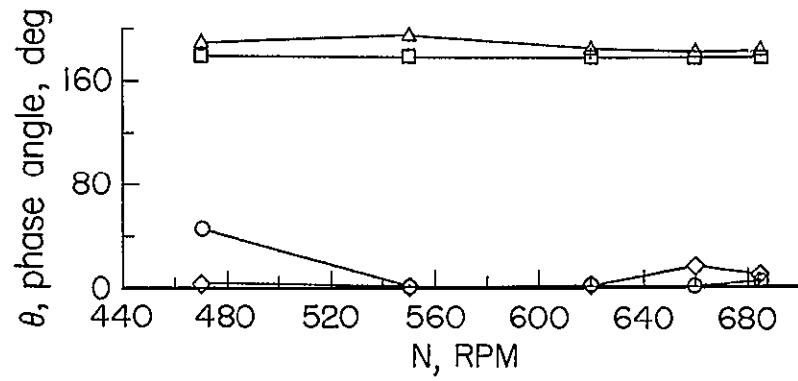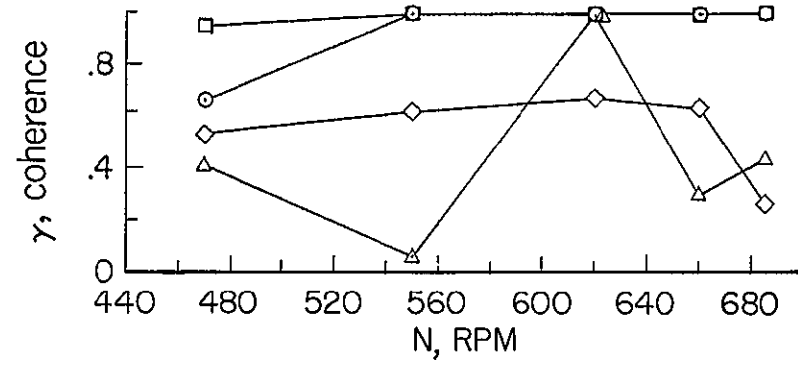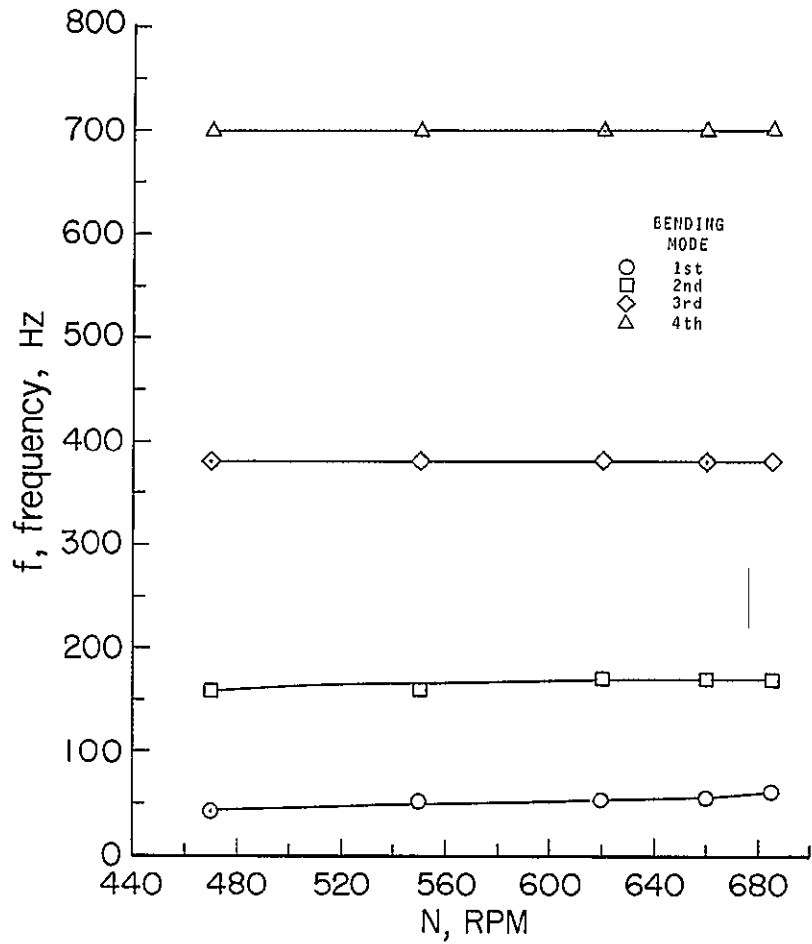
(h) Gages 6,12; p_t = 101.59X10^3 N/m^2 (30 in. Hg).

Figure 10.- Continued.
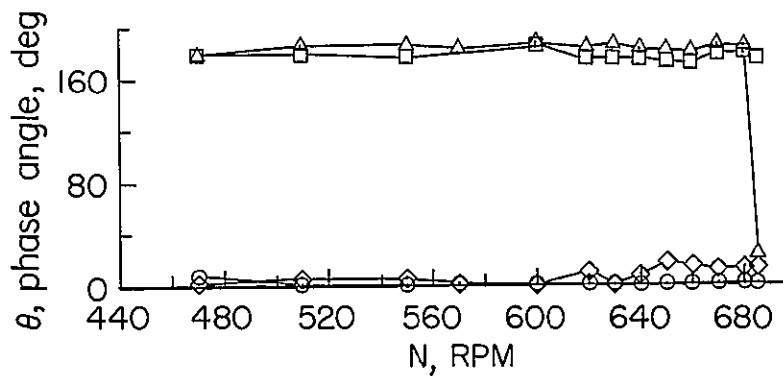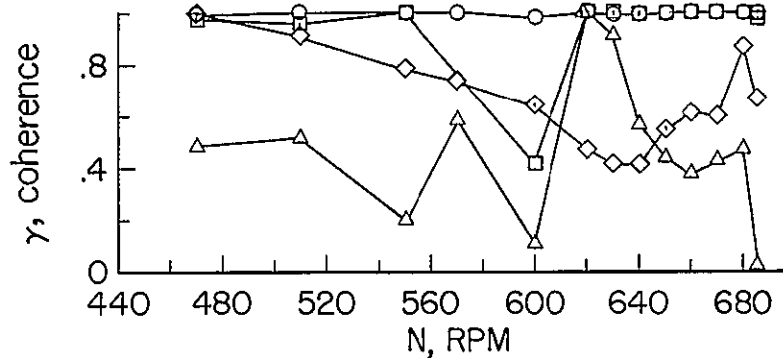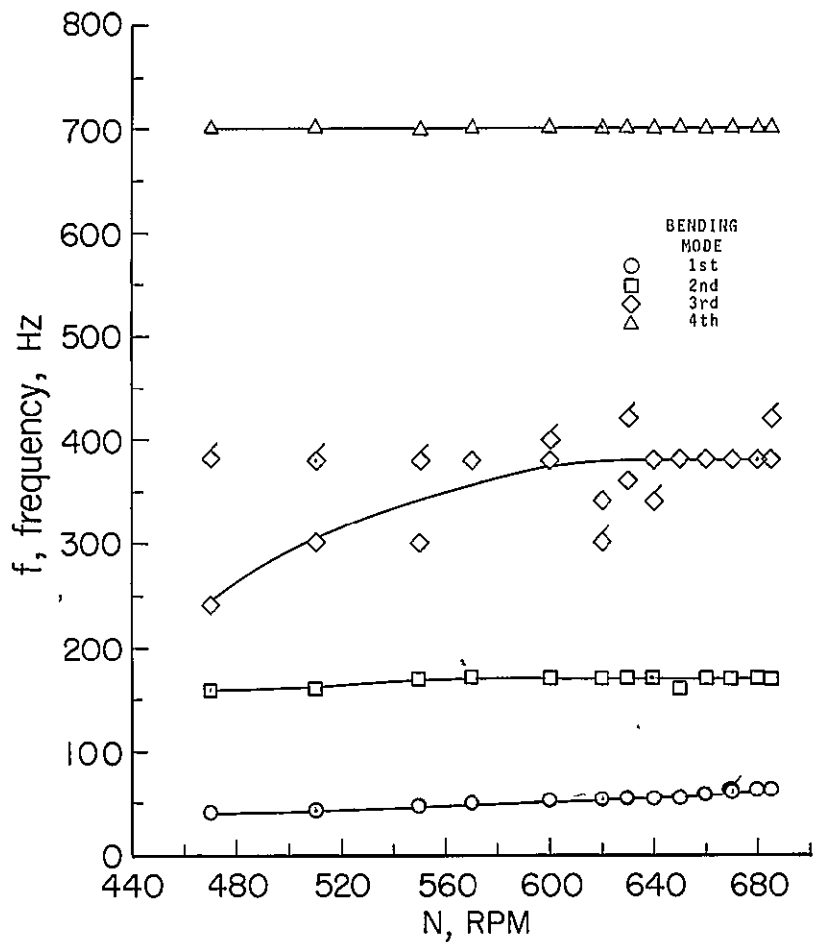
(i) Gages 6,12; p_t = 152.39X10^3 N/m^2 (45 in. Hg).

Figure 10.- Continued.
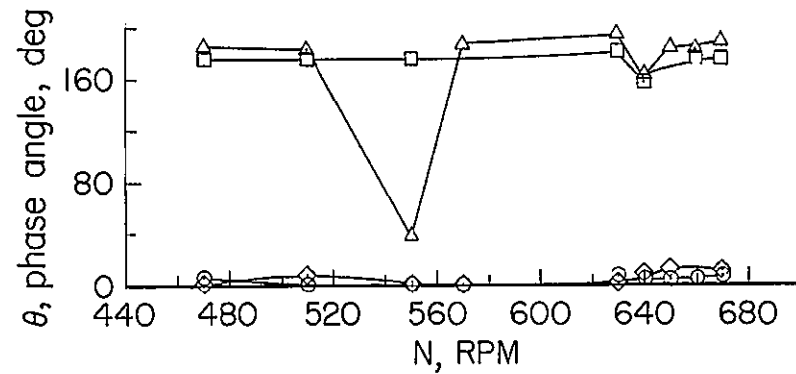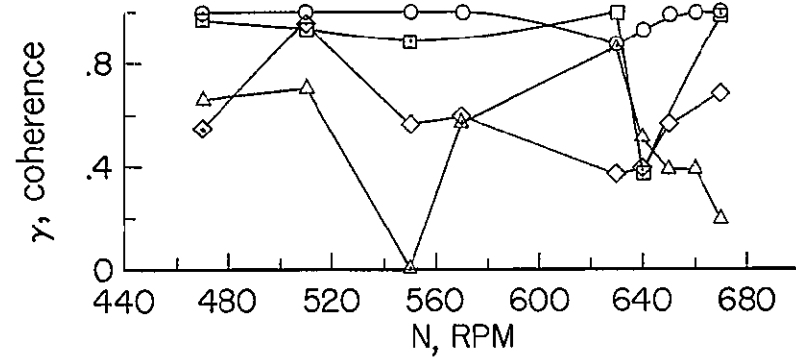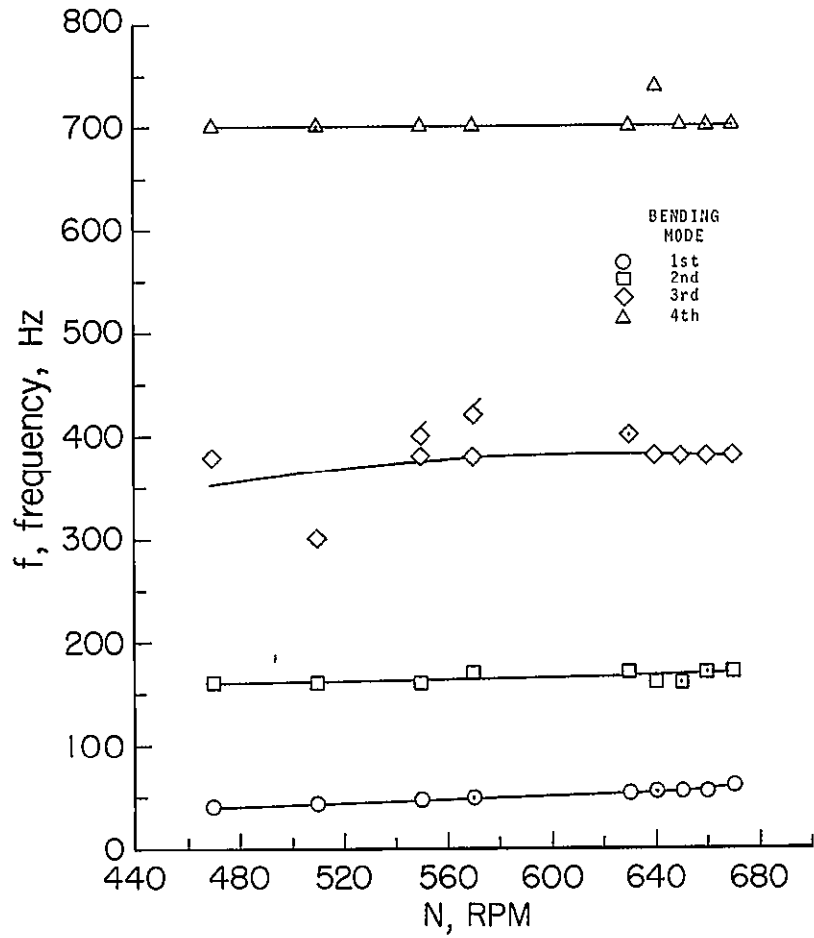
(j) Gages 6,12; p_t = 220.12X10^3 N/m^2 (65 in. Hg).

Figure 10.- Continued.
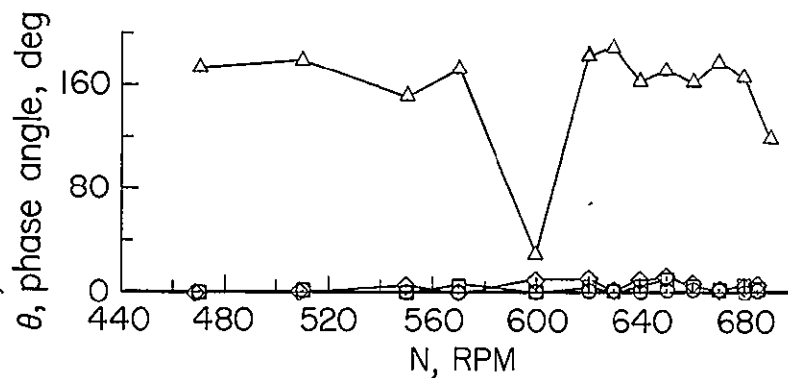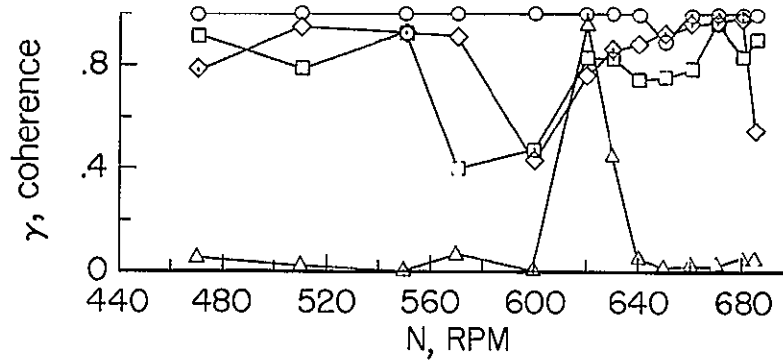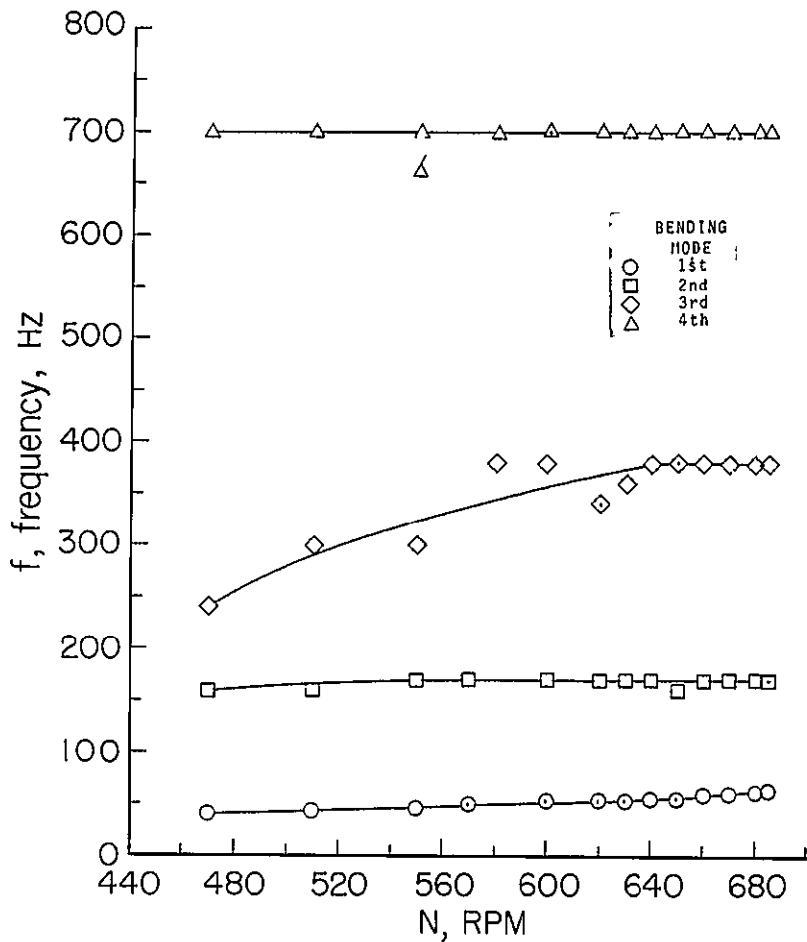
(k) Gages 6,11; p_t = 152.39X10^3 N/m^2 (45 in. Hg).

Figure 10.- Continued.
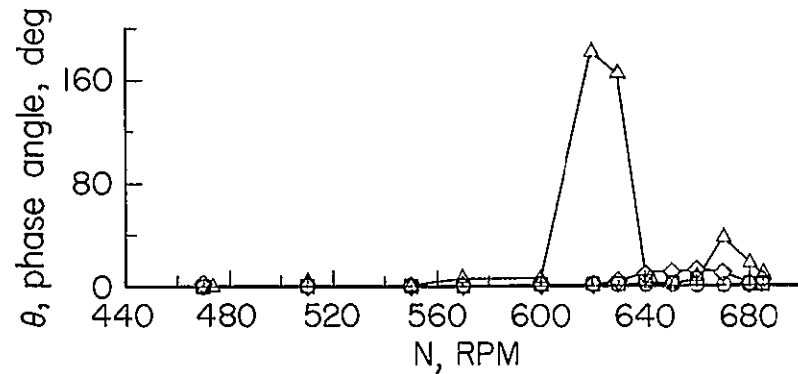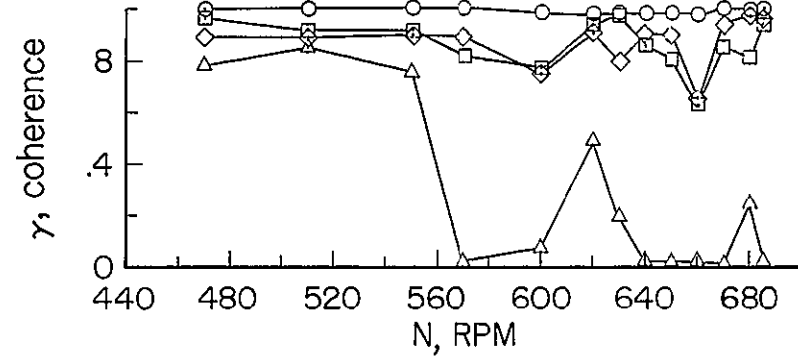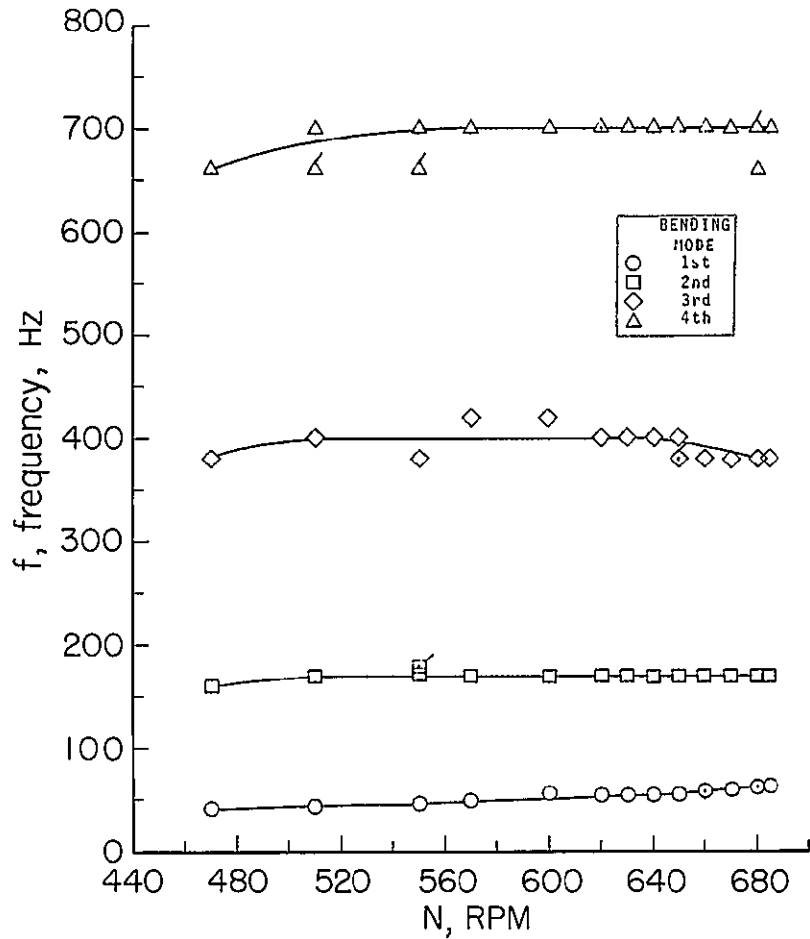
(1) Gages 13,14; p_t = 152.39X10³ N/m² (45 in. Hg).

Figure 10.- Continued.
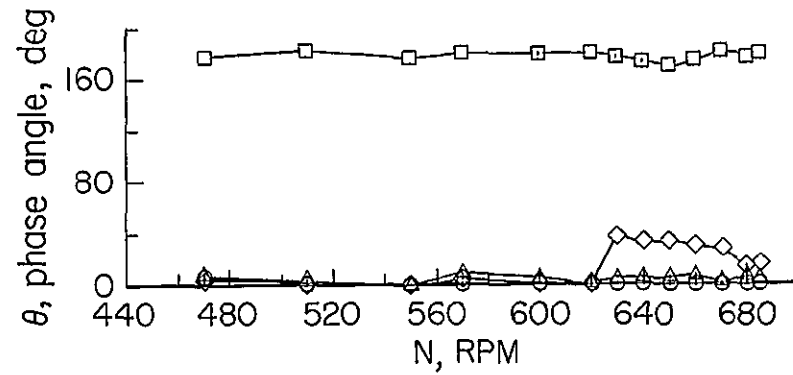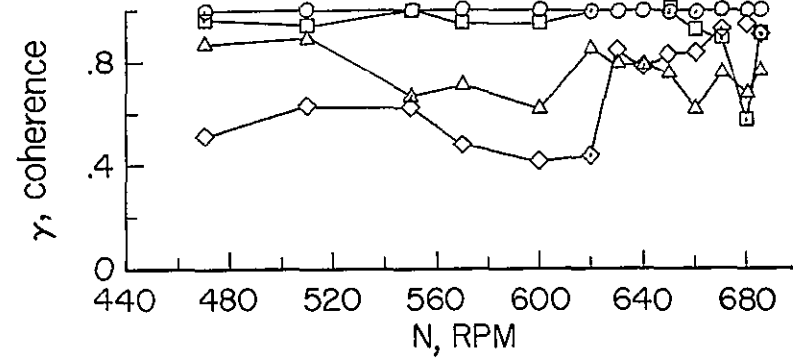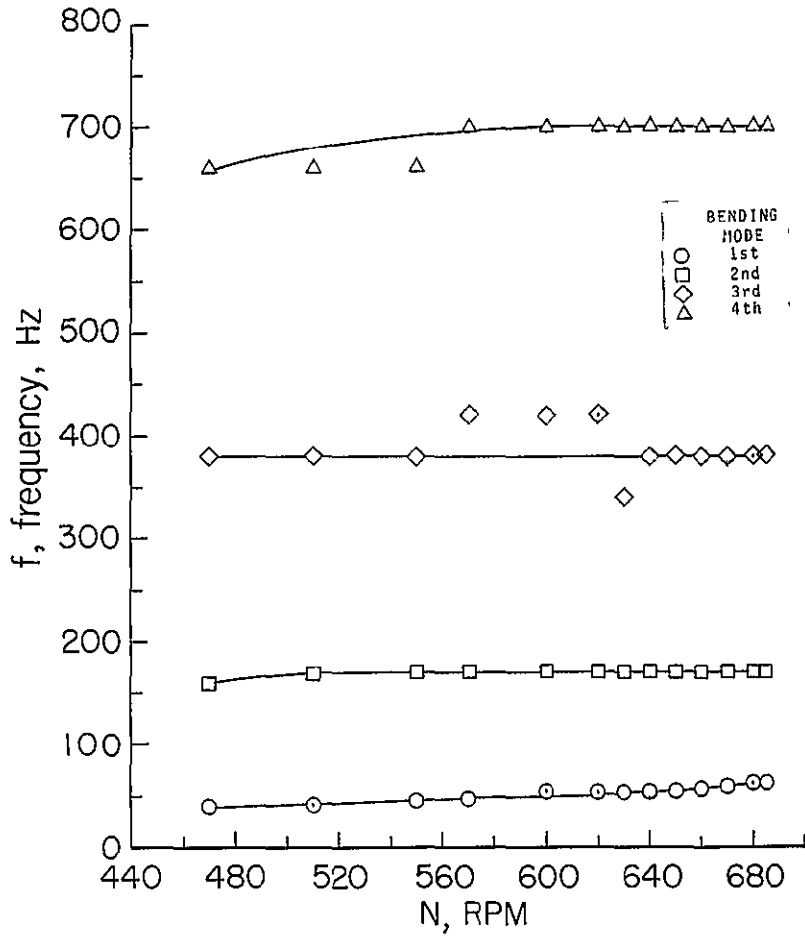
(m) Gages 14,15; $p_t = 152.39 \times 10^3$ N/m^2 (45 in. Hg).

Figure 10.- Concluded.
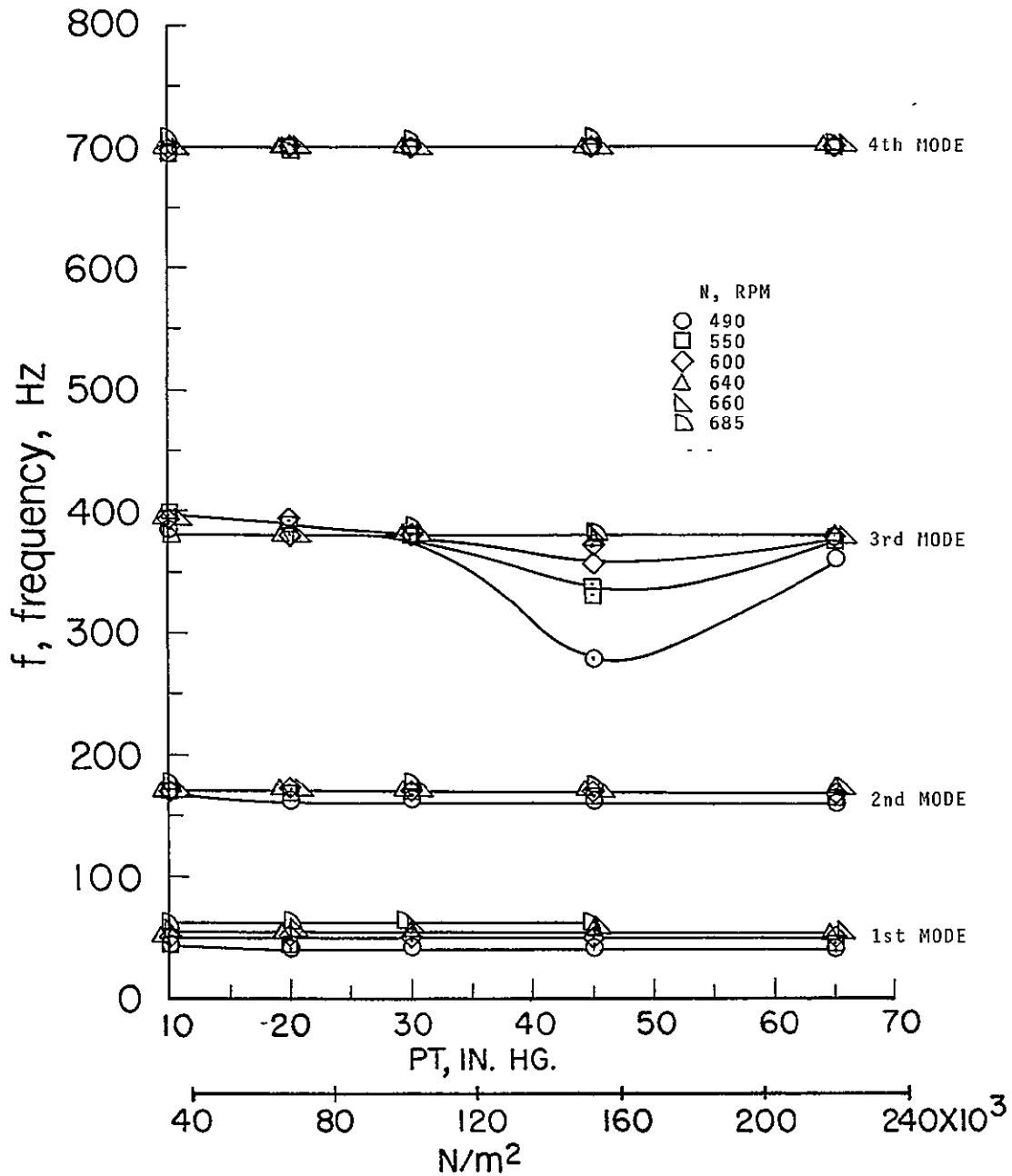
(a) |Modal| frequencies for gages 4,5,6,12.

Figure 11.- Variation of the frequency, phase angle, and coherence
for the first four bending modes of the blade with tunnel total
pressure for various gage combinations and compressor speeds.
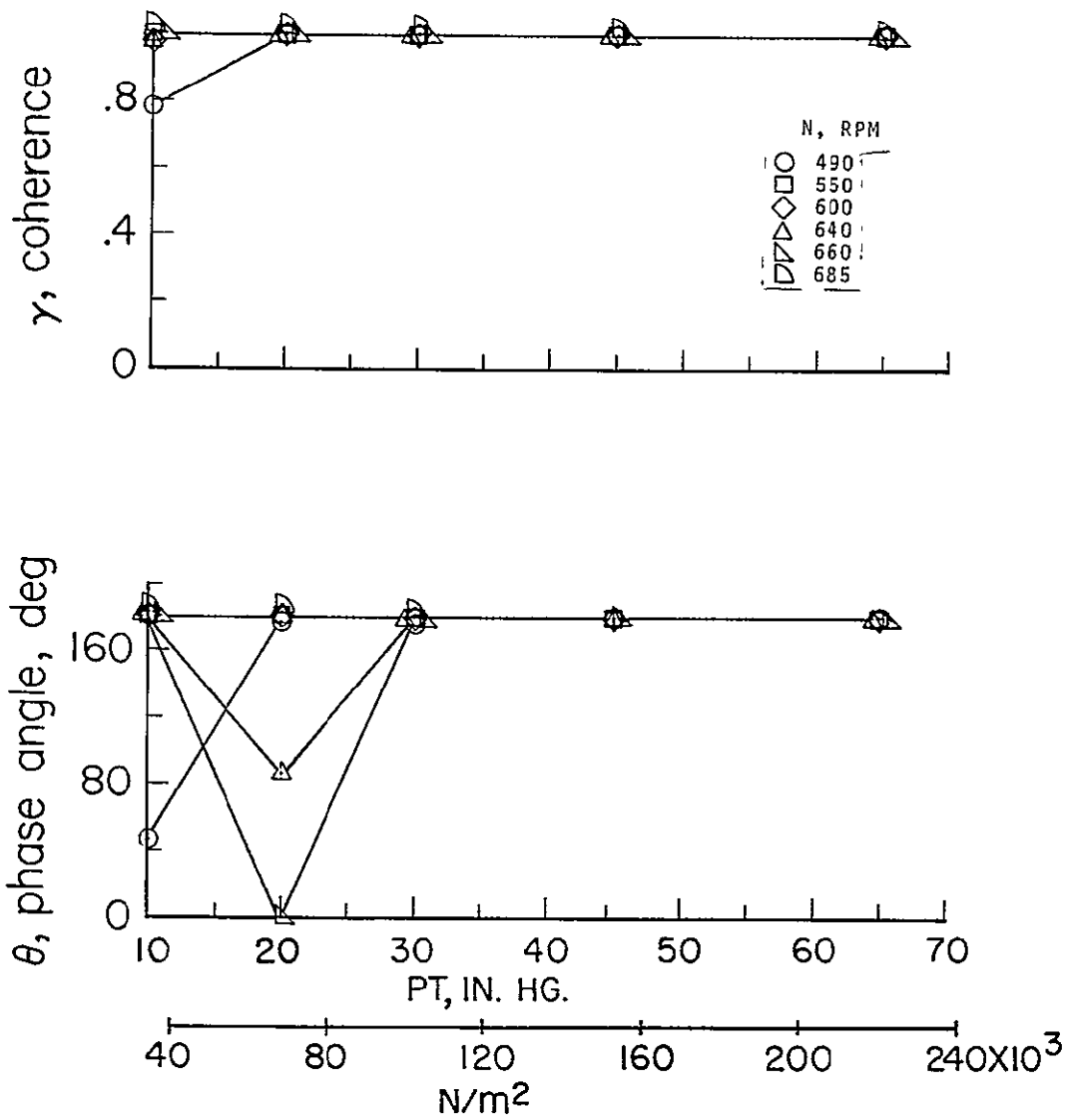
(b) 1st mode θ and γ for gages 4,5.

Figure 11.- Continued.
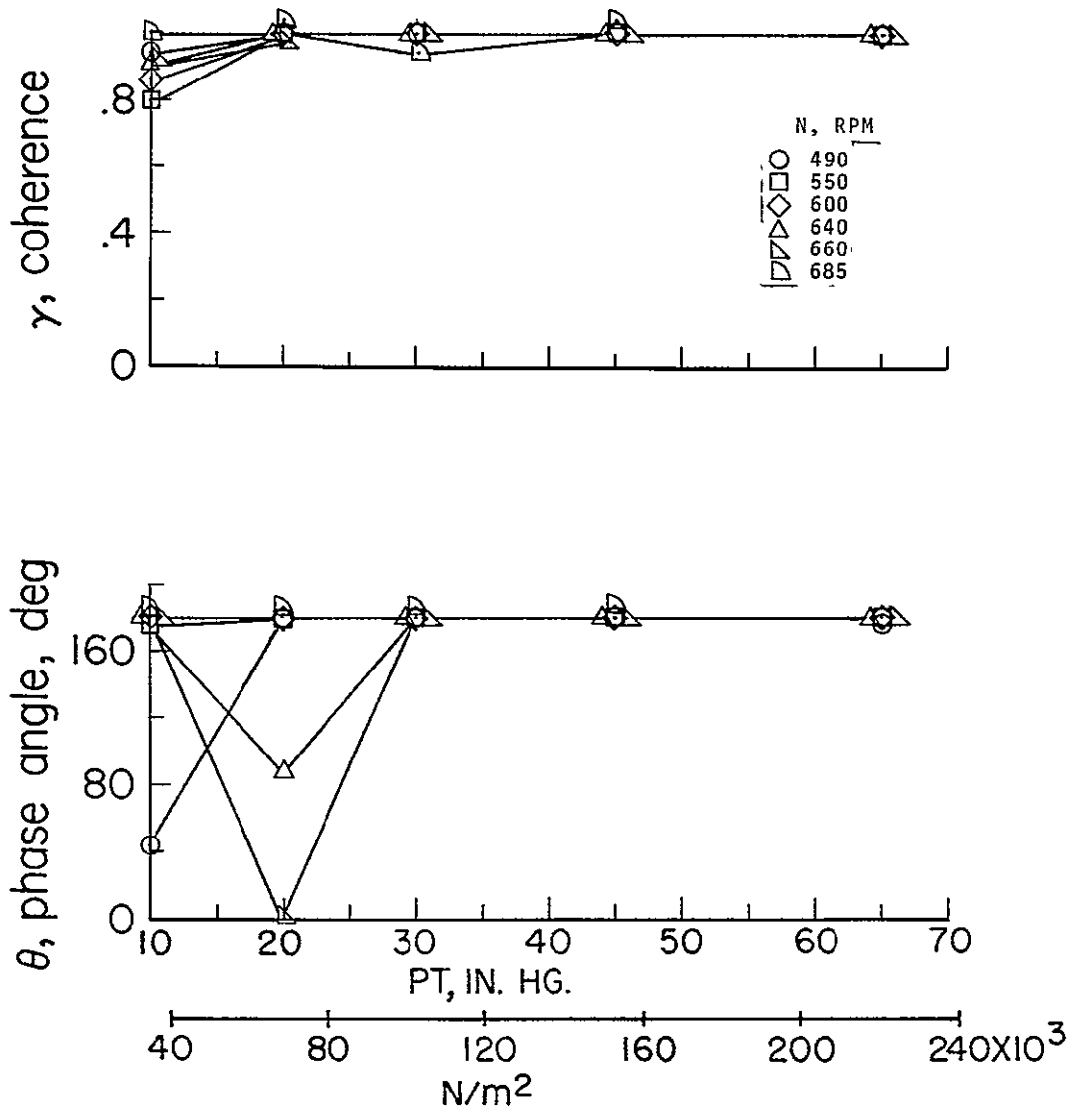
(c) 2nd Mode θ and γ for gages 4,5.

Figure 11.- Continued.
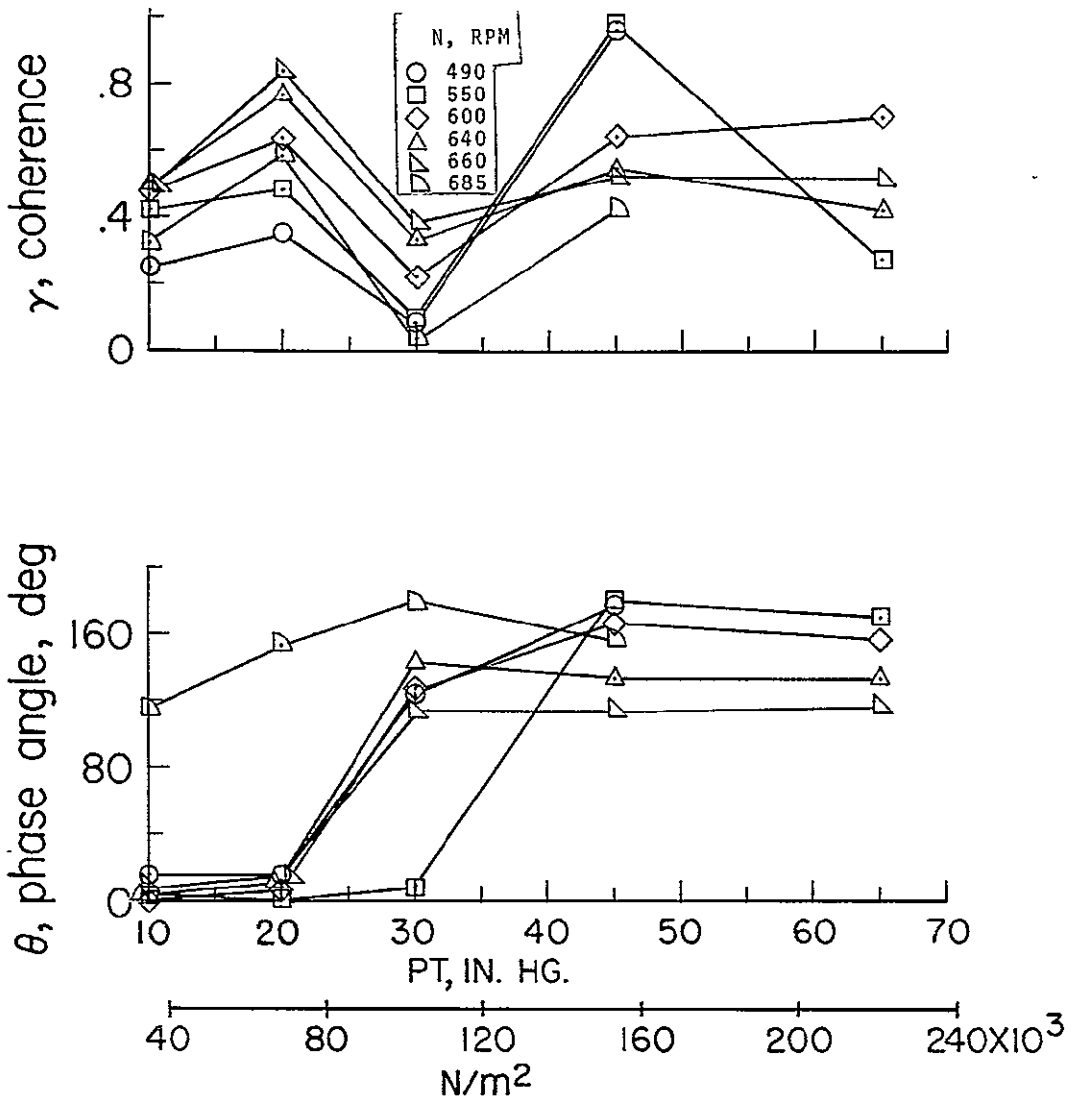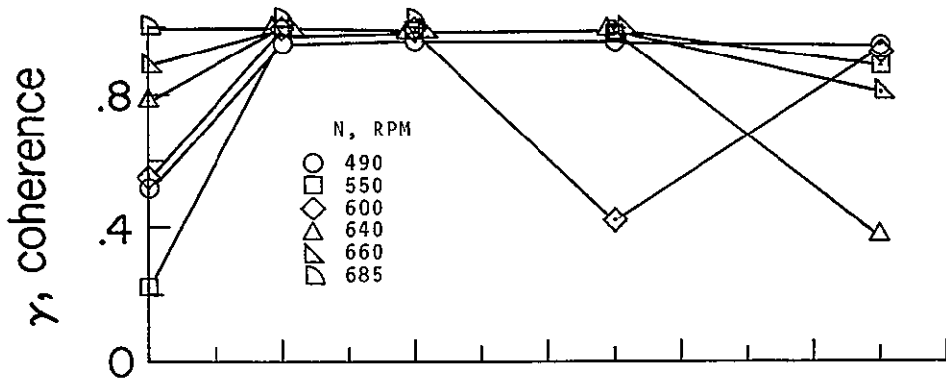
(d) 3rd mode θ and γ for gages 4,5.

Figure 11.- Continued.
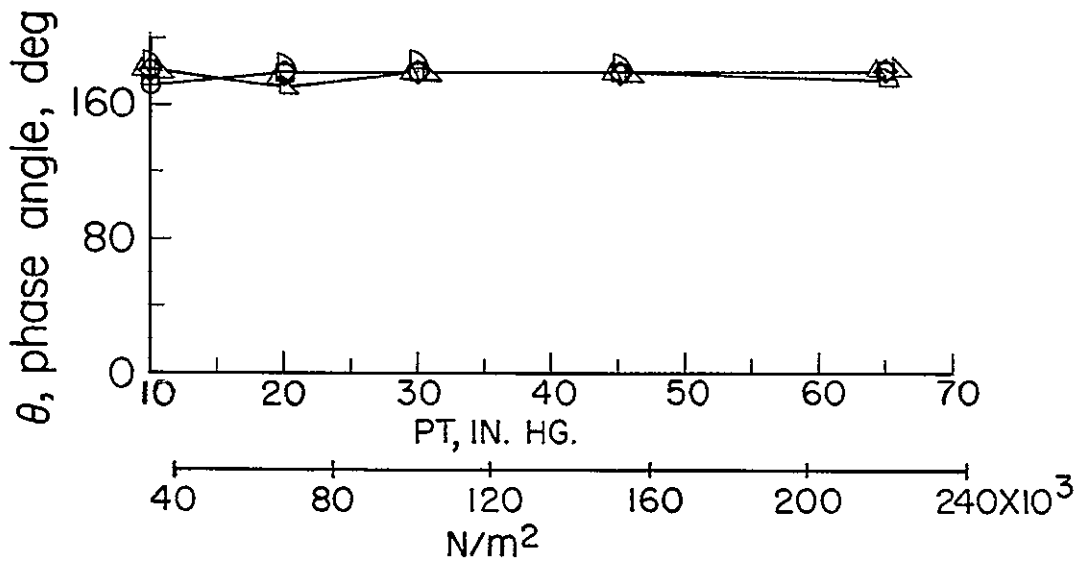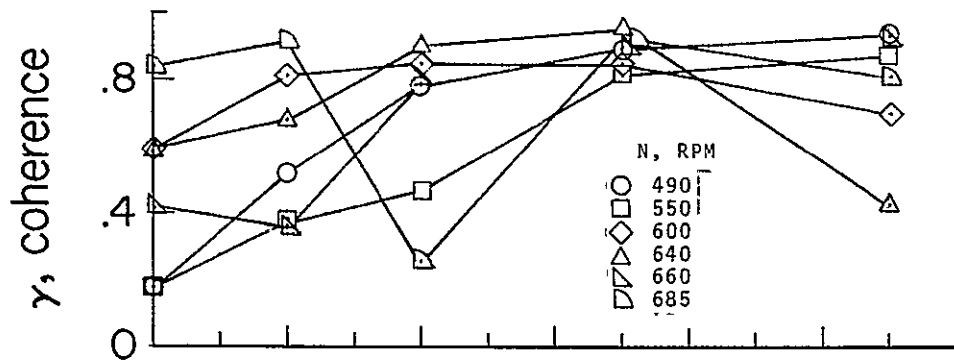
(e) 4th mode θ and γ for gages 4,5.
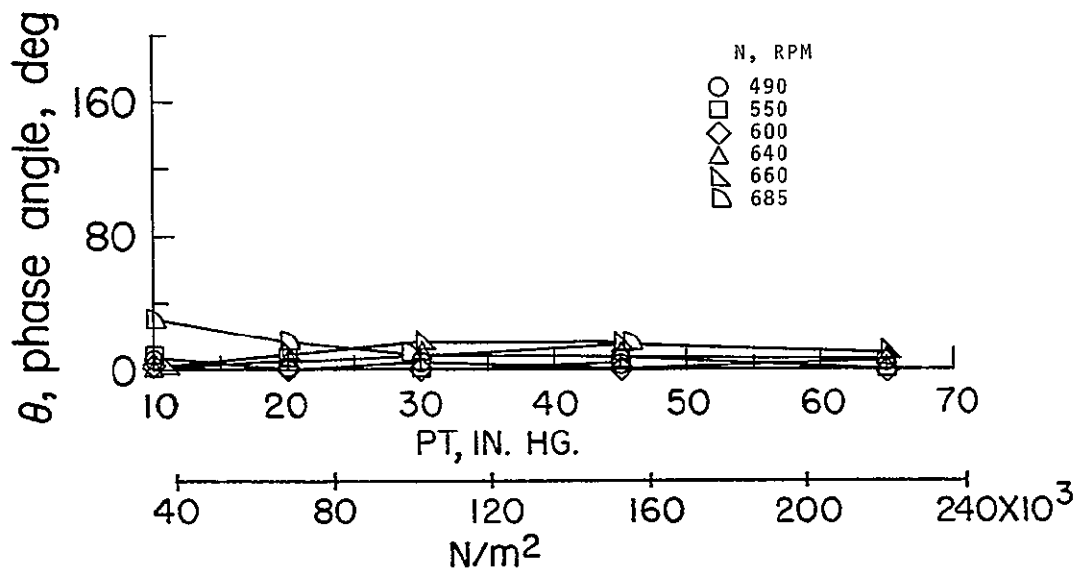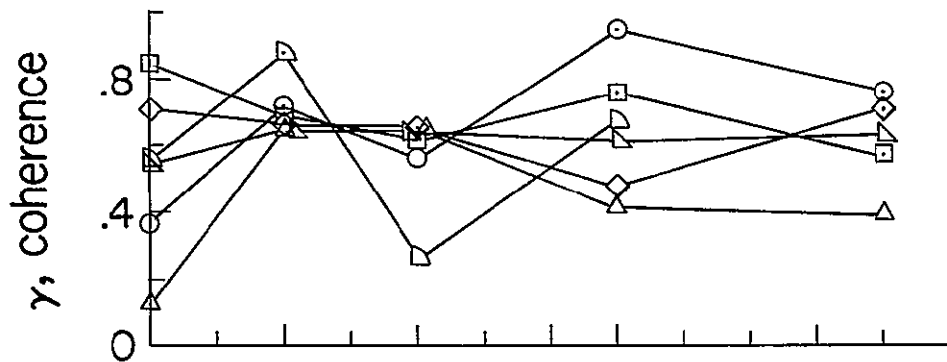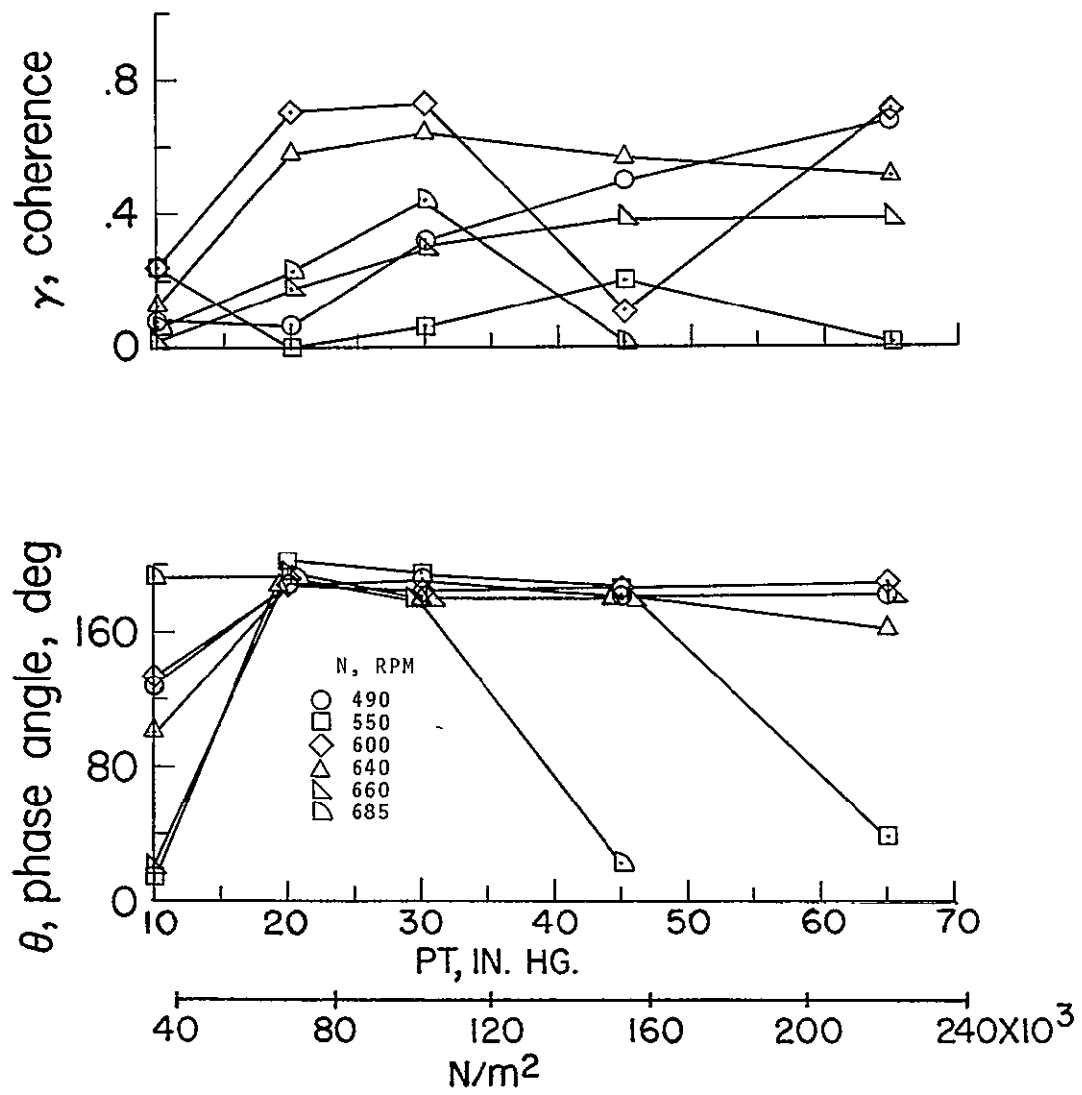
Figure 11.- Continued.
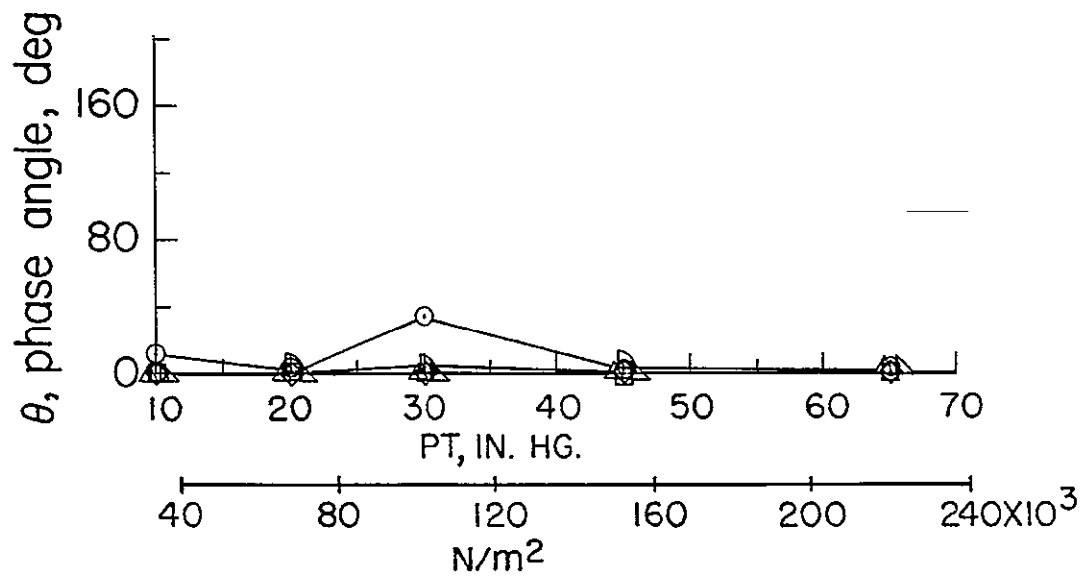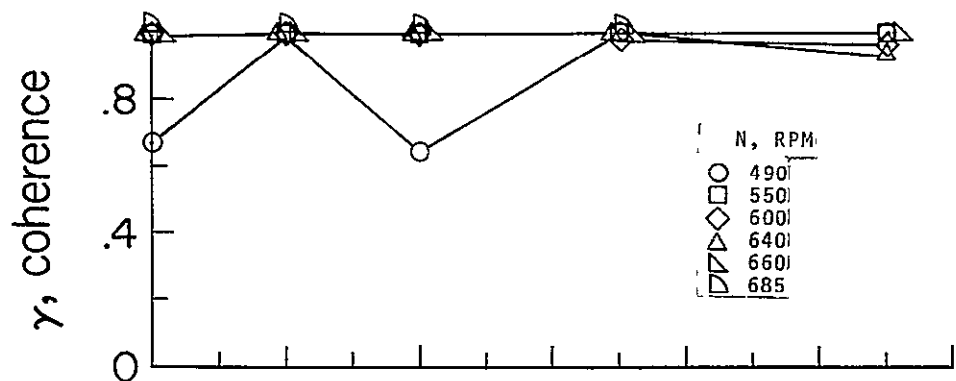
(f) 1st mode θ and γ for gages 6,12.

Figure 11.- Continued.
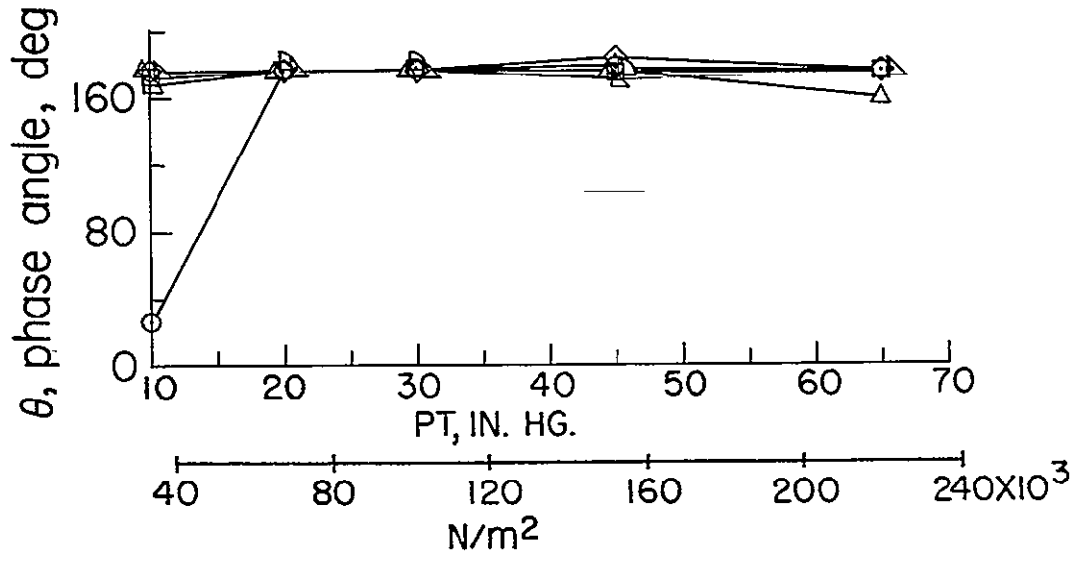
(g) 2nd mode θ and γ for gages 6,12.

Figure 11.- Continued.

(h) 3rd mode θ and γ for gages 6,12.
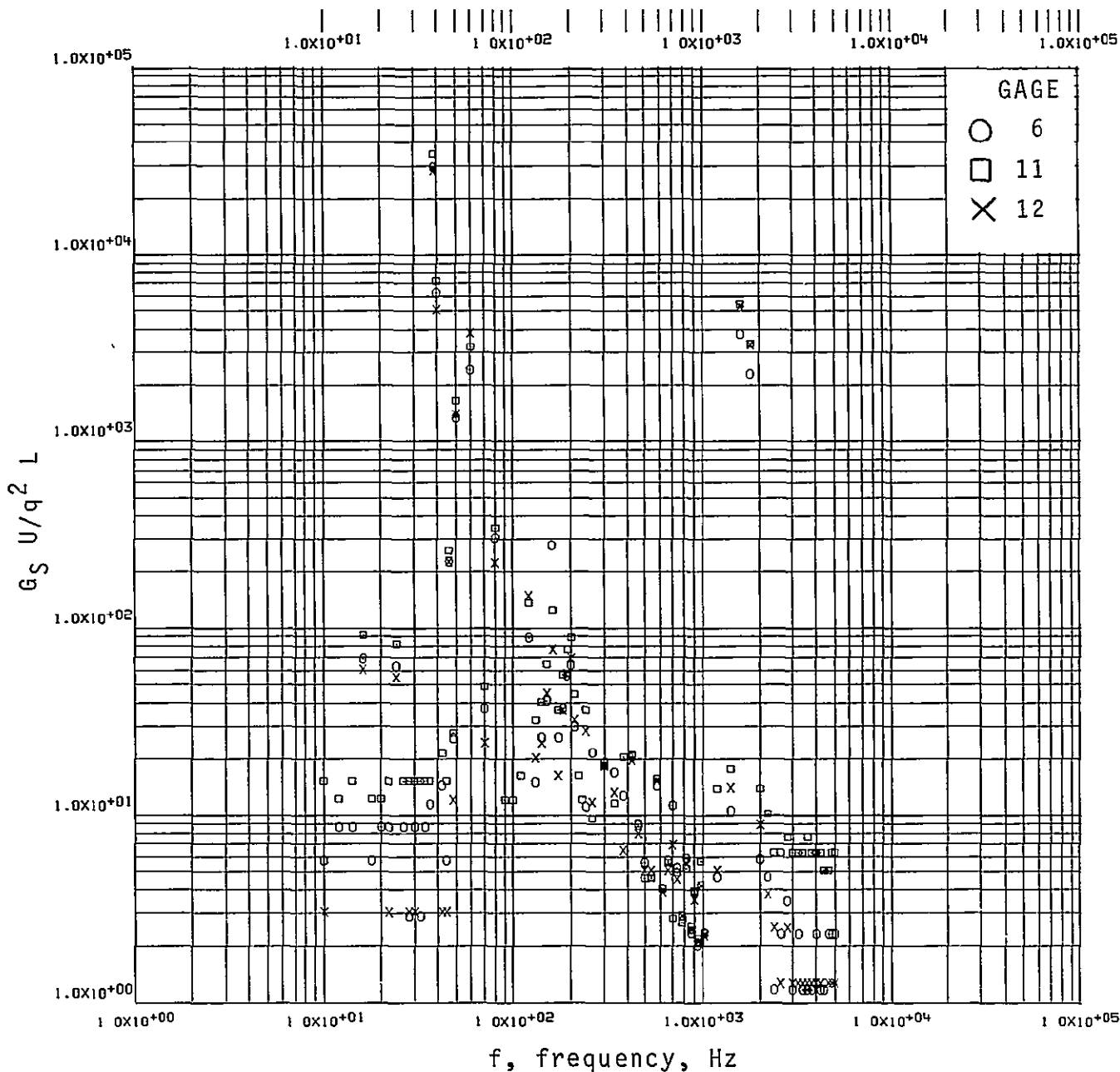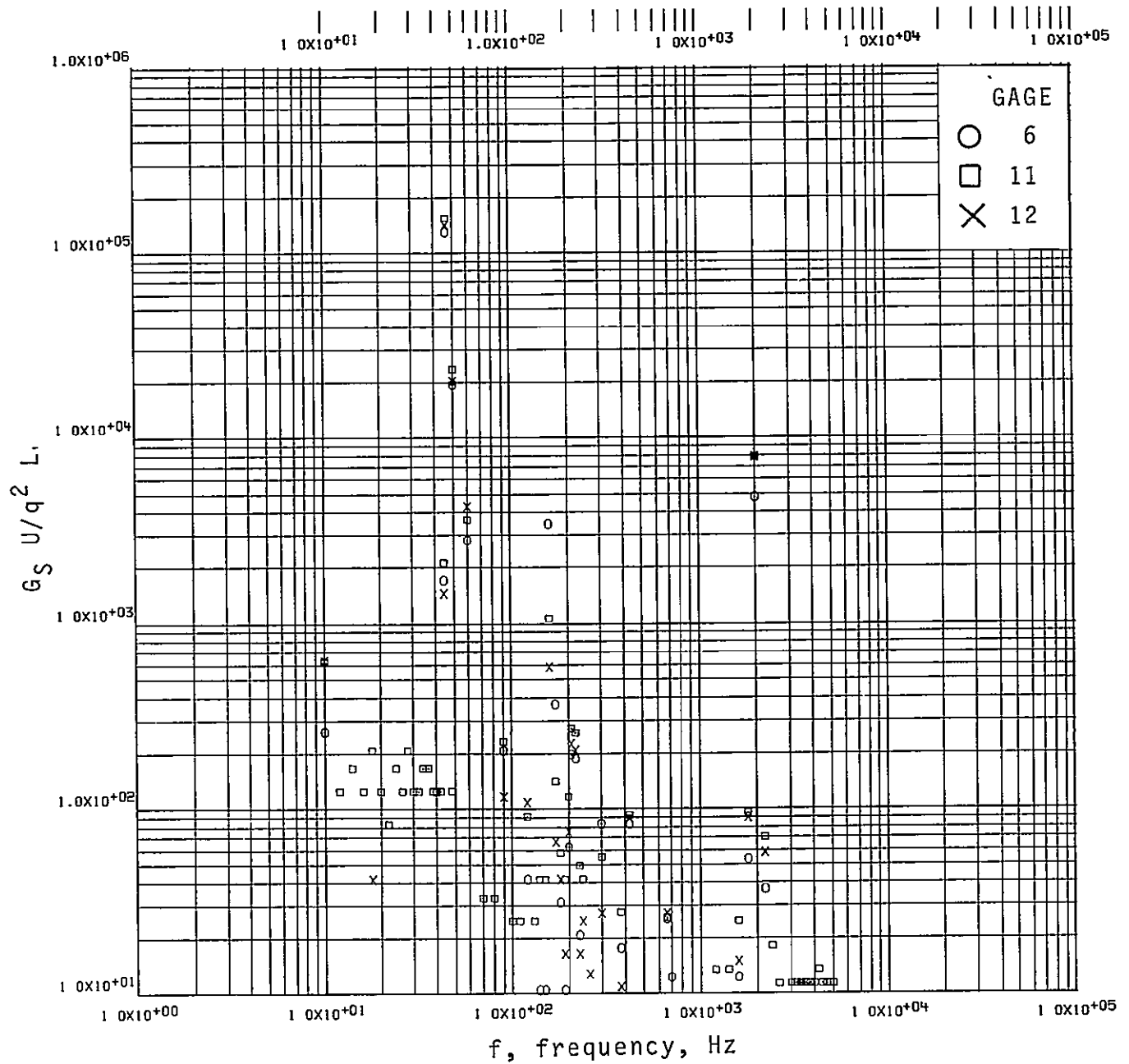
Figure 11.- Continued.

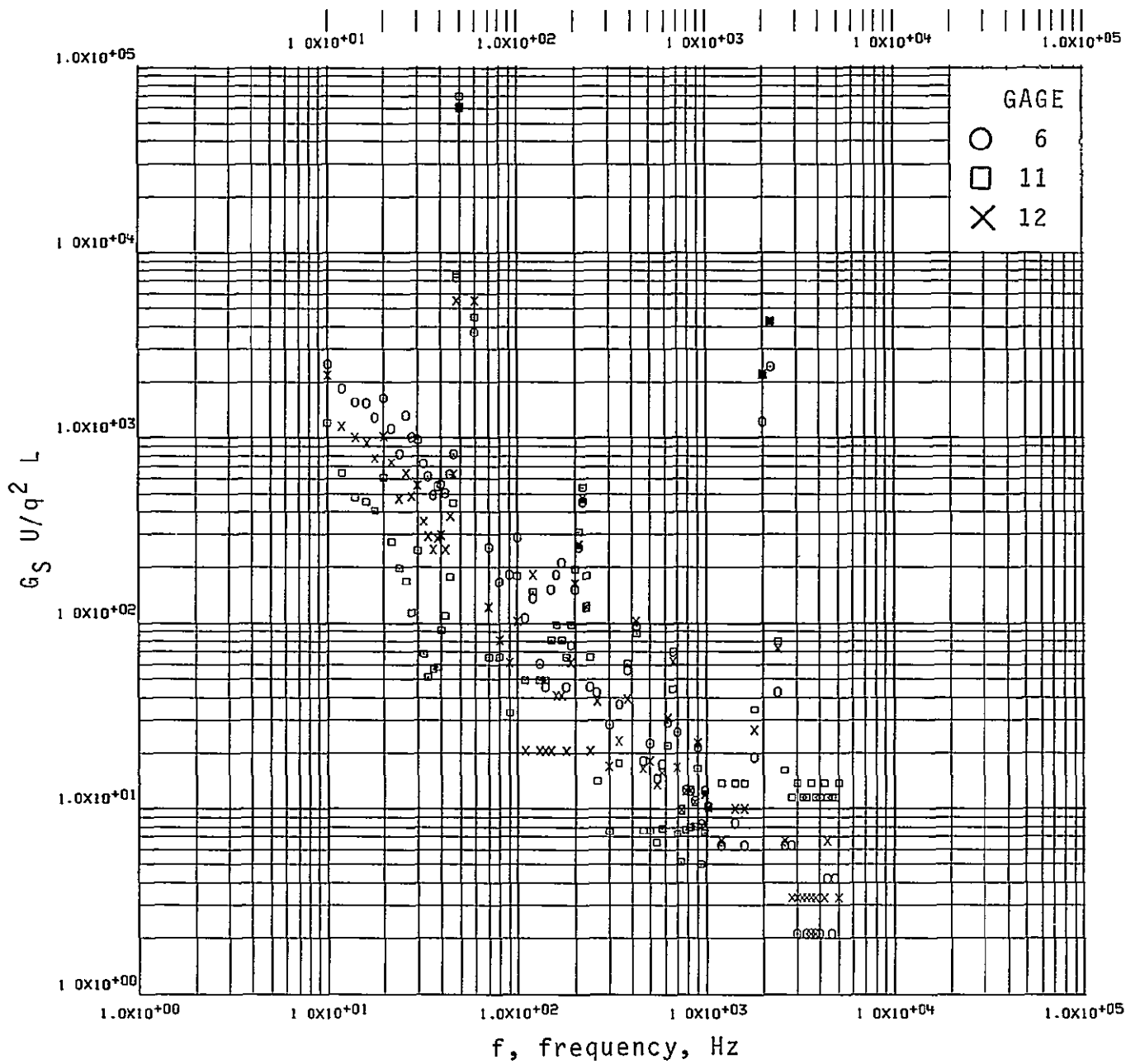(i) 4th mode θ and γ for gages 6,12.

Figure 11.- Concluded.

(a) N = 470; $M_\infty \cong 0.65$.

Figure 12.- Power spectrum of the dynamic stresses in the compressor blade for frequencies up to 20 kHz at various compressor speeds; p_t = 152.39X10^3 N/m^2 (45 in. Hg).

(b) N = 550; $M_\infty \cong 0.83$.

Figure 12.- Continued.
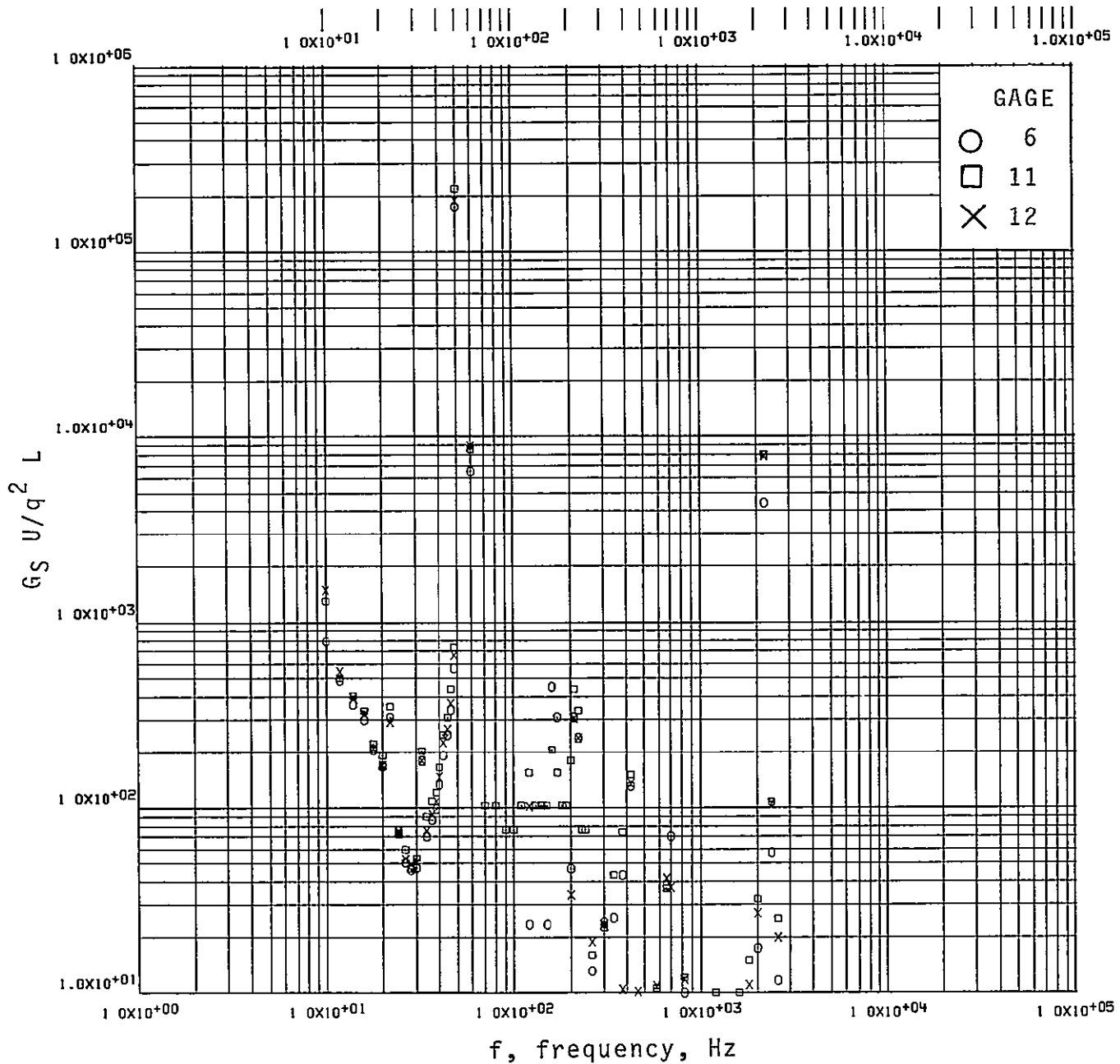
(c) N = 600; $M_\infty \cong 0.98$.

Figure 12.- Continued.
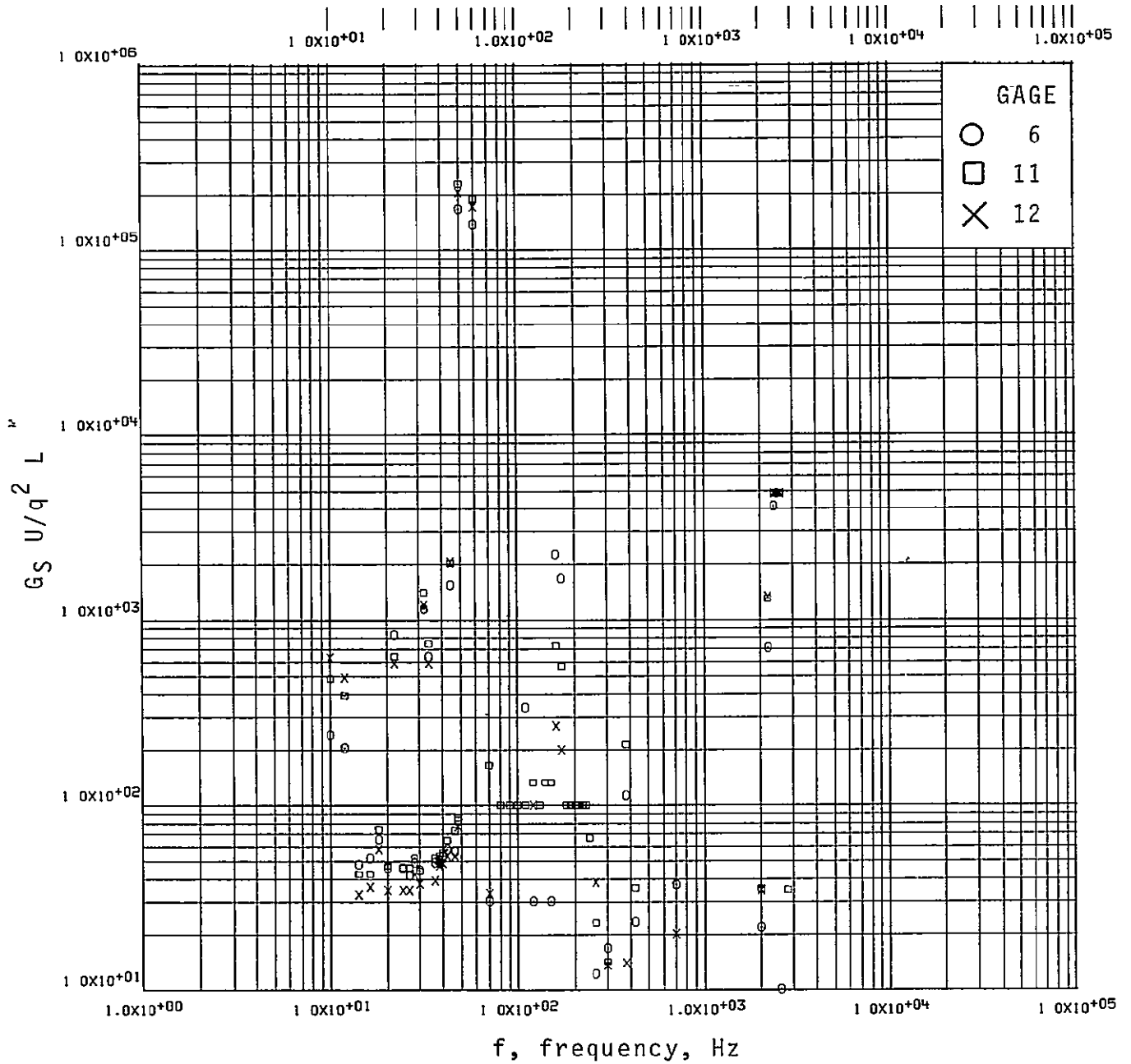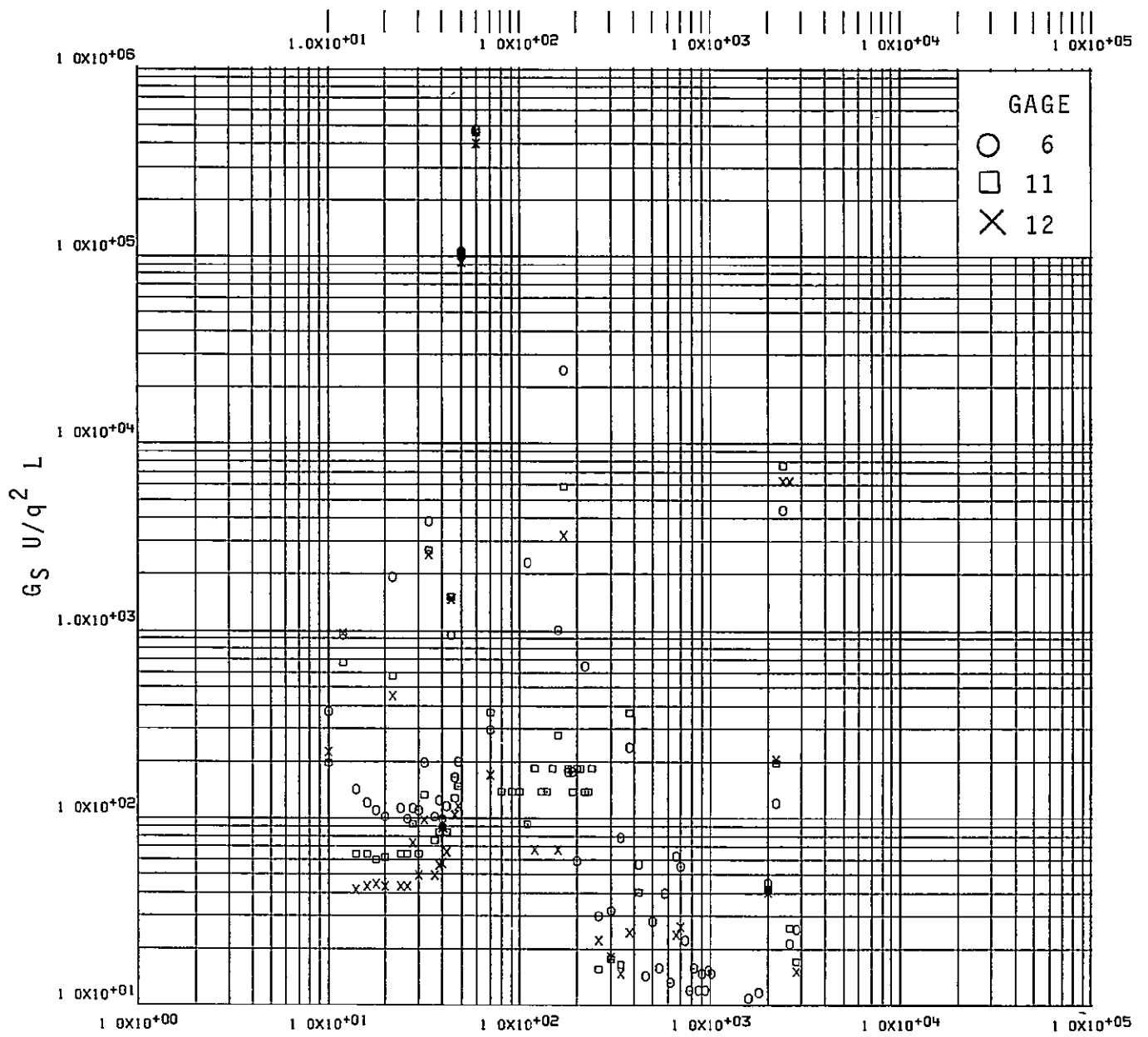
(d) $N = 640$; $M_\infty \cong 1.14$.

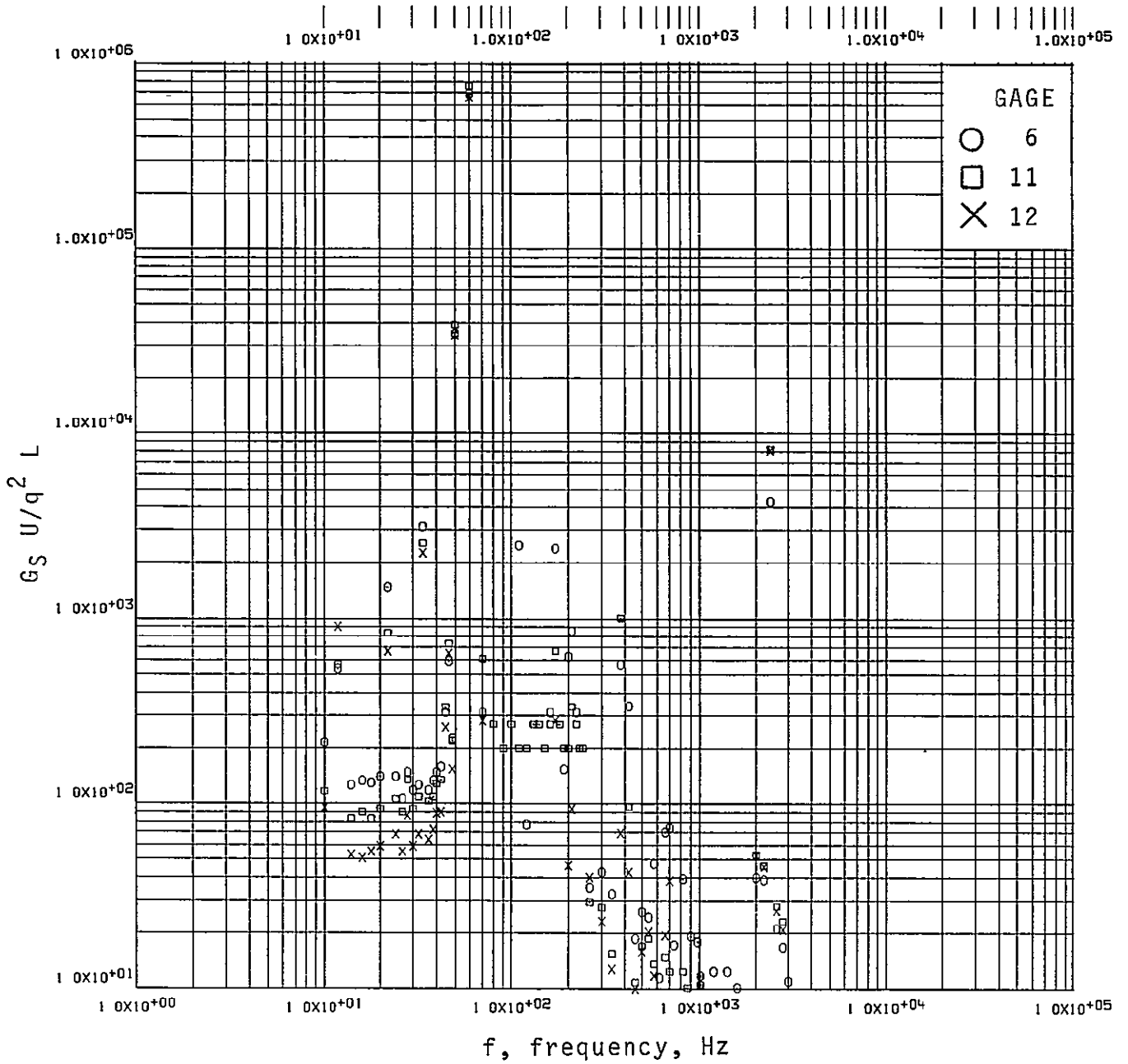Figure 12.- Continued.

(e) $N = 660$; $M_\infty \cong 1.22$.

Figure 12.- Continued.

f, frequency, Hz

(f) N = 670; $M_\infty \cong 1.25$.

Figure 12.- Continued.

(g) $N = 680$; $M_\infty \cong 1.26$.

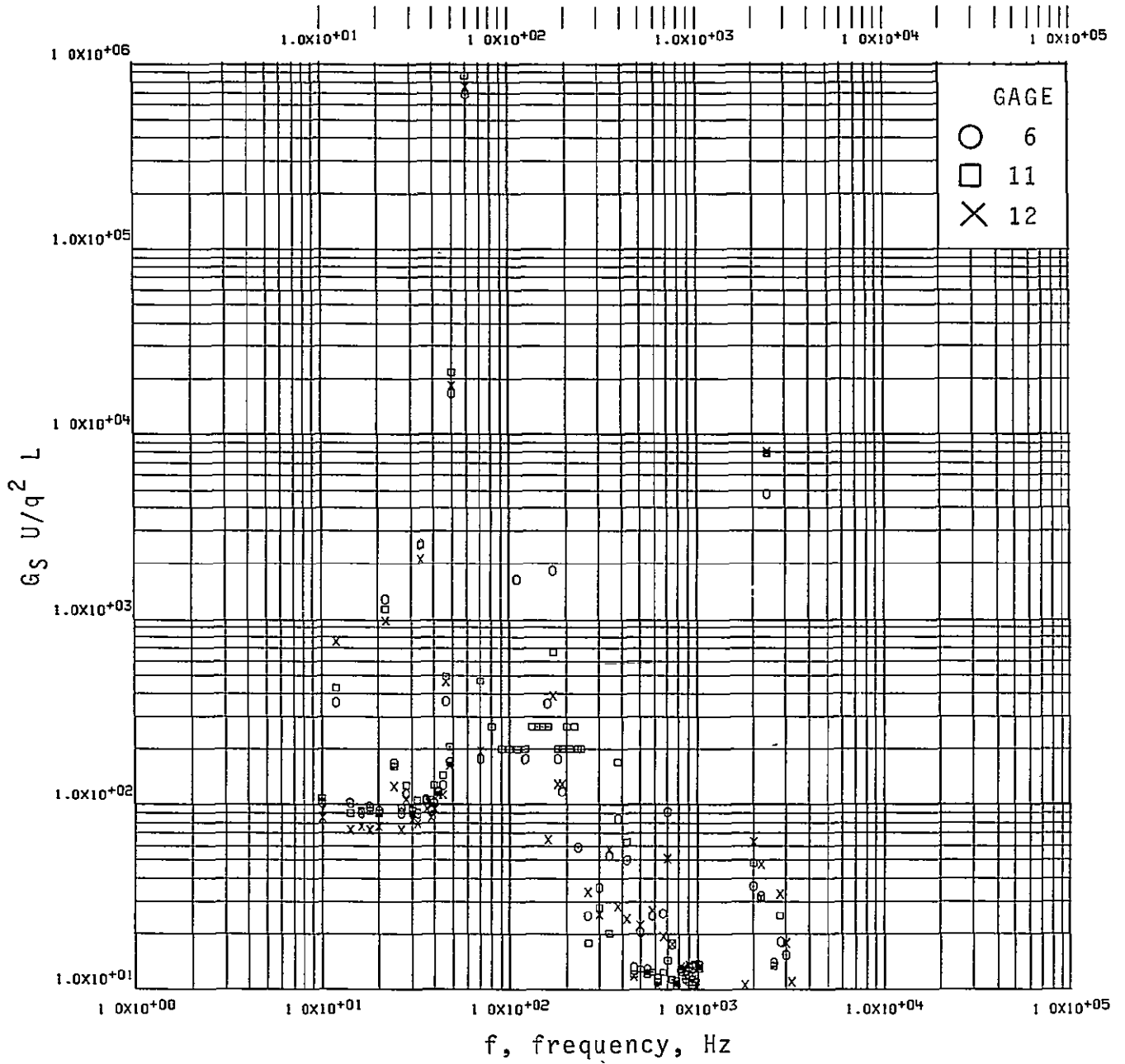Figure 12.- Continued.

(h) $N = 685$; $M_\infty \cong 1.27$.

Figure 12.- Concluded.
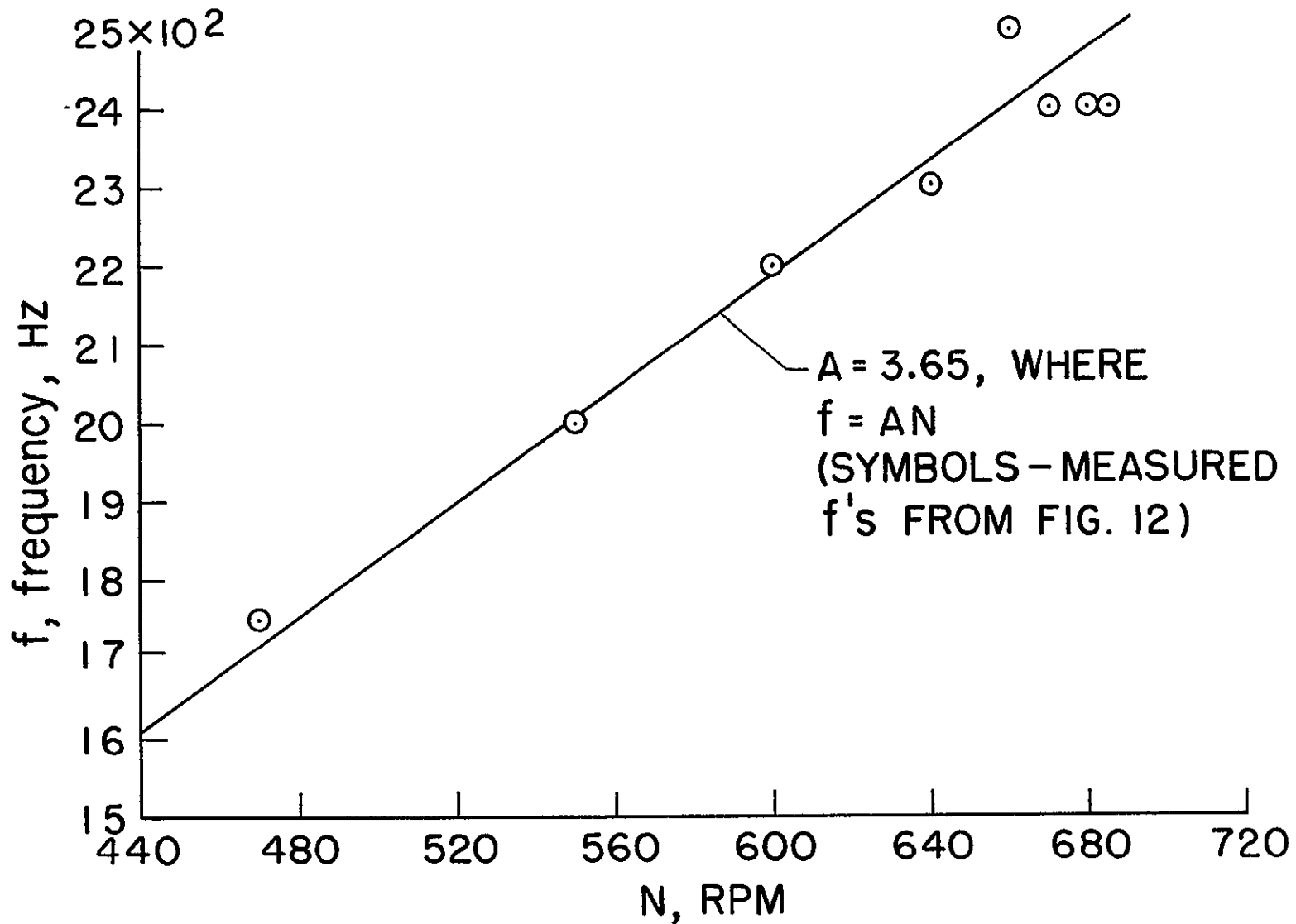
Figure 13.- Variation of the frequency of the noise peaks observed at frequencies above 1 kHz with compressor speed; p_t = 152.39X10^3 N/m^2 (45 in. Hg).
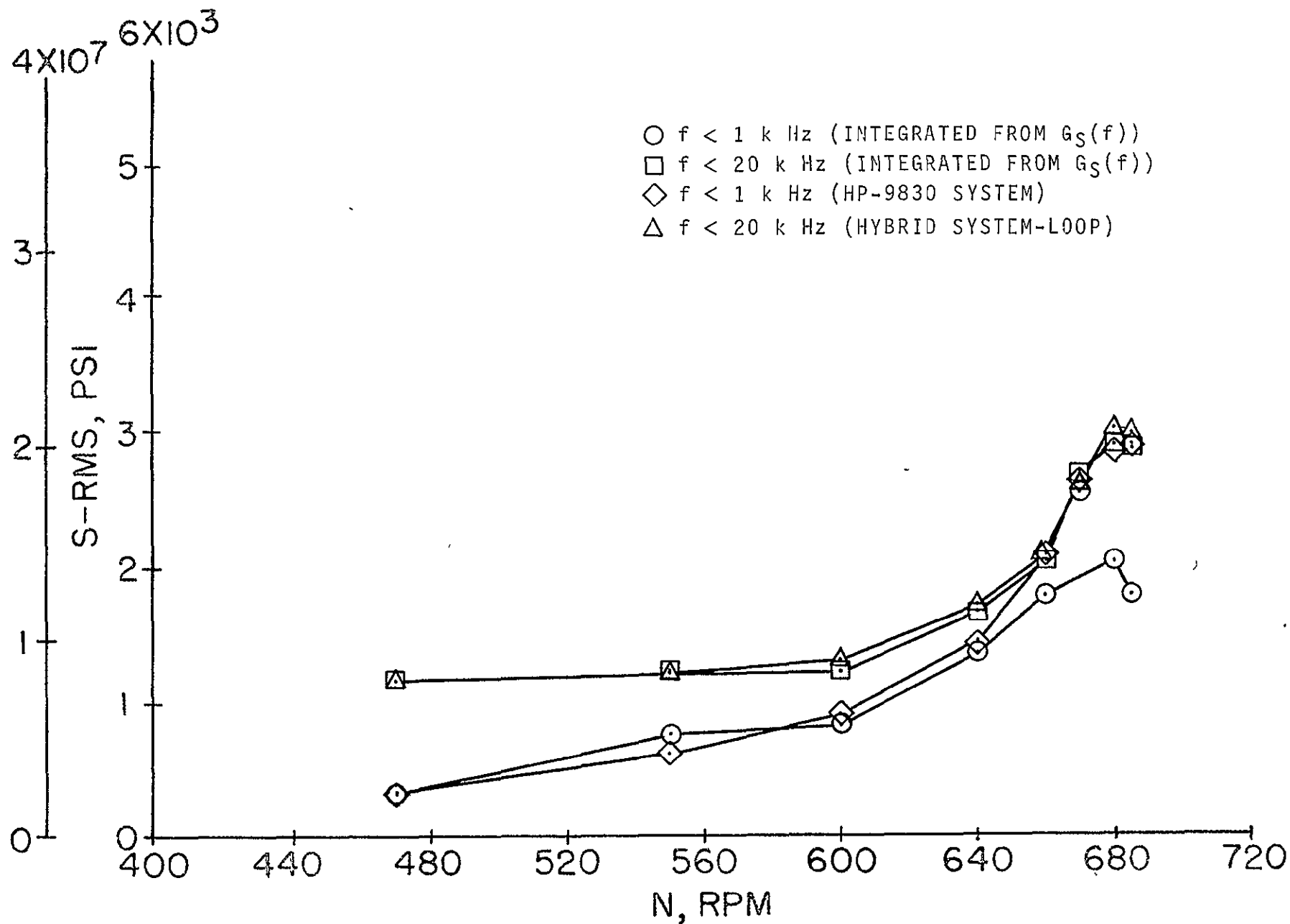
(a) Gage 6.

Figure 14.- Variation of the dynamic blade stresses with compressor speed illustrating the effect of noise peaks at frequencies above 1 kHz; p_+ = 152.39X10^3 N/m^2 (45 in. Hg).
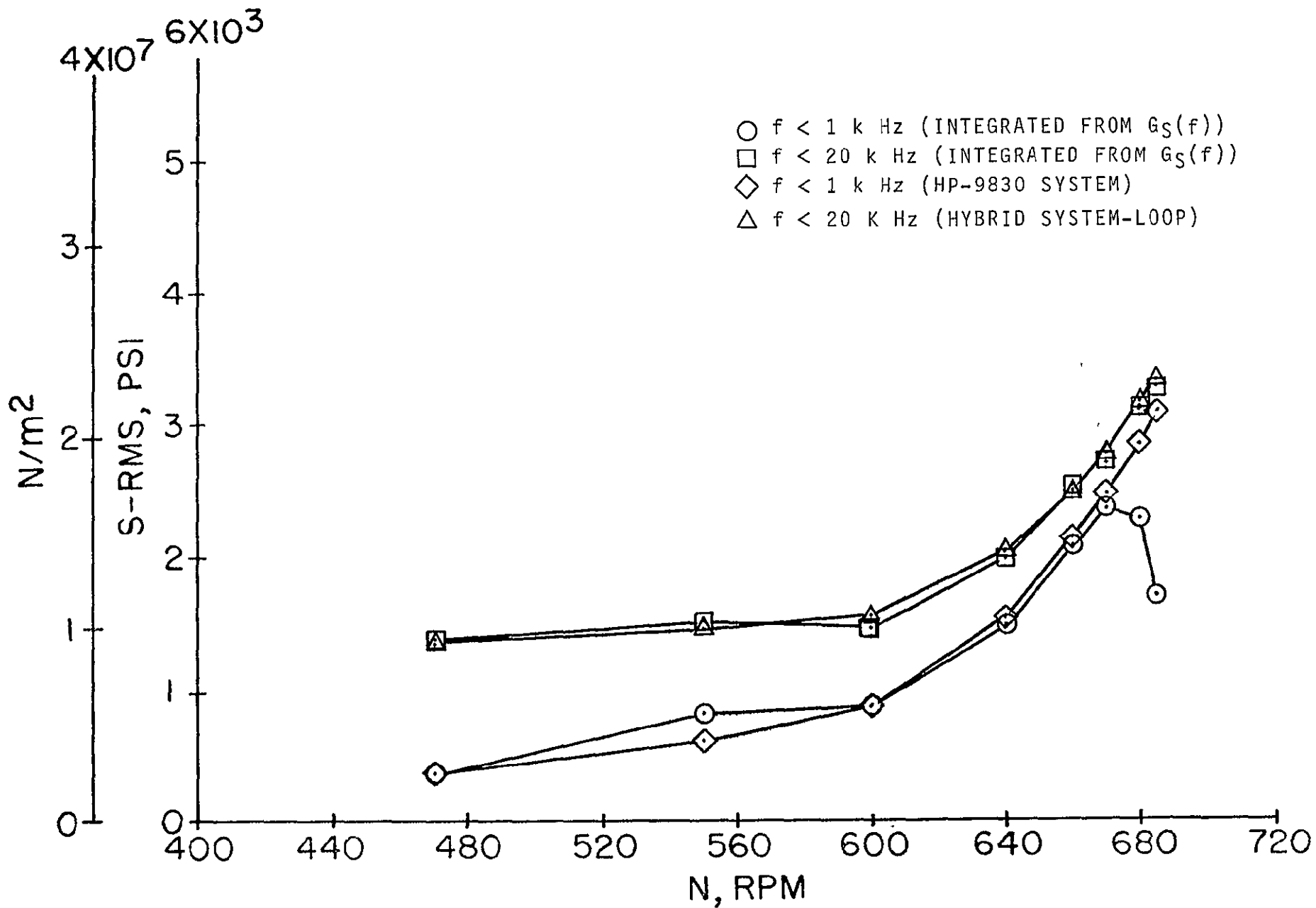
(b) Gage 11.

Figure 14.- Continued.

(c) Gage 12.

Figure 14.- Concluded.

1 Report No NASA CR- 152083	2 Government Accession No	3 Recipient's Catalog No

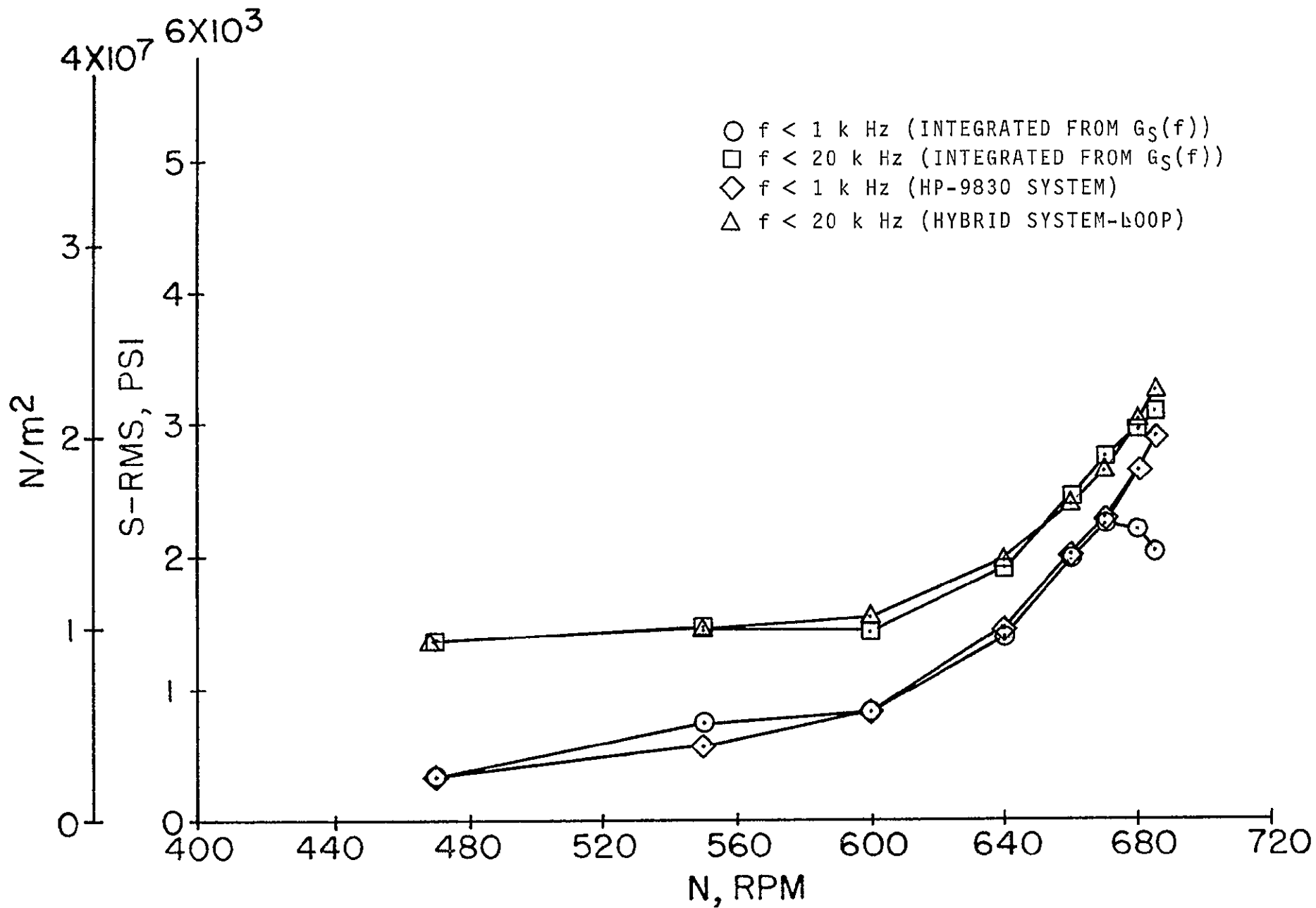| 4 Title and Subtitle "An Analysis of the Rotor Blade Stresses of the Three Stage Compressor of the Ames Research Center 11- by 11-Foot Transonic Wind Tunnel"		5 Report Date November, 1977
		6 Performing Organization Code

7 Author(s) Jules B. Dods, Jr.	8 Performing Organization Report No
	10 Work Unit No

9 Performing Organization Name and Address Raman Aeronautics.Research and Engineering, Inc. Palo Alto, CA 94301	11 Contract or Grant No NAS 2-9112
	13 Type of Report and Period Covered Final Report

12 Sponsoring Agency Name and Address National Aeronautics & Space Administration Washington, D. C. 20546	
	14 Sponsoring Agency Code

15 Supplementary Notes

16 Abstract

The static and dynamic rotor blade stresses of the 3-stage compressor of the Ames Research Center 11- by 11-Foot Transonic Wind Tunnel were measured over the operational range of the wind tunnel. A maximum total blade stress (static plus dynamic) of 62.36×10^6 N/m^2 (9045 psi) occurs on the third stage blade at a distance of 0.5461 m (21.5 in) outboard from the root of the blade for a tunnel total pressure of 220.12×10^3 N/m^2 (65 in Hg). The static stress accounts for 88.6- percent of the total stress, and the dynamic stress accounts for the remaining 11.4-percent of the total stress. A band-pass frequency analysis of the data indicated that the dynamic stresses are primarily due to vibrations in the first bending mode.

17 Key Words (Suggested by Author(s)) Rotor Blade Stresses Static Stresses Dynamic Stresses Transonic Wind Tunnels	18 Distribution Statement UNCLASSIFIED - UNLIMITED

19 Security Classif (of this report) UNCLASSIFIED	20 Security Classif (of this page) UNCLASSIFIED	21 No of Pages	22 Price*